Microwave Electronics

Enhancement of Microwave Properties of Planar Filters and Antennas using Photonic Bandgap (PBG) Structures

Thesis submitted to

Cochin University of Science and Technology

in partial fulfilment of the requirements

for the award of the degree of

DOCTOR OF PHILOSOPHY

by

Sreedevi K Menon

Under the guidance of

Prof. P. Mohanan

Department of Electronics
Cochin University of Science and Technology
Cochin 6820 22
India

October 2006

CERTIFICATE

Certified that the work presented in this thesis entitled "Enhancement of Microwave Properties of Planar Filters and Antennas using Photonic Bandgap (PBG) Structures" is based on the bonafide research work done by Ms. Sreedevi K Menon under my guidance in the Department of Electronics, Cochin University of Science and Technology, Cochin 682 022, and has not been included in any other thesis submitted previously for the award of any degree.

Kochi-22
October 4, 2006

Prof. P. Mohanan
Supervising Guide,
Centre for Research in Electromagnetics and Antennas (CREMA)
Department of Electronics,
Cochin University of Science and Technology
Kochi-22

DECLARATION

I hereby declare that the present work entitled "Enhancement of Microwave Properties of Planar Filters and Antennas using Photonic Bandgap (PBG) Structures" is based on the original work done by me under the guidance of Prof. P. Mohanan, Centre for Research in Electromagnetics and Antennas (CREMA), Department of Electronics, Cochin University of Science and Technology, Kochi-22 and has not been included in any other thesis submitted previously for the award of any degree.

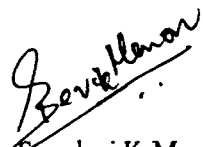

Kochi-22
October 4, 2006

Sreedevi K Menon

ACKNOWLEDGEMENT

With immense pleasure I extend deep sense of gratitude to Prof. P. Mohanan, Centre for Research in Electromagnetics and Antennas (CREMA), Department of Electronics, Cochin University of Science and Technology for his excellent guidance and constant encouragement throughout the course.

I am thankful to Prof. K. Vasudevan, Head, Department of Electronics, Cochin University of Science and Technology and Dr. C.K. Aanandan, Reader, Department of Electronics, for providing the necessary facilities and for their valuable suggestions in shaping my research work.

I remember with gratitude Prof. K.T. Mathew, Prof. Sasindharan Pillai and Prof. Tessamma Thomas for their support and encouragement at various stages of my work and also grateful to Dr. Rajaveerappa, Ms. Supriya M. H and Mr. James Kurian, Faculty, Department of Electronics for their support and help.

Along with that I would like to extend my sincere gratitude to Dr. Ratheesh, Scientist, C-MET and Prof. Ramesh Babu, Department of Physics for their valuable suggestions and advice.

I am thankful to all the teaching and non-teaching staff of the Department of Electronics for their amicable relation and sincere co-operation.

I am extremely thankful to all the Research Scholars in the Department of Electronics, from whom I have benefited immensely towards the accomplishment of this work.

I wish to thank Council for Scientific and Industrial Research (CSIR), India for financial assistance in the form of Senior Research Fellow (SRF) awarded to me and also acknowledge Department of Science and Technology (DST), Govt. of India for financial assistance at the earlier stages of my work.

I am extremely grateful to my parents and well-wishers for the support and encouragement rendered to me. Finally, I owe a lot to Manoj for his unconditional love, encouragement, understanding and support. Above all, there is that supreme power without whose blessings and kindness we cannot achieve anything in this world.

Sreedevi K Menon

Abstract

In this thesis, we explore the design, computation, and experimental analysis of photonic crystals, with a special emphasis on structures and devices that make a connection with practically realizable systems. First, we analyze the properties of photonic-crystal: periodic dielectric structures that have a band gap for propagation. The band gap of periodically loaded air column on a dielectric substrate is computed using Eigen solvers in a plane wave basis. Then this idea is extended to planar filters and antennas at microwave regime. The main objectives covered in this thesis are:

- Computation of Band Gap origin in Photonic crystal with the abet of Maxwell's equation and Bloch-Floquet's theorem
- Extension of Band Gap to Planar structures at microwave regime
- Predict the dielectric constant – *synthesized dielectric constant* of the substrates when loaded with Photonic Band Gap (PBG) structures in a microstrip transmission line
- Identify the resonant characteristic of the PBG cell and extract the equivalent circuit based on PBG cell and substrate parameters for microstrip transmission line
- Miniaturize PBG as Defected Ground Structures (DGS) and use the property to be implemented in planar filters with microstrip transmission line
- Extended the band stop effect of PBG / DGS to coplanar waveguide and asymmetric coplanar waveguide.
- Formulate design equations for the PBG / DGS filters
- Use these PBG / DGS ground plane as ground plane of microstrip antennas
- Analysis of filters and antennas using FDTD method

CONTENTS

4. PLANAR FILTERS WITH PHOTONIC BAND GAP STRUCTURES – DESIGN & ANALYSIS

5. PLANAR ANTENNAS: REFLECTION AND RADIATION CHARACTERISTICS ON PHOTONIC BANDGAP SUBSTRATES

1

INTRODUCTION

Contents

Photonic crystals have attracted much attention these years. The sincere effort in this thesis is to extend the principle of Photonic Bandgap to Microwave regime. A brief introduction to the concept of Photonic crystals and a review of past work is presented in this chapter of the thesis. Different theoretical approaches used for analysis is also presented. The chapter concludes with a layout of the organization of the thesis.

1.1 Dynamical theory of the electromagnetic field

In 1864, James Clerk Maxwell revealed the equations underlying all phenomena in electricity and magnetism through "A dynamical theory of the electromagnetic field" [1]. This remarkable work laid bare the deep connections between the electricity of Franklin, the magnetic lodestones of the ancient mariners, and the light that had filled the first eyes gazing into the heavens. The theory shortly thereafter verified by Heinrich Hertz and thus began the new age of wireless communication. And yet Maxwell's equations, encompassing as they are, were only the beginning. Maxwell's electromagnetism has figured prominently in every subsequent advance of physics, from quantum mechanics to relativity to the "standard model" of particle theory. Today, the same basic theory provides us with the use of radio, television and mobile phones.

Of course, it is not enough to understand electricity and magnetism - one must also comprehend the material upon and within which those forces operate. Maxwell knew the behavior of certain kinds of materials, such as dielectrics and has predicted in his equations the reflection, refraction and dispersion of the electromagnetic waves when they interact with these materials. This knowledge led the quest to know "what sort of material can afford control over wave propagation?"

1.2 Waves Trapped?

The importance of waves in the natural and the man-made world can hardly be overestimated. We see and we hear through waves. We transmit information through waves. We understand and control the electrical, magnetic and other properties of metals and semi-conductors through electronic waves.

Imagine an electron propagating through a semiconductor crystal. The crystal lattice provides a periodic potential to the electron allowing propagation only in certain energy bands in certain directions. Strong lattice potential can extend the forbiddance in all possible directions resulting in a complete band gap, as between valence and conduction bands. Energy bandgap concept of solid state electronic materials can be extended to electromagnetics which provide a means to control and manipulate electromagnetic waves.

Optical analogy of electronic semiconductors the *Photonic crystals* (PC) allows tailoring the properties of photons thus controlling the flow of light. The underlying concept of these materials stems from the early notions by Yablonovitch [2]. The first proposed Photonic crystal was for spontaneous emission control. Spontaneous emission of light is a major natural phenomenon, which is of great practical and commercial importance. For example, in semiconductor lasers, spontaneous emission is the major sink for threshold current, which must be surmounted in order to initiate lasing. In hetero-junction bipolar transistors (HBTs), which are non-optical devices, spontaneous emission nevertheless rears its head. In some regions of the transistor current-voltage characteristic, spontaneous optical recombination of electrons and holes determines the HBT current gain. In solar cells, surprisingly, spontaneous emission fundamentally determines the maximum available output voltage. We shall also see that spontaneous emission

determines the degree of photon number state squeezing, an important new phenomenon in the quantum optics of semiconductor lasers. Thus the ability to control spontaneous emission of light is expected to have a major impact on technology. The easiest way to understand the effect of a photonic bandgap on spontaneous emission is to take note of Fermi's golden rule. At high frequencies, metals become more and more lossy. These dissipative losses allow for virtual modes, even at frequencies which would normally be forbidden. Therefore it makes sense to consider structures made of positive-dielectric-constant materials such as glasses and insulators, rather than metals. These can have very low dissipation, even all the way up to optical frequencies. This is ultimately exemplified by optical fibers which allow the light propagation over many kilometers, with negligible losses. Such positive-dielectric constant materials can have an almost purely dielectric response with low resistive losses. If arrayed into a three-dimensionally periodic dielectric structure, a photonic bandgap should be possible, employing a purely real reactive dielectric response and the structure proposed by Yablonovitch for spontaneous emission control is shown in Figure 1.2.1.

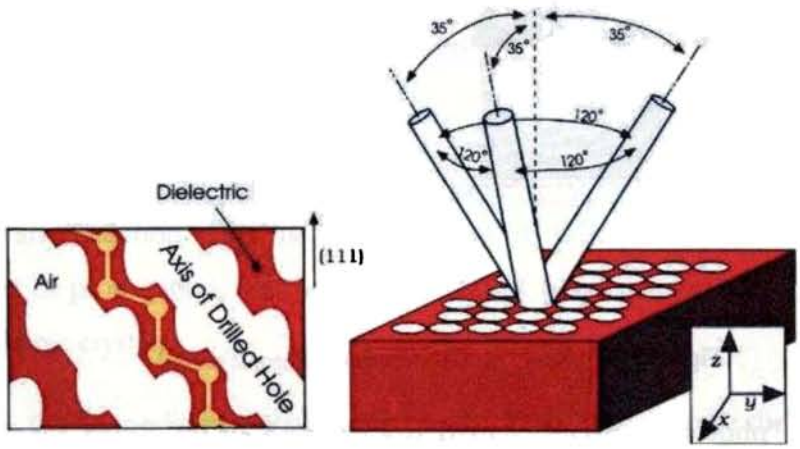

Figure 1.2.1 The Yabonovite structure consists of a dielectric slab in which a triangular array of holes is drilled. (1989)

Actually, a form of photonic crystal can be found in nature, producing the iridescent colors of abalone shells, butterfly wings, and some crystalline minerals. Some naturally occurring photonic crystals - Morph butterfly and Peacock Feather is shown in Figure 1.2.2. But, these beautiful materials archetypically comprise alternating microscopic layers of two substances (or two arrangements of the same substance) and are only periodic in *one* direction.

Indeed there was no assurance in 1987 that any photonic band gap materials could ever be produced experimentally with available refractive indexes. The search for a three dimensional (3-D) photonic band gap entailed numerous blind alleys and false starts, culminating in 1990 with the remarkable theoretical discovery that the diamond crystal geometry provided an ideal system for gaps at microwave frequencies and first experimental demonstration of a 3-D photonic band gap material was done.

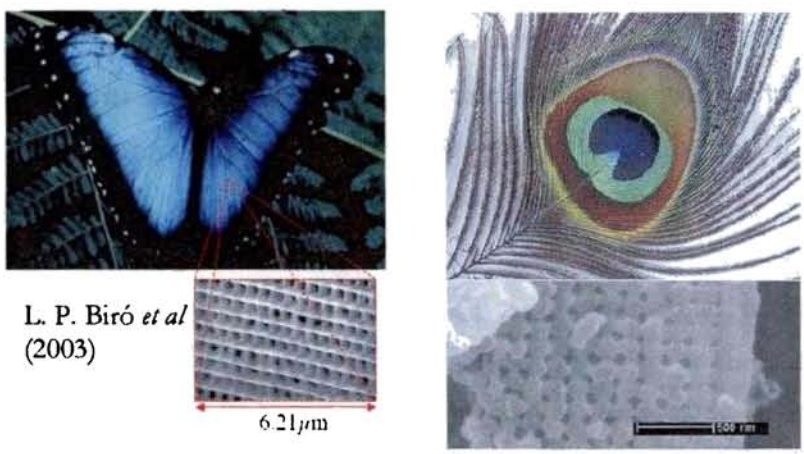

L. P. Biró *et al* (2003)

J. Zi *et al* (2003)

Figure 1.2.2 Some natural occurring Photonic crystals

The idea of "photonic crystals" started from the notion of Bragg condition in periodic structures under which light at particular wavelengths completely reflects off such structures

Vector-wave-based solutions implemented using the plane wave expansion (PWE) method for Maxwell's equations, being developed by Leung *et al.* [3], Zhang *et al.* [4], and Ho *et al.* [5], offered the potential of finding a true two-dimensional (2-D) photonic band-gap structure. Indeed, soon thereafter, a structure that possesses a full photonic band-gap was identified. Theoretical work by Ho *etal* [5] confirmed the existence and structure of the first (3-D) photonic crystal, the diamond dielectric structure.

As shown in Figure 1.2.3, there are three different types of periodic structures; namely, one-dimensional (1D), two-dimensional (2D), and three-dimensional (3D) periodic structures [6].

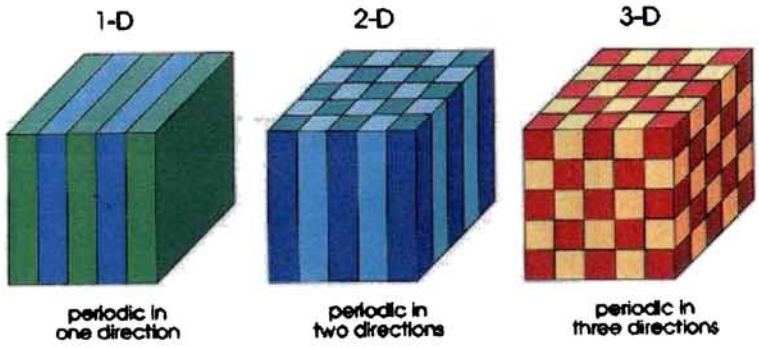

Figure 1.2.3. Examples of one, two and three-dimensional photonic crystals. The different colors represent different values of the dielectric constant.

The main advantage of 3D over 2D periodic structures is their flexibility to channel light in any direction. This means, regardless of the type of polarization or the direction of propagation, light in certain band of frequencies cannot propagate in 3D photonic crystals.

In a PC, the "periodic potential is due to a lattice of macroscopic dielectric media instead of atoms. If the dielectric materials of the crystals are different enough, and the absorption of light by the material is minimal, then the scattering at the

interfaces can produce many of the same phenomena for photons as atomic potential does for electrons. Photonic crystals have periodic scatterers and when the period (separation between the scatterers) is in the order of wavelength of light the reflections and refractions will cancel the scattered as well the forward moving light. Energy being conserved, these are forbidden from entering the crystal. This happens no matter what direction the light is coming from, in a certain range of wavelengths called the *photonic band gap* (PBG). The basic physical reason for the rise of gaps lays in the coherent multiple scattering and interference of waves inside the crystal – the Bragg resonance of the waves with the crystal structure. Such a medium impervious to light can be used to make "optical wire" (by carving a tunnel through the material) from which no light can deviate or a cavity at the center of the crystal in which a beam of light is trapped – "optical cage". The opal suggested by S.John etal is shown in Figure 1.2.4.

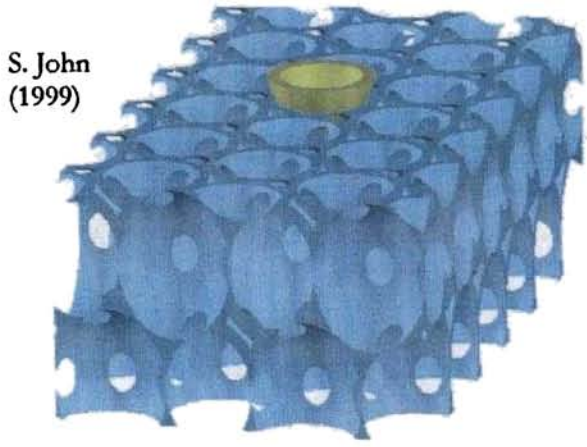

Figure 1.2.4 Opal

1.3 Band Gap at Microwave Regime

Electromagnetic wave propagation in periodic dielectric media is analogous to electron-wave propagation in semiconductor crystals. Although fundamentally different propagation mechanisms are involved, preliminary results suggest that at

microwave and millimeter-wave frequencies the propagation characteristics of these crystals can be manipulated by carefully designing and fabricating structures composed of regions of differing dielectric constants. McCall *et al.* [7] were the first to calculate and measure microwave propagation and reflection in a two-dimensional (2-D) array of low-loss high-dielectric-constant cylinders. A dielectric structure that exhibits complete band gap (3-D) for microwaves developed by Yablonovitch [6] by drilling air cylinders in a material of refractive index 3.6 is shown in Figure 1.3.1.

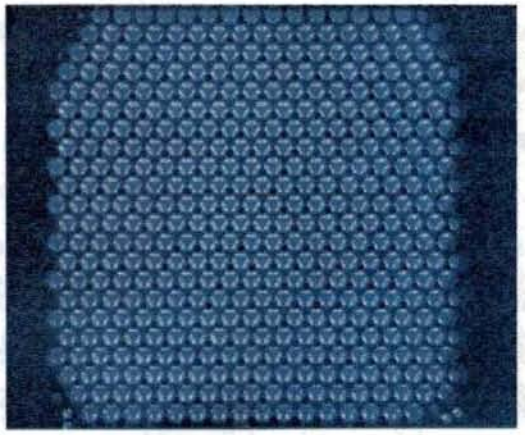

Figure 1.3.1 PBG offering Complete Bandgap for Microwaves

PBG properties in the optical region are scalable to wide range of frequencies. Photonic crystals or Photonic band gap (PBG) materials in general referred as *electromagnetic band-gap (EBG)* materials or *electromagnetic crystals (EC)* are inhomogeneous structures composed of periodic regions of material with a specific permittivity immersed in a homogeneous background of different permittivity. These artificial, composite structures have been found to have unique properties that are advantageous in applications involving semiconductor integrated circuits. The possible applications of these photonic crystals are numerous, including inhibition and enhancement of spontaneous emission [3], fabrication of waveguides from planar slabs [8] and filters [9, 10]. Photonic crystal

finds applications in suppressing harmonics in microstrip patch antenna [11, 12] increases the power output and efficiency of power amplifiers [13], Frequency tuning [14] and also in design of reflectors [15] and microstrip filter superconducting films[16]. Periodic electromagnetic structures are commonplace in many of the items we rely on every day – from the magnetron in a microwave oven to the ultraviolet radiation protection provided by polarized sunglasses.

Although previous research had focused almost exclusively on optical and quasi-optical applications for the PBG materials, it quickly became apparent that numerous applications for similar periodic structures in the microwave and infrared frequency range were being developed. It is the purpose of this work to analyze periodic structures to determine effective and realizable uses for microwave circuits and antennas. The easiest way proposed to implement an Electromagnetic crystal in microwave region consists in etching a periodic pattern of circles on the ground plane [17]. This way, deep and wide stop bands are obtained while employing a technique compatible with monolithic technology. Two-dimensional (2D) periodic patterns were first used, although taking advantage only of the periodicity along the conductor strip direction (effective 1D structure). In fact, due to the high confinement of the fields around the conductor strip, it is possible to use 1D periodic patterns [18] obtaining similar behavior as the 2D structures, while reducing the transversal dimension of the device. Due to the unique feature of wide rejection band in the millimeter wave or microwave range, PBG structures have been widely applied to microwave devices to improve their performances [19, 20]. In Shielded Structures Electromagnetic Bandgap Metal Plates is used for Parallel Plate Mode Suppression [21]. The concept of PBG in microstrip technology is extended to coplanar wave guide (CPW) for band rejection [22, 23, 24] which helps in the application of MMIC applications. Subsequent experimental demonstration in the microwave domain, have led to extensive theoretical and experimental activity, aimed at the optimization of PBG structures for the visible domain and the exploration of their potential applications.

1.4 Some Applications of Photonic Band Gap materials

The absence of any propagating modes in a photonic crystal can suppress spontaneous emission for photons with frequencies within the gap. The ability to confine and control electromagnetic waves in three dimensions would have important implications for quantum optics and quantum-optical devices: the modification of black-body radiation, the localization of light to a fraction of a cubic wavelength, and thus the realization of single-mode light-emitting diodes, are but a few examples. PBG materials can also be used in frequency selective mirrors, band-pass filters and resonators. By introducing controlled line or point defects in the crystals one can observe localization of electromagnetic waves leading to the fabrication of planar waveguides that can bend at sharp angles (even 90°). Some of the applications of PBG are illustrated in detail in the following section.

Periodic thin-film dielectric resonator: Photonic technology, using light instead of electrons as a unit of information, is increasingly replacing electronics in communication and information management systems. Light has several advantages over the electron. It can travel in a dielectric material at much greater speeds than an electron in a metallic wire. Light can also carry a large amount of information per second. The bandwidth of dielectric materials is significantly larger than that of metals. Furthermore, photons are not as strongly interacting as electrons, which help reduce energy losses.

Periodic thin-film dielectric resonator with the presence of *localized* modes with high Q-factors can be manufactured using PBG technology. The bandgap in transverse wave vector (at fixed frequency) created by the grating can also be used to reduce the number of guided modes that would otherwise appear in a layer of the same average refractive index. In this way, multi-mode waveguide can be made in which all but the highest order modes are suppressed, rendering the structure signal-mode.

Photonic Bandgap Dielectric Waveguide Filter. Conventional metallic waveguide filter, although shows very good performance, is difficult to manufacture due to its large size and sensitive to fine-tuning. A structure that keeps almost all significant properties of a conventional metallic rectangular waveguide which is much easier for mass production and is much smaller in size can be achieved using PBG technology. PBG dielectric waveguide filter is a guiding structure which comprises three rows of plated-through-holes at each side of the PBG dielectric waveguide and two plated through- holes are used as the coupling structure between two resonators. These two plated-through-holes can be fabricated using the same process as the PBG array. The input and output coupling structure is formed by two similar plated-through holes. It directly couples the energy from the feeding 50 Ω microstrip lines. The radiation loss caused by wide microstrip width is not a problem for the new filter, because its substrate dielectric constant is relatively high. Tuning is not required for this PBG dielectric waveguide filter because the fabrication tolerance of the PCB process can be controlled relatively well than that of the machined metallic waveguide. Thus a dielectric waveguide filter [49] can be made by a two dimensional PBG structure. Two 50 Ω microstrip lines incorporating with a newly proposed external coupling structure fed the filter. This filter has demonstrated small size, low loss, and easy to manufacture. The PBG waveguide filter is shown in the Figure 1.4.1.

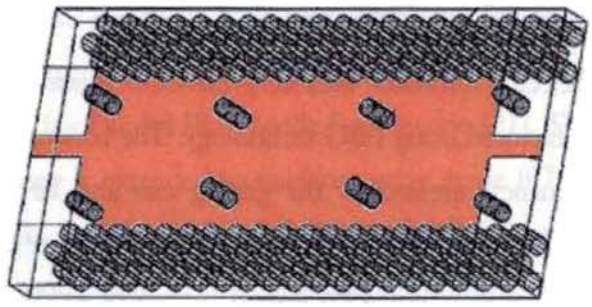

Chi-Yang Chang (2002)

Figure 1.4.1. The Photonic Bandgap Dielectric Waveguide Filter

Parallel Plate Mode Suppression in Shielded Structures: Metal plate structure incorporated with electromagnetic bandgap holes finds use as metal shields with the capability of suppressing the propagation of unwanted parallel plate mode. The holes can be of any shape and the periods of those holes should be selected to half the guided wavelength of the parallel plate mode at a desired center frequency of suppression. At X-band these PBG structures parallel mode suppression practically with an additional attraction of avoiding crosstalk [50]. The parallel plate guide excited with H-plane horn is depicted in Figure 1.4.2.

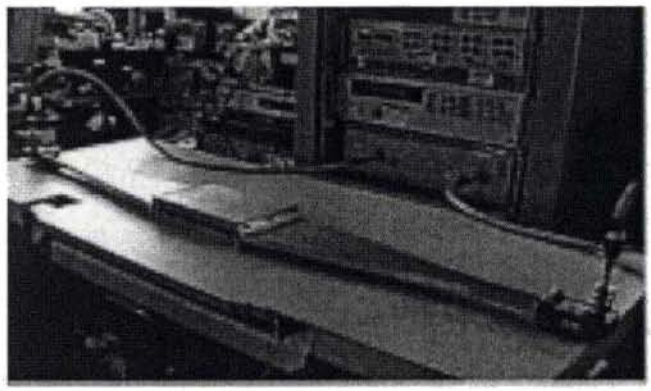

Debasis
Dawn (2002)

Figure 1.4.2 Parallel plate guide excited with H-plane horn

Microstrip Hybrid Ring: PBG cells can be incorporated into the curved microstrip line, where it has no extra insertion loss introduced in the ring hybrid. Compact microstrip 180° ring hybrid incorporating six curved PBG cells embedded in the ring as shown in Figure 1.4.3.

In addition, the slow-wave effect generated by the periodic PBG cells reduces the overall physical size of the ring hybrid. This design is potentially useful for applications in microwave-integrated circuits. The PBG cells do no affect the bandwidth and amplitude of the transmission coefficients when embedded into the microstrip device. Therefore, we can use conventional procedures to design the ring hybrid [51].

Kam Man Shum (2001)

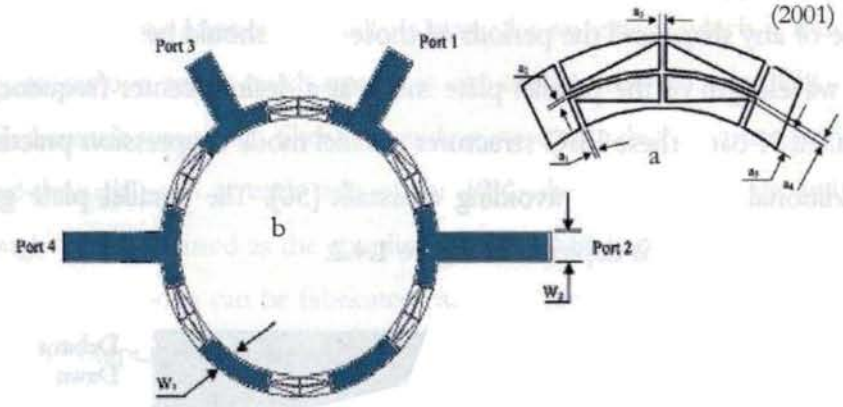

Figure 1.4.3 (a) Curved PBG cell layout, (b) Layout of the ring hybrid with the proposed PBG cells.

Low-Pass Filter: Filtering is one of the most important parts of microwave circuit systems. Filters can be implemented with shunt stubs or stepped-impedance lines in a microstrip circuit, but these techniques require large circuit layout size and provide a narrow band and a spurious pass band in stop band. Photonic bandgap (PBG) structures have been considered as an alternate to solve these problems in microwave circuit applications. Many researchers have proposed and demonstrated several PBG structures for microstrip circuit application with filtering characteristics [11], [13], [17]. A serial connection of several different PBG structures for wide rejection bandwidth requires large size and had a limitation of compactness in microstrip circuit applications. Some of the PBG structures used as filters are demonstrated in Figure 1.4.4 and that offers a wide bandwidth in Figure 1.4.5.

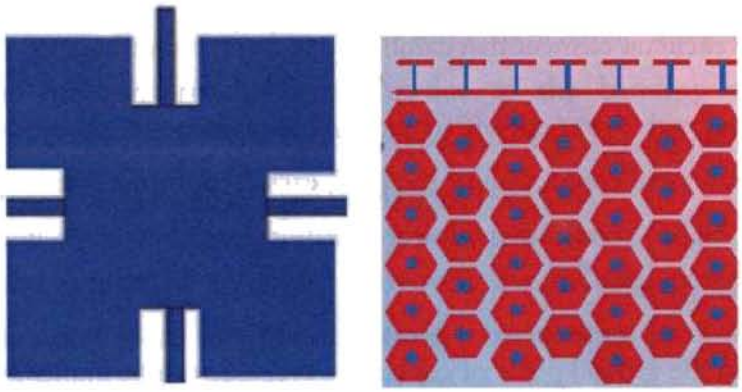

Figure 1.4.4 Two of PBG structures that are used as filter

Wide stop band can also be achieved by two new lattices to build up two PBG structures which have different stop bands [52]. This builds up two different stop bands, and it results in a wide stop band with good performance. Because it is achieved with a parallel connection of two different PBG structures, this structure has the wide stop band characteristic without an increment in size.

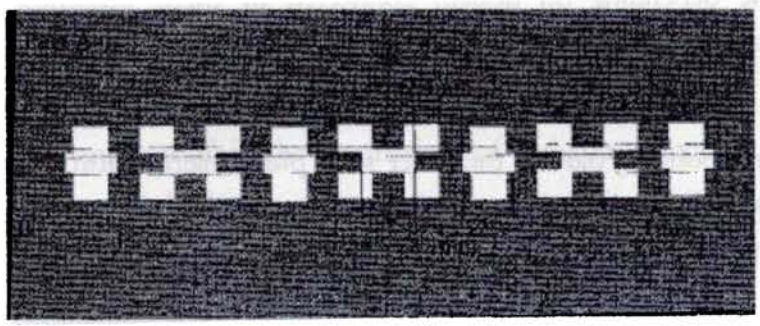

Figure 1.4.5 PBG structures for creating wide stop bands (2000)

The 1-D periodic PBG structure for the finite-width conductor-backed coplanar waveguide (FW-CBCPW) can act as a band stop filter [23]. Unlike the conventional PBG structures for the microstrip line and the coplanar waveguide (CPW), which are typically placed on one of the signal strips and the ground plane, this PBG cell

is etched on both the signal strip and the upper ground plane of FW-CBCPW, resulting in a novel circuit element that exhibits remarkable stop band effect.

The low-pass filter with lower cut-off frequency and wider rejection bandwidth is constructed from a serial connection of the PBG cells. This forms a structure with more flexibility, higher compactness, lower radiation loss, and easier integration with the uni-planar circuits.

PBG structures in the ground plane of coplanar waveguide can be implemented by etching holes in the ground plane with an open connected with the gap between strip line and ground plane [22]. At the resonant frequencies of the periodic structure, there exists a stop band for the transmission of microwave signals. This provides an effective method to suppress higher order harmonics in active circuits.

Mixed-Signal System Applications: PBG structure with alternating impedance PBG (AI-PBG) can be used for isolation in mixed signal systems [53]. PBG structure can be realized with metal patches etched in the ground plane (or in the power plane depending on design) connected by metal branches to form a distributed L-C network (where L is inductance and C is capacitance). In this structure, a metal branch introduces additional inductance while the metal patch and the corresponding part of the other solid plane mainly form the capacitance and is presented in Figure 1.4.6

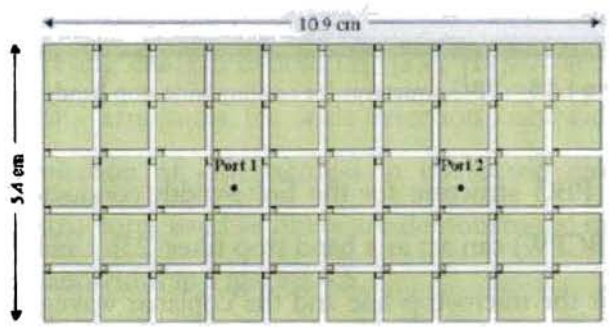

Jinwoo Choi (2004)

Figure 1.4.6 PBG that can be used for Mixed-Signal System Applications

Substrate for Antennas: PBG structures have been integrated with patch antennas for enhanced performance due to the bandgap of surface-wave suppression [12]–[15]. They have also been used as ground planes of spiral and curl antennas to achieve low profile designs [54], [55].

For active integrated antennas, moreover, the radiated power of microstrip antennas needs to be very low at harmonic frequencies. In order to meet these requirements, two one-dimensional (1-D) photonic bandgap (PBG) structures, namely, the defected ground structure (DGS) and the compact microstrip resonant cell (CMRC), can be applied to the feed line of microstrip antennas[11], [15], [20]. The characteristic impedance of the microstrip line is controlled by the additional effective inductance of the PBG structure. Additionally, the second harmonic of the proposed antennas is properly suppressed compared to a conventional antenna. The PBG structures are quite effective for harmonic suppression [22]. Thus these antennas are suitable for active integrated antennas. In addition the PBG structures will lead to a reduction in pattern side lobes resulting in improvements in radiation pattern front-to-back ratio and overall antenna efficiency. Photonic crystals will reduce surface waves and prohibit the formation of substrate modes, which are commonly known inhibitors of patch antenna designs. By reducing or eliminating the effects of these electromagnetic inhibitors with photonic crystals, a broadband response can be obtained from inherently narrowband antennas. The surface-wave suppression effect of the PBG structure and its application to reduce the mutual coupling of microstrip antenna leads to the potential application in arrays. Some of the PBG structures that prove to improve antenna characteristics is shown in Figure 1.4.7.

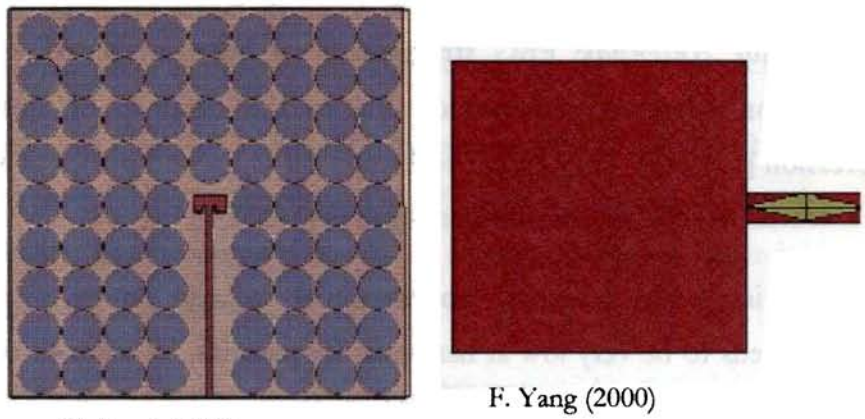

Y. Horri (1999)

F. Yang (2000)

Figure 1.4.7 PBG used for improvement of antenna characteristics

Realization of a uni-planar compact photonic bandgap (UC-PBG) substrate whose applications to planar slow-wave structures and low-leakage conductor-backed coplanar waveguide have been recently presented [22], [23]. Advantageous features of this crystal substrate include simple, low-cost manufacturing (no vias are necessary) and compatibility with standard monolithic microwave integrated circuits (MMIC's) fabrication technology. This UC-PBG substrate is successfully used to reduce surface-wave losses for an aperture-coupled fed patch antenna on a thick high dielectric-constant substrate. UC-PBG substrate is effective in reducing the mutual coupling among the patch elements in a phased array configuration. The array performance with UC-PBG was improved in terms of the active return loss (wider scan angles) and active pattern of the center element (elimination of blind spots), by using only two unit cells between adjacent elements. Moreover the PBG assisted ground plane enhances broadside gain of a patch antenna. A microstrip patch antenna with two-dimensional (2-D) PBG to control harmonic is reported in [56]. Lin proposed a compact PBG to suppress harmonics for CPW-fed loop-slot antenna [57] shown in Figure 1.4.8. Also, the high-order harmonics can be reduced by PBG microstrip circuits.

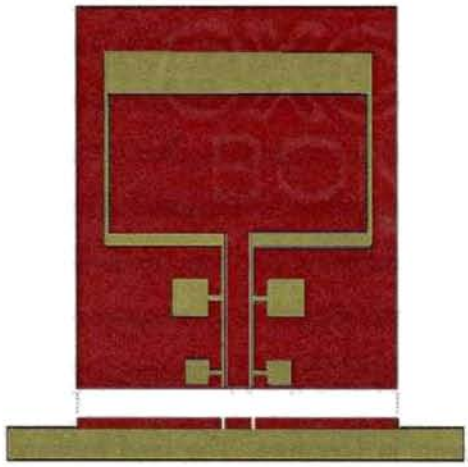

X. Lin (2003)

Figure 1.4.8 PBG to suppress harmonics for CPW-fed loop-slot antenna

Defected Ground Structures: A new type of PBG structure which reduced the size of circuits came to picture in 2000 proposed by Dal Ahn [60]. This new structure called Defected Ground Structure (DGS) can give band gap characteristics in some frequency bands with only one or more unit lattices as shown in Figure 1.4.9.

Dal Ahn (2000)

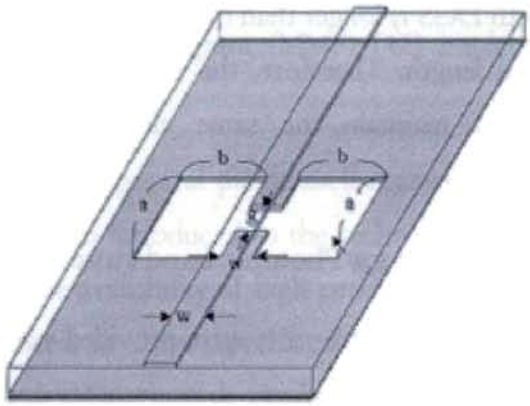

Figure 1.4.9 DGS unit lattice etched in the ground plane of a microstrip line

The equivalent circuit of the defected ground unit structure can be derived by means of three-dimensional field analysis methods. Band pass filters using defected ground structure (DGS) sections simultaneously realize a resonator and an inverter [61, 65, and 66]. So a coupled-line band pass filter with DGS provides compact size with low insertion-loss characteristic. DGS is useful for mounting an active device, and finds application to a microwave oscillator [62]. The DGS circuit is convenient for mounting active and passive devices with out any via holes.

A Novel Frequency Doubler Using Feed forward Technique and Defected Ground Structure [63] is also seen in literature. The feed forward loop in the frequency doubler suppresses the fundamental component and the DGS diminishes the higher order harmonics such as third, fourth, and so on. Due to the combination of feed forward structure and DGS, only the doubled frequency component appears at the output port and the other unwanted components are suppressed excellently. Defected Ground Structure finds application in reducing the size of Amplifiers [64].

The DGS on the ground plane of microstrip line provides additional effective inductive component which enables a microstrip line with very high impedance to be realized and shows a slow-wave characteristics. The resultant electrical length of the microstrip line with DGS is longer than that of the conventional microstrip line for the same physical length. Therefore, the microstrip line with DGS can be shortened in order to maintain the same electrical length, matching, and performances of the basic (original) amplifier.

1.5 A brief review of analysis for Photonic band structures

For many years, electromagnetic theorists were provided with two primary means of predicting electromagnetic phenomena: measurements and analytical solutions. Measurements of electromagnetic systems provide the scientist/engineer with reams of data and a physical intuition for the mechanisms involved in producing

the response. However, the feasibility of fabricating new devices for each design change can be time-consuming and, depending on the architecture or application, expensive. These two limitations are often addressed by using analytical techniques to predict electromagnetic behavior. Solution techniques including asymptotic analysis, Variational analysis, integral transforms, contour integration, and perturbation theory are the staple of analytical electromagnetic prediction and design. Improvements in computer speed and memory helped to provide the framework for the rapid development of computational electromagnetics (CEM) methods including, but not limited to, the finite element method (FEM), the finite difference methods in both time (FDTD) and frequency domains (FDFD), the transmission line matrix (TLM) method, and method of moments (MoM) solutions. CEM techniques have added significantly to the toolboxes of scientists and engineers alike. In fact, the hybridization of many of the aforementioned techniques to solve large and complex problems may provide revolutionary new solution capabilities for the near future.

Other methods that were used for Electromagnetic crystals are the Finite Difference Time Domain (FDTD) [42 - 43], the transfer matrix method [44], the Finite Element Method (FEM) [45], the Boundary Element Method (BEM) [46] and the Multiple Multipole Program (MMP) [47] implemented in the MaX-1 software [48].

With the recent advent of general purpose electromagnetics (EM) codes, a third solution method has been introduced to the technical community, *simulation*. One might conclude that the availability of high performance commercial EM software has mitigated the need to solve specific electromagnetic problems by writing original computer codes. For example, the late availability of commercial codes that incorporate periodic boundary conditions is a prime example of a recent simulation tool that has renewed the interest in developing new circuit and antenna devices.

Certainly, one of the advantages of the general EM solver is its ability to solve a wide variety of problems. The disadvantage of the general EM solver is its inability to address specific theoretical or numerical issues that can significantly affect the accuracy of a solution. This is not to say that general EM solvers are not extremely useful for design and have not revolutionized the way that electromagnetics research is being performed. However, every CEM code writer will attest to the many nuances and small singular changes that must be included in an original numerical code to achieve maximum performance. Complex, real-world problems are not always amenable to general purpose solutions and often require customized solutions and programs to solve them. Computational electromagnetics which includes electromagnetic theory, sophisticated analytical techniques, and numerical methods is used to characterize and analyze the merits and demerits of a new design.

The rapidly growing field of wireless communications is providing new opportunities to develop novel structures that will enhance or even replace existing circuits and antennas. Devices that incorporate periodicity as a key feature of the design are promising unrivaled performance in microwave circuits and antennas. Periodic electromagnetic structures are commonplace in many of the items we rely on every day – from the magnetron in a microwave oven to the ultraviolet radiation protection provided by polarized sunglasses. Commenting on the recent inundation of applications for periodic structures, Maddox [57] remarks, "If only it were possible to make materials [photonic band-gap materials] in which electromagnetic waves cannot propagate at certain frequencies, all kinds of almost-magical things would happen." It is important, nevertheless, to dispel some of the myths about what photonic band-gap (PBG) materials are and are not. PBG are periodic dielectric and/or metallic structures that when designed and implemented correctly can improve the performance of specific devices. PBG are not magical structures that defy basic laws of physics and have only of late appeared in the literature.

Researchers from the diverse fields of classical electromagnetics, solid-state physics, optics, material science, condensed matter physics, and semiconductor physics, are actively contributing to the base of electromagnetic crystal knowledge [27, 29-33]. Active areas of electromagnetic and photonic crystal research include but are not limited to microwave and millimeter-wave antenna structures, quasi-optical microwave arrays, photonic crystal integrated circuits, high- and low-Q electromagnetic resonators, quantum optical electromagnetic cavity effects, and optical nano-cavities. In addition, sonic band-gap materials or artificial acoustic crystal substrates are being developed and could impact sonar. From solid-state theory, we know that semiconductors allow electron conduction without scattering only for electrons that have energies within a specific range of energy, often termed *band-gaps*. Electromagnetic wave propagation in periodic dielectric media is analogous to electron-wave propagation in semiconductor crystals. Although fundamentally different propagation mechanisms are involved, preliminary results suggest that at microwave and millimeter-wave frequencies the propagation characteristics of these crystals can be manipulated by carefully designing and fabricating structures composed of regions of differing dielectric constants. Early work by Yablonovitch [2] successfully demonstrated that light propagation could be inhibited in certain frequency gaps in special photonic band-gap crystals (PBGs). Scalar-wave-based theories were developed to determine a suitable candidate for the first three-dimensional (3-D) photonic crystal. However, it became apparent that scalar-wave-based solutions were inadequate for the task. Vector-wave-based solutions implemented using the plane wave method for Maxwell's equations, being developed concurrently by [34 - 38] and offered the potential of finding a true photonic band-gap structure. Indeed, soon thereafter, a structure that possesses a full photonic band-gap was identified. Theoretical work by Ho *etal.* [5] confirmed the existence and structure of the first (3-D) photonic crystal, the diamond dielectric structure. Concurrently, band structures for two-dimensionally

periodic structures were being calculated in a similar manner by Plihal *et al.* [58]. However, it was McCall *et al.* [7] who were the first to calculate *and* measure microwave propagation and reflection in a two-dimensional (2-D) array of low-loss high-dielectric-constant cylinders. With the confirmation of realizable 2-D and 3-D photonic crystal structures, attention shifted to applying these materials in new designs and architectures.

1.6 Thesis Outline

It is the purpose of this work to analyze periodic structures to determine effective and realizable uses for microwave circuits and antennas.

Chapter 2 deals with the methodology involved in experimental measurements. This chapter also gives a brief introduction to the planar filters and antennas assisted with PBG ground plane. An introduction to the theoretical analysis is presented in this chapter.

In Chapter 3, Maxwell's equations are subjected to periodic boundary conditions and solutions are developed and implemented to determine the band structure (propagating modes) of a periodic, two - dimensional inhomogeneous dielectric region. The geometry and Maxwell's integral equation(s) are discretized and the matrix equation is solved numerically. A nontrivial solution for the fields requires the matrix determinant to be zero, which results in a characteristic equation. The Eigen values (propagation constants) are obtained from the roots of this equation. For a lossless structure, the propagation constants of a guided wave are real numbers. However, in the stop bands, the propagation constants are complex-valued. To validate the solution obtained the solution of the exact Eigen value equation for the two-dimensional periodic problem is also obtained using the plane wave expansion (PWE) method.

In Chapter 4, the band structure (propagating modes) of a periodic, two-dimensional inhomogeneous dielectric region is determined at microwave regime. Photonic Band gap structures are incorporated to the ground plane of planar transmission lines and the reflection and transmission properties are studied in detailed. A new class filter at microwave frequencies is designed, developed and analyzed. Experimental results are authenticated by developing equivalent circuit and by commercially available softwares. To simplify two-dimensional periodic media to a one-dimensional equivalent structure the *synthesized dielectric constant* of the two-dimensional PBG is derived. An extension of PBG as DGS is also studied in detail for microstrip line and coplanar wave guide which provides a wide band gap depending on the lattice dimensions.

A number of researchers have designed electromagnetic crystal structures for use in planar antenna and circuit applications, particularly for use as reflectors in planar dipole antennas. Chapter 5 puts light to the property of PBG structures as substrate for planar antennas. By designing special artificial substrates, surface wave formation may be reduced or even eliminated in some planar antennas. This would dramatically increase both the available bandwidth and gain to levels usually reserved for non-planar antennas. To this end, periodic structures may serve as the material that can change the physical properties of substrates used in fabricating planar circuits and antennas. For planar antennas operating at a frequency in the band-gap of the three-dimensional PBG crystal, energy which would have been radiated into the substrate is reflected.

Chapter 5 concludes the work illustrating the significant results obtained. What future holds for PBG materials is also discussed in this chapter. Finally, the appendix of the thesis deals with a new class of dielectric resonator antenna and various feeding techniques involved to increase its properties.

References

1. J. Clerk Maxwell, "A Dynamical Theory of the Electromagnetic Field," *Philosophical Transactions of the Royal Society of London* **155**, 459–512 (1865). Abstract: *Proceedings of the Royal Society of London* **13**, 531–536 (1864).

2. E. Yablonovitch, "Inhibited Spontaneous Emission in Solid-state Physics and Electronics," Physical Review Letters. **58**, 1110 (1987).

3. K. M. Leung and Y. F. Liu, "Full vector calculation of photonic band structures in face-centered-cubic dielectric media," *Physical Review Letters.* **65**, 2646–2649, (1990).

4. Z. Zhang and S. Satpathy, "Electromagnetic wave propagation in periodic structures: Bloch wave solution of Maxwell's equations," *Physical Review Letters*, **65**, 2650–2653 (1990).

5. K. M. Ho, C. T. Chan, and C. M. Soukoulis, "Existence of a photonic gap in periodic dielectric structures," *Physical Review Letters.* **65**, 3152–3155 (1990).

6. E. Yablonovitch, "Photonic Band-Gap Structures," *Journal of Optical Society of America B.* **10**, 283-295 (1993).

7. S. L. McCall, P. M. Platzman, R. Dalichaouch, D. Smith, and S. Schultz, "Microwave propagation in two-dimensional dielectric lattice," *Physical Review Letters.* **67** 2017–2020(1991).

8. J. G. Maloney, M. P. Kelser, B. L. Shirely and G. S. Smith, "A Simple Description for Wave Guiding in Photonic Bandgap Materials," *Microwave and Optical Technology Letters.* **14**, 261-266 (1997).

9. Q. Xue, K. M. Shum and C. H. Chan, "Novel 1-D Microstrip PBG Cells," *IEEE Microwave and Guided Wave Letters.* **10**, 403-405 (2000).

10. Yang, F. R. et al. "A novel uniplanar compact PBG structure for filter and mixer application". IEEE MTT-S, **47**, 1509–1514 (1999).

11. Y. Horii and M. Tsutsumi, "Harmonic Control by Photonic Bandgap on Microstrip Patch Antenna," *IEEE Microwave and Guided Wave Letters.* **9**, 13-15 (1999).

12. Coccioli, R., et al. "Aperture-coupled patch antenna on UC-PBG substrate". *IEEE Transactions on Microwave Theory and Techniques*, **47**, 2123–2130 (1999).

13. V. Radisic, Y. Qain and T. Itoh, "Broad Band Power Amplifier Using Dielectric Photonic Bandgap Structure," *IEEE Microwave and Guided Wave Letters.* **8**, 13-14 (1998).

14. Laso, M. A. G., et al. "Multiple-frequency-tuned photonic bandgap structure". *IEEE Microwave and Guided Wave Letters*, **10**, 220–222 (2000).

15. H. Nakano, K. Hitosugi, N. Tatsuzawa, D. Togashi, H. Mimaki and J. Yamauchi "Effects on the Radiation Characteristics of Using a Corrugated Reflector with a Helical Antenna and an Electromagnetic Band-Gap Reflector With a Spiral Antenna," *IEEE Transactions on Antennas and Propagation.* **53**, 191-199 (2005).

16. Hui-Fen Huang, Jun-Fa Mao, Xiao-Chun Li, and Zhengfan Li, "Photonic Bandgap Microstrip Filter" *IEEE Transactions on Applied Superconductivity.* **15**, 3827-3830 (2005).

17. V. Radisic, Y. Qian, R. Coccioli, and T. Itoh, "Novel 2-D Photonic Bandgap Structure for Microstrip Lines" *IEEE Microwave Guided Wave Letters.* **8**, 69-71, (1998).

18. Falcone, F., T. Lopetegi and M. Sorolla, *Microwave and Optical Technology Letters.* **22**, 411-413 (1999).

19. I. Ederra, R. Gonzalo, C. Mann, P. de Maagt, "(Sub) mm-wave components and subsystems based on PBG technology", *IEEE Antennas and Propagation Society International Symposium* **2** 1087 - 1090 (2003)

20. Z. W. Du, K. Gong, J. S. Fu, B. X. Gao, and Z. H. Feng "A compact planar inverted-F antenna with a PBG-type ground plane for mobile communications", *IEEE Transactions on Vehicular Technology.* **52** 483- 489 (2003)

21. D Dawn, Y Ohashi,and T Shimura, "A Novel Electromagnetic Bandgap Metal Plate for Parallel Plate Mode Suppression in Shielded Structures" *IEEE Wireless Component Letters.* **12**, 166-168 (2002).

22. Y.Q Fu, G.H. Zhang, and N.C. Yuan "A Novel PBG Coplanar Waveguide" *IEEE Wireless Component Letters.* **11**, 447-448 (2001).

23. S.G. Mao and M.Y. Chen "A Novel Periodic Electromagnetic Band gap Structure for Finite-Width Conductor-Backed Coplanar Waveguides" *IEEE Wireless Component Letters.* 11, 261-263 (2001).

24. F. Martín, F. Falcone, J. Bonache, T. Lopetegi, M. A. G. Laso, and M. Sorolla " New Periodic-Loaded Electromagnetic Band gap Coplanar Waveguide with Complete Spurious Pass band Suppression" *IEEE Wireless Component Letters.* **12**, 435-437 (2002).

25. Brillouin, L., "Wave Propagation in Periodic Structures", 2nd edition (New York : Dover), (1946).

26. Yeh, P., and YARiv, A," Optidal Waves in Layered Media (New York : Wiley), (., 1988)

27. John, S ., *Phys . Rev. Lett .*, **58**, 2486, (1987).

28. Brown, E . R ., Parker, C. D ., and Yablonovitch, E ., *J. opt . Soc . Am. B*, **10**, 404, (1993).

29. Kurizki, G ., *Phys . Rev A*, **42**, 2915, (1998).

30. Adler, C . L ., and Lawandy, N. M., *Phys. Rev. Lett.*, **66**, 2617,(19919).

31. Martorell, J., and Lawandy, N. M ., *Phys . Rev. Lett .*, **65**, 1877 ,(1990).

32. John, S., and Wang, J ., *Phys . Rev. Lett .*, **64**, 2418, (1990) .

33. Dowling, J ., and Bowden, C. M., *Phys . Rev. A*, **46**, 612, (1992)

34. K. Sakoda, "Optical Properties of Photonic Crystals",Springer, Berlin, (2001).

35. J. D. Joannopoulos, R. D. Meade, J. N. Winn, "Molding the Flow of Light", Princeton University Press, (1995).

36. K. M. Ho, C. T. Chan, and, C. M. Soukolis, "Existance of a Photonic Gap in Periodic Dielectric Structures", *Phys. Rev Lett.*, **65**, pp. 3152-3155,(1990).

37. S. G. Johnson, and J. D. Joannopoulos, "Block-iterative frequency-domain methods for Maxwell's equations in a planewave basis", *Opt. Express*, **8**, pp. 173-190, 2001.

38. R. D. Meade, A. M. Rappe, K. D. Brommer, J. D. Joannopoulos, and O. L. Alerhand, "Accurate theoretical analysis of photonic band-gap materials", *Phys. Rev B*, **48**, pp. 8434-8437, (1993).

39. H. S. Söuzüer, J. W. Haus, and R. Inguva, "Photonic bands: Convergence problems with the plane-wave method", *Phys. Rev B*, **45**, pp. 13962- 13972, 1992.

40. D. Hermann, M. Frank, K. Busch and P. Wölfle, "Photonic band structure computations", *Opt. Express*, **8**, pp. 167-172, (2001).

41. K. Ohtaka, T. Ueta, and K. Amemiya, "Calculation of photonic bands using vector cylindrical waves and reflectivity of light for an array of dielectric rods", *Phys. RevB*, **57**, pp. 2550-2568, (1998(.

42. C. T. Chan, Q. L. Yu, and K. M. Ho, "Order-N spectral method for electromagnetic waves", *Phys. RevB*, **51**, pp. 16 635-16 642, (1995(.

43. M. Qui and S. He, "A non-orthogonal finite-difference time-domain method for computing the band structure of a two-dimensional photonic crystal with dielectric and metallic inclusions", *J. Appl. Phys.*, **87**, pp.8268-8275, (2000(.

44. J. B. Pendry and A. MacKinnon, "Calculation of Photon Dispersion Relations", *Phys. Rev Lett.*, **69**, pp. 2772-2775, (1992).

45. W. Axmann and P. Kuchment, "An efficient finite element method for computing spectra of photonic and acoustic band-gap materials", *J. Comput. Phys.*, **150**, pp. 468-481, 1999. 179 *ACES journal*, (2003)

46. P. A. Knipp, and T. L. Reinecke, "Boundary-element calculations of electromagnetic band-structure of photonic crystals", *Physica E*, **2**, pp.920-924, (1998(.

47. Ch. Hafner, "Post-modern Electromagnetics Using Intelligent MaXwell Solvers", John Wiley & Sons, (1999(.

48. Ch. Hafner, "MaX-1: A visual electromagnetics platform", John Wiley & Sons, (1998(.

49. Chi-Yang Chang and Wei-Chen Hsu "Photonic Bandgap Dielectric Waveguide Filter" *IEEE Microwave and Wireless Components Letters*, **12**, 137-139, (2002).

50. Debasis Dawn, Y. Ohashi and T. Shimura "A Novel Electromagnetic Bandgap Metal Plate for Parallel Plate Mode Suppression in Shielded Structures, *IEEE Microwave and Wireless Components Letters*, **12**, 166-168,(2002)

51. Kam Man Shum, Quan Xue, and Chi Hou Chan "A Novel Microstrip Ring Hybrid Incorporating a PBG Cell" *IEEE Microwave and Wireless Components Letters*. **11**, 258-260, (2001).

52. Taesun Kim and Chulhun Seo "A Novel Photonic Bandgap Structure for Low-Pass Filter of Wide Stopband *IEEE Microwave and Wireless Components Letters* **10**, 13-15, (2000).

53. Jinwoo Choi, Vinu Govind, and Madhavan Swaminathan "A Novel Electromagnetic Bandgap (EBG) Structure for Mixed-Signal System Applications"

54. T. H. Liu,W. X. Zhang, M. Zhang, and K. F. Tsang, "Low profile spiral antenna with PBG substrate," *Electron. Lett.*, **36**, , pp. 779–780, (2000)

55. F. Yang and Y. Rahmat-Samii, "A low profile circularly polarized curl antenna over electromagnetic band-gap (EBG) surface," *Microwave Opt. Technol. Lett.*, **31**, pp. 165–168, (2001).

56. Y. Horri and M. Tsutsumi, "Harmonic control by photonic bandgap on microstrip patch antenna," *IEEE Microw. Guided Wave Lett.*, **9**, pp. 13–15, (1999).

57. X. Lin, L. Wang, and J. Sun, "Harmonic suppression by photonic bandgap on CPW-fed loop-slot antenna," *Microw. Opt. Tech. Lett.*, **41**, pp. 154–156, (2004).

58. M. Plihal, A. Shambrook, A. A.Maradadin, and P. Sheng, "Two-dimensional photonic band structures," *Optics Communications*, **80**, pp. 199–204, (1991).

59. Dal Ahn, Jun-Seok Park, Chul-Soo Kim, Juno Kim, Yongxi Qian, and Tatsuo Itoh "A Design of the Low-Pass Filter Using the Novel Microstrip Defected Ground Structure" *IEEE Transactions On Microwave Theory and Techniques*, **49**, 86-93, (2001)

60. Jun-Seok Park, Jun-Sik Yun, and Dal Ahn, "A Design of the Novel Coupled-Line Band pass Filter Using Defected Ground Structure with Wide Stop band Performance" *IEEE Transactions On Microwave Theory and Techniques* , **50** , 2037-2044, (2002).

61. Jun-Seok Park and Myeong-Sub Jung, "A Novel Defected Ground Structure for an Active Device Mounting and Its Application to a Microwave Oscillator" *IEEE Transactions On Microwave Theory and Techniques*,. **14**, 198-200, (2004).

62. Yong-Chae Jeong, and Jong-Sik Lim "A Novel Frequency Doubler Using Feed forward Technique and Defected Ground Structure" *IEEE Transactions On Microwave Theory and Techniques*, **14**, 557- 559, (2004).

63. Jong-Sik Lim, Jun-Seok Park, Young-Taek Lee, Dal Ahn, , and Sangwook Nam, "Application of Defected Ground Structure in Reducing the Size of Amplifiers" *IEEE Transactions On Microwave Theory and Techniques*, **12**, 261-263, (2002).

64. A Abdel-Rahman, A. K. Verma, A. Boutejdar, and A. S. Omar " Compact Stub Type Microstrip Bandpass Filter Using Defected Ground Plane" *IEEE Microwave And Wireless Components Letters*, **14**, 136 -138, (2004).

65. Adel B. Abdel-Rahman, Anand K. Verma, Ahmed Boutejdar, and A. S. Omar, "Control of Bandstop Response of Hi–Lo Microstrip Low-Pass Filter Using Slot in Ground Plane" *IEEE Transactions On Microwave Theory and Techniques*, **52**, 2004, 1008-1013, (2004).

2

MAXWELL'S EQUATIONS AND PHOTONIC BAND GAP

Contents

This chapter deals with the fundamental understanding of the electromagnetic waves in a periodic medium. The Band Gap origin in Photonic crystal is explained with the help of Maxwell's equation and Bloch-Floquet's theorem. Band Gap is computed by treating Maxwell's equations as Eigen value problem. Band Gap in a one dimensional system is discussed and computed in detail.

2.1 Propagation of Waves in a Periodic Medium

A fundamental understanding of how electromagnetic fields behave in a periodic medium is provided in this section. The origin of the band gap in Electromagnetic crystals is derived from the properties of Maxwell's equations [1] and the Bloch-Floquet's theorem [2]. Maxwell equations are treated as Hermitian Eigen value problem and are solved for the band gap. All macroscopic electromagnetism, including wave propagation in Electromagnetic crystals is governed by Maxwell's equations represented as:

$$\nabla x \vec{E} = -\frac{\partial \vec{B}}{\partial t} \qquad 2.1$$

$$\nabla x \vec{H} = J + \frac{\partial \vec{D}}{\partial t} \qquad 2.2$$

$$\nabla \cdot \varepsilon \vec{E} = \rho \qquad 2.3$$

$$\nabla . \vec{H} = 0 \qquad 2.4$$

E and **H** are the electric and magnetic field intensity respectively, the electric current density **J** and electric charge density ρ are the sources of the electromagnetic fields. Now, consider a mixed dielectric with composite regions of

homogeneous dielectric material with no free charges or currents. $\therefore \ \rho = J = 0$. Combining equations (2.1) and (2.2)

$$\nabla x \frac{1}{\varepsilon} \nabla x \vec{H} = \frac{\partial^2 \vec{H}}{\partial t^2} \qquad 2.5$$

This equation can be compared to Schrödinger's equation from quantum mechanics.

$$\left(\frac{p^2}{2m} + V(r) \right) \Psi_E(r) = E \, \Psi_E(r) \qquad 2.6$$

Equation (2.5) has a Hermitian (self-adjoint) "Hamiltonian" *operator* $\nabla x \frac{1}{\varepsilon} \nabla x$ on the left hand side and a time derivative $\frac{\partial^2}{\partial t^2}$ on the right. Instead of the periodic potential V in the Schrödinger's equation here we have periodicity in dielectric constant $\frac{1}{\varepsilon}$. Now, like in quantum mechanics, we look for time-harmonic states whose time dependence is $e^{-i\omega t}$ for some (angular) frequency ω, then all possible solutions can be expressed using this form, since the equation is linear, $\therefore$ equation (2.5) $\Rightarrow$

$$\nabla x \frac{1}{\varepsilon} \nabla x \vec{H} = \left(\frac{\omega}{c} \right)^2 \vec{H} \qquad 2.7$$

Identifying the differential operator $\Theta = \nabla x \frac{1}{\varepsilon} \nabla x$ we have the master equation (2.6) as

$$\Theta \vec{H} = \left(\frac{\omega}{c} \right)^2 \vec{H} \qquad 2.8$$

This is the Hermitian Eigen value problem over the infinite domain and generally produces a continuous spectrum of Eigen frequencies. One important property of Maxwell's equations in general and of equation (2.5) in particular is that they are

scale-independent. Because of this scale invariance, it is convenient to use dimensionless units for distance and time: we pick some natural length scale d in the system (usually the periodicity), and then express all distances as a multiple of d and all angular frequencies ω as a multiple of $\frac{2\pi}{d}$.

The solution of wave equation in periodic media is usually derived using a form of Bloch-Floquet's theorem. The Bloch-Floquet's theorem [1] tells us that, for a Hermitian Eigen problem whose operators are *periodic* functions of position, the solutions can always be chosen of the form $e^{ik.x}$, a periodic function. A number of similarities can be seen in the solution of electron wave propagation in semiconductors and electromagnetic wave propagation in periodic dielectric media, and Bloch's theorem can be extended to electromagnetic wave propagation in periodic media. So the solution of equation (2.5) for a periodic ε can be chosen of the form:

$$\bar{H} = e^{i(k.x - \omega t)} \bar{H}_k \qquad 2.9$$

H_k (Electric field can also be used) is a periodic function of position. Substituting equation (2.8) into equation (2.5) we find that the function H_k satisfies the reduced Hermitian Eigen value problem:

$$(\nabla + ik) \times \frac{1}{\varepsilon} (\nabla + ik) \times \bar{H}_k = \omega^2 \bar{H}_k \qquad 2.10$$

As $\bar{H}_k$ is periodic, Eigen problem over a finite domain is only needed to be considered – over the unit cell of periodicity. There is a general theorem that Eigen problems with a finite domain have a *discrete* set of Eigen values. Thus, the Eigen frequencies ω are a countable sequence of continuous functions $\omega_n(k)$ (for n = 1,2,3,...) . When they are plotted as a function of the wave vector k, these

frequency "bands" form the *band structure* of the photonic crystal as shown in Figure 2.1.1.

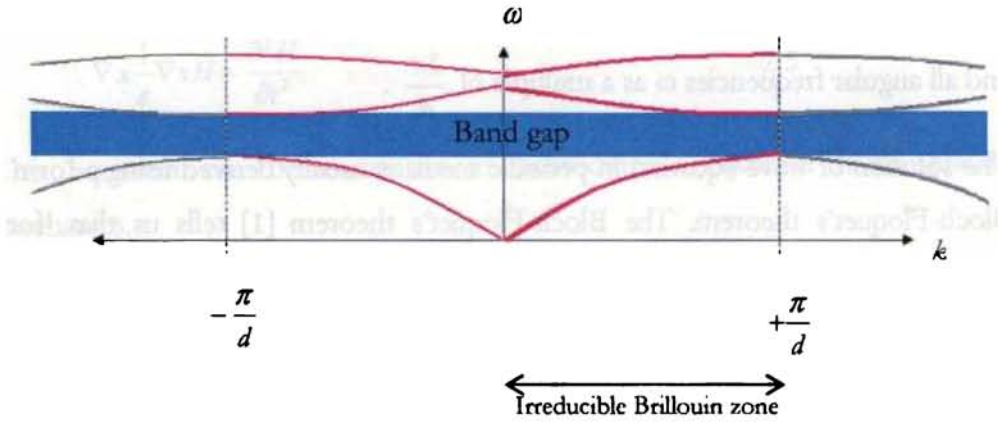

Figure 2.1.1. The Band Structure

Consider a 1-D structure with period d, $(\varepsilon(x+d)=\varepsilon(x))$ and consider the Eigen states for the wave vector $k+\frac{2\pi}{d}$. The function $e^{i\frac{2\pi x}{d}}$ is periodic (with period d) so this part of equation (2.8) can be absorbed into the function H_k. The resulting expression then solves the Eigen problem for a wave vector k, and those solutions are unique, we can therefore conclude that the Eigen solutions at $k+\frac{2\pi}{d}$ are the same as those at k. Because k is only unique to within multiples of $\frac{2\pi}{d}$, then, it is sufficient to *only* solve the Eigen problem for in a finite range, $-\frac{\pi}{d}$ *to* $\frac{\pi}{d}$ called the *first Brillouin zone* [2]. Applying time-reversal symmetry, $-k$ to k produces same results as $k = 0$ *to* $\frac{\pi}{d}$ thus reducing the range of wave vectors. This symmetry-reduced region is called the *irreducible Brillouin zone*, and in three dimensions is given by well-known polyhedra [2] shown in Figure 2.1.2 (whose vertices have canonical,

obscure labels like Γ,X, M, *etc.*). If the crystal has *translational symmetry* ($d \rightarrow 0$) the irreducible Brillouin zone extends to k = ∞ , and is called a *dispersion relation.*

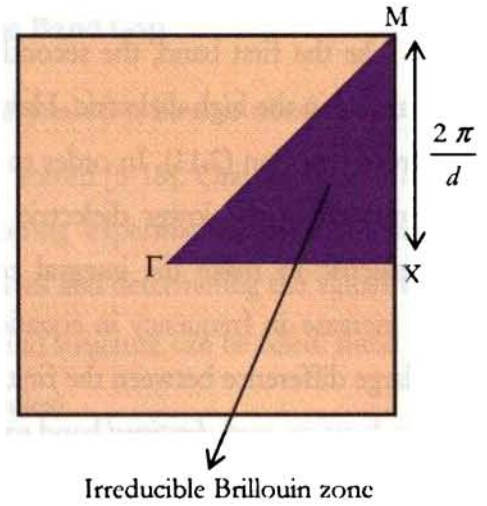

Figure 2.1.2 Symmetry-reduced region – The irreducible Brillouin zone

2.2 The Origin of the Photonic band gap

In a Hermitian Eigen value problem all the Eigen functions must be orthogonal leading the inner products (integral over a unit cell) to zero so [3], for any two Eigen states (m ≠ n) at a given k point we have:

$$\int \vec{H}_k^{(m)} \cdot \vec{H}_k^{(n)} = 0 \qquad 2.11$$

Lowest band solves a *Variational problem*:

$$\omega_1(k)^2 = \min_{H_k} \frac{\int \left|(\nabla + ik) \times \vec{H}_k\right|^2 / \varepsilon}{\int \left|\vec{H}_k\right|^2} c^2 \qquad 2.12$$

In order to minimize the Variational problem of equation (2.11), the field for the lowest band should try to satisfy two conditions. First, its curl should not be too big - that is, it should vary slowly, and not contain any fast oscillations. This is

analogous, in quantum mechanics, to having a low kinetic energy. Second, the curl - the electric field - should be concentrated in regions of *high* dielectric constant; this is analogous to having a low potential energy. In order to see the gap, we naturally must look at the *second* band. Like the first band, the second band also wants to oscillate slowly and be concentrated in the high dielectric. However, it must also be orthogonal to the first band from equation (2.11). In order to accomplish this, the second band must be concentrated in the lower dielectric and/or have a sign oscillation inside the high dielectric to make the integral zero - both of these possibilities will incur a large increase in frequency in equation (2.12), so a band gap. There will generally be a large difference between the first and second bands, a "gap" at each point. In order to have an *omni-directional* band gap, however, the gaps at *all* points must overlap in some frequency range. For this reason, a fairly large contrast in between the high and low dielectric regions is usually necessary to make the gaps in different directions large enough to intersect. The situation is even worse than that, however, because the fields have a direction as well as a sign and a magnitude. In order to be orthogonal to the first band according to equation (2.11), the second band need only be perpendicular to the first, without sacrificing its concentration in the high dielectric. To combat this phenomenon, we need to make use of the boundary conditions on the fields, from Maxwell's equations that apply at dielectric interfaces. In particular, the surface- tangential component of the curl of H is allowed to be discontinuous across a dielectric boundary, while the surface-normal component must be continuous. Now, suppose that our high dielectric consists of thin veins surrounded by lower dielectric. In that case, the numerator of equation (2.12) can be "weighted" *discontinuously* in these veins for electric fields running parallel to them, but *not* for electric fields perpendicular to the veins. This allows us to discriminate between bands with fields in different directions, and makes a complete band gap possible despite the variety of field polarizations. When these conditions are satisfied, the periodic crystal will have a complete photonic

band gap in three dimensions. How band gap is computed is explained in detail in the next section.

2.3 Computing the Band Gap

Given a photonic crystal $\varepsilon(r)$, how to obtain the band structure functions $\omega_n(k)$ is the problem to be solved [6-18]. One alternative is to manufacture a large crystal and perform scattering experiments. By irradiating the crystal with a beam of electromagnetic waves and determining the values of Δk that are allowed at a given frequency ω the band structure can be filled. Band structure can be calculated from *ab initio* (first principles).

Consider a cubic crystal of an isotropic medium represented by the cubic lattice in R^3. The crystal is assumed to be ideal with the lattice R that fills the whole space. It is clear that the group of symmetry of this crystal $S_3(R)$ contains, in particular, the following orthogonal transformations:

$$\alpha_1 = \begin{pmatrix} 0 & 1 & 0 \\ -1 & 0 & 0 \\ 0 & 0 & 1 \end{pmatrix} \qquad \alpha_2 = \begin{pmatrix} 0 & 0 & 1 \\ 0 & 1 & 0 \\ -1 & 0 & 0 \end{pmatrix} \qquad \alpha_3 = \begin{pmatrix} 1 & 0 & 0 \\ 0 & 0 & 1 \\ 0 & -1 & 0 \end{pmatrix}$$

i.e. α_1 is the rotation on $\frac{\pi}{2}$ about the z-axis, α_2 is the rotation on $\frac{\pi}{2}$ about the y-axis and α_3 is the rotation on $\frac{\pi}{2}$ about the x-axis. Since these three rotations preserve the lattice R, the dielectric constant tensor $\{\varepsilon_k^i\}$ is invariant under those symmetry operations. Writing it in analytical form, we denote $\{\varepsilon_k^i\}$ as the matrix A; then $A_i' = \alpha_i A \alpha_i^{-1} = A$ for any $i = 1, 2, 3$. Computing the matrix A_i' we have

$$A_1' = \begin{pmatrix} \varepsilon_2^2 & -\varepsilon_1^2 & \varepsilon_3^2 \\ -\varepsilon_2^1 & \varepsilon_1^1 & -\varepsilon_2^1 \\ \varepsilon_2^3 & -\varepsilon_1^3 & \varepsilon_3^3 \end{pmatrix} = \begin{pmatrix} \varepsilon_1^1 & \varepsilon_2^1 & \varepsilon_3^1 \\ \varepsilon_1^2 & \varepsilon_2^2 & \varepsilon_3^2 \\ \varepsilon_1^3 & \varepsilon_2^3 & \varepsilon_3^3 \end{pmatrix} = A .$$

It follows that $\varepsilon_1^1 = \varepsilon_2^2$ and computing in the same manner $A_2^{'}$ *and* $A_3^{'}$ leads to $\varepsilon_1^1 = \varepsilon_2^2 = \varepsilon_3^3$. The group $S_3(R)$ contains three more transformations:

$$\beta_1 = \begin{pmatrix} -1 & 0 & 0 \\ 0 & -1 & 0 \\ 0 & 0 & 1 \end{pmatrix} \qquad \beta_2 = \begin{pmatrix} -1 & 0 & 0 \\ 0 & 1 & 0 \\ 0 & 0 & -1 \end{pmatrix} \qquad \beta_3 = \begin{pmatrix} 1 & 0 & 0 \\ 0 & -1 & 0 \\ 0 & 0 & -1 \end{pmatrix}$$

$\beta_1 = \alpha_1^2$ is the rotation on π about the z-axis, $\beta_2 = \alpha_2^2$ is the rotation on π about the y-axis and $\beta_3 = \alpha_3^2$ is the rotation on π about the x-axis. Again the lattice is transformed into itself, which gives us $\varepsilon_3^1 = \varepsilon_3^2 = \varepsilon_1^3 = \varepsilon_2^3 = 0$, or in general $\varepsilon_j^i = 0$ *for* $i \neq j$. Thus finally $A = \{\varepsilon_k^s\} = \varepsilon \begin{pmatrix} 1 & 0 & 0 \\ 0 & 1 & 0 \\ 0 & 0 & 1 \end{pmatrix}$ i.e. $\varepsilon_k^s = \varepsilon\, \delta_k^s$ where ε is a scalar.

We have shown the following: the permittivity of the cubic crystal is isotropic (does not depend on the direction as for isotropic materials). This result is not necessarily physically obvious since one might expect that for instance permittivity in the direction of the crystal edge would differ from that in the diagonal direction.

Adding the empirical material equations to the Maxwell system we obtain for a nonmagnetic medium as

$$\nabla^2 E - \frac{n^2}{c^2}\frac{\partial^2 E}{\partial t^2} = \nabla(\nabla . E) \qquad 2.13$$

$$\nabla . (n^2 E) = 0 \qquad 2.14$$

$n = n(x) = \sqrt{\mu\varepsilon}$, the periodic refractive index. According to Floquet's-Bloch theory the linear Maxwell equations (2.14) with periodic n(x) can be reduced to a spectral problem for the vector function with ω as the Eigen value and $\psi(x)$ the Eigen vector.

$$E(x,t) = \psi(x) e^{-i\omega t} \qquad 2.15$$

When $n_0(x)$ is a periodic function in x, y, z with periods x_0, y_0, z_0, respectively, the Eigen vector $\psi(x)$ has the form of a Bloch wave

$$\psi(x) = \psi(x) e^{i(k_x x = k_y y = k_z z)} \qquad 2.16$$

$\psi(x)$ is periodic in x, y, and z with periods x_0, y_0, and z_0, and $\omega = \omega(k_x, k_y, k_z)$. No band gaps exist in the linear spectrum for low-contrast photonic crystals. As a result, a bounded Bloch functions $\psi(x)$ will exist for any value of $\omega \in R$. Highly contrast photonic crystals may however exhibit band gaps for some configurations of the linear refractive index $n^2(x)$.

2.4 Bragg resonance and the Brillouin construction

When the optical material is homogeneous, such that $n(x) = n_0$ is constant, the linear spectrum of the Maxwell equations (2.13) is defined by the free transverse waves,

$$E(x,t) = e_k \; e^{i(k.x - \omega t)} \qquad 2.17$$

where e_k is the polarization vector, $k = (k_x, k_y, k_z)$ is the wave vector, and $\omega = \omega(k)$ is the wave frequency. It follows from the system (2.13) that

$$k.e_k = 0 \qquad 2.18$$

$$\omega^2 = \frac{c^2}{n_0^2}\left(k_x^2 + k_y^2 + k_z^2\right) \qquad 2.19$$

When the optical material is periodic, such that $n(x + x_0) = n(x_0)$, the linear spectrum of the Maxwell equations (2.13) is defined by the Bloch waves:

$$E(x,t) = \psi(x)\, e^{i(k.x - \omega t)} \qquad 2.20$$

$\psi(x + x_0) = \psi(x)$ is the periodic envelope. The geometric configuration of the photonic crystal is defined by the fundamental (linearly independent) lattice vectors

$x_{1,2,3}$ and fundamental reciprocal lattice vectors $k_{1,2,3}$, such that $x_j = 2\pi\delta_{i,j}$ where $1 \le i, j \le 3$. Therefore, the basis $k_{1,2,3}$ is dual to the basis $x_{1,2,3}$ and the linear refractive index n(x) can be expanded into triple Fourier series:

$$n(x) = n_0 \sum_G \alpha_G e^{iGx} \qquad 2.21$$

G is the vector in dual basis $G = nk_1 + mk_2 + lk_3$, (n, m, l) $\in Z^3$ and the factor n_0 is included for convenience. If n_0 is the mean value of $n(x)$, then $\alpha_{0,0,0} = 1$. Let the wave vector k in the incident Bloch wave (2.20) be fixed $k = k_{in}$. The incident wave vector k_{in} is expanded in terms of the lattice vectors: $k_{in} = \frac{1}{2}(pk_1 + qk_2 + rk_3)$ where $(p, q, r) \in R^3$.

The Bloch wave (2.20) is represented by triple Fourier series for $\psi(x)$ such that $E(x, t)$ consists of an infinite superposition of free transverse waves with the wave vectors $k' = k_{out}^{(n,m,l)}$.

$$k' = k + G \qquad 2.22$$

As the scattering of light is considered to be elastic, we introduce the following energy and momentum constraint on the resonating waves.

For $\Delta k = G$, k = G, the resonance condition is

$$2k.G + G^2 = 0 \qquad 2.23$$

This is the central result in the theory of elastic scattering in a periodic lattice. The identical result occurs in the theory of the electron energy band structure of crystals. Notice that if G is a reciprocal lattice vector, −G is also one; thus we can equally well write (2.23) as

$$2k.G = G^2 \qquad 2.24$$

The Brillouin zone gives a vivid geometrical interpretation of the resonance condition $2k.G = G^2$ or

$$k \cdot \left(\frac{1}{2}G\right) = \frac{1}{2}G^2 \qquad 2.25$$

We construct a plane normal to the vector G at the midpoint; any vector k from the origin to the plane will satisfy the resonance condition. The plane thus described forms a part of the zone boundary. An incident wave on the crystal will be diffracted if it's wave vector has the magnitude and direction required by (2.25), and the diffracted wave will be in the direction of the vector k − G. The set of planes that are the perpendicular bisectors of the reciprocal lattice vectors are of particular importance in the theory of the wave propagation in crystals, because a wave whose wave vector drawn from the origin terminates on any of these planes will satisfy the condition for diffraction. These planes divide the Fourier space of the crystal into bits and pieces. The central square is a primitive cell of the reciprocal lattice. It is called the first Brillouin zone. The first Brillouin zone of the cubic lattice in two dimensions The Brillouin construction exhibits all the incident wave vectors which can be Bragg-reflected by the crystal.

The number of waves resonant to the incident k_{in} is less then the number of nodes of the reciprocal lattice G lying inside the sphere of the radius $2|kin|$ centered at the origin. To prove this, consider a simple cubic crystal, where the fundamental lattice vectors and reciprocal lattice vectors are all orthogonal. The coordinate axes (x, y, z) are oriented along the axes of the simple cubic crystal. The set of resonant Bloch waves is given by the set of triples:

$$S = \{(n, ml) \in Z^3 : n(n+p) + m(m+q) + l(l+r) = 0)\} \qquad 2.26$$

The set S always has a zero solution: $(n, m, l) = (0, 0, 0)$. When (p, q, r) $\in Z^3$ and $|p| + |q| + |r| \neq 0$, the set S has at least one non-zero solution: $(n, m, l) = (-p, -q, -r)$.

2.5 Classification of resonances

The classification of resonances can be based on algebraic equation (2.26). When (p, q, r) $\in Z^3$, resonant triples (n, m, l) can be all classified analytically. However, when $(p, q, r) \notin Z^3$, additional resonant triples may also exist. Here we review particular resonant sets S for integer and non-integer values of (p, q, r).We introduce spherical angles (θ,φ) such that the incident wave vector k_{in} is

$$k_{in}=k(\sin\theta\cos\varphi, \sin\theta\sin\varphi,\cos\theta), k\in R, 0\le\theta\le\pi, 0\le\varphi\le 2\pi \qquad 2.27$$

When $\theta=0$, the wave vector k_{in} is perpendicular to the (x, y) crystal plane. Then

$$p=\frac{2k}{k_0}\sin\theta\cos\varphi \quad q=\frac{2k}{k_0}\sin\theta\sin\varphi \quad p=\frac{2k}{k_0}\cos\theta \qquad 2.28$$

2.5.1 One-dimensional resonances of counter-propagating waves

The one-dimensional Bragg resonance occurs when the incident wave is coupled with the counter-propagating reflected wave, such that the set S has at least one non-zero solution: $(n, m, l) = (0, 0, -r)$, where $r \in Z_+$. The values of p and q are not defined for the Bragg resonance, when $n = m = 0$. As a result, the spherical angles θ and φ in the parameterization (2.27) are arbitrary, while the wave number k satisfies the Bragg resonance condition:

$$rk_0=2k\cos\theta \qquad 2.29$$

$$\Rightarrow r\lambda=2d\cos\theta \qquad 2.30$$

The one-dimensional Bragg resonance is generalized in three dimensions for $p = q = 0$ and $r \in Z_+$, when the geometric configuration for the Bragg resonance (2.29) is fixed at the specific value $\theta=0$ and

$$k_{in}=\frac{\pi}{d}(0,0,r) \qquad k_{out}^{(0,0,-r)}=\frac{\pi}{d}(0,0,-r) \qquad 2.31$$

The incident wave is directed to the z-axis of the cubic lattice crystal and the wavelength is $\lambda = 2d/r$. The family of Bragg resonances with $p = q = 0$ and r ∈ Z_+, may include not only the two counter-propagating waves (2.31) but also other Bloch waves in three-dimensional photonic crystals. The dimension of S depends on the total number of all possible integer solutions for (n, m, l).

2.5.2 Two-dimensional resonances of counter-propagating waves

Two-dimensional Bragg resonances occur when the incident wave vector k_{in} is resonant to the counter-propagating reflected wave vector $k_{out}^{(-p,-q,0)}$, as well as to two other diffracted wave vectors $k_{out}^{(0,-q,0)}$ and $k_{out}^{(-p,0,0)}$, where $(p,q) \in Z_+^2$. The value of r is not defined for the two-dimensional resonance, such that the angle θ in the parameterization (2.27) is arbitrary, while k and φ satisfy the resonance conditions:

$$\varphi = \arctan(\frac{q}{p}) \qquad \sqrt{p^2+q^2}\, k_0 = 2k\sin\theta \qquad 2.32$$

The two-dimensional Bragg resonances are generalized in three dimensions for $(p,q) \in Z_+^2$ and $r = 0$, when the geometric configuration for the Bragg resonance (2.32) is fixed at the specific value $\theta = \frac{\pi}{2}$ and

$$k_{in} = \frac{\pi}{d}(p,q,0), \qquad k_{out}^{(-p,-q,0)} = \frac{\pi}{d}(-p,-q,0) \qquad 2.33\ (a)$$

$$k_{out}^{(0,-q,0)} = \frac{\pi}{d}(p,-q,0) \qquad k_{out}^{(-p,0,0)} = \frac{\pi}{d}(-p,q,0) \qquad 2.33\ (b)$$

The incident wave k_{in} is directed along the diagonal of the (px, qy)-cell of the cubic lattice crystal and the wavelength is $\lambda = 2d/\sqrt{p^2+q^2}$. The families of Bragg

resonances with $(p,q)\in Z_+^2$ and $r = 0$ may include not only the four resonant waves (2.33) but also other Bloch waves in three-dimensional photonic crystals.

The dispersion surface $\omega = \omega(k)$ for the Bloch waves (2.20) in the periodic electromagnetic crystal is defined by the profile of the refractive index $n(x)$. We shall consider the asymptotic approximation of the dispersion surface $\omega = \omega(k)$ in the limit when the electromagnetic crystal is low-contrast, such that the refractive index n(x) is given by

$$n(x) = n_0 + \varepsilon\, n_1(x) \qquad 2.34$$

n_0 is a constant and ε is small parameter. The Bloch waves are smooth functions of ε such that the asymptotic solution of the Maxwell equations as $\varepsilon \to 0$ takes the form of the perturbation series expansions:

$$E(x,t) = E_0(x,t) + \varepsilon E_1(x,t) + O(\varepsilon^2) \qquad 2.35$$

The leading-order term $E_0(x, t)$ consists of free transverse waves with wave vectors $k_{out}^{(n,m,l)}$ given by (2.17), such that the asymptotic form (2.35) represents the Bloch wave (2.20) as $\varepsilon \neq 0$. Coupled-mode equations are derived by separating resonant free waves from non-resonant free waves in the Bloch wave (2.20), where the resonant set S with $N = \dim(S) < \infty$ is defined by (2.26). Let $E_0(x, t)$ be a linear superposition of N resonant waves with wave vectors k_j at the same frequency ω:

$$E_0(x,t) = \sum_{j=1}^{N} A_j(X,T)\, e_{k_j}\, e^{i(k_j x - \omega t)}, \quad X = \frac{\varepsilon x}{k}, \quad T = \frac{\varepsilon t}{\omega} \qquad 2.36$$

$A_j(X,T)$ is the envelope amplitude of the j^{th} resonant wave (2.17) and (X,T) are slow variables. The slow variables represent a deformation of the dispersion surface $\omega = \omega(k)$ for free waves (2.18) due to the low-contrast periodic photonic crystal. The degeneracy in the polarization vector is neglected by the assumption that the

incident wave is linearly polarized with the polarization vector $e_m = ek_{in}$. The triple Fourier series (2.21) for the cubic-lattice crystal is simplified as follows with $\alpha_{0,0,0} = 0$:

$$n_1(x) = n_0 \sum_{(n,m,l)\in Z^3} \alpha_{n,m,l}\, e^{ik_{in}(nx+my+lz)} \qquad 2.37$$

The Fourier coefficients $\alpha_{n,m,l}$ satisfy the constraints $\alpha_{n,m,l} = \bar{\alpha}_{-n,-m,-l}$ due to the reality of $n_1(x)$, $\alpha_{n,m,l} = \alpha_{m,n,l} = \alpha_{n,l,m} = \alpha_{l,n,m}$ due to the crystal isotropy in the directions of x,y,z - axes, and $\alpha_{-n,m,l} = \alpha_{n,m,l}$, $\alpha_{n,-m,l} = \alpha_{n,m,l}$ and $\alpha_{n,m,-l} = \alpha_{n,m,l}$ due to the crystal symmetry with respect to the origin (0, 0, 0) (the latter property can be achieved by a simple shift of (x, y, z)). It follows that all coefficients $\alpha_{n,m,l}$ for $(n,m,l)\in Z^3$ are real-valued.

It follows from (2.13), (2.34), and (2.35) that the first-order correction term $E_1(x, t)$ solves the non-homogeneous linear problem:

$$\nabla^2 E_1 - \frac{n_0^2}{c^2}\frac{\partial^2 E_1}{\partial t^2} = 2\frac{n_0^2}{c^2}\omega\frac{\partial^2 E_0}{\partial T\,\partial t} - 2k(\nabla.\nabla_x)E_0 + \frac{2n_0 n_1(x)}{c^2}\frac{\partial^2 E_0}{\partial t^2} + \frac{2}{n_0}\nabla(\nabla n_1 . E_0) = 0 \qquad 2.38$$

where $\nabla x = (\partial x, \partial y, \partial z)$ and the second equation (2.13) has been used. The right hand side of the non-homogeneous equation (2.38) has resonant terms, which are parallel to the free-wave resonant solutions of the homogeneous problem. The resonant terms lead to the secular growth of $E_1(x, t)$ in t, unless they are identically zero. The latter conditions define the coupled-mode equations for amplitudes $A_j(X,T)$, j = 1,2, ... N in the general form:

$$2ik^2\left(\frac{\partial A_j}{\partial T} + \left(\frac{k_j}{k}.\nabla x\right)A_j\right) + \sum_{k\neq j} a_{j,k}A_k = 0 \qquad 2.39$$

2.5.3 Coupled-mode equations for one-dimensional resonance

The lowest-order Bragg resonance for two counter-propagating waves occurs for $r = 1$, when

$$k_1 = \frac{\pi}{d}(0,0,1), \qquad k_2 = \frac{\pi}{d}(0,0,-1) \qquad 2.40$$

Let $A_1 = A_+(Z,T)$ and $A_2 = A_-(Z,T)$ be the amplitudes of the right (forward) and left (backward) propagating waves, respectively. The envelope amplitudes are not modulated across the (X, Y)-plane, since the coupled-mode equations for A± are essentially one-dimensional. The polarization vectors are chosen in the x-direction, such that $e_{k_1} = e_{k_2} = (1, 0, 0)$ and $E_0 = (E_{0,x}(z,Z, T)e^{-i\omega t}, 0, 0)$. The non-homogeneous equation (2.38) at the x-component of the solution E_1 at $e^{-i\omega t}$ takes the form:

$$\nabla^2 E_{1,x} - k^2 E_{1,x} = -2ik^2 \frac{\partial^2 E_{0,x}}{\partial T} - 2k \frac{\partial^2}{\partial Z \partial z} E_{0,x} - \frac{2k^2 n_1(x)}{n_0} E_{0,x} + \frac{2}{n_0} \frac{\partial^2 n_1(x)}{\partial x^2} E_{0,x}$$

By removing the resonant terms at $e^{\pm ikz}$, the coupled-mode equations for amplitudes $A_\pm(Z, T)$ take the form:

$$i\left(\frac{\partial A_+}{\partial T} + \frac{\partial A_+}{\partial Z}\right) + \alpha A_- = 0 \qquad 2.41$$

$$i\left(\frac{\partial A_-}{\partial T} - \frac{\partial A_-}{\partial Z}\right) + \alpha A_+ = 0 \qquad 2.42$$

The coupled-mode equations (2.41)–(2.42) can be defined on the interval $0 \le Z \le L_z$ for $T \ge 0$, where the end points at $Z = 0$ and $Z = L_z$ are the left and right (x, y)-planes, which cut a slice of the photonic crystal.

The stationary transmission problem follows from the separation of variables in the coupled-mode equations (2.39):

$$A_j(X,T) = d_j(X)\, e^{-\Omega T} \qquad 2.43$$

j = 1, ...,N, and Ω is the detuning frequency. After separation of variables (2.43), the linear coupled-mode equations (2.41) – (2.48) reduce to the following ODE system:

$$i\frac{\partial d_+}{\partial Z} + \Omega d_+ + \alpha d_- = 0 \qquad 2.44$$

$$-i\frac{\partial d_-}{\partial Z} + \Omega d_- + \alpha d_+ = 0 \qquad 2.45$$

The problem (2.44) – (2.45) is defined on the interval $0 \le Z \le L_z$. When the incident wave is illuminated to the photonic crystal from the left, the linear system (2.44) – (2.45) is completed by the boundary conditions:

$$d_+(0) = \alpha_+ \ \text{and}\ d_-(L_z) = 0 \qquad 2.46$$

where α_+ is the given amplitude of the incident wave at the left (x, y)-plane of the crystal. The general solution of the ODE system (2.44) – (2.45) is given explicitly as follows:

$$\begin{pmatrix} d_+ \\ d_- \end{pmatrix} = c_+ \begin{pmatrix} \alpha \\ \Omega + ik \end{pmatrix} e^{kZ} + c_- \begin{pmatrix} \alpha \\ \Omega - ik \end{pmatrix} e^{-kZ} \qquad 2.47$$

where $c_\pm \in C$ are arbitrary and $k \in C$ is the root of the determinant equation:

$$k = \sqrt{\alpha^2 + \Omega^2} \qquad 2.48$$

When $k = iK, K \in R$, the linear dispersion relation $\Omega = \Omega(K)$ follows from the quadratic equation:

$$\Omega^2 = \alpha^2 + K^2 \qquad 2.49$$

The two branches of the dispersion relation (2.49) correspond to the two counter propagating resonant waves. Their resonance leads to the photonic stop band, which is located in the interval: $|\Omega| < |\alpha|$. Let $\Omega = 0$ for simplicity, i.e. the detuning

frequency is fixed in the middle of the stop band. The unique solution of the boundary-value problem (2.44) – (2.46) follows from the general solution (2.47):

$$\begin{pmatrix} d_+ \\ d_- \end{pmatrix} = \frac{\alpha_+}{\cosh \alpha L_z} \begin{pmatrix} \cosh \alpha (L_z - Z) \\ -i \sinh \alpha (L_z - Z) \end{pmatrix} \qquad 2.50$$

The transmittance T and reflectance R are defined from the other boundary values of the solution (2.50) such that the balance identity T + R = 1 is satisfied.

$$T = \left| \frac{d_+(L_z)}{d_+(0)} \right|^2 = \frac{1}{\cosh^2 \alpha L_z}$$

$$R = \left| \frac{d_-(0)}{d_+(0)} \right|^2 = \frac{\sinh^2 \alpha L_z}{\cosh^2 \alpha L_z}$$

Thus getting the transmission or reflection from a photonic crystal can give the band gap.

2.6 Band Gap of the One Dimensional System

Consider electromagnetic wave propagation in one-dimensional system which consists of alternating layers of two dielectric materials. For the determination of photonic band gap, we are focusing only those materials, which show the band gap for all polarization and direction of propagation. In this section we have derived the analytical solution for photonic band gap by using assumptions those are given by John and Wang [4,5] that the photon always encounters precisely the same periodic index inside the Photonic band gap material for any of the polarization or propagation direction.

For studying the properties of electromagnetic waves in one dimension system, a alternating layered structure of dielectric material which having the refractive indexes $n_1 \left(\sqrt{\varepsilon_1}\right)$, $n_2 \left(\sqrt{\varepsilon_2}\right)$ with width a and b respectively is chosen. The variation

in refractive index is considered periodically along the x-axis normal to layers. The refractive index profile is described from the geometry of considered structure as shown in Figure 2.6.1. Origin is at the center of one of the layer of length b. Here, we have defined three regions whose widths are a, b and a respectively.

From the figure it can see that the refractive index of first region lies between $\frac{-b}{2} < x < \frac{a+b}{2}$ and for second region lies between $\frac{-b}{2} < x < \frac{b}{2}$ regions. As the third region is the repetition of first region so we can express with $n(x+md) = n(x)$ n where d is the period of the lattice which is defined as $d = a + b$ and $m = 0, \pm 1, \pm 2, \pm 3$.

Now, for the propagation of electromagnetic waves in one-dimensional system Maxwell's equation (2.13) are reduce to in a simple form

$$\frac{d^2 E(x)}{dx^2} + \frac{n^2(x)\omega^2}{c^2} E(x) = 0 \qquad 2.51$$

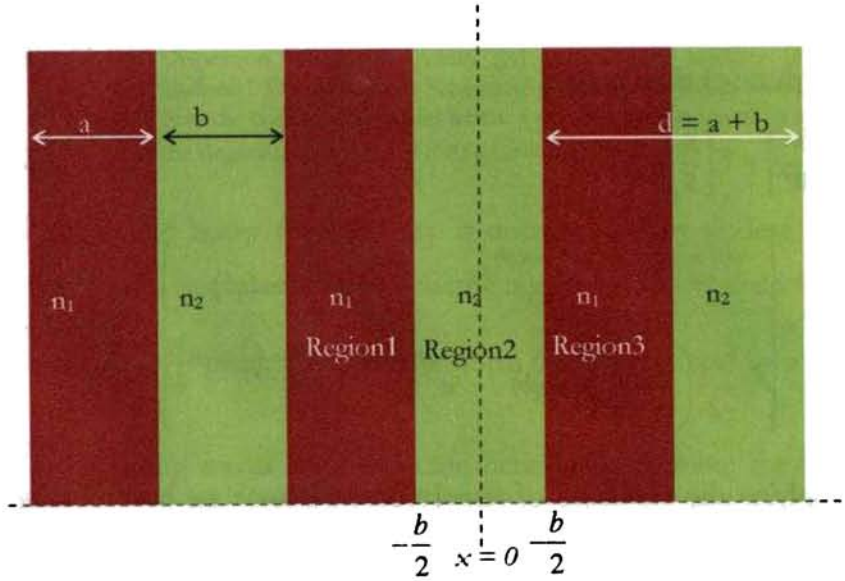

Figure 2.6.1 One Dimensional PBG structure

$n(x)$ represents the refractive index of various regions shown in the figure. The solution of equation (2.51) in three regions as can be written as:

In region 1 $E_1(x) = R\,e^{ipx} + S\,e^{-ipx}$ 2.52

In region 2 $E_2(x) = T\,e^{iqx} + U\,e^{-iqx}$ 2.53

In region 3 $E_3(x) = V\,e^{ipx} + W\,e^{-ipx}$ 2.54

Where p and q are unit less parameters which is defined as $p = \frac{n_1 \omega}{c}$ and $q = \frac{n_2 \omega}{c}$.

Since refractive index is varying periodically, it will not change by translation by a lattice constant. This condition leads that a bounded solution must exit that satisfy:

$$E(x+d) = e^{ikd}\,E(x) \qquad 2.55$$

Applying boundary condition that the tangential component of E and B and there derivative must be continuous at the boundary of dielectric interface in equation (2.55) the unknown coefficients R, S, V and W can be solved. These equations can be realized in matrix form, which relates the traveling wave coefficient of first region to those of third region

$$\begin{bmatrix} V \\ W \end{bmatrix} = T \begin{bmatrix} R \\ S \end{bmatrix} \qquad 2.56$$

Where $T = \begin{bmatrix} e^{-iqb\left(\cos(qb) + \frac{i}{2}\left(\frac{p}{q} + \frac{q}{p}\right)\sin(qb)\right)} & \frac{i}{2}\left(\frac{q}{p} - \frac{p}{q}\right)\sin(qb) \\ \frac{-i}{2}\left(\frac{q}{p} - \frac{p}{q}\right)\sin(qb) & e^{ipb\left(\cos(qb) - \frac{i}{2}\left(\frac{p}{q} + \frac{q}{p}\right)\sin(qb)\right)} \end{bmatrix}$ 2.57

Now, applying the condition of translation invariance we have obtained another matrix equation for same unknown coefficient. The solution of such equations can be obtained if and only if the determinant of coefficient matrix should be zero. So after solving these matrix equations we have got an analytical solution for dispersion relation of the form [6]:

$$k(\omega)=\frac{1}{d}\cos^{-1}\left[\begin{array}{l}\cos\left(\frac{n_1\omega a}{c}\right)\cos\left(\frac{n_2\omega b}{c}\right)-\frac{1}{2}\left(\frac{n_1}{n_2}+\frac{n_2}{n_1}\right)\\ \times\ \sin\left(\frac{n_1\omega a}{c}\right)\sin\left(\frac{n_2\omega b}{c}\right)\end{array}\right] \quad 2.58$$

Plot of $k(\omega)$ gives us the desired band diagram for a specified frequency range for a periodic structure as in Figure 2.6.2 is given below.

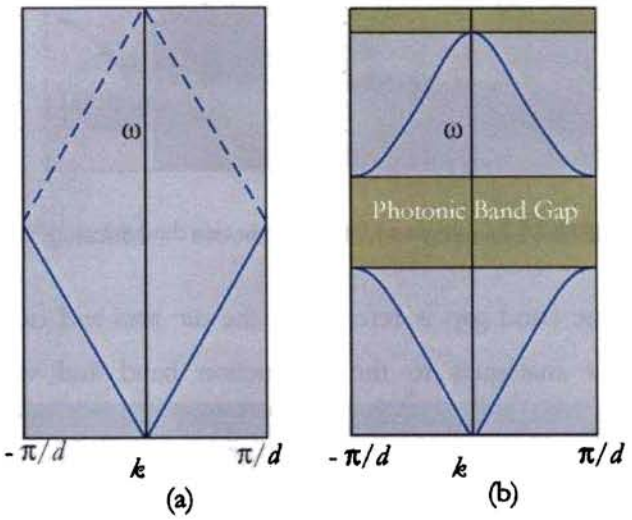

Figure 2.6.2. (a) Dispersion relation frequency (ω) versus wave number (k), of a uniform1-D medium **(b)** Schematic effect on the bands of a physical periodic dielectric variation where a gap has been opened by splitting the degeneracy at the $k = \pm\pi/d$ Brillouin-zone

The bands above and below the band gap is distinguished by finding where the power of their modes lies – in the high dielectric region or the low dielectric region. The degenerate $k=\pm\frac{\pi}{d}$ plane waves of a uniform medium are split into $\cos\left(\frac{\pi x}{d}\right)$ and $\sin\left(\frac{\pi x}{d}\right)$ standing waves by a dielectric periodicity, forming the lower and upper edges of the band gap, respectively - the former has electric - field peaks in the high dielectric (ε , high) and so will lie at a lower frequency than the latter (which peaks in the low dielectric). A schematic origin of the band gap in one dimension is illustrated in Figure 2.6.3.

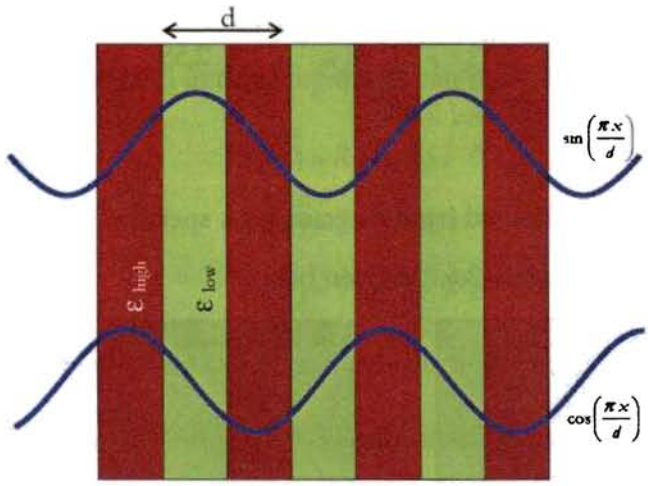

Figure 2.6.3. Origin of Band Gap in one dimension

Band above a photonic band gap is referred as the *air band* and one below as the *dielectric band* which is analogues to the conduction band and valence band in semiconductors. In one dimension a gap occurs between every set of bands, at either the Brillouin zone's edge or centre. The band structure is as plotted in Figure 2.6.4.

For any dielectric constant band gap appears in one dimension. The smaller the dielectric contrast, the smaller the gaps, but the gap is formed as soon as $\frac{\varepsilon_1}{\varepsilon_2} \neq 1$.

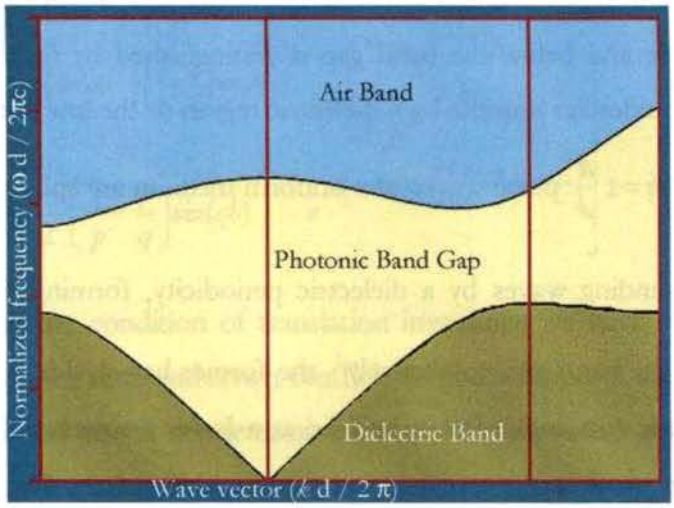

Figure 2.6.4. Band Structure in one dimension

When air columns are drilled in a substrate a same periodic variation of dielectric constant is observed. For different period d and radius of air column the band gap formed for a periodic structure as in Figure 2.6.5 is depicted in the following plots.

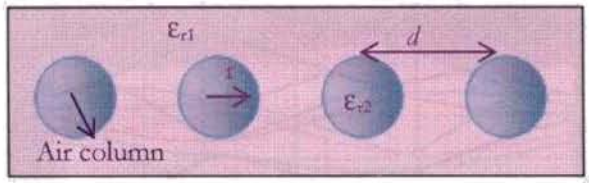

Figure 2.6.5 Periodically drilled air column in a substrate

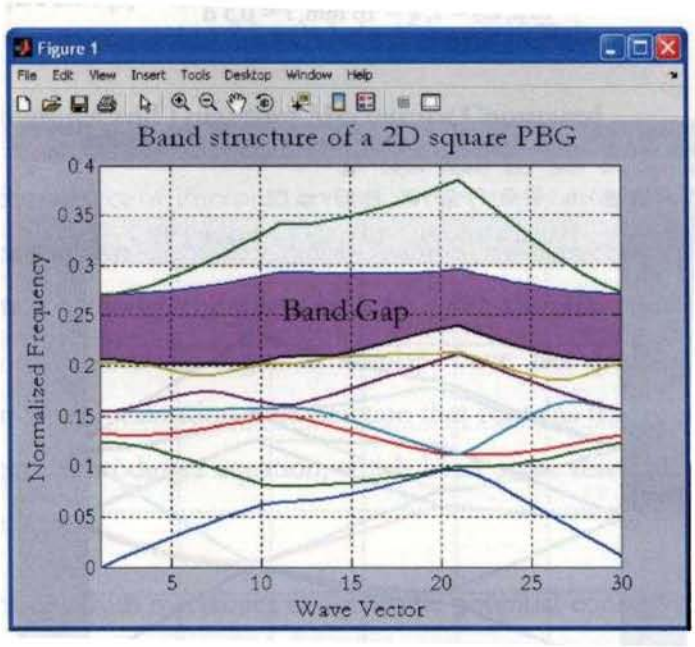

Figure 2.6.6 **(a)** Band Diagram of periodically loaded air cylinders $\varepsilon_{r1} = 10.2$, $\varepsilon_{r2} = 1$, $d = 10$ mm, $r = 0.25$ d

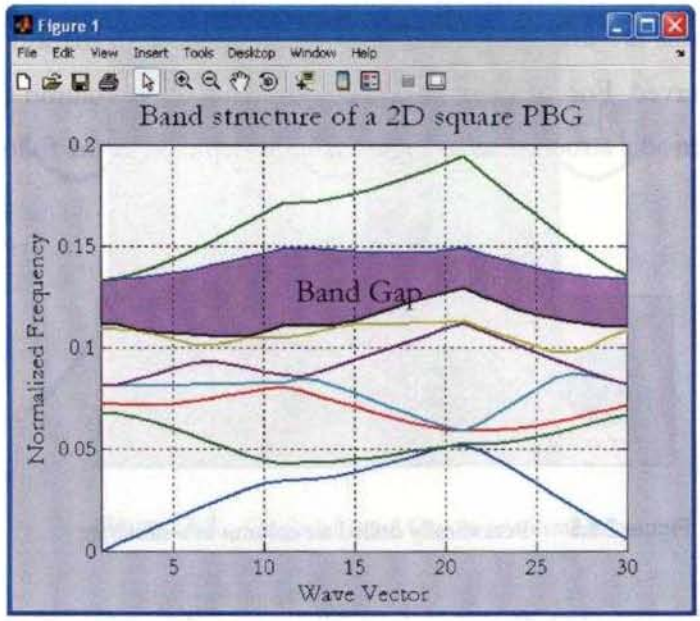

Figure 2.6.6 **(b)** Band Diagram of periodically loaded air cylinders ε_{r1} = 10.2, ε_{r2} = 1, d = 10 mm, r = 0.5 d

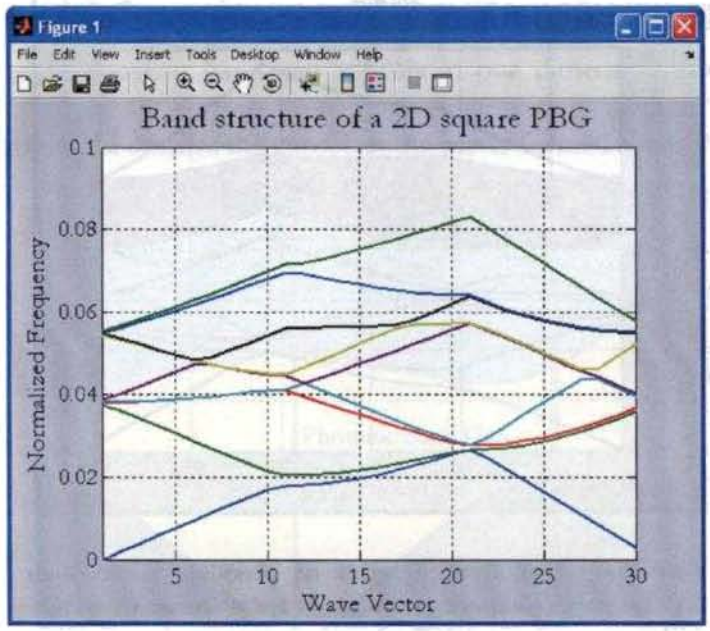

Figure 2.6.6 **(c)** Band Diagram of periodically loaded air cylinders ε_{r1} = 10.2, ε_{r2} = 1, d = 10 mm, r = d

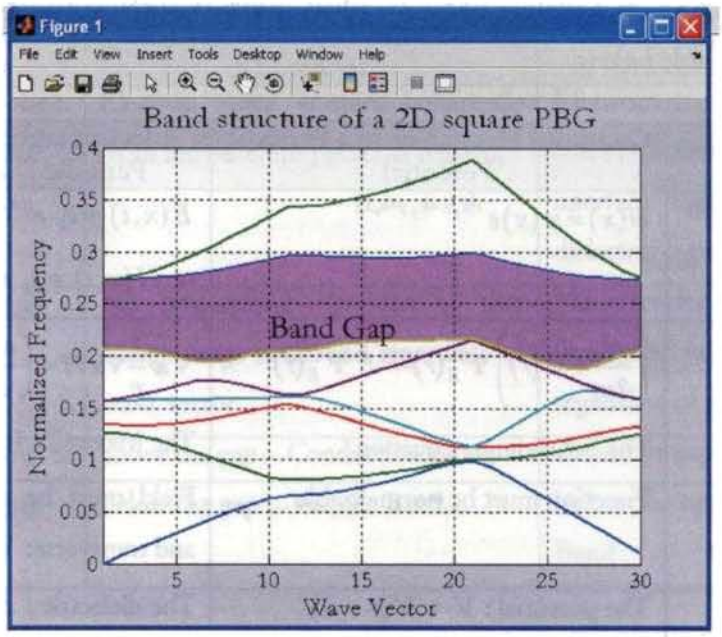

Figure 2.6.6 (d) Band Diagram of periodically loaded air cylinders $\varepsilon_{r1} = 9.8$, $\varepsilon_{r2} = 1$, $d = 10$ mm, $r = 0.25$ d

2.7 Electrodynamics and Quantum Mechanics Compared

The heart of the subject of Photonic crystals is the propagation of electromagnetic waves in the periodic medium. In a sense Quantum mechanics is also the study of wave propagation, although the waves are a bit more abstract. At the atomic scale, particles (like the electron) begin to display wave like properties, including interference and non-localization. The function that contains the information about the particle obeys Schrödinger equation, which bears some resemblance to familiar wave equation.

So the study of quantum mechanics in a periodic potential contains direct parallels to the study of electromagnetism in periodic dielectrics. Sine the quantum mechanics of periodic potentials is the basic theory of solid-state physics, the field of photonic crystals can also inherit some of these theorems and terminology of

solid-state physics, in a slightly modified form. Some of these correspondences are listed in the Table below.

	Quantum Mechanics in a Periodic Potential	Electromagnetism in a Periodic Dielectric
Master function	$\psi(x) = \psi(x) e^{i(k_x x = k_y y = k_z z)}$	$E(x,t) = e_k \; e^{i(k.x-\omega t)}$ or $H(x,t) = e_k \; e^{i(k.x-\omega t)}$
Master Equation	$\left(\frac{p^2}{2m} + V(r)\right) \Psi_E(r) = E \, \Psi_E(r)$ The Schrödinger equation	$\nabla x \frac{1}{\varepsilon} \nabla x H = \left(\frac{\omega}{c}\right)^2 H$ The Maxwell's Equation
Conditions on main function	Function must be normalizable	Field must be normalizable and transverse: $\nabla . H = 0$
Periodicity	The potential : $V = V(r+R)$	The dielectric : $\varepsilon = \varepsilon(r+R)$
Interaction between the normal modes	Electron – electron repulsive interaction	No strong interaction of light modes
Normal Modes	Eigen states with different energies are orthogonal; they have real Eigen values and can be found using Variational principle.	Modes with different frequencies are orthogonal; they have real Eigen values and can be found using Variational principle.
Physical Energy of the System	Eigen value E of the Hamiltonian	The Electromagnetic energy
Allowed values of wave vector k	Lies in the Brillouin Zone	Lies in the Brillouin Zone
Heuristic that goes along with Variational theorem	Wave function concentrates in the regions of low potential, while remaining orthogonal to lower states	Fields concentrates their energy in high dielectric constant regions, while remaining orthogonal to lower modes

	Quantum Mechanics in a Periodic Potential	Electromagnetism in a Periodic Dielectric
Physical origin of band Gap	Electron wave scatters coherently from the different potential regions	Electromagnetic fields scatter coherently at the interface between different dielectric regions
Inside the gap	No propagating electrons in that energy range is allowed regardless of wave vector	No extended modes in the frequency range is allowed regardless of wave vector
Bands below & above the gap	above the gap – Conduction Band below the gap – Valence Band	above the gap – Air Band below the gap – Dielectric Band

References

1. J. Clerk Maxwell, "A Dynamical Theory of the Electromagnetic Field," *Philosophical Transactions of the Royal Society of London* **155**, 459–512 (1865). Abstract: *Proceedings of the Royal Society of London* **13**, 531–536 (1864).

2. N. W. Ashcroft and N. D. Mermin, "Solid State Physics" (Holt Saunders, Philadelphia, (1976).

3. J. Singh, "Quantum Mechanics: Fundamentals and Applications to Technology:, John Wiley & Sons, Inc., New York, NY (1997).

4. L. Brillouin, "Wave Propagation in Periodic Structures", McGraw-Hill, New York, NY, 1946.

5. J. D. Joannopoulos, R. D. Meade, and J. N. Winn, "Photonic Crystals: Molding the Flow of Light", Princeton, (1995).

6. S.John and W. Wang, *Phys. Rev B*, **43**, 12772-12789 (1991).

7. Jonathan P. Dowling and Charles M. Bowden, J. of Modern Optics, **41**, 345-351(1994)

8. John, W. *Phys. Rev Lett.*, **63**, 2169 (1984)

9. M. S. P. Eastham "The Spectral Theory of Periodic Differential Equations". Scottish Acad. Press, Edinburgh, London, (1973).

10. P.Kuchment "Floquet Theory for Partial Differential Operators" Birkhauser, Basel.

11. M. Reed and B. Simon "Methods of Modern Mathematical Physics", **4**: Analysis of Operators. Academic Press, New York, (1978).

12. A. Figotin and P. Kuchment "Band-gap structure of the spectrum of periodic and acoustic media. II. Two-dimensional photonic crystals." SIAM J. Appl. Math. **56**, 1561–1620, (1994).

13. P. Kuchment "The mathematics of photonic crystals, Mathematical Modeling in Optical Sciences" SIAM, Philadelphia, (1999).

14. W. Strauss "Partial Differential Equations: an Introduction", Wiley & Sons, New York, (1992).

15. A. Arraf and C.M. de Sterke "Coupled-mode equations for quadratically nonlinear deep gratings", Phys. Rev. E **58**, 7951–7958 (1998).

16. *Electromagnetics*, **41**, Special issue on theory and applications of photonic band-gap structures (1999).

17. C. H. Chan, "Analysis of frequency selective surfaces in Frequency Selective Surface and Grid Array", T. K. Wu, editor, chapter 2, pp. 27–85, John Wiley & Sons, Inc., New York, NY, (1985).

18. D. N. Chigrin, A. V. Lavrinenko, D. A. Yarotsky, and S. V. Gaponenko, "Observation of total omni-directional reflection from a one-dimensional dielectric lattice," *Applied Physics A*, **68**, pp. 25—28, (1999).

3

INTRODUCTION TO PLANAR FILTERS AND ANTENNAS, METHODOLOGY– EXPERIMENT & THEORETICAL ANALYSIS

Contents

A brief introduction to the soul of the thesis is presented in this chapter. Impact of Photonic Band Gap (PBG) on the transmission, reflection and radiation characteristics of planar filters and antennas is discussed. The methodology adopted for experimental and theoretical analysis of planar filters and antennas on PBG substrates at microwave regime is also illustrated. Analysis is carried out using Finite Difference Time – Domain Method (FDTD).

A microwave filter is two –port network used to control the frequency response at a certain point in a microwave system providing transmission at frequencies with in the pass band region of interest and attenuation in the stop band of the filter. In any analog circuits sometimes high-frequency signals has to be manipulated in such a way as to enhance or attenuate certain frequency ranges or bands and so filters come into use. There are generally four types of filters: *low-pass, high-pass, band-pass* and *band-stop.* The low-pass filter allows low-frequency signals to be transmitted from the input to the output port with little attenuation. However, as the frequency exceeds a certain *cut-off* point, the attenuation increases significantly with the result of delivering reduced amplitude signal to the output port. The opposite behavior is true for a high pass filter, where the low frequency signal components are highly attenuated or reduced in amplitude, while beyond a cut-off frequency point the signal passes the filter with little attenuation. Band-pass and band-stop filters restrict the pass band between specific lower and upper frequency points where the attenuation is either low (band-pass) or high (band-stop) compared to the remaining frequency bands. At microwave frequencies filters can be realized using microstrip technology because the microstrip has the advantage of small size, light weight, low cost and ease of fabrication. Various kinds of filters can be

realized by using microstrip type structures [1]. In this thesis attempts are provided only on planar structures because of the reasons given above.

3.1 Microstrip Lines

A typical microstrip transmission line is illustrated in Figure 3.1.1. Microstrip transmission lines are open planar waveguides where classical engineering designs are based upon the quasi-TEM propagation model. It consists of a single conducting strip of width W placed on a low loss dielectric substrate of thickness h and located on a ground plane.

The important parameters for designing these transmission lines are the characteristic impedance (Z_0), effective dielectric constant (ε_{re}), attenuation constant (α), discontinuity reactance, frequency dispersion, surface wave excitation, and radiation. Several methods to determine these parameters are summarized in [3–7]. The characteristic impedance is given as:

$$Zo = \frac{\eta}{2\pi\sqrt{\varepsilon_{re}}} \ln\left(\frac{8h}{W} + 0.25\frac{W}{h}\right) \quad for \frac{W}{h} \le 1 \qquad 3.1(a)$$

$$Zo = \frac{\eta}{\sqrt{\varepsilon_{re}}}\left(\frac{W}{h} + 1.393 + 0.667\ln\frac{W}{h} + 1.444\right)^{-1} \quad for \frac{W}{h} \ge 1 \qquad 3.1(b)$$

$$\eta = 120\pi \ and \ \varepsilon_{re} = \frac{\varepsilon_r + 1}{2} + \frac{\varepsilon_r - 1}{2} F\left(W/h\right) \qquad 3.1\ (c)$$

$$F\left(W/h\right) = \left(1 + 12\, h/W\right)^{-1/2} + 0.041\left(1 - W/h\right)^2 \ for \frac{W}{h} \le 1 \qquad 3.1\ (d)$$

$$F\left(W/h\right) = \left(1 + 12\, h/W\right)^{-1/2} \ for \frac{W}{h} \ge 1 \qquad 3.1(e)$$

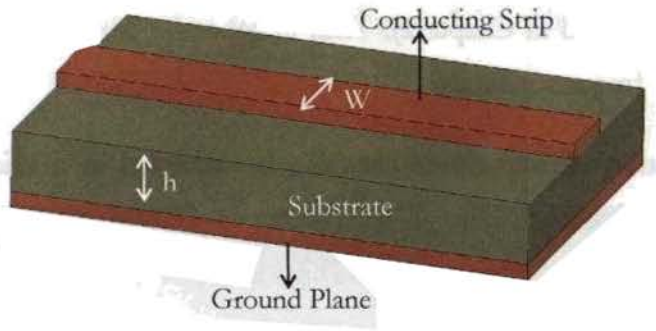

Figure 3.1.1 Microstrip line

A microstrip line can act as a filter when loaded with stubs, coupled lines or by stepping the impedance [2]. Figure3.1.2 depicts different kinds of microstrip filters.

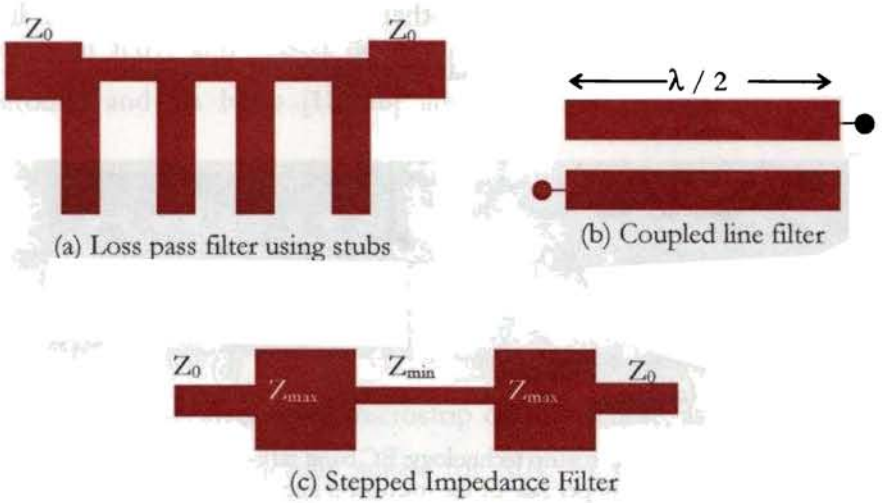

Figure 3.1.2 Different types of Microstrip Filters

Consider the case of a Stepped Impedance filter, the periodic variation of impedance through the microstrip line leads to the filtering action. Periodic structures generally exhibit pass band and stop band characteristics in various

bands of wave length determined by the nature of the structure. The presence or absence of propagating wave can be determined by inspection of the k-β or ω-β diagram (as explained in Chapter2). Thus in general a periodic structure acts as a filter to certain frequency bands.

Periodic variation of impedance can also be achieved in a microstrip line by incorporating Photonic Band Gap Structures [3]. Microstrip PBG can be considered as a wide stop-band filter. This idea could be extended to the ground plane of the microstrip line allowing a periodic fluctuation in impedance and thus restricting some frequencies in the pass band. The proposed ways to produce band gap in microstrip technology are to drill a periodic pattern of cylinders in the dielectric [4] or to etch circles in the ground plane of the microstrip substrate following a periodic pattern [5] as in Figure 3.1.3.

The PBG effect can be extended to other planar transmission lines like the coplanar wave guide, asymmetric coplanar wave guide etc

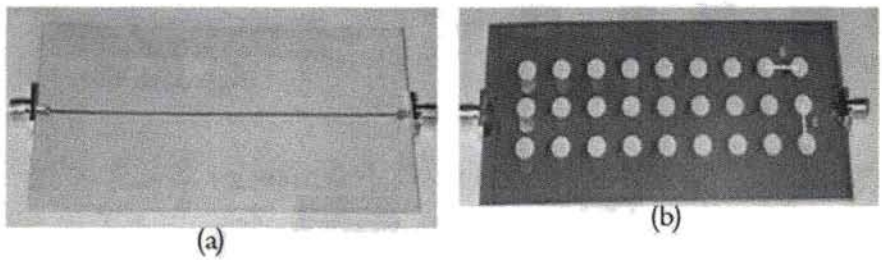

Figure 3.1.3. EC in microstrip technology: EC band reflector.
(a) The upper side of the microstrip line shows the conductor strip on the substrate and (b) the ground plane shows the etched holes for a 2D periodic pattern

3.2 Coplanar Waveguide

A coplanar waveguide (CPW) fabricated on a dielectric substrate was first demonstrated by C. P. Wen [6] in 1969. Since that time, tremendous progress has been made in CPW based microwave integrated circuits (MICs) as well as

monolithic microwave integrated circuits (MMICs) [7 - 10]. A conventional CPW on a dielectric substrate consists of a center strip conductor with semi-infinite ground planes on either side as shown in Figure 3.2.1. This structure supports a quasi-TEM mode of propagation.

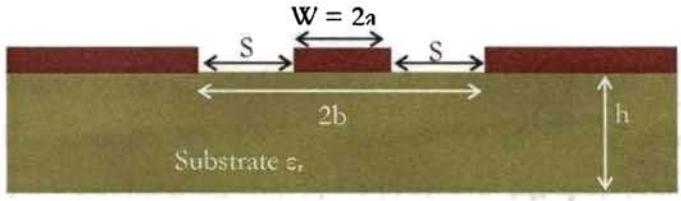

Figure 3.2.1 Coplanar waveguide

The CPW offers several advantages over conventional microstrip line: First, it simplifies fabrication: second, it facilitates easy shunt as well as series surface mounting of active and passive devices [11 - 15]; third, it eliminates the need for wraparound and via holes [11, 16] and fourth, it reduces radiation loss [11]. Furthermore the characteristic impedance is determined by the ratio of $\frac{a}{b}$, so size reduction is possible without limit, the only penalty being higher losses [17]. In addition a ground plane exists between any two adjacent lines; hence cross talk effects between adjacent lines are very week [11]. As a result, CPW circuits can be made denser than conventional microstrip circuits. These, as well as several other advantages, make CPW ideally suited for MIC as well as MMIC applications. Coplanar waveguides can be broadly classified as follows: Conventional CPW, Conductor backed CPW and Micromachined CPW. In a conventional CPW, the ground planes are of semi-infinite extent on either side. However, in a practical circuit the ground planes are made of finite extent. The conductor-backed CPW has an additional ground plane at the bottom surface of the substrate. This lower ground plane not only provides mechanical support to the substrate but also acts as

a heat sink for circuits with active devices. The micromachined CPWs are of two types, namely, the micro-shield line and the CPW suspended by a silicon dioxide membrane above a micromachined groove.

A conventional CPW can be designed using the method of conformal mapping. The characteristic impedance of the line is given as;

$$Z_c = \frac{\eta_0}{\sqrt{\varepsilon_e}} \frac{K(k')}{4K(k)} \qquad 3.2$$

$$\eta_0 = \sqrt{\frac{\mu_0}{\varepsilon_0}} = 377\Omega \qquad 3.3$$

The substrate is assumed to be infinitely thick and $K(k)$ is the complete elliptical integral of the first kind with modulus $k = \frac{W}{d}; d = 2S + W$, $k' = \sqrt{1-k^2}$ and $\varepsilon_e = \frac{\varepsilon_r + 1}{2}$.

$$Z_c = \frac{\eta_0}{\sqrt{\varepsilon_e}} \left[\frac{\ln 2 + 2\tanh^{-1}\sqrt{1-\left(\frac{W}{d}\right)^2}}{4\pi} \right] \text{for } \frac{W}{d} \le 0.7 \qquad 3.4$$

$$Z_c = \frac{\eta_0}{\sqrt{\varepsilon_e}} \left[\frac{\pi}{4\left(\ln 2 + 2\tanh^{-1}\sqrt{1-\left(\frac{W}{d}\right)^2} \right)} \right] \text{for } 0.7 \le \frac{W}{d} \le 1 \qquad 3.5$$

Coupled CPWs have several applications in the design of microwave components such as, directional couplers and filters. When an electromagnetic wave propagates along a conductor backed CPW considerable amount of energy leakage takes place. The energy that leaks, propagates along the transverse directions away from the

line, and excites a parallel plate mode between the CPW top and bottom ground planes. The parasitic parallel plate mode is the leading cause for crosstalk between adjacent circuits. The cross talk can be suppressed by constructing a photonic band gap lattice on the CPW top ground planes as demonstrated in [20]. Another PBG-CPW structure is proposed by Yun and Chang in [21], where a pattern of rectangular apertures are etched in the ground plane just adjacent to the slot, and well defined frequency band gap has been observed. Later Yun-Qi Fu etal [26] proposed a PBG structure by etching holes in the ground plane with an open connected with the gap between strip line and ground plane and the structure is as shown in Figure3.2.2.

Design and analysis of Photonic Band Gap structures in the ground plane of a microstrip line and coplanar wave guide is studied in detail in Chapter 4.

The methodology adopted in the theoretical analysis is presented in the next section.

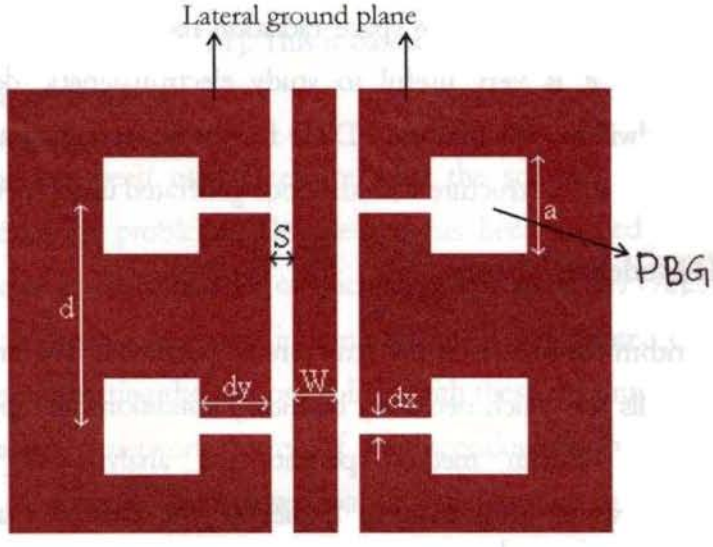

Figure 3.2.2 Top view of PBG – CPW Yun-Qi Fu etal (2001)

3.3 Finite Difference Time-Domain (FDTD)

The analysis of PBG structures is done using Finite Difference Time-Domain (FDTD) method. The finite difference time domain (FDTD) method is an efficient tool for electromagnetic analysis and can be conveniently applied to study PBG structures. Finite Difference Time Domain (FDTD) method is an efficient tool for directly solving time harmonic Maxwell's equation using finite difference techniques. In the FDTD method the spatial and time derivatives are approximated by centered differences, which are accurate to second order in time or space. With Maxwell's equations reduced to a set of coupled difference equations, the solution is readily obtained by time stepping, where the new value for field components are calculated from the previous values. Hence the method is termed as 'leap-frog' method.

The finite size photonic Band Gap materials present very accurate anisotropic properties according to the finite dimensions and the periodicity of the structure. To analyze this anisotropy, a plane wave expansion of the electromagnetic fields inside the PBG crystal is performed using the FDTD method and space-time Fourier transforms. With this "k-space" analysis we obtain the excited propagating modes useful to predict the free space radiation modes. Since FDTD is a time domain method, it is very useful to study electromagnetic devices in broad frequency bandwidths. We first use FDTD for the scattering parameters of a two dimensional (2D) PBG structure with the code generated using MATLAB 7.2.

3.4 FDTD Modeling Theory

FDTD algorithm for analyzing the structure is generated. The entire structure is divided into cells for which necessary boundary conditions are applied. The finite difference time domain method permits the analysis of interactions of electromagnetic waves with material bodies of the desired shapes. The finite difference time domain method was originated by Yee in 1966 [27] and applied to electromagnetic problems in two dimensions. The FDTD method calculates the

electric and magnetic fields on a discrete mesh by approximating the first order derivatives in the differential form of Maxwell's vector curl equations. The discrete electric and magnetic fields are interleaved in space to obtain centered difference approximations to the spatial derivatives. The time derivatives are calculated in a leap-frog manner to obtain the centered differences in time. Space and time discretizations are selected to bind the errors in sampling process and to ensure numerical stability of the problem. The electric and magnetic field components are interleaved in space to permit a natural satisfaction of the tangential field continuity conditions at media interfaces.

Applications of FDTD techniques to various electromagnetic problems are available in literature [28], [29], [30]. In the case of arbitrary shaped patches application of Yee's algorithm has been found to be extremely accurate in finding the current and field distribution across the patch. One practical difficulty with this method is that for devices containing small structures or strongly varying fields, it needs very fine mesh. When using finer meshes it needs longer CPU time and memory. An improved method for reducing the number of time steps is implemented by Lubbers *et al.* [31]. This is based on using a source with an external resistance to excite the circuit.

FDTD method has been used extensively for the solution of two and three dimensional scattering problems. The method has been applied to calculate the frequency dependent characteristics of microstrip discontinuities [32]. Analysis of microstrip discontinuities has great importance, since complicated circuits can be realized by interconnecting the microstrip lines with these discontinuities and using transmission lines and network theory. If the discontinuities are too close to each other the use of network concept will not be accurate due to the interaction of evanescent waves. To analyze the circuits accurately the entire structure has to be simulated in one computation. In time domain analysis a broadband pulse may be

used as the excitation and frequency domain parameters may be calculated over the entire frequency range of interest by Fourier Transform of the transient results [30].

The formulation of the FDTD method begins by considering the differential formulae of Maxwell's curl equations which govern the propagation of electromagnetic waves. The media are assumed to be piecewise uniform, isotropic and homogeneous.

$$-\frac{\partial B}{\partial t} = \nabla \times E \qquad 3.6$$

$$\frac{\partial D}{\partial t} = \nabla \times H - J \qquad 3.7$$

$$B = \mu H \qquad 3.8$$

$$D = \varepsilon E \qquad 3.9$$

In Cartesian co-ordinate system the above equations may be written as

$$-\frac{\partial B_x}{\partial t} = \frac{\partial E_z}{\partial y} - \frac{\partial E_y}{\partial z} \qquad 3.10$$

$$-\frac{\partial B_y}{\partial t} = \frac{\partial E_x}{\partial z} - \frac{\partial E_z}{\partial x} \qquad 3.11$$

$$-\frac{\partial B_z}{\partial t} = \frac{\partial E_y}{\partial x} - \frac{\partial E_x}{\partial y} \qquad 3.12$$

$$\frac{\partial D_x}{\partial t} = \frac{\partial H_z}{\partial y} - \frac{\partial H_y}{\partial z} - J_z \qquad 3.13$$

$$\frac{\partial D_y}{\partial t} = \frac{\partial H_x}{\partial z} - \frac{\partial H_z}{\partial x} - J_y \qquad 3.14$$

$$\frac{\partial D_z}{\partial t} = \frac{\partial H_y}{\partial x} - \frac{\partial H_x}{\partial y} - J_z \qquad 3.15$$

The system of six coupled partial difference equations forms the basis of the FDTD numerical algorithm for electromagnetic wave interaction with general three dimensional objects.

The basic Yee algorithm helps to solve both electric and magnetic fields in time and space using the Maxwell's curl equations. The grid points for the E- filed and H-field are chosen as shown in Figure 3.4.1. The boundary condition for a perfectly conducting surface is that the tangential components of the electric field vanish at the boundary. This implies that the normal component of the magnetic field vanishes on the surfaces. The conducting surfaces will therefore be approximated by a collection of surfaces of cubes, the sides of which are parallel to the coordinate axes. Plane surfaces are perpendicular to the x-axis will be chosen so as to contain points where E_x and E_y are defined [27].

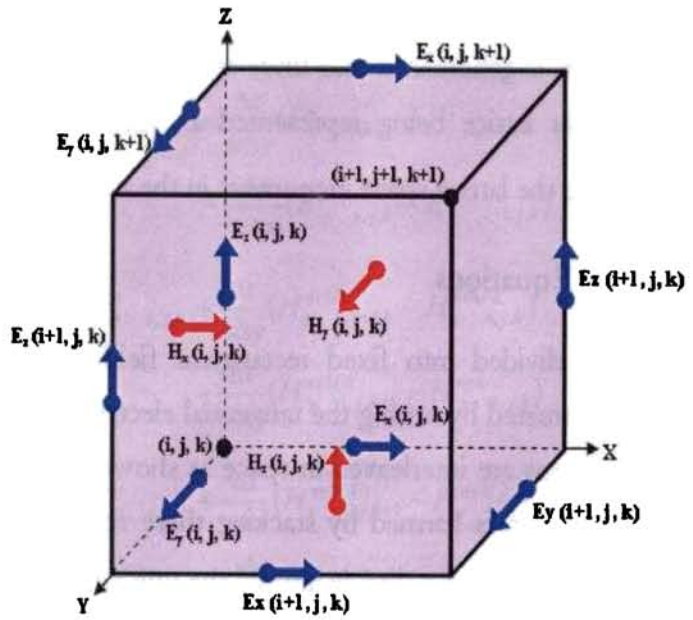

Figure 3.4.1 Field component placements in the FDTD unit cell

Each Yee cell contains six field components E_x, E_y, E_z and H_x, H_y, H_z. All the fields are offset by half a space step as in Figure The Yee algorithm centers its $\overline{E}$ and $\overline{H}$ components in a three dimensional space so that every $\overline{E}$ component is surrounded by four circulating $\overline{H}$ components and every $\overline{H}$ component by four circulating $\overline{E}$ components.

3.4.1 FDTD Problem Definition

The FDTD method is formulated by discretizing Maxwell's equations over a finite volume and approximating the derivatives with centered difference approximations. Conducting surfaces are treated by setting the tangential electric field components to be zero. The walls are treated separately to prevent reflections from the mesh terminations. In the present analysis, space grids are selected such that the electromagnetic filed does not vary significantly over one increment. The notation used for analysis is generalized into three spatial dimensions, space points in a uniform rectangular lattice being represented as, $(i,j,k) = (i\Delta_x, j\Delta_y, k\Delta_z)$. Here Δ_x, Δ_y and Δ_z are the lattice space increments in the *x*, *y*, and *z* directions.

3.4.2 FDTD Principal Equations

The PBG structure is divided into fixed rectangular field locations and each conducting surfaces are treated by setting the tangential electric field component to zero. The six field locations are interleaved in space as shown in Figure 3.4.1. The entire computational domain is formed by stacking these rectangular cells into a rectangular volume. The *x*, *y*, and *z* dimensions of the unit cell are Δx, Δy, and Δz respectively. This field arrangement has an advantage that the centered differences are realized in the calculation of each field component and the boundary condition of tangential field component is automatically satisfied at the dielectric material interfaces.

Since there are six field components within the unit cell, six field components touching the shaded upper eighth of the unit cell in the figure are considered to be a unit node with subscript indices (i, j, k) in the x, y, and z directions. The notation implicitly assumes the $\pm\frac{1}{2}$ space indices and thus can be directly used for computations. The time step is indicated with subscripts, n. The explicit finite difference approximations to (3.18) to (3.23) are as given by Sheen *et al.* [117]

$$H_x^{n+1/2}{}_{i,j,k} = H_x^{n-1/2}{}_{i,j,k} + \frac{\Delta t}{\mu\Delta z}(E_y^n{}_{i,j,k} - E_y^n{}_{i,j,k-1}) - \frac{\Delta t}{\mu\Delta y}(E_z^n{}_{i,j,k} - E_z^n{}_{i,j-1,k}) \quad 3.16$$

$$H_y^{n+1/2}{}_{i,j,k} = H_y^{n-1/2}{}_{i,j,k} + \frac{\Delta t}{\mu\Delta x}(E_z^n{}_{i,j,k} - E_z^n{}_{i-1,j,k}) - \frac{\Delta t}{\mu\Delta z}(E_x^n{}_{i,j,k} - E_x^n{}_{i,j,k-1}) \quad 3.17$$

$$H_z^{n+1/2}{}_{i,j,k} = H_z^{n-1/2}{}_{i,j,k} + \frac{\Delta t}{\mu\Delta y}(E_x^n{}_{i,j,k} - E_x^n{}_{i,j-1,k}) - \frac{\Delta t}{\mu\Delta x}(E_y^n{}_{i,j,k} - E_y^n{}_{i-1,j,k}) \quad 3.18$$

$$E_x^{n+1}{}_{i,j,k} = E_x^n{}_{i,j,k} + \frac{\Delta t}{\varepsilon\Delta y}(H_z^{n+1/2}{}_{i,j+1,k} - H_z^{n+1/2}{}_{i,j,k}) - \frac{\Delta t}{\varepsilon\Delta z}(H_y^{n+1/2}{}_{i,j,k+1} - H_y^{n+1/2}{}_{i,j,k}) \quad 3.19$$

$$E_y^{n+1}{}_{i,j,k} = E_y^n{}_{i,j,k} + \frac{\Delta t}{\varepsilon\Delta z}(H_x^{n+1/2}{}_{i,j,k+1} - H_x^{n+1/2}{}_{i,j,k}) - \frac{\Delta t}{\varepsilon\Delta x}(H_z^{n+1/2}{}_{i+1,j,k} - H_z^{n+1/2}{}_{i,j,k}) \quad 3.20$$

$$E_z^{n+1}{}_{i,j,k} = E_z^n{}_{i,j,k} + \frac{\Delta t}{\varepsilon\Delta x}(H_y^{n+1/2}{}_{i+1,j,k} - H_y^{n+1/2}{}_{i,j,k}) - \frac{\Delta t}{\varepsilon\Delta y}(H_x^{n+1/2}{}_{i,j+1,k} - H_x^{n+1/2}{}_{i,j,k}) \quad 3.21$$

The half time steps indicate that $\vec{E}$ and $\vec{H}$ are alternatively calculated in order to achieve centered differences for the time derivatives. This algorithm is referred to as 'leap-frog' algorithm. Here the permittivity and permeability are set to appropriate values depending on the location of each filed component. For the electric field component in the air-dielectric interface the average of two permittivities $(\varepsilon_0 + \varepsilon_1)/2$, where ε_0 and ε_1 are the permittivity of the free space and medium is used. The error is second order in both space and time steps and are proportional to Δl, and the global error is $O(\Delta l^2)$. The maximum time step is limited by the Courant Stability criterion of the finite difference equations [117]

$$\Delta t \leq \frac{1}{v_{\max}} \left(\frac{1}{\Delta x^2} + \frac{1}{\Delta y^2} + \frac{1}{\Delta z^2} \right)^{-\frac{1}{2}} \qquad 3.21$$

where $v_{\max}$ is the maximum velocity of light in the computational volume.

3.4.3 Source Consideration

The time dependence of the source is chosen depending on the problem to be solved. For applications where frequency dependent data is to be generated, a pulse is used such that its frequency content covers the desired frequency range. A Gaussian pulse has a smooth waveform in time, and its Fourier Transform is also a Gaussian pulse centered at zero frequency. This unique property makes it a perfect choice for investigating the frequency dependent characteristics of the microstrip discontinuities via Fourier Transform of the pulse response.

To simulate, a voltage source excitation is necessary to impose the vertical electric field in a rectangular region above the ground plane. The launched wave has a nearly unit amplitude and is Gaussian which is given by

$$f_s(t) = e^{-(t-t_0)^2/T^2} \qquad 3.25$$

where T is the half width and t_0 is the time delay.

The choice of t_0 and T is such that the truncation of the source pulse does not introduce unwanted high frequencies in the spectrum and does not waste computation time on determining values of the fields that are essentially zero i.e., T depends on the maximum frequency of computation and t_0 ensures the field to be zero in the initial condition. Usually the width of the pulse is chosen to be at least 20 points per wavelength at the highest frequency of interest. However, if we proceed straight way, the computational time is large to achieve the stability condition. Lubbers *et al.* [31] introduced a new concept to reduce the computational time, by introducing a source resistance R_s in series with the voltage source.

The equivalent circuit for a voltage source which includes an internal source resistance R_s is illustrated in Figure 3.4.2. If the source resistance R_s is set to zero then the FDTD electric field at the source is given by

$$E_z^n(i_s, js.ks) = \frac{V_s[n\,\Delta t]}{\Delta z} \qquad 3.26$$

V_s is the Gaussian pulse. When the source resistance is included, the calculation of source field at each time step is complicated.

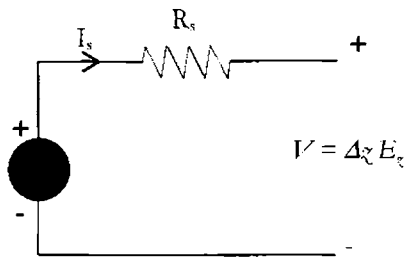

Figure 3.4.2 FDTD Source with source Resistance R_s

To determine the terminal voltage V of Figure 3.4.2, the current through the source must be determined. The current through the source is given by

$$I_s^{n-1/2} = [H_x^{n-1/2}(i_s . j_s - 1 k_s) - H_x^{n-1/2}(i_s . j_s k_s)]\Delta x + [H_y^{n-1/2}(i_s . j_s k_s) - H_y^{n-1/2}(i_s - 1 . j_s k_s)]\Delta y \quad 3.27$$

And the electric source field is given by

$$E_s^n(i_s . j_s k_s) = \frac{V_s(n\Delta t)}{\Delta z} + \frac{I_s^{n-1/2} R_s}{\Delta z} \quad `3.28$$

The value of the source resistance cannot be too large or instabilities can occur due to neglecting the displacement current through the FDTD cell containing the source [31].

Once the pulse amplitude drops, the source voltage becomes essentially zero, any reflections from the antenna which returns to the source, is totally reflected back. The inclusion of an internal resistance to the source provides an additional loss mechanism to dissipate energy introduced into the calculation space that will reduce the computational time appreciably [121].

3.4.4 Absorbing Boundary conditions

Absorbing boundary conditions are applied at the boundary mesh walls of finite difference, to simulate an unbounded space. The most common, and generally most practical, method used to derive absorbing boundary conditions are based on asymptotic expansion of one–way wave equation. Many researchers have developed theories to these approximate boundary conditions [27].

The difference equations cannot be used to evaluate the field components tangential to the outer boundaries since they would require the values of field components outside the mesh. One of the six mesh boundaries is a ground plane and its tangential electric field values are forced to zero. The tangential

electric field components on other five mesh walls are represented in such away that outgoing waves are not reflected using the absorbing boundary conditions. For this structure the pulses on the microstrip line will be considered as incident normally to the mesh walls. This results in a simple approximate continuous absorbing boundary condition that the tangential fields on the outer boundaries will obey the one –dimensional wave equation in the direction normal to the mesh wall. For the y normal wall the one dimensional wave equation is

$$\left(\frac{\partial}{\partial y}-\frac{1}{v}\frac{\partial}{\partial t}\right)E_{\tan}=0 \qquad 3.29$$

v is the velocity of light in the medium.

This equation is Mur's first order approximate boundary condition and may be easily discretized using only field components on or just inside the mesh walls, yielding an implicit finite difference equation [29].

$$E_0^{n+1}=E_1^{n}+\frac{v\Delta t-\Delta y}{v\Delta t+\Delta y}\left(E_1^{n+1}-E_0^{n}\right) \qquad 3.30$$

Here E_0 is the tangential electric field components on the mesh wall and E_1 represents the tangential electric field components one node inside the mesh wall. The normal incidence assumption is not valid for the fringing fields which are propagating tangential to the wall and therefore the side walls should be far away, so that the fringing fields are negligible at the walls. Also the radiation will not be exactly normal to the mesh walls.

Finite difference equations are used with the above boundary and source conditions to simulate the propagation of broadband Gaussian pulse on the

microstrip structure. The most important aspects of the time domain algorithm are as follows:

- Initially at $t = n = 0$ all the fields are forced to zero.
- The following steps are repeated until the response is ≈ 0
- Gaussian excitation is imposed at port.
- $H^{n+\frac{1}{2}}$ is calculated from the finite difference equations.
- $E^{n+\frac{1}{2}}$ is calculated from the finite difference equations.
- Tangential E is set to 0 on conductors.
- Save the desired field quantities
- Increment the time $n \rightarrow n+1$
- Update the equation
- Compute scattering matrix coefficients from time domain results.

To eliminate the reflections from the circuit, to reflect it again by the source wall, the circuit is placed a sufficient distance away from the source. After the Gaussian pulse has been launched, the absorbing boundary condition is switched on at the boundary walls.

3.5 Analysis of PBG backed Transmission line using FDTD method

As explained the finite difference equations are used to simulate the desired structure along with the source excitation and absorbing boundary conditions. The spatial parameters $\Delta x, \Delta y$ and Δz are chosen for integral number of modes to exactly fit within the structure. The microstrip transmission line with periodic square shaped slots in the ground plane is presented in Figure 3.4.3.

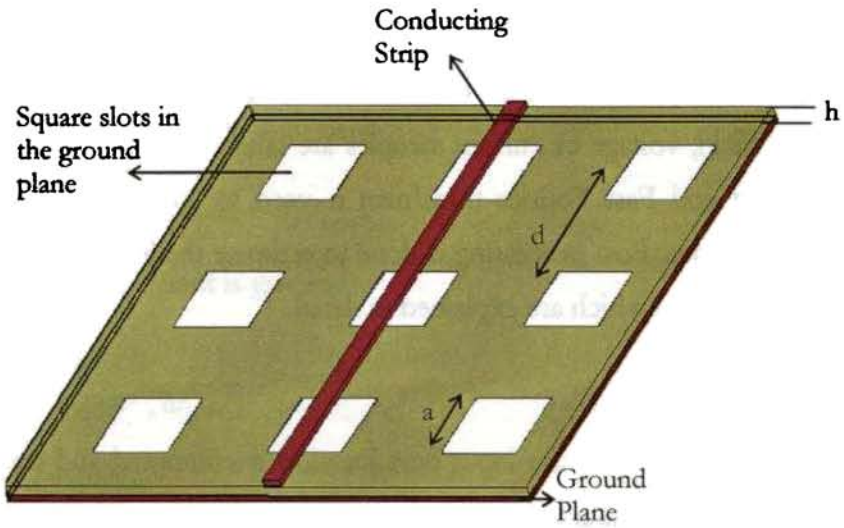

Figure 3.4.3. Microstrip Line with PBG ground plane

Excitation is given at ports P_1 and P_2. PBG backed microstrip transmission line is modeled with $\Delta x=0.5mm, \Delta y=0.5mm$ and $\Delta z=0.32\,mm$. Enough cells are given in the outside domain ensuring the pulse to converge.

The computational domain of analysis is presented in Figure 3.4.4.

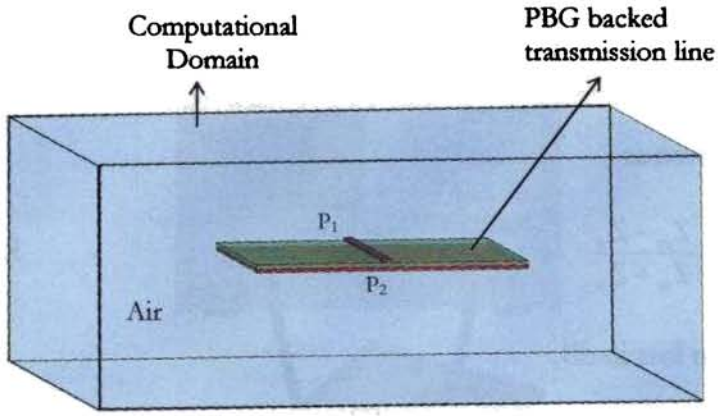

Figure 3.4.4. Computational domain for FDTD analysis

3.5.1 Extraction of Filter properties

FDTD algorithm performs the transient analysis of the problem under investigation. Field, voltage or current samples are taken from the fixed points in the FDTD grid and Fast Fourier transform is used to compute the frequency domain in formations. Post processing is done to estimate the S-parameters (return loss and insertion loss) which are explained in detail.

3.5.1(a) Return Loss

The voltage $V_n = V(n.\Delta t)$ at the input port location is computed and saved from the E_z field component at the grid point over the entire simulation time intervals (say N steps). Similarly the current I^{n-1} is also computed based on the Ampere's Law applied to the tangential H loop around the feed point. The samples are suitably padded with zeros and the FFT is computed separately. The input impedance of the antenna is computed as the ratio of the FFT of voltage derived from E field values at the feed point, over the entire time steps, to the FFT of current at the same point, derived from the H field values.

$$Z_{in}(\omega) = \frac{FFT(V^n, P)}{FFT(I^{n-1}, P)} \qquad 3.31$$

Assuming that characteristic impedance (Z_0) of the feed line ($Z_0 = Zs$), reflection coefficient is given as

$$\Gamma(\omega) = \frac{Z_{in} - Z_o}{Z_{in} + Z_o} \qquad 3.32$$

Then the return loss in dB,

$$S_{11} = 20 \log_{10} \Gamma(\omega) \qquad 3.33$$

3.5.1 (b) Insertion Loss

Using the FDTD algorithm, the periodic dielectric PBG structure is meshed. At port 2 the reflected voltage is given as

$$V_{(at P_2)} = E_{z\,(at P2)}\,\Delta z - R_s\, I_{s\,(at P_2)} \qquad 3.34$$

Transmission coefficient is given as

$$T = \frac{FFT\left(V_{(at\,P2)}\right)}{FFT\left(V_{n\,\Delta t_{(at\,P1)}}\right)} \qquad 3.35$$

$$S_{21} = 20\log_{10} T \qquad 3.36$$

The computed results are presented along with the experimental and simulated results in chapter 4.

3.6 Methodology of Measurement

For the measurement of the transmission (S_{21}) and reflection (S_{11}) a Vector Network Analyzer (HP 8510 C) is used. For error free measurement a full 2-port calibration is done using standard open, short, load and thru.

After the calibration, the PBG backed transmission lines are connected across the two ports of the S-parameter test set and the reflection and transmission studies are carried out. The measurement set up is shown in the Figure 3.6.1.

Figure 3.6.1. Measurement setup for reflection and transmission studies

The magnitude and phase of the measured S_{11}/ S_{12} is the acquired and stored in ASCII format in the computer using the CREMASOFT, indigenously developed by the Department of Electronics, Cochin University of Science and Technology. The stop band center frequency is determined from the S_{12}/S_{21} curves.

3.7. Microstrip Antennas Using Photonic Crystal Substrates – An Introduction

The current trend in commercial communication systems has been to develop low cost, light weight, low profile antennas that are capable of maintaining high performance over a large spectrum of frequencies. This technological trend has focused much effort into the design of microstrip (patch) antennas. With a simple geometry, patch antennas offer many advantages not commonly exhibited in other antenna configurations. For example, they are extremely low profile, lightweight, simple and inexpensive to fabricate using modern day printed circuit board technology, compatible with microwave and millimeter-wave integrated circuits (MMIC), and have the ability to conform to planar and non-planar surfaces. In addition, once the shape and operating mode of the patch are selected, designs become very versatile in terms of operating frequency, polarization, pattern, and impedance. The variety in design that is possible with microstrip antennas probably exceeds that of any other type of antenna element [1].

Despite the many advantages of patch antennas, they do have some considerable drawbacks. One of the main limitations with patch antennas is their inherently narrowband performance due to its resonant nature. With bandwidths as low as a few percent [2], broadband applications using conventional patch designs are limited. Other characteristics of patch antennas include low efficiency, limited power capacity, spurious feed radiation, poor polarization purity, and manufacturing tolerance problems [3]. The simplest and most direct approach to increase the bandwidth is to use thick substrate of low dielectric constant [3].

This can extend efficiency (as much as 90% if the surface waves are not included) and bandwidth (up to 35%) [4]. However, surface waves must be included, since surface waves extract power from the direct radiation pattern, resulting in increased side lobe levels, antenna loss, and a decrease in efficiency. The probability of surface wave formation increases as the thickness of the substrate increases. As a patch antenna radiates, a portion of the total available power for direct radiation becomes trapped along the surface of the substrate. This trapped electromagnetic energy leads to the development of surface waves [5]. In fact, the ratio of power that radiates into the substrate compared to the power that radiates into air is approximately $\varepsilon_r^{3/2}$:1 [5]. This is governed by the rules of total internal reflection, which state that any field line radiated into the substrate at angles greater than the critical angle $\theta c = \sin^{-1}\left(\sqrt{\varepsilon_r}\right)$ are totally internally reflected at the top and bottom surfaces. This is illustrated in Figure 3.7.1 Therefore, for a substrate with dielectric constant ε_r = 10.2, nearly $\frac{1}{3}$ of the total radiated power is trapped in the substrate with a critical angle of roughly 18.2 degrees.

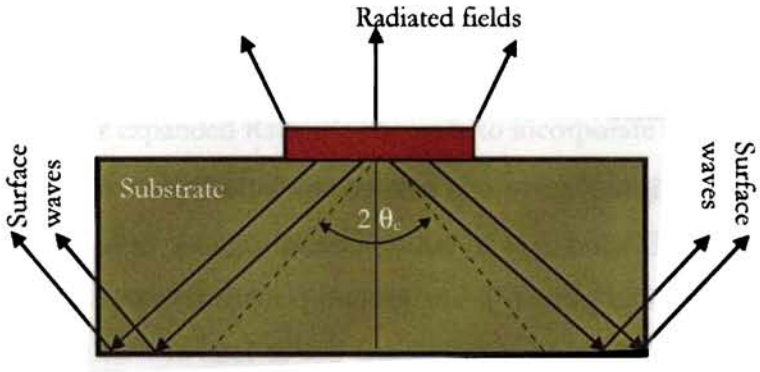

Figure 3.7.1. Field lines radiating from a patch antenna; illustrates the formation of surface waves

Surface wave effects can be eliminated by using cavities or stacked substrate techniques [5]. However, this has the fundamental drawback of increasing the weight, thickness, and complexity of the microstrip antenna, thus negating many of the advantages of using microstrip antennas. These complications prevent microstrip antennas from becoming the standard in the microwave telecommunications community.

A recently developed method for improving the bandwidth and efficiency of a patch antenna is the insertion of a photonic crystal array into the substrate. With the ability to completely prohibit the propagation of electromagnetic energy at specific frequencies, photonic crystals and their respective band gaps correlate well with the development of next-generation microstrip antennas. The insertion of photonic crystals into the substrate does not change any of the fundamental characteristics that exist for patch antennas. In other words, the antenna designer must still chose between using a thick or thin substrate. The only requirement is that the refractive index ratio between the substrate and crystals be large enough (> 2:1) [7] for the bandgap to exist. This section compares two methodologies of introducing photonic crystals into patch antenna designs. Namely, thick and thin substrate approaches. This section concludes with a novel technique, which combines properties of both approaches when using the photonic crystal structure.

3.7.1 Thick Substrates

The concept of designing microstrip antennas on a thick photonic crystal substrate is to utilize quasi-3D band gaps to radiate electromagnetic field from the antenna, without using a ground plane [7]. The ground plane is removable because the 3D bandgap creates an equivalent ground plane due to total internal reflections caused by the high index ratios in the vertical axis (perpendicular to the patch), as shown in Figure 3.7.2.

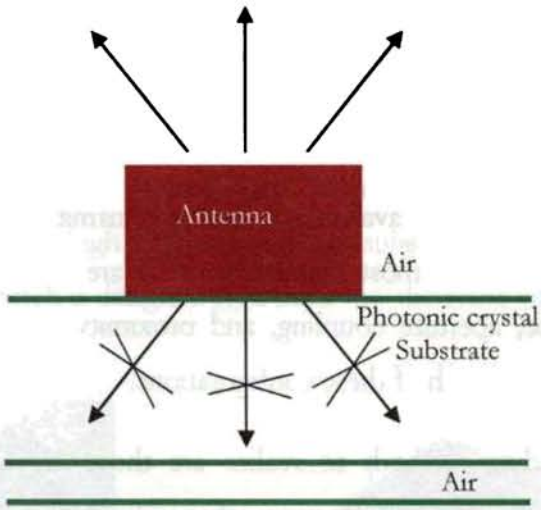

Figure 3.7.2. Cross-sectional view of a Patch Antenna radiating from a thick substrate with PBG

3.7.2 Thin Substrates

The concept of using thin substrates containing photonic crystals to design microwave devices was first conceived by Radisic et al. in 1998. In their approach, microstrip filters were fabricated by simply etching a two-dimensional triangular pattern into the ground plane of a conventional microstrip line. This resulted in nearly 100% reflection loss over a span of frequencies governed by the lattice spacing, opposed to the typical 100% transmission expected from a microstrip line.

Coccioli et al. later expanded Radisic's concepts to incorporate this approach in the development of microstrip antennas printed on thin substrates containing similar photonic crystals [9]. Experimental measurements of this type of antenna illustrated a 10dB side lobe level reduction and minimal reduction in front-to-back ratios [9] when compared to a patch without the photonic crystals. These thin substrate designs exhibit comparable results to that of the thick substrate designs. The only drawback, however, is that the band gap is reduced to two dimensions, due to the

inclusion of the ground plane – total internal reflections condition scarified. To reestablish the third dimension of the band gap, a new approach is required.

3.8 Feeding Methods

There are several techniques available to feed or transmit electromagnetic energy to a microstrip antenna. The most popular methods are the microstrip transmission line, coaxial probe, aperture coupling, and proximity coupling [10, 11 and 12]. Figure 3.8.1 illustrates each of these configurations.

The simplest feeding methods to realize are those of the coaxial probe and microstrip transmission line. Both approaches utilize direct contact with the patch to induce excitation. The point of excitation (contact point) is adjustable, enabling the designer to control the impedance match between feed and antenna, polarization, mode of operation, and excitation frequency.

Generally, for direct contact feeds, the best impedance match is obtained when the contact point is off-centered. This produces asymmetries in the patch excitation, which generate higher order modes [10]. These higher order modes induce a cross-polarized component in the principal plane antenna patterns, which draw power from the dominant TM_{010} mode and results in degradation of the antenna's main beam. Therefore, oftentimes, a trial-and-error approach is used to obtain the optimum match for the direct contact feeds. Another disadvantage of the direct contact feeds is that they are inherently narrowband devices. These feeds, whether coaxial or microstrip, are "matched" to specific impedances (in most cases 50Ω) for a select range of frequencies. Operation outside this range automatically degrades antenna performance due to the inherent mismatch between the antenna and the feed. To overcome some of the shortcomings of the direct-coupled feeds, a variety of "non-contacting coupled feeds" has been developed. The two main configurations are the aperture-coupled and proximity-coupled feeds. The

aperture-coupled configuration consists of two parallel substrates separated by a ground plane.

Excitation of the patch is accomplished by coupling energy from a microstrip line through a small aperture in the ground plane. With this arrangement, the microstrip feed is designed on a thin-high dielectric constant substrate, which tightly binds the field lines, while the patch is designed on a thick-low dielectric constant substrate.

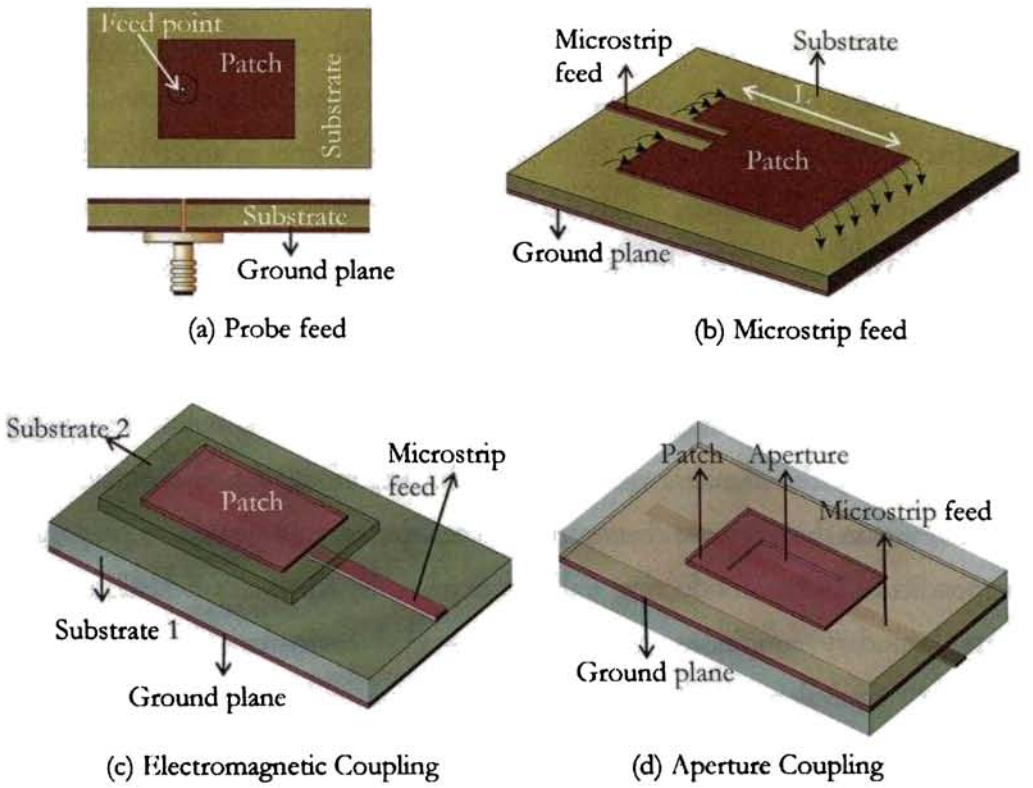

Figure 3.8.1 Feeding techniques to Microstrip Antenna

The ground plane isolates the feed from the patch, and thus minimizes spurious radiation from the feed, which would interfere with the antenna pattern [12]. Therefore, the design of the patch and the transmission line are independent. In

contrast, the proximity-coupled technique operates in a manner similar to that of the aperture-coupled configuration except the ground plane is removed. Both non-contacting feeds have similar advantages with the exception that the thickness changes with removal of the ground plane.

3.9 Analytical Evaluation of a Patch Antenna

In common practice, microstrip antennas are evaluated using one of three synthesis methods – the transmission line model, the cavity model, or the full-wave model [10]. Since the inception of these techniques, several complex analytical models have been developed that account for fringing effects, special geometries, complex substrates, and mutual coupling from neighboring elements in an array. The most direct approach to evaluate patch antennas with reasonably accurate results is to use the cavity model. In the cavity model, a patch antenna is represented as a dielectric loaded cavity. The cavity is formed via a substrate that is truncated on the top and bottom by two perfectly conducting electric boundaries – the patch and ground plane. The sidewalls are perfectly conducting magnetic boundaries that are determined by the dimensions of the patch. Therefore, the electric field lines contain within the substrate (between the patch and ground plane) are propagating perpendicular to the conducting walls, as required by Maxwell's Equations. Using these boundary conditions, the dielectric loaded cavity can be evaluated via Huygens' equivalence principle. The equivalence principle works such that fictitious equivalent sources may be envisioned to replace the actual source of radiation, which in this case is an antenna. These fictitious sources are said to be equivalent within a region because they produce the same fields within that region as the antenna itself [10]. Huygens' Principle is based on the uniqueness theorem, which states that a solution that satisfies a differential equation (e.g. Maxwell's equations) and the boundary conditions is unique [13]. In the case of a patch antenna, equivalent electric current densities J_t and J_B are formed on the top and

bottom surfaces of the patch, respectively. The four sidewalls of the cavity are represented via equivalent electric and magnetic current densities. These equivalent currents are illustrated in Figure 4.4.1 and are written in general as

$$\vec{J}_s = \hat{n} \times \vec{H}_z \qquad 3.37$$

$$\vec{M}_s = -\hat{n} \times \vec{E}_z \qquad 3.38$$

where E_z and H_z represent the electric and magnetic fields along the walls of the cavity, respectively.

In most practical patch designs, the substrate height-to-patch width ratio is very small, thus allowing only a small amount of current to flow to the top surface [10] so $J_t \sim 0$. This ideally would not create any tangential magnetic field components (H_a) to the edges of the patch. Therefore, the equivalent electric current densities along the sidewalls are essentially zero, as illustrated in Figure 3.9.1. The only nonzero current density is the equivalent magnetic current density (M_s) along the sidewalls of the cavity. To simplify the model, image theory is used to account for the ground plane such that the equivalent magnetic current density becomes

$$\vec{M}_s = -2\hat{n} \times \vec{E}_z \qquad 3.39$$

(a) J_t, M_s with ground plane

(b) J_t= 0, M_s with ground plane

(c)M, with no ground plane

Figure 3.9.1 Equivalent current densities on four sides of a rectangular patch antenna as specified using the Cavity Model

This reduced model is similar to a cavity with four apertures or "slots" where radiation can occur. However, the equivalent current densities of length L and height h cancel, since they are equal magnitude and 180 degrees out of phase. Thus, these two sidewalls are referred to as non-radiating slots [10].

Therefore, only two slots radiate, each of width W and height h, are both equal in magnitude and phase, as shown in Figure 3.9.2. These components will thus add in phase, in a direction normal to the patch.

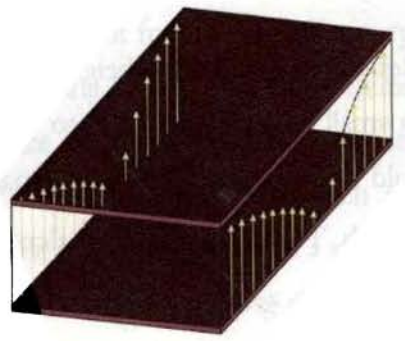

Figure 3.9.2 Current densities of non-radiating slots of a rectangular patch antenna

Using Aperture Theory, an approximate formula for the radiated fields from a rectangular patch antenna can be derived. For this analysis, the E-field is assumed to be uniformly distributed along the patch with amplitude $E_{ax} = E_0$. Based on this theory, a uniform source radiating in the yz-plane can be evaluated using

$$P_x = \int_S \int_a E_{ax}(y', z') e^{j\beta(y' \sin\theta\cos\phi + z' \cos\theta)} dy' dz' \qquad 3.40$$

$$E_\theta = j\beta \frac{e^{-j\beta r}}{2\pi r}(P_x \cos\phi) \qquad 3.41$$

$$E_\phi = j\beta \frac{e^{-j\beta r}}{2\pi r}(-P_x \sin\phi) \qquad 3.42$$

$\therefore (3.42) \Rightarrow$

$$P_x = E_0 \frac{\sin(Y)}{Y} \frac{\sin(Z)}{Z} \qquad 3.43$$

$$Y = \frac{\beta W}{2} \sin\theta \sin\phi, \quad Z = \frac{\beta h}{2} \cos\theta \qquad 3.44$$

For very thin substrates $\beta h << 1$ and as the limit of $Z \to 0$, equation (3.43) reduces to

$$P_x = E_0 \frac{\sin(Y)}{Y} \qquad 3.45$$

This expression is valid for only a single radiating slot. The expression when both slots radiate simultaneous is calculated using array theory. The normalized array factor for two elements, of the same magnitude and phase, separated by a distance L along the x-axis is

$$AF(\theta,\phi) = \cos\left(\frac{\beta L}{2} \sin\theta \cos\phi\right) \qquad 3.46$$

The far-field expression for a patch are evaluated from equations (3.45) and (3.46) to produce

$$E_\theta = E_0 \cos\phi (f(\theta,\phi)) \qquad 3.47$$

$$E_\theta = -E_0 \cos\theta \sin\phi (f(\theta,\phi)) \qquad 3.48$$

$$f(\theta,\phi) = \frac{P_x}{E_0} AF(\theta,\phi)$$

$$= \frac{\sin\left(\frac{\beta W}{2} \sin\theta \sin\phi\right)}{\left(\frac{\beta W}{2} \sin\theta \sin\phi\right)} \cos\left(\frac{\beta L}{2} \sin\theta \cos\phi\right) \qquad 3.49$$

The cavity model provides a description of how the fields radiating from the surface of the patch antenna. The radiation mechanism could easily be understood from Figure3.9.3.

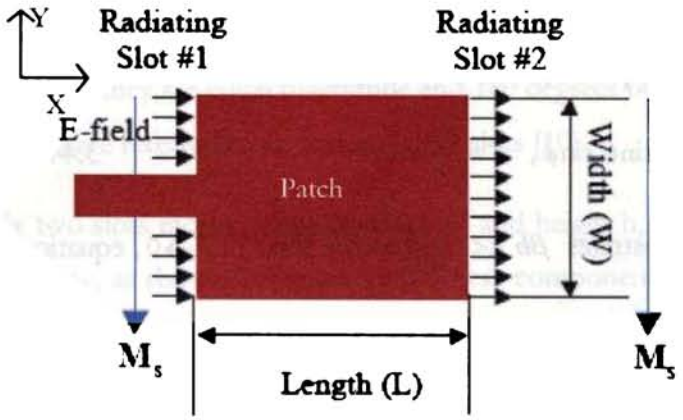

Figure 3.9.3 Fringing electric fields that is responsible for radiation along with the equivalent magnetic surface (*Ms*) currents

3.10 FDTD analysis of Antennas with PBG substrate

The Rectangular Microstrip Antenna (RMSA) on a PBG substrate is modeled a similar way as explained in section 3.4. The spatial parameters are kept same as that used for analysis of transmission line. The computational domain is presented in Figure 3.10.1.

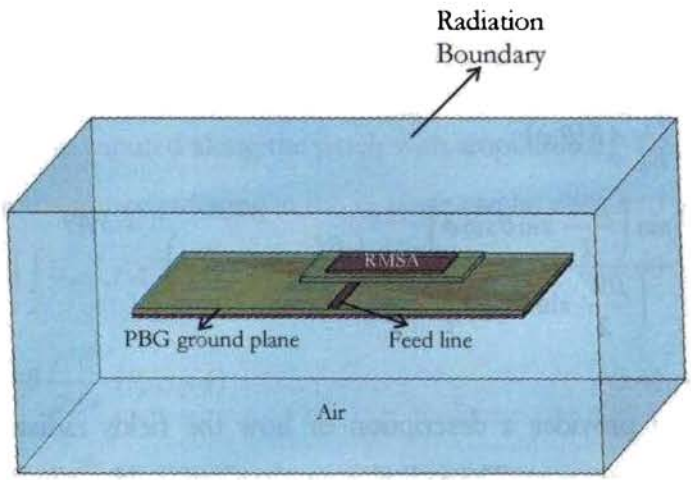

Figure 3.10.1. Computational domain

3.10.1 Extraction of Return Loss of the antenna

The return loss is extracted as explained in section 3.5.1. From the reflection coefficient $\Gamma(\omega) = \frac{Z_{in} - Z_o}{Z_{in} + Z_o}$, the return loss in dB is obtained as $S_{11} = 20\log_{10}\Gamma(\omega)$.

3.10.2 Resonant frequency and Bandwidth

From the return loss the resonant frequency is identified as the frequency point with maximum dip. The frequency points with -10 dB power are noted on either side of the resonant frequency which gives the bandwidth.

3.11 Parameters involved in Antenna Measurements

The various parameters studied in this thesis are

- resonant frequency of the patch antenna
- bandwidth offered by the antenna
- gain in the resonant band and the
- radiation pattern in the band

3.11.1 Measurement of Resonant Frequency and Bandwidth

For identifying the resonant frequency and the bandwidth offered the reflection characteristics of the antenna is measured. For that at first, the port-1 of the vector network analyzer is calibrated by using the suitable standard short, open and load. The antenna is then connected to the Port-1 of the network analyzer S-parameter test set as shown in the Figure 3.11.1.

The magnitude and phase of the measured S_{11} logmag data is acquired and stored in ASCII format in the computer using the CREMASOFT. The resonant frequency is determined from the return loss curve in logmag form, by identifying the frequency for which the curve shows maximum dip. The return loss is the number

in dB that the reflected signal is below the incident signal. As the VSWR=2 corresponds to the reflection co-efficient, $\rho = \frac{VSWR + 1}{VSWR - 1} = \frac{1}{3}$, then $20 \log\left(\frac{1}{3}\right) \approx -10\ dB$. Thus 2:1 bandwidths are determined by observing the range of frequencies (Δf_r) about the resonant frequency, f_r for which the return loss curves show a -10 dB value. The bandwidth is then calculated as $\frac{\Delta f_r}{f_r}$.

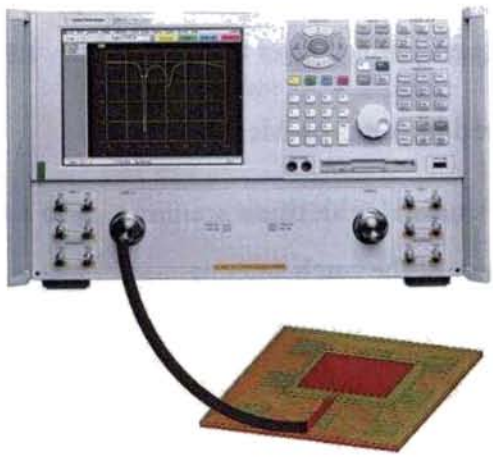

Figure 3.11.1 Measurement set up for Resonant Frequency and Bandwidth

3.11.2 Measurement of Radiation pattern and Gain

Radiation pattern measurement is carried out using the setup consisting of the network analyzer and anechoic chamber as depicted in Figure 3.11.2. An automatic turn table assembly kept in the quiet zone is used to mount the test antenna inside the anechoic chamber. The principal E and H-plane radiation patterns (with both co and cross-polar patterns) of the test antenna are measured by keeping the test antenna inside the chamber in the receiving mode. A standard wideband ridge horn antenna is used as the transmitter. The horn is then connected to port-1 and the test antenna in port-2 of the S-parameter test set. The analyzer is configured to

make the S_{21} measurements in the step mode with proper averaging. The radiation patterns of the antenna under test at multiple frequency points can be measured in a single rotation of the positioner using CREMASOFT.

The antenna set up for measuring the radiation pattern can be used for the measurement of gain using gain transfer method. A standard horn antenna is connected on the turn table and bore-sighted. A thru calibration is done in the Network Analyzer. Standard antenna is replaced with the test antenna and bore-sighted. The gain of the antenna is then the gain of the standard antenna added up to the reading on the Network Analyzer.

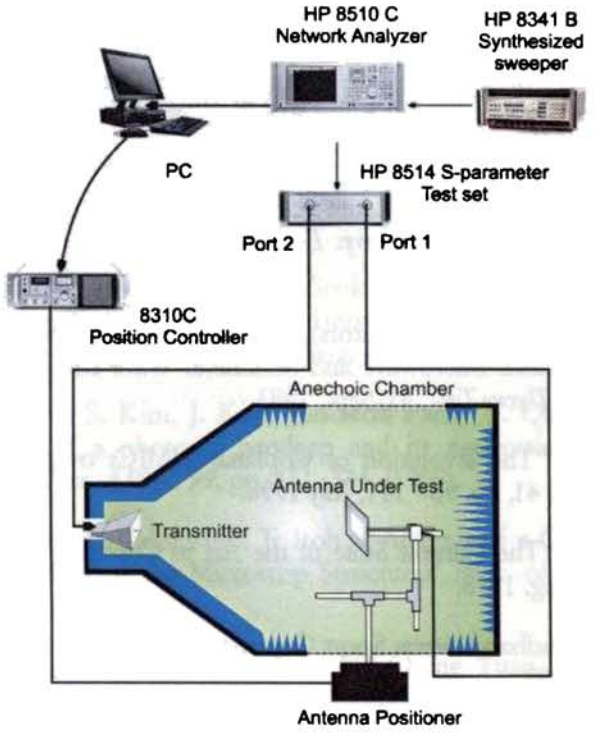

Figure 3.11.2 Measurement set up for Radiation Pattern and Gain

The experimental and theoretically predicted results are presented in detail in chapter 5.

References

1. R. M. Barrett and M. H. Barnes "Microwave Printed Circuits" *Radio T V News* **46**, 16 (1951).

2. D.D. Grieg, and H.F. Englemann *"Microstrip- A* new transmission technique for the kilomegacycle range" *Proc. IRE* . **40**, 1644-1650 (1952).

3. K.C. Gupta et al. *Microstrip Lines and Slotlines* 2nd ed., Norwood, MA: Artech House, (1996).

4. E. O. Hammerstad "Equations for Microstrip Circuit Design," *Proc. European Microwave Conf.*, 268–272 (1975).

5. Wheeler, H. A., "Transmission Line Properties of Parallel Strips Separated by a Dielectric Sheet," *IEEE Trans. Microwave Theory Tech*, **13**, 172–185 (1965)

6. C. P. Wen, "Coplanar Waveguide: A Surface Strip Transmission Line Suitable for Nonreciprocal Gyromagnetic Device Applications", *IEEE Trans. Microwave theory Tech.*, **17**, pp. 1087Ð1090, Dec. 1969.

7. J. L. B. Walker, "A Survey of European Activity on Coplanar Waveguide", *1993 IEEE MTT-S Int. Microwave Symp. Dig.*, **2**, pp. 693 - 696, Atlanta, Georgia, June 14-18, 1993.

8. A. K. Sharma and T. Itoh (Editors), Special Issue on Modeling and Design of Coplanar Monolithic Microwave and Millimeter-Wave Integrated Circuits, *IEEE Trans. Microwave Theory Tech.*, **41**, Sept. 1993.

9. T. Sporkmann, "The Evolution of Coplanar MMICs over the past 30 Years", *Microwave Journal*, **41**, pp. 96 - 111, July 1998.

10. T. Sporkmann, "The Current State of the Art in Coplanar MMICs" *Microwave J.*, **41**, pp. 60-74, Aug. 1998.

11. J. Browne, "Broadband Amps Sport Coplanar Waveguide", *Microwaves RF*, **26**, pp. 131-134, Feb. 1987.

12. Technology Close-Up, *Microwaves RF*, **27**, pp. 79, April 1988.

13. J. Browne, "Coplanar Waveguide Supports Integrated Multiplier Systems" *Microwaves RF*, **28**, pp.137-138, March 1989.

14. J. Browne, "Coplanar Circuits Arm Limiting Amp with 100-dB Gain," *Microwaves RF*, **29**, pp. 213-220, April 1990.

15. J. Browne, "Broadband Amp Drops through Noise Floor" Microwaves *RF*, **31**, pp. 141-144, Feb. 1992.

16. J. Browne, "Coplanar MIC AmpliPer Bridges 0.5 To 18.0 GHz," *Microwaves RF*, **26**, pp. 194*D*195, June 1987.

17. R. E. Stegens and D. N. Alliss, "Coplanar Microwave Integrated Circuit for Integrated Subsystems," *Microwave Sys. News Comm. Tech.*, **17**, pp. 84-96, Oct. 1987.

18. Wheeler, H. A., "Transmission Line Properties of a Strip on a Dielectric Sheet on a Plane," *IEEE Trans. Microwave Theory Tech.*, **25** , 631–647(1977).

19. Bahl, I. J., and D. K. Trivedi, "A Designer's Guide to Microstrip Line," *Microwaves*, **16**, pp. 174–182 (1977).

20. F.-R. Yang, K.-P. Ma, Y. Qian, and T. Itoh, "A Uniplanar Compact Photonic-Bandgap (UC-PBG) Structure and Its Applications for Microwave Circuits" *IEEE Trans. Microwave Theory Tech.*, **47**, pp. 1509-1514, (1999).

21. T.-Y. Yun and K. Chang, "One-dimensional photonic bandgap resonators and varactor tuned resonators," in *IEEE MTT-S Dig.* , pp. 1629–1632, (1999).

22. C. S. Kim, Jun-Seok Park,, D. Ahn, and J. B. Lim, "A novel 1-D periodic defected ground structure for planar circuits," *IEEE Microwave Guided Wave Lett.*, **10**, pp. 131–133, (2000).

23. Jong-Sik Lim, Ho-Sup Kim, Jun-Seok Park, Dal Ahn, and Sangwook Nam "A Power Amplifier with Efficiency Improved Using Defected Ground Structure" *IEEE Microwave and Wireless Components Letters*, **11**, 170-172, (2001).

24. J. I. Park, C. S. Kim, J. Kim, Jun-Seok Park,, Y. Qian, D. Ahn, and T. Itoh, "Modeling of a photonic bandgap and its application for the low-pass filter design," in *Proc. APMC'99*, pp. 331–334, (1999).

25. C, C, Chang., C, Caloz., and T, Itoh. : 'Analysis of a Compact Slot Resonator in the Ground Plane for Microstrip Structures' Proc. of APMC 2001, pp. 1100 – 1103, (2001).

26. Yun-Qi Fu, Guo-Hua Zhang, and Nai-Chang Yuan, "A Novel PBG Coplanar Waveguide" *IEEE Microw Wireless Comp. Lett.*, **11**, pp. 447–449, (2001).

27. Kane S Yee, "Numerical solution of Initial boundary value problems involving Maxwell's equations in isotropic media", *IEEE Trans. Antennas and Propagat.*, **14**, pp.302-307,(1966).

28. Allen Taflove and Morris E. Brodwin, "Numerical solutions of steady state electromagnetic scattering problems using the time–dependent Maxwell's equations", *IEEE Trans. Microwave Theory and Techn.*, **23**, pp.623-630, (1975).

29. Gerrit Mur, "Absorbing boundary conditions for the finite-difference approximation of the time -domain electromagnetic field equations", *IEEE Trans. Electromagnetic Compatibility*, **23**, pp.377-382, (1981).

30. Alain Reineix and Bernard Jecko, "Analysis of microstrip patch antennas using Finite -Difference Time -Domain method", *IEEE Trans. Antennas and Propagat.* **37**, pp.1361-1369, (1989).

31. David M. Sheen, Sami M. Ali, Mohamed D. Abouzahra and Jin Au Kong, "Application of the three –dimensional Finite-Difference Time–Domain method to the analysis of planar microstrip circuits", *IEEE Trans Antennas and Propagat.*, **38**, pp.849-857, (1991).

32. Raymond Lubbers, Li Chen ,Toru Uno and Saburo Adachi , " FDTD calculation of radiation patterns ,impedance and gain for a monopole antenna on a conducting box", *IEEE Trans. Antennas and Propagat* ., 40, pp.1577-1583, (1992).

33. Martin L. Zimmerman and Richard Q. Lee, "Use of the FDTD method in the design of microstrip antenna arrays", *Int. Journal of Microwave and Millimeter – Wave Computer Aided Eng.*, *4*, pp. 58-66, (1994).

34. A.Taflove, "Reinventing Electromagnetics: Emerging applications of FDTD computation, *IEEE Computational Science and Eng.*, pp.24-34, (1995).

35. R.J. Lubbers and H.S Langdon, "A simple feed model that reduces time steps needed for FDTD antenna and microstrip calculations", *IEEE Trans. Antennas and Propagat.*, **44**, pp.1000-1005, (1996).

36. Jose A.Perada *et al.*, :Numerical dispersion and stability analysis of the FDTD technique in lossy dielectrics", *IEEE Microwave and Guided wave Lett.* **8**, pp.245-248, (1998).

4

PLANAR FILTERS WITH PHOTONIC BAND GAP STRUCTURES – DESIGN & ANALYSIS

Contents

This chapter deals with the design and analysis of planar filters with Photonic Band Gap (PBG) structures at microwave regime. The filter property is studied for Microstrip Transmission Line, Coplanar Waveguide (CPW) and Asymmetric Coplanar Waveguide (ACPW). Equivalent circuit of the filters is extracted by simple circuit theory. Analysis of the filters is presented using Finite Difference Time – Domain Method (FDTD) and empirical relations are presented for the design. Validation is done by experiment are verified by Zeland's IE3D simulation software.

Periodic structures, some of which are known as photonic band gap(PBG) crystals finds foremost application in the optical frequency bands to control the light wave propagation, can also be scaled for use at microwave and millimeter-wave frequencies. With the properly designed PBG structure, the propagation of electromagnetic waves is forbidden in some specified frequency bands. In this work, a PBG structure is implemented with different geometric periodic patterns is used to improve the band stop characteristics.

Several designs of Photonic Crystals in the microwave region have been proposed using micro-machined dielectrics and holed ground plane in microstrip technology. The last approach is simpler to fabricate as well as compatible with monolithic technology with a deeper and wider frequency response in the rejected frequency band. The distance d between the centers of two adjacent etched circles is kept constant throughout the structure. In principle, only three rows of circles are necessary to implement the two-dimensional (2D) periodic pattern due to the high confinement of the fields around the conductor strip. On the top plane, there is a classical conductor strip having a width w corresponding to a characteristic impedance $Z_0 = 50\ \Omega$ for a conventional (unperturbed) microstrip line. This

microstrip PC can be analyzed like a single-mode Bragg reflector or grating satisfying the Bragg condition with guided wave number k in the perturbed microstrip line and d the period of the perturbation as

$$2\,d\sin\theta = n\,\lambda$$

When $\theta = 90^{\circ}$ and for the first mode

$$2d = n\lambda$$

$$2\cdot\frac{2\pi}{\lambda} = \frac{2\pi}{d}$$

So we have

$$2k = \frac{2\pi}{d} \qquad 4.1$$

and the guided wavelength λg is

$$\Rightarrow \lambda_g = 2d \qquad 4.2$$

The performance of this structure shows a deep and broad rejected frequency band around the design frequency. In a microstrip PC band reflector, there is a design trade-off since the bigger the circle radius, the higher the rejection amplitude and bandwidth, but also the more reinforced the amplitude of the side lobes and, therefore, the pass-band ripple. This concept of band rejection is studied in detail in this chapter.

4.1 Bandgap and Optimization of PBG parameters - Experiment, Simulation, Design and Theoretical Analysis

Filtering action on Microstrip Line can be achieved by etching or drilling periodic patterns in the ground plane of a 50 Ω microstrip line and the stop band centre frequency is a function of the period d of the structure and it acts a PBG structure. Radisic et al ; optimized the aspect ratio r/d for a 2D square lattice with circles etched in the ground plane of a microstrip transmission line as r/d = 0.25, r being the radius of the circle etched. Using equation (4.1) one can predict the cut-off

frequency for a given period or vice versa. The geometry of the perturbed transmission line with Photonic Band Gap structures is shown in Figure 4.1.1. The periodic patterns etched could be of any shape as this would disturb the electric field distribution and thus give PBG property.

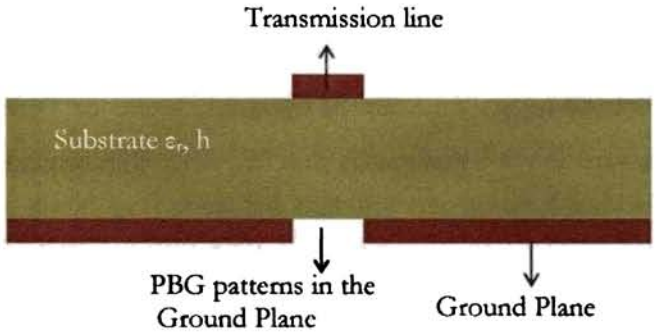

Figure 4.1.1. Transmission Line with PBG backing

A typical transmission line with PBG structures in the ground plane as shown in Figure 4.1.2 is studied in detail.

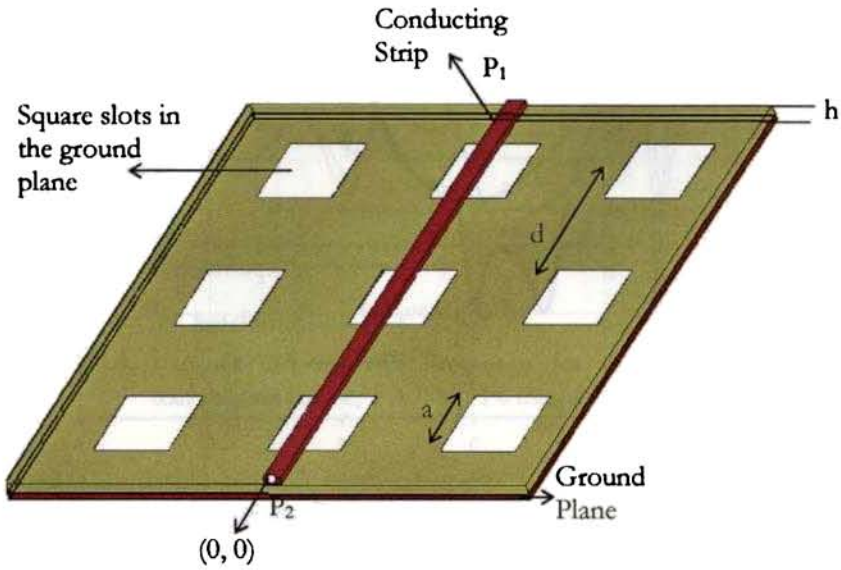

Figure 4.1.2. Microstrip Line with square shaped slots as PBG in the ground plane

For ease of fabrication square slots with dimension '*d*' are etched in the ground plane of a 50 Ω microstrip line on a substrate with dielectric constant ε_r = 4.7 and thickness h = 1.6mm.

Using equation (4.1) the cut-off frequency for a period *d* = 30 mm in this substrate would be 2.3 GHz. The simulated and measured S-parameters showed the stop band to be centered on 2.9 GHz with area of the square equivalent to a circle with $r = 0.25d$. The simulated and experimental results are analyzed by finite Difference Time – Domain (FDTD) method. The variation of S-parameters with frequency is shown in Figure 4.1.3.

The figure confirms the existence of band gap in the transmission characteristics with a shift in the pole frequency. The return loss in the stop band is ~ 0 dB confirming the band gap. As per equation (4.1) the pole frequency should be 2.4 GHz but experimental results showed it to be at 2.9 GHz. The experimental and simulated results are in good agreement. This aspect is discussed in detail and a correction is applied in the later part of the thesis.

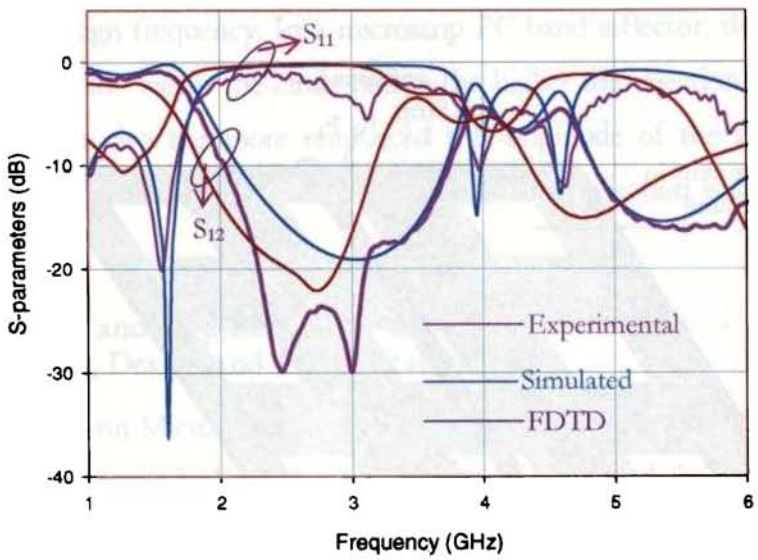

Figure 4.1. 3. Variation of S-parameters with Frequency with square shaped periodic perforations in the ground plane *d* = 30 mm, $\frac{a}{d}=0.44$, ε_r = 4.7 h = 1.6 mm

4.1.1 Effect of the position of the transmission line

The effect of the position and orientation of the transmission line with respect to the PBG ground plane is studied. When the transmission line was just above the centre of PBG structures in the ground plane, the S_{21} characteristics showed reasonable width and depth in the stop band. As the transmission line got shifted from the centre of the PBG structure the stop band depth and width are found to decrease. Figure 4.1.4 shows the S_{12} of the PBG structure for different position of the transmission line with respect to the PBG structure in the ground plane. So it could be concluded that the maximum bandwidth with reasonable rejection in S_{21} is observed with the transmission line exactly at the centre of the PBG cells in the ground plane.

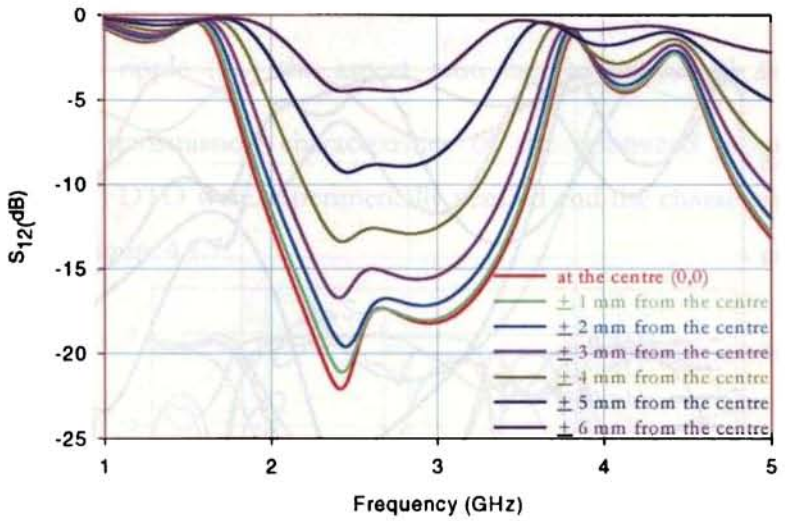

Figure 4.1.4. Variation of S_{21} with Frequency for different position of the transmission line $\varepsilon_r = 4.7$, h = 1.6 mm, $d = 30$ mm, $r = 0.25$d

4.1.2 Optimization of Aspect Ratio

Squares of different size (the lattice constant) *'a'* for a particular period were simulated to optimize the band gap performance. The stop band effect of the

PBG structure for different aspect ratio $\frac{a}{d}$ was studied. For small size of the square the stop band is very small. In the limiting case $a \to 0$; $\frac{a}{d} \to 0$ there is no stop band and the structure behaved as a standard microstrip line, as expected. As the square dimension is increased the stop band becomes more distinctive. For very large $\frac{a}{d}$, ripples in the pass band is found to increase. Figure 4.1.5 shows the S_{12} of the PBG structure for different aspect ratios.

On a close look to the reflection characteristics obtained for these structures, plotted in Figure 4.1.6 a perfect reflection characteristic is seen for an aspect ratio $\frac{a}{d}$=0.44 .

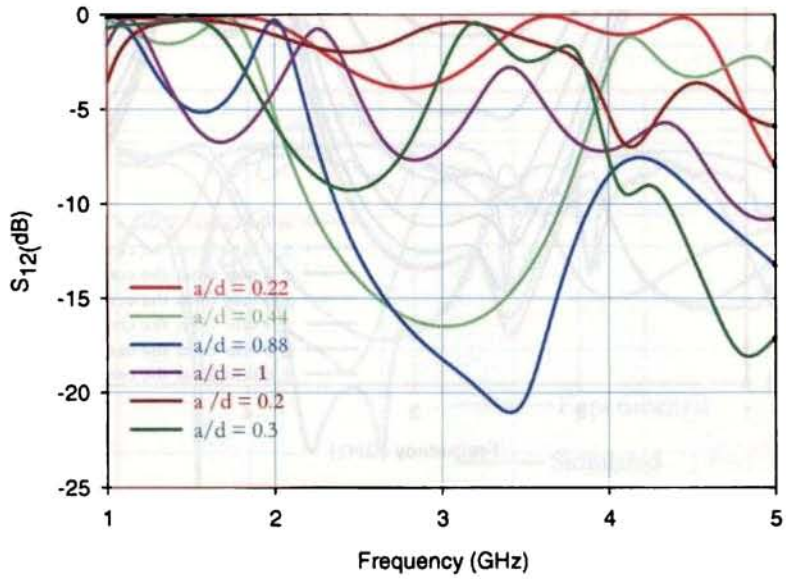

Figure 4.1.5. Variation of Transmission characteristics with Frequency for different aspect ratio ε_r = 4.7, h = 1.6 mm, d = 30 mm

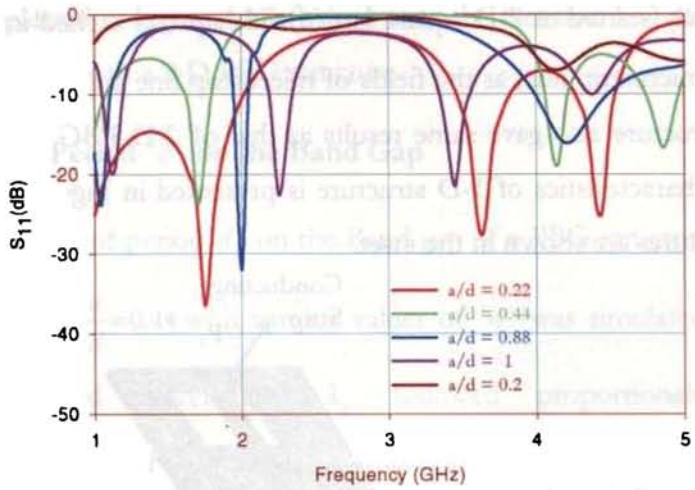

Figure 4.1.6. Variation of S_{11} with Frequency with Frequency for different aspect ratio $\varepsilon_r = 4.7$, h = 1.6 mm, d = 30 mm

Though $\frac{a}{d}=0.88$ gave wide stop band the pass band ripple was more in this case. So considering the fact that PBG should give significant stop band depth (S_{12}) with less pass band ripple (S_{11}) the aspect ratio can be optimized as $\frac{a}{d}=0.44$. The reflection and transmission characteristics of the optimized ground plane by simulation and FDTD were experimentally verified and the characteristic obtained is depicted in Figure 4.1.7.

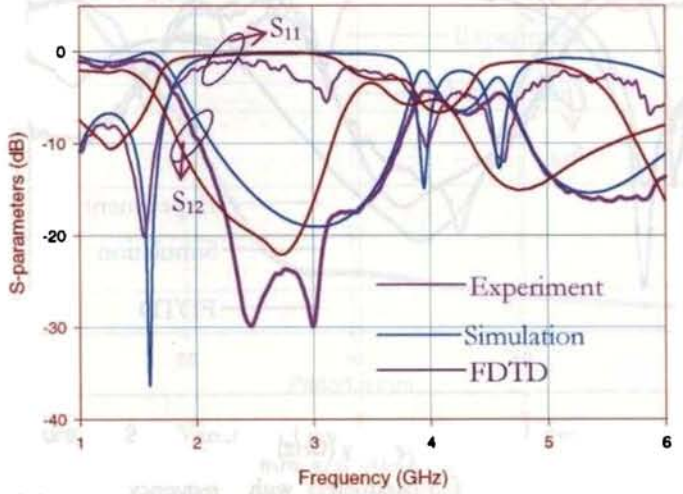

Figure 4.1.7 Variation of S-parameters with Frequency d = 30 mm, $\frac{a}{d}=0.44$, $\varepsilon_r = 4.7$, h = 1.6 mm

Though the study started in 2-D square lattice with squares etched in the ground plane of 50 Ω microstrip line; as the fields of microstrip line are concentrated near the line 1-D structure also gave same results as that of 2-D PBG structures. The geometry and characteristics of 1-D structure is presented in Figure 4.1.8 and the respective structures are shown in the inset.

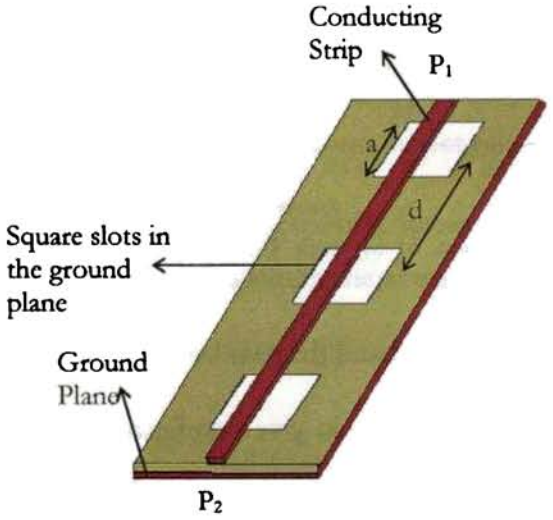

Figure 4.1.8(a) Geometry 1-D PBG structures

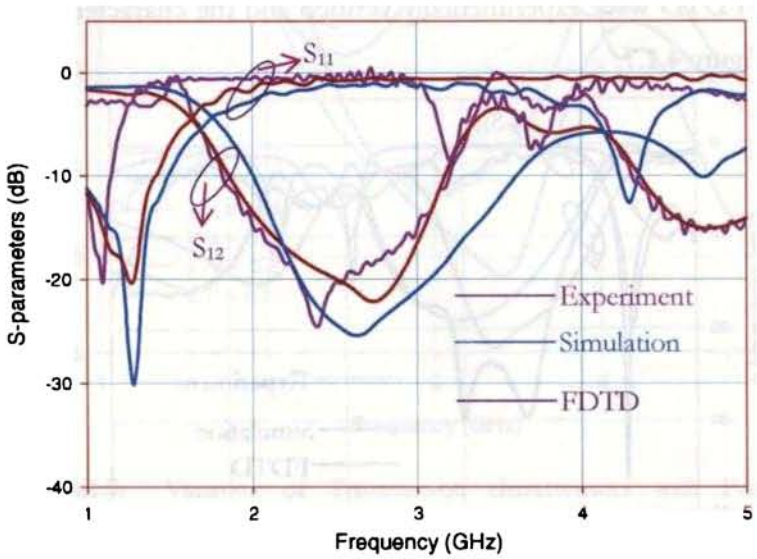

Figure 4.1.8(b) Variation of S-parameters with Frequency for 1-D PBG structures d = 30 mm, $\frac{a}{d} = 0.44$, ε_r = 4.7, h = 1.6 mm

The results plotted in Figure 4.1.9 (b) points to the fact that 1-D structure behaves more or less similar to a 2-D PBG structure.

4.1.3 Effect of Period 'd' on the Band Gap

To find the effect of period'd' on the Band gap of a PBG structure; square lattice with aspect ratio $\frac{a}{d}$=0.44 with various values of 'd' was simulated. It was found that the guided wavelength λ_g followed proportionality with the period'd'$\Rightarrow \lambda_g \propto d$. Experimental verification pointed to the same results as obtained by simulation. So it could be inferred that the location of the band gap is decided by the period'd' of the PBG structure and the depth of the band gap by the aspect ratio$\frac{a}{d}$. Plot of the dependence of the stop band centre frequency on the period is depicted in Figure 4.1.9.

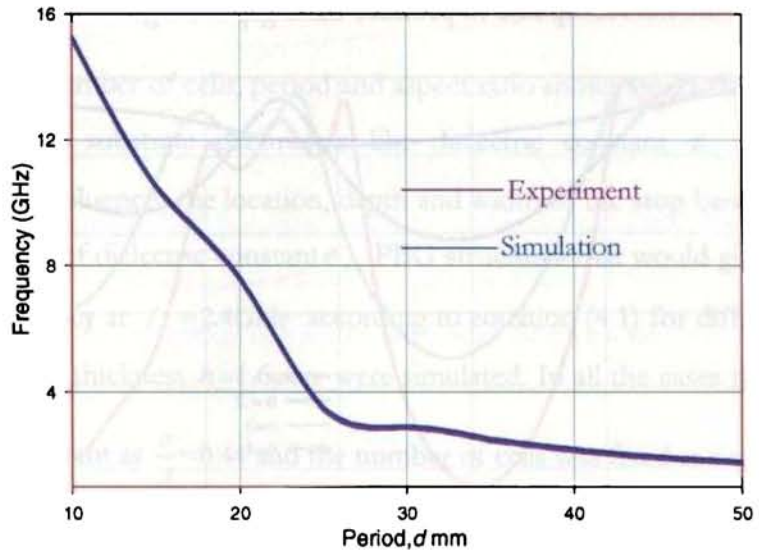

Figure 4.1.9. Variation of cut-off frequency with period ε_r = 4.7, h = 1.6 mm, a/d =0.44

This again confirms that there is a close agreement between experiment and simulation. It I s also noted that there is much disagreement in the pole frequency obtained experimentally and that predicted from equation (4.2).

4.1.4 Effect of Number of Perforations *'n'*

How many periodic cells are needed in a PBG structure for significant stop band is studied in detail in this section. The depth of rejection in the transmission characteristics is found to increase with number of cells *n*. The depth of stop band with number of cells is as shown in Figure 4.1.10. From exhaustive experimental and simulation studies, a linear relation is derived between the depth of rejection at the stop band centre frequency $S_{12}\,(dB)$ and the number of cells *n* given as

$$S_{12} = 4.16 + (-6.89)\,n \qquad 4.3$$

Equation (4.3) can predict the transmission coefficient for a given number of cells or vice versa with precision. It is found that more than one cell is needed in the ground plane of the microstrip line to produce band gap for a given PBG structure.

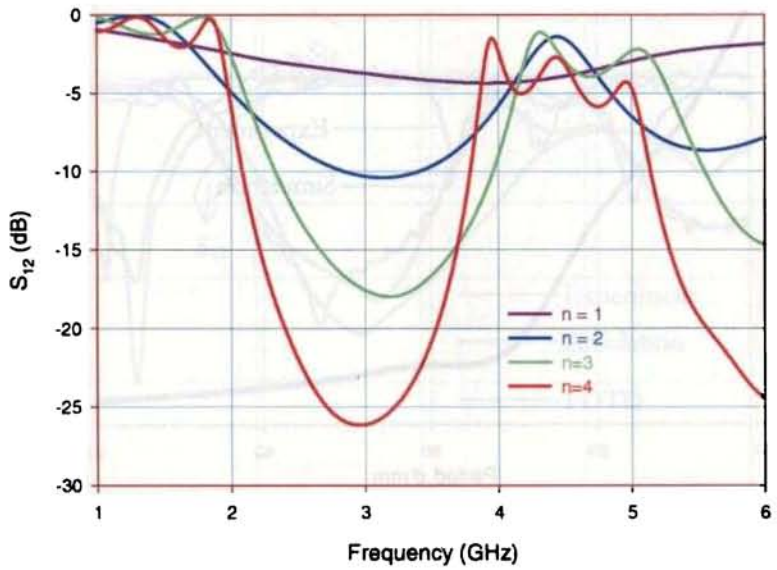

Figure 4.1.10. Depth of rejection with number of cells experimental ε_r = 4.7, h = 1.6 mm, *d* = 30 mm

The depth of rejection predicted from equation (4.3) and that obtained by experiment is presented in Table 4.1.11. As the number of cells increases the depth of rejection also increases and when $n=\infty$ we have $S_{12}=\infty$ which points to a complete band gap as explained by Joannopoulos.

No: of cells (n)	Rejection Depth	
	Predicted as per equation (4.3)	experiment
1	-2.7	-3.7
2	-9.6	-10
3	-16.5	-17
4	-23.4	-26
5	-30.3	-30
6	-37.9	-34

Table 4.1.11. Depth of rejection with number of cells $\varepsilon_r = 4.7$, h = 1.6 mm, $d = 30$ mm

4.1.5 Effect of Substrate Parameters on Band Gap

Though the number of cells, period and aspect ratio shows similar behavior in each substrate; the substrate parameters like dielectric constant ε_r and substrate thickness h influences the location, depth and width of the stop band. To ascertain the influence of dielectric constant ε_r, PBG structures that would give a stop band centre frequency at $f_c = 2.4GHz$ according to equation (4.1) for different dielectric materials with thickness $h=1.6\,mm$ were simulated. In all the cases the aspect ratio was kept constant as $\frac{a}{d}=0.44$ and the number of cells was fixed as $n=3$.

The microstrip line was fabricated to have characteristic impedance $Z_0=50\Omega$ with respect to the dielectric constant ε_r of the host material. More over, for a substrate to show PBG properties the dielectric constant between the etched and the un-

etched portion of the substrate should be in the ratio $\geq 2:1$. For this reason substrate having dielectric constant $\varepsilon_r \geq 4$ is only considered for the study. For all the materials under study it was found that the stop band centre frequency f_c was centered around 3 GHz and not at 2.4 GHz as predicted from equation (4.1). The pole frequency is found to decrease with the dielectric constant.

The results obtained are shown in Figure 4.1.12. $\Rightarrow$ This shows that equation (4.1) needs a correction for precise prediction of the stop band centre frequency.

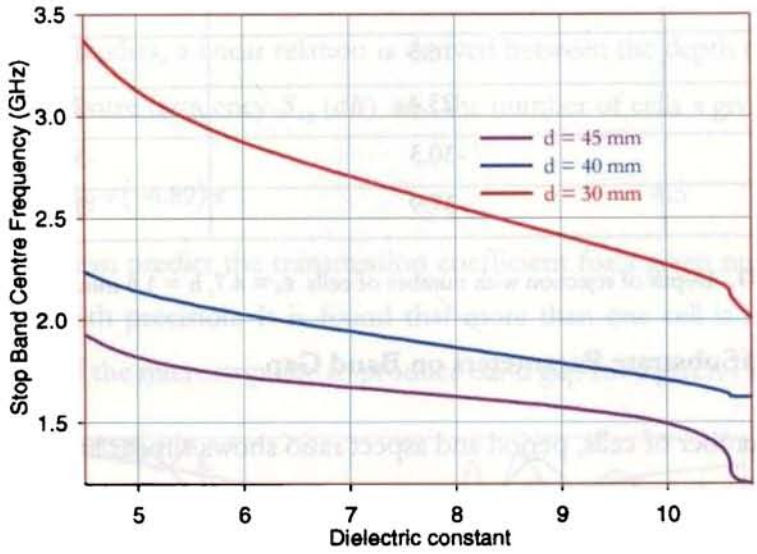

Table 4.1.12. Dependence of stop band centre frequency f_c on dielectric constant for h = 1.6 mm

When the substrate thickness was varied the width and depth of the stop band was influenced considerably. The cut-off frequency f_c is found decreasing with increase of substrate thickness. But for thick substrates cut-ff frequency is virtually independent of the thickness of the substrate. A 50 Ω microstrip line was fabricated on each of the substrate with different thickness h for a particular dielectric constant ε_r. Thick substrates are found to have narrow stop band compared to thin substrates.

The influence of substrate thickness on the PBG characteristics is shown in Figure 4.1.13.

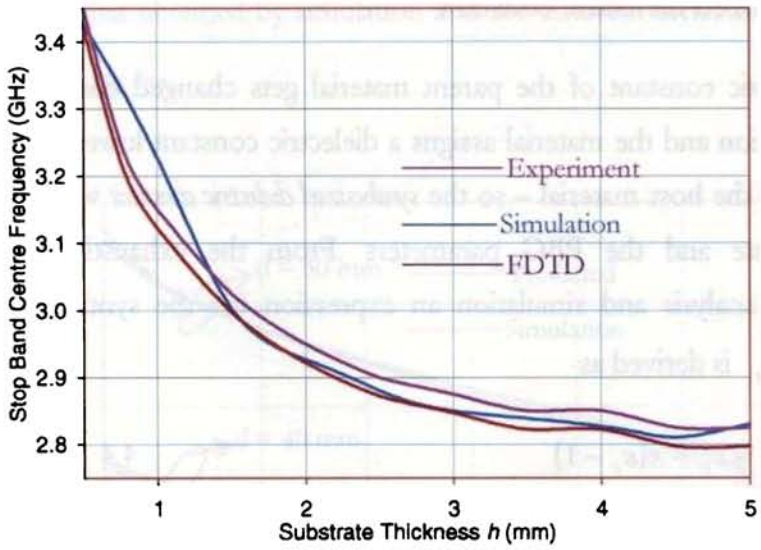

Figure 4.1.13. Variation of stop band centre frequency f_c with substrate thickness for $\varepsilon_r = 4.36$, d = 30mm, $a/d = 0.44$.

In all the cases, the stop band central frequency by experiment, simulation and FDTD are in close agreement. But there is a considerable shift in the stop band centre frequency f_c from equation (4.1) which points that a correction is needed for precise prediction of f_c. When etched with periodic patterns in the ground plane of a microstrip line, a dielectric contrast is achieved between the etched and un-etched portion of the substrate due to the fringing of electric field. That means some of the electric and magnetic fields are lying surrounding air medium in the slots. This will reduce the effective dielectric constant of the substrate. This shows that a variation occurs for the dielectric constant when the substrate is having periodic perforations in the ground plane. So for the accurate prediction of f_c, instead of dielectric constant ε_r, corrected or *synthesized dielectric constant* ε_{rs} has to be used. The synthesized dielectric constant has to be a function of the substrate

and the PBG parameters. This dielectric constant the substrate achieves as a result of periodic perforations is presented in the following section.

4.2 Synthesized dielectric constant

The dielectric constant of the parent material gets changed due to the periodic etched portion and the material assigns a dielectric constant lower to the dielectric constant of the host material – so the *synthesized dielectric constant* which is related to the substrate and the PBG parameters .From the exhaustive experimental, theoretical analysis and simulation an expression for the synthesized dielectric constant ε_{rs} is derived as

$$\varepsilon_{rs} = \varepsilon_r - x(\varepsilon_r - 1) \qquad 4.4$$

ε_{rs} is the synthesized dielectric constant, ε_r is the relative dielectric constant of the substrate and x is the correction factor dependent on the area of the etched portion and the period. The correction factor x is given as,

$$x = k\left(\frac{W}{h}\right)\left(\frac{A}{d^2}\right) \qquad 4.5$$

W is the width of the transmission line and A is the area of the etched portion. Value of k is dependent on the dielectric constant of the parent material,

$$\begin{aligned} &k = 1.25 \; for \; \varepsilon_r \le 6.2 \\ &k = 1.85 \; for \; 6.2 \le \varepsilon_r \le 9.8 \\ &k = 2.45 \; for \; \varepsilon_r \ge 9.8 \end{aligned} \qquad 4.6$$

Appling this correction to equation (3.3) leads to more accurate prediction of stop band centre frequency. Since the above expression is a function of the area of the

etched portion rather than the shape it holds good for any arbitrary shaped geometry in the ground plane. The pole frequency predicted using the equation is compared with that obtained by simulation and for different dielectric constant is depicted in Figure 4.2.1.

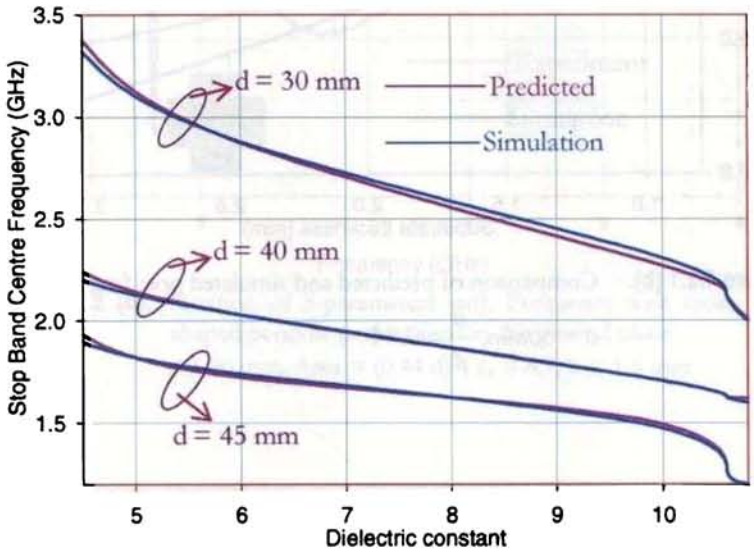

Figure 4.2.1 (a). Comparison of predicted and simulated pole frequency

h = 1.6 mm, $\frac{a}{d} = 0.44$

To verify the shift in the cut-off frequency different geometrical shapes having same area as that of the square ($a = 0.44\ d$) was simulated and studied experimentally. S-parameter characteristics shows almost identical behavior as compared with square patterns for ground planes with periodic patterns of different shapes and is plotted in Figure4.2.2. The geometrical shape for the periodic slots used in the study is shown in the inset.

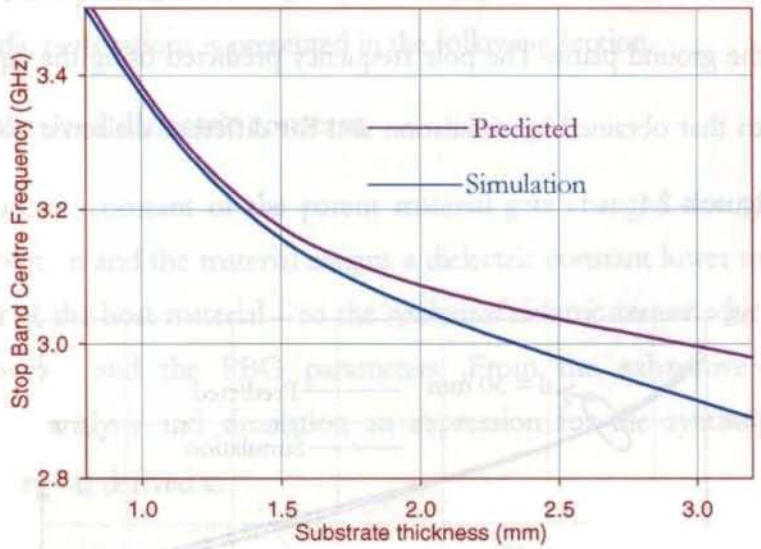

Figure 4.2.1 (b). Comparison of predicted and simulated pole frequency

d = 30mm, $\frac{a}{d} = 0.44$

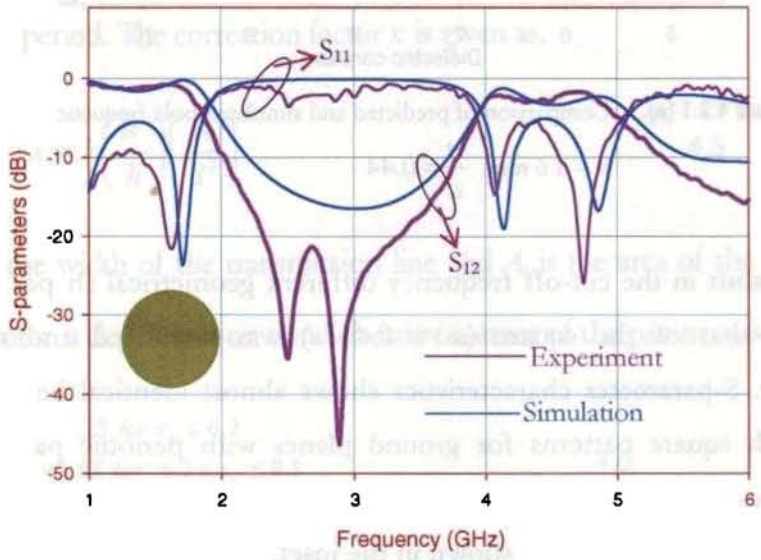

Figure 4.2.2 (a). Variation of S-parameters with Frequency with circular periodic perforations in the ground plane d = 30 mm, Area = $(0.44\ d)^2$, ε_r = 4.7 h = 1.6 mm

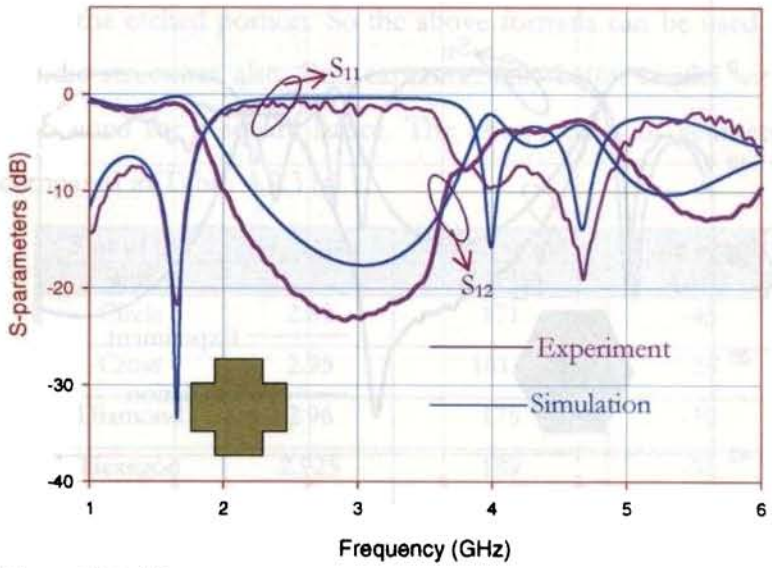

Figure 4.2.2 (b). Variation of S-parameters with Frequency with cross-shaped periodic perforations in the ground plane d = 30 mm, Area = (0.44 d)^2, ε_r = 4.7, h = 1.6 mm

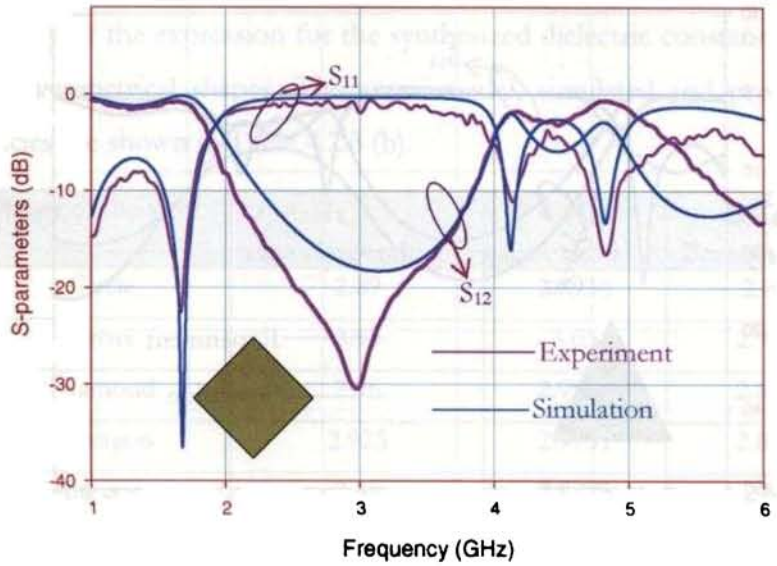

Figure 4.2.2 (c). Variation of S-parameters with Frequency with diamond-shaped periodic perforations in the ground plane d = 30 mm, Area = (0.44 d)^2, ε_r = 4.7, h = 1.6 mm

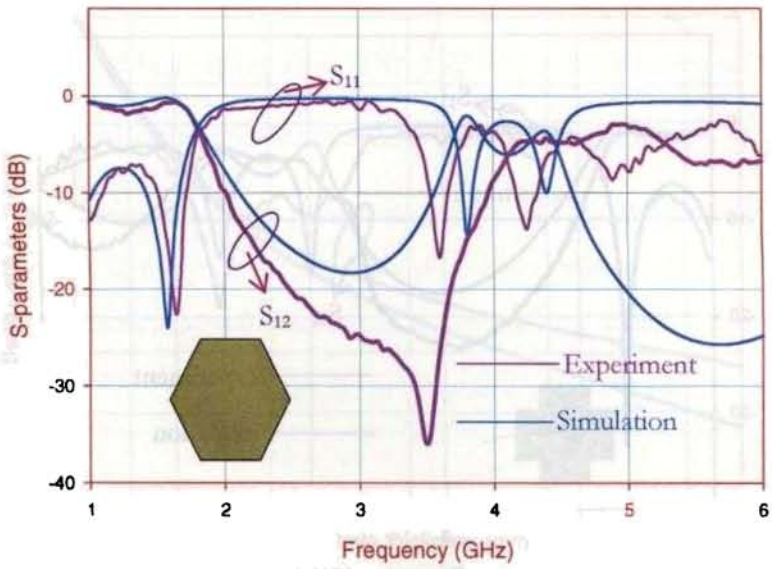

Figure 4.2.2 (d). Variation of S-parameters with Frequency with hexagonal-shaped periodic perforations in the ground plane d = 30 mm, Area = (0.44 d)^2, ε_r = 4.7, h = 1.6 mm

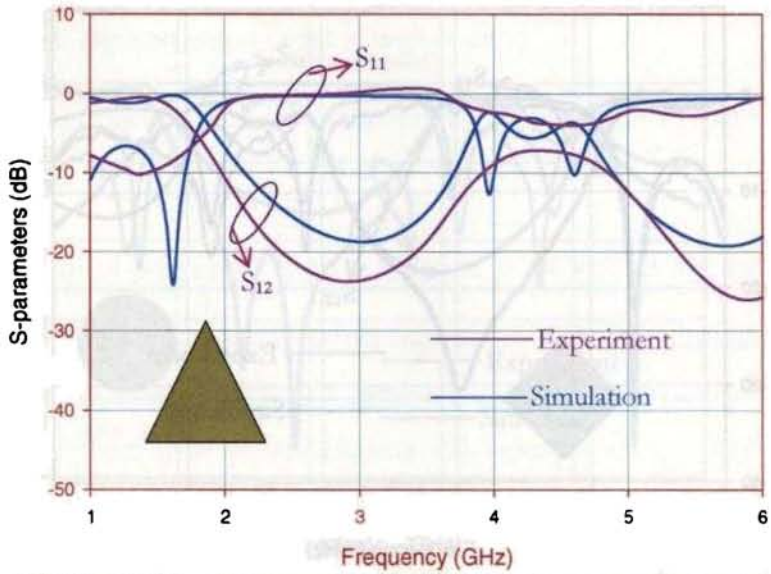

Figure 4.2.2 (e). Variation of S-parameters with Frequency with triangular-shaped periodic perforations in the ground plane d = 30 mm, Area = (0.44 d)^2, ε_r = 4.7, h = 1.6 mm

From the above observations, it is concluded that the pole frequency is controlled by the area of the etched portion. So the above formula can be used for arbitrary shaped periodic structures also. But, experimentally better results with minimum ripple are obtained for a square lattice. The observations of geometrical shaped slots are compared in Table. 4.2.3 (a).

Slot of the slot	f_c GHz	Band width (MHz)	Pole depth (dB)
Circle	2.89	171	-45
Cross	2.95	161.5	-23
Diamond	2.96	175	-30
Hexagon	2.925	189	-35
Square	2.89	175	-39
Triangle	2.995	170	-23

Table 4.2.3(a). Comparison of predicted and simulated pole frequency for different PBG structures $\varepsilon_r = 4.7$, h = 1.6 mm, d = 30 mm, Area = $(0.44\ d)^2$

The validity of the expression for the synthesized dielectric constant is verified for different geometrical shapes. The experimental, simulated and predicted cut-off frequencies are shown in Table 4.2.3 (b).

Shape of the slot	f_c GHz experimental	f_c GHz simulated	f_c GHz Present model
Circle	2.89	2.8936	2.899
Cross	2.95	3.03	2.9034
Diamond	2.96	2.9596	2.8986
Hexagon	2.925	2.9751	2.8986
Square	2.89	2.8875	2.889
Triangle	2.995	2.9947	2.95

Table 4.2.3(b). Comparison of predicted and simulated pole frequency for different PBG structures $\varepsilon_r = 4.7$, h = 1.6 mm, d = 30 mm, Area = $(0.44\ d)^2$

The observed results validate the expression for the synthesized dielectric constant for any geometrical shaped PBG lattice in the ground plane of the microstrip line. In all the cases the experimental and predicted pole frequency are in good agreement and the maximum error is < 2%. This establishes the concept of synthesized dielectric constant and can be conveniently used for the design of PBG structured Microstrip line.

The band stop characteristics for these optimized parameters for different period are shown in the Figure 4.2.4.

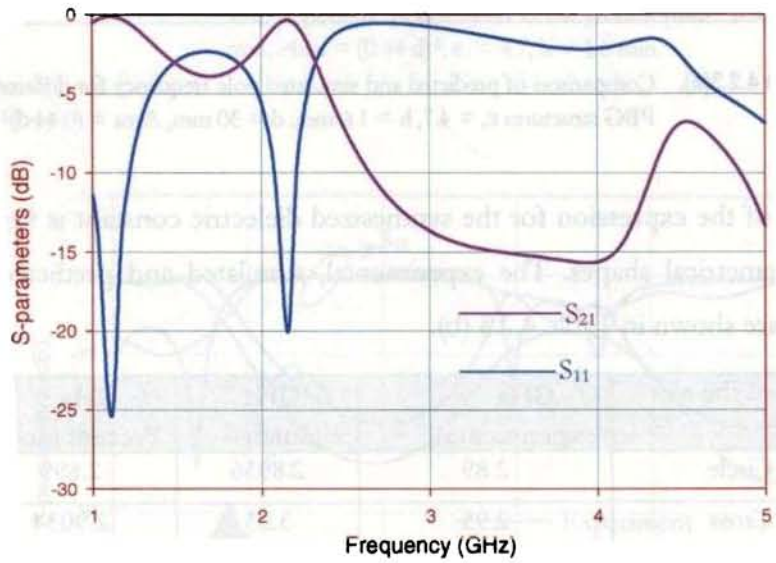

Figure 4.2.4 (a). Variation of S-parameters with Frequency with square-shaped periodic perforations in the ground plane d = 23 mm, Area = $(0.44\ d)^2$, ε_r = 4.7, h = 1.6 mm

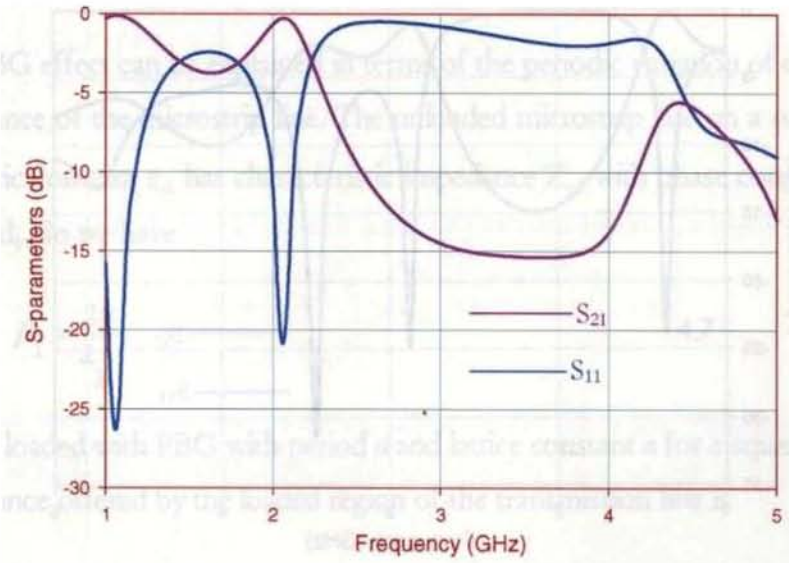

Figure 4.2.4 (b). Variation of S-parameters with Frequency with square-shaped periodic perforations in the ground plane d = 25 mm, Area = $(0.44\ d)^2$, $\varepsilon_r = 4.7$, h = 1.6 mm

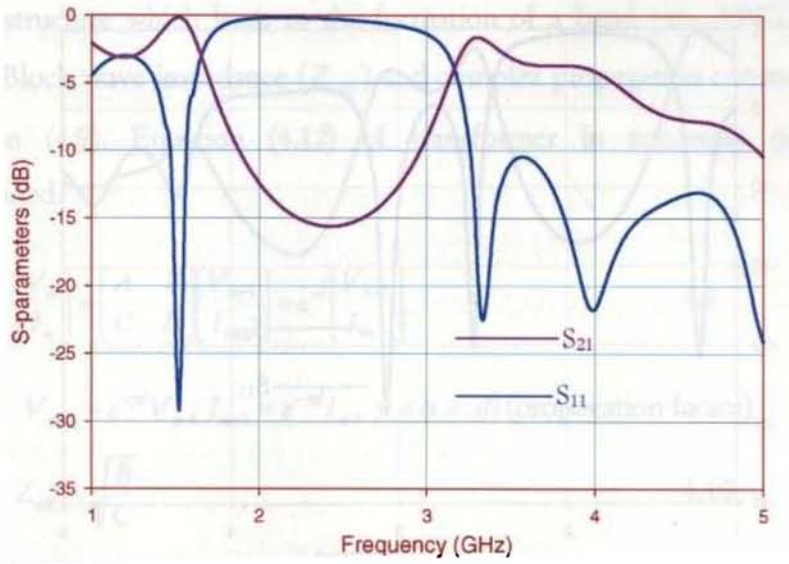

Figure 4.2.4 (c). Variation of S-parameters with Frequency with square-shaped periodic perforations in the ground plane d = 35 mm, Area = $(0.44\ d)^2$, $\varepsilon_r = 4.7$, h = 1.6 mm

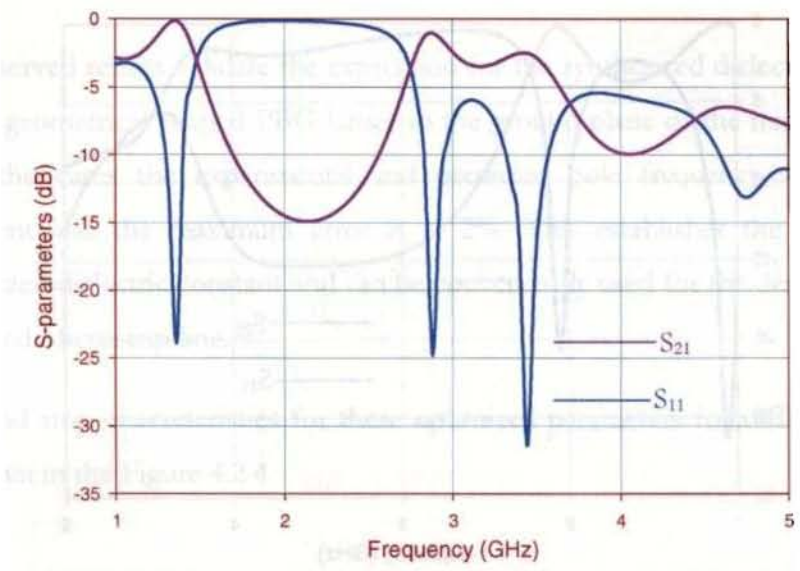

Figure 4.2.4 (d). Variation of S-parameters with Frequency with square-shaped periodic perforations in the ground plane d = 40 mm, Area = (0.44 d)^2, ε_r = 4.7, h = 1.6 mm

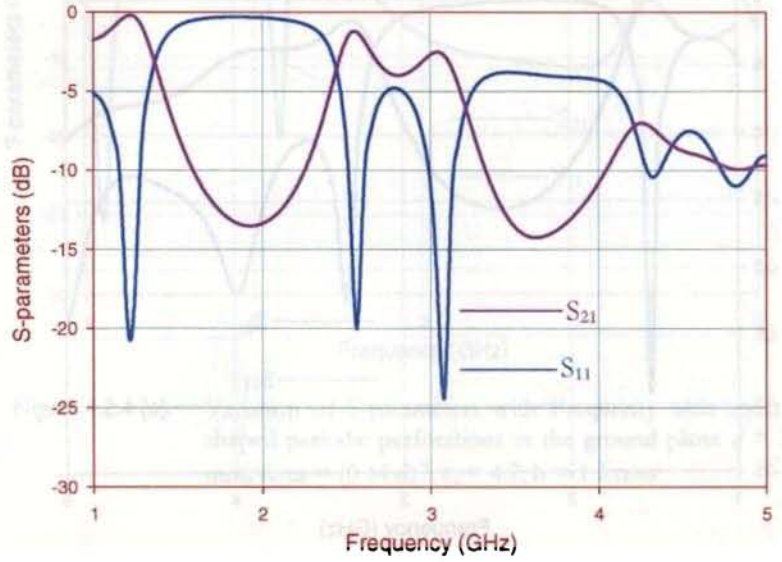

Figure 4.2.4 (e). Variation of S-parameters with Frequency with square-shaped periodic perforations in the ground plane d = 45 mm, Area = (0.44 d)^2, ε_r = 4.7, h = 1.6 mm

4.3 Formation of Band Gap

The PBG effect can be explained in terms of the periodic variation of characteristic impedance of the microstrip line. The unloaded microstrip line on a substrate with dielectric constant ε_{r1} has characteristic impedance Z_{o1} with phase constant β_1 for a length d_1. So we have

$$\beta_1 = \frac{2\pi}{\lambda_g} \qquad 4.7$$

When loaded with PBG with period d and lattice constant a for a square lattice, the admittance offered by the loaded region of the transmission line is

$$Y = jY_o \tan(\beta_1 a) \qquad 4.8$$

Thus the PBG loaded transmission line has a periodic change in the characteristic impedance. The applied signal experiences periodic low-high impedance along the planar structure which leads to the formation of a band gap. ABCD parameters define Bloch wave impedance (Z_{cell}) and complex propagation constant written as equation (4.9). Equation (4.12) of transformer in scattering parameters is determined.

$$\begin{bmatrix} V_n \\ I_n \end{bmatrix} = \begin{bmatrix} A & B \\ C & D \end{bmatrix} \begin{bmatrix} V_{n+1} \\ I_{n+1} \end{bmatrix} = e^{\gamma d} \begin{bmatrix} V_{n+1} \\ I_{n+1} \end{bmatrix} \qquad 4.9$$

Where $V_{n+1} = e^{-\gamma d} V_n$, $I_{n+1} = e^{-\gamma d} I_n$, $\gamma = \alpha + j\beta$ (propagation factor)

$$Z_{cell} = \sqrt{\frac{B}{C}} \qquad 4.10$$

From the ABCD parameters we have the propagation constant 'γ' is given as

$$\cosh \gamma d = \cosh \alpha d \cos \beta d + j \sinh \alpha d \sin \beta d = \frac{A + D}{2} \qquad 4.11$$

The S-parameters are given as

$$\begin{bmatrix} S_{11} & S_{12} \\ S_{21} & S_{22} \end{bmatrix} = \begin{bmatrix} \dfrac{A+\dfrac{B}{Z_0}-CZ_0-D}{A+\dfrac{B}{Z_0}+CZ_0+D} & \dfrac{2(AD-BC)}{A+\dfrac{B}{Z_0}+CZ_0+D} \\ \dfrac{2}{A+\dfrac{B}{Z_0}+CZ_0+D} & \dfrac{-A+\dfrac{B}{Z_0}-CZ_0+D}{A+\dfrac{B}{Z_0}+CZ_0+D} \end{bmatrix} \quad 4.12$$

For a propagating wave in the periodic structure we have a low pass band when $\alpha = 0, \beta \neq 0$. When $\alpha \neq 0, \beta = 0, \pi$ the wave doesn't propagate and results in a stop band.

4.4 Resonance of PBG cells

The transmission characteristics of a PBG backed microstrip line show a stop band which points to the formation of a resonant block. According to transmission line theory if the values of inductance L and Capacitance C are varied periodically, the transmission line can exhibit band stop characteristics. So it is possible to derive an L-C equivalent circuit for the PBG cell and by connecting identical cells in series, the periodic structure exhibits band stop characteristics. The effective capacitance C_{eff} and inductance L_{eff} of the PBG backed transmission line with n number of cells of any arbitrary area A and periodicity d on a substrate with dielectric constant ε_r is

$$C_{eff} = \frac{\varepsilon_0 \varepsilon_r A}{d} \quad 4.13$$

$$L_{eff} = k n^2 \sqrt{\frac{a}{d}} \mu_0 h \left(\frac{a}{d-a} \right) \quad 4.14$$

ε_0 and μ_0 are the permittivity and permeability of free space, a is the maximum perturbation width of the unit cell and h is the substrate height. The correction factor k is calculated as

$$k = 1.25 \text{ for } \varepsilon_r \leq 6,$$
$$k = 1.2 \text{ for } 6 \leq \varepsilon_r \leq 9.8 \qquad 4.15$$
$$k = 0.74 \text{ for } \varepsilon_r \geq 9.8$$

Then the stop band center frequency can be calculated from the equation,

$$f_o = \frac{1}{2\pi\sqrt{L_{eff} C_{eff}}} \qquad 4.16$$

and the -10 dB bandwidth is given as

$$\Delta f = f_0 \frac{\sqrt{\frac{L_{eff}}{C_{eff}}}}{\eta} \qquad 4.17$$

η is the characteristic impedance of free space. Lower and upper cut of frequencies is then

$$f_1 = f_0 - \frac{\Delta f}{2} \qquad f_2 = f_0 + \frac{\Delta f}{2} \qquad 4.18$$

These equations help in an ease to predict the frequency response if physical parameters are known or vice versa. The reactance part is neglected assuming negligible conductor loss. The reflection and transmission characteristics obtained from the present model are in accord with that obtained by experiment and simulation thus validating the model. In experiment, simulation and present model S_{11} is found to be ~ 0 dB in the entire -10 dB stop band of S_{21} which shows that there is little radiation loss and thus confirms PBG property in design and analysis. The equivalent circuit is presented in Figure 4.4.1.

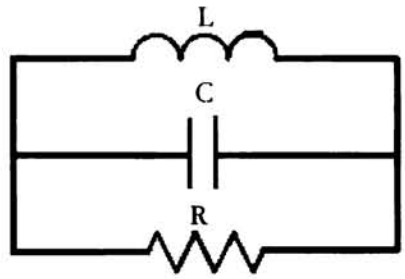

Figure 4.4.1. Equivalent circuit of the PBG cell

The stop band characteristics obtained for 2D square lattice in the ground plane is shown in Figure 4.4.2 (a). The calculated effective capacitance C_{eff} and inductance L_{eff} of the PBG backed transmission line is used to simulate the equivalent model in Figure 4.4.1 and this variation is plotted in Figure 4.4.2 as present model.

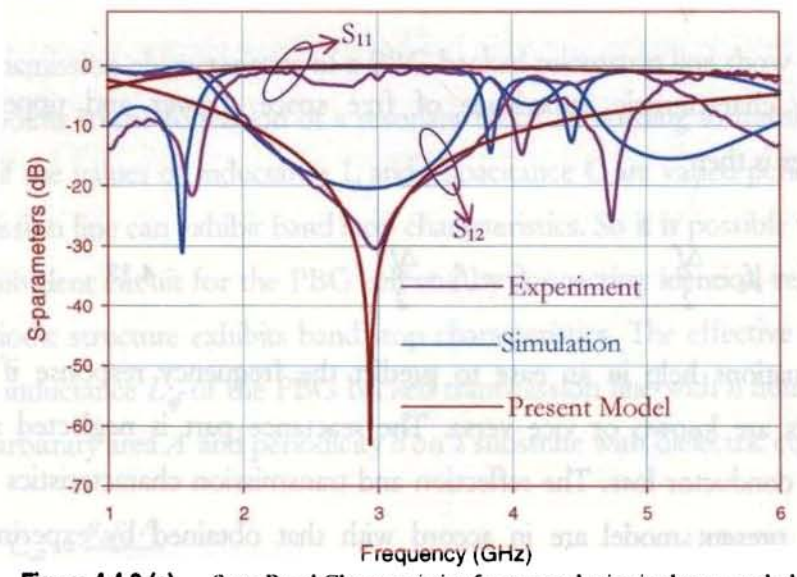

Figure 4.4.2 (a) Stop Band Characteristics for square lattice in the ground plane, ε_r = 4.7, h = 1.6mm, d = 30mm, n = 3, A = 176.625 mm^2

For all the periodic structures S-parameter characteristics shows almost identical behavior. Simulated values of cut-off frequency and -10 dB bandwidth are found to be in good agreement with the predicted values and these results are tabulated in Table.4.4.2 (b).

Slot Geometry	Stop band		
	Experimental	IE3D	Present model
Circle	2.05 – 3.765	2.1 – 3.675	2.04 – 4.23 (same for all geometries)
Cross	2.015 -3.66	2.2 – 3.65	
Diamond	2.085 -3.835	2.1 – 3.742	
Hexagon	2.015 -3.94	2.05 – 3.62	
Square	2.05 -3.730	2.0 – 3.575	
Triangle	1.98 -3.8	2.0 – 3.85	

Table 4.4.2 (b) -10 dB bandwidth obtained for different slot geometries
$\varepsilon_r = 4.7$, h = 1.6mm, d = 30mm, n = 3, A = 176.625 mm²

Variation of stop band center frequency with dielectric constant is studied. Results obtained by IE3D simulation is compared with the numerically predicted values and is plotted in Figure 4.4.3 (a). The predicted and simulated -10 dB bandwidths are shown in Table.4.4.3 (b).

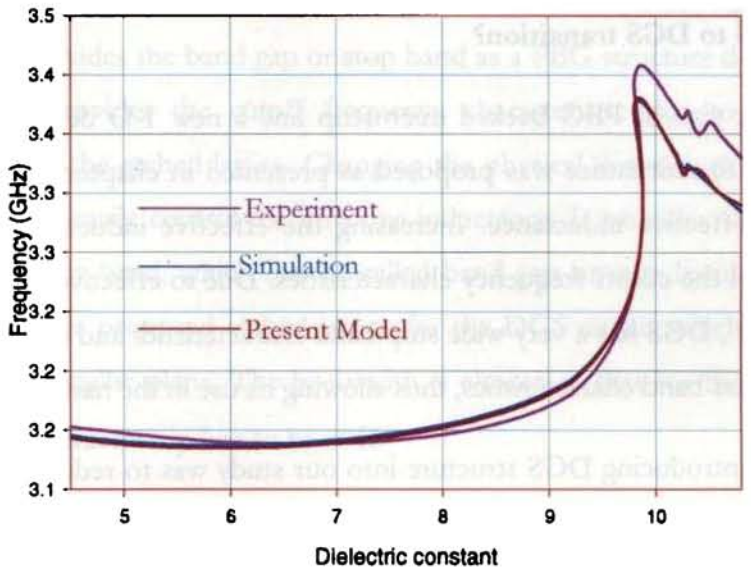

Figure 4.4.3 (a) Variation of cut-off frequency with dielectric constant

Dielectric Constant	-10 dB Bandwidth	
	Present model	IE3D
4.5	2.239 – 4.148	2.22 – 3.93
4.8	2.218 – 4.066	2.1 – 3.52
6	2.207 – 3.859	2.28 – 3.85
9.2	2.525 – 3.859	2.52 – 3.76
9.8	2.769 – 4.063	2.6 – 3.78
10.2	2.749 – 4.017	2.74 – 3.79
10.4	2.738 – 3.994	2.925 – 3.775
10.8	2.719 – 3.951	2.98 – 3.78

Table 4.4.3 (b) Predicted and simulated -10 dB bandwidths

Thus an equivalence relation is derived between the PBG parameters and effective capacitance and inductance of the perturbed Microstrip transmission line.

4.5 Why PBG to DGS transition?

To reduce the size of PBG backed microstrip line a new 1-D defected ground structure (DGS) unit lattice was proposed as presented in chapter 3 in order to improve the effective inductance. Increasing the effective inductance makes it easy to control the cutoff frequency characteristics. Due to effective additional L-C components , DGS has a very wide stop band characteristics and does not show the periodic pass band characteristics, thus allowing its use in the harmonic tuning.

Prime aim in introducing DGS structure into our study was to reduce the overall structure that offers band gap. It is concluded earlier that at least 3 cells are needed for effective band gap formation for a PBG structure and there are too many design parameters, which effect on the bandgap properties, such as the number of lattice, lattice shapes, lattice spacing, and relative volume fraction. Better

performance can easily be achieved with a single DGS cell and this property is studied elaborately in the following section.

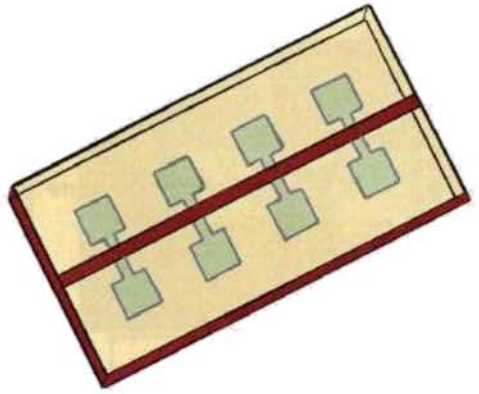

Figure 4.5.1 DGS structure proposed by Kim etal (2000)

4.6 DGS for Microstrip Line

In our study the proposed as a defected ground structure (DGS) has a single unit cell which provides the band gap or stop band as a PBG structure does. The DGS unit lattice provides the cutoff frequency characteristic due to the effective inductance of the etched lattice. Changing the physical dimensions of the etched lattice we can easily control the effective inductance. It provides the rejection of some frequency band, which can be called band gap or stop band effect. Figure 4.6.1 shows the proposed etched lattice for the DGS circuit which is located on the ground metallic plane. The line width is chosen as that for the characteristic impedance of microstrip line to be 50Ω.

The DGS consists of narrow and wide etched areas in backside metallic ground plane, which give rise to increasing the effective capacitance and inductance of a transmission line. A dumbbell shaped single lattice was etched in the ground plane

of microstrip line. For band gap to occur in the transmission characteristics, the separation between the two squares l should be $l \geq W$.

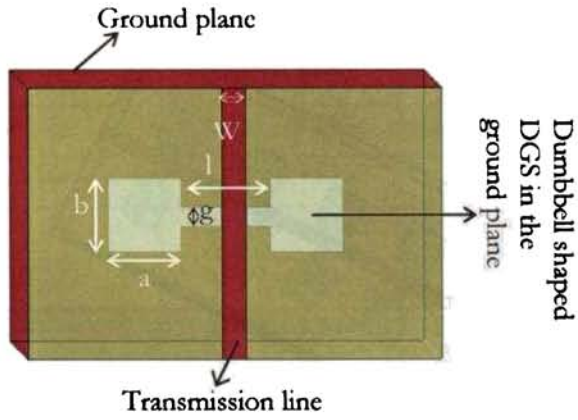

Figure 4.6.1 Dumbbell DGS structure in the ground plane of a microstrip line

For ease of calculation the condition $l = W$ was taken for the studies. Measurements and simulation of the fabricated DGS structures show that the cut-off and stop band center frequency characteristics depend on the physical dimension a, b of the proposed DGS unit lattice. So by changing the physical dimensions of the etched lattice one can easily control the effective inductance and thus the rejection of signals at some frequency band.

The lattice shape etched in the ground plane disturbs the current distribution thus increases the effective capacitance and inductance of the signal strip. So the proposed DGS circuit can be represented by an equivalent LCR circuit. So the effective capacitance and inductance of the DGS lattice can be extracted following as

$$R = 2 Z_0 \left(\frac{1}{|S_{11}|^2} - 1 \right) \qquad 4.19$$

$$C = \frac{\sqrt{|S_{11}|^2 (R + 2Z_0)^2 - 4Z_0^2}}{2Z_0 R \sqrt{1 - |S_{11}|^2} (f_2 - f_1)} \qquad 4.20$$

$$L = \frac{1}{4\pi^2 f_0^2 C} \qquad 4.21$$

In the equations C is the capacitance, L is the inductance Z_o characteristic impedance, f_o is the pole frequency or the stop band center frequency and f_2-f_1 is the *-10 dB* bandwidth of S_{12} curve. The frequency response of this DGS filter obtained from simulation, experiment and extracted equivalent circuit (Figure4.6.2 (a)) are in good agreement and is shown in Figure 4.6.2 (b).

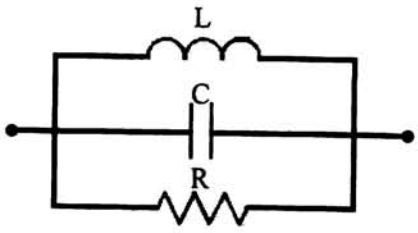

Figure 4.6.2(a) Equivalent circuit of the Dumbbell shaped DGS structure in the ground plane of a microstrip line

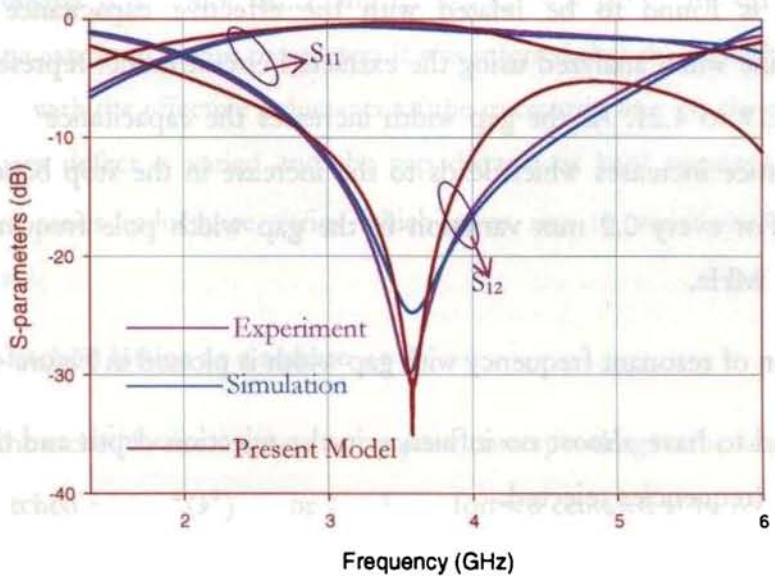

Figure 4.6.2 (b) Stop Band Characteristics for dumbbell shaped DGS in the ground plane, ε_r = 4.7, h = 1.6mm, a = b = 8mm, g = 0.2mm, l =W = 3mm

From the extracted equivalent circuit using equations (4.19 to 4.21) the band stop characteristics of the dumbbell shaped DGS can be explained. In the lower frequency band, the inductor dominates and determines the cut-off frequency. With the increase in frequency, the series inductance due to the DGS section increases the reactance of the microstrip line, and then it starts to reject some frequency regimes. The combination of effective inductance and capacitance provides the attenuation pole, which is the resonant frequency of the LC tank circuit. As the operational frequency increases the capacitor is dominated and the reactance of the capacitance decreases. Thus a band gap occurs between the propagating frequency bands.

The DGS is composed of two square defected areas and a narrow connecting slot or the gap width. The effect of each portion in the band stop characteristics is studied in detail in the following sections.

4.6.1 Effect of the gap width 'g' in the stop band characteristics

Gap width is found to be related with the effective capacitance of the microstrip line when analyzed using the extracted circuit model represented by equations 4.19 to 4.21. As the gap width increases the capacitance offered by the DGS lattice increases which leads to the increase in the stop band center frequency. For every 0.2 mm variation in the gap width pole frequency gets shifted ~20 MHz.

The variation of resonant frequency with gap width is plotted in Figure 4.6.3.

Gap is found to have almost no influence in the rejection depth and the band width of the frequencies rejected.

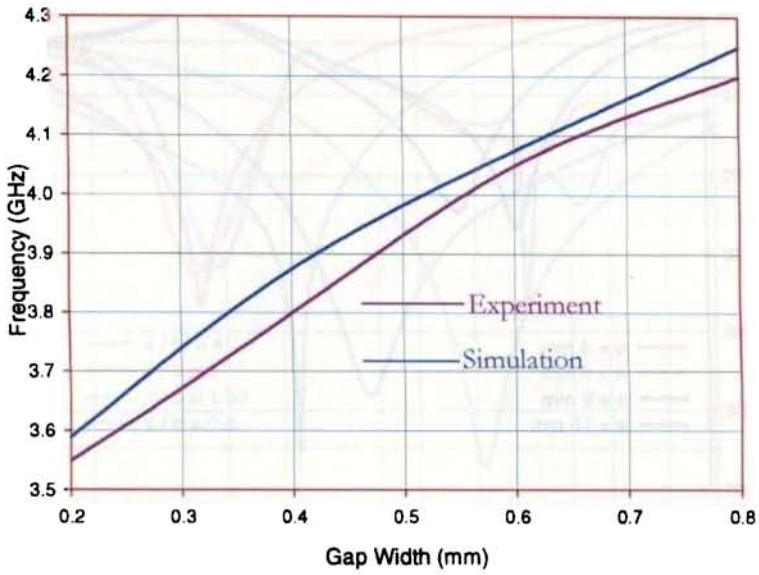

Figure 4.6.3. Variation of stop band center frequency with gap width 'g' ε_r = 4.7, h = 1.6mm, a= b= 8mm

4.6.2 Effect of lattice dimension a,b on band stop characteristics

To find the influence of etched lattice dimension on the transmission characteristics square slot lattice and rectangular slot lattice are studied in detail. From the extracted circuit parameters it was inferred that the etched square defect is related with the effective inductance of the microstrip line. As the etched area of the square defect is varied and the gap distance is kept constant as $l = W$, the effective series inductance varies which gives rise to variations in the cutoff frequency.

4.6.2.1 Etched lattice as a square $a = b$

When the etched lattice was kept as a square corresponding to the lattice dimension or the etched area a^2 (b^2) a stop band was formed centered at f_0. As the dimension increased the pole frequency varied inversely. The observed results are plotted in Figure 4.6.4.

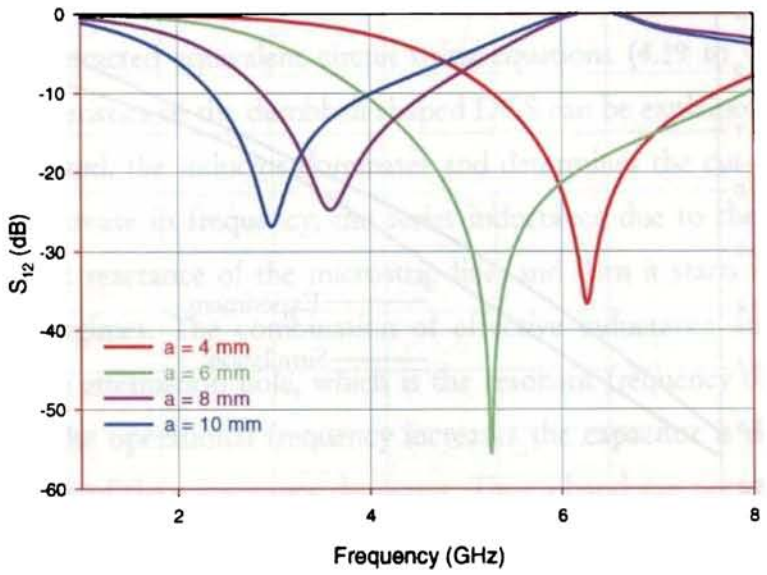

Figure 4.6.4 Stop Band Characteristics for dumbbell shaped DGS in the ground plane, ε_r = 4.7, h = 1.6mm, g = 0.2mm, l =W = 3mm

4.6.2.2 Etched lattice as a rectangle

The transmission characteristics showed a pass band characteristic in the frequency response for rectangular DGS in the ground plane. Corresponding to the dimension a and b of the lattice two pole frequencies f_{o1} and f_{o2} is obtained. If the ratio $\frac{a}{b}$ was maintained with in certain range we have a pass band in the frequency response in between the stop bands.

When the square DGS was made rectangular by varying the vertical dimension b, a pass band was observed between two stop bands when $\frac{a}{b} \geq 4$ and beyond this the stop band was found to become wider compared to the structure which had $a=b$. As the ratio becomes smaller the band shifted towards the lower side of the frequency spectrum. The transmission characteristics for different $\frac{a}{b}$ is shown in Figure 4.6.5

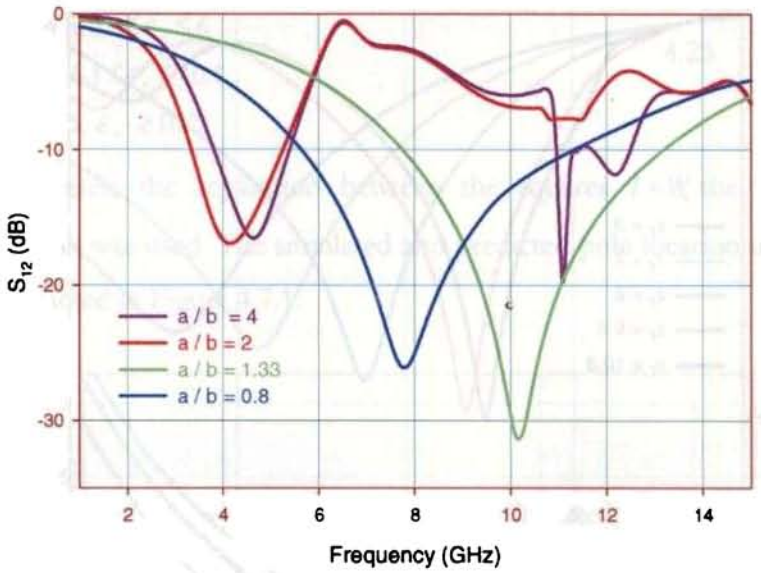

Figure 4.6.5 Stop Band Characteristics for dumbbell shaped DGS in the ground plane, ε_r = 4.7, h = 1.6mm, a = 8mm, g = 0.2mm, l =W = 3mm

Similar behavior is obtained when the rectangle is oriented the other way.

4.6.3 Effect of Substrate parameters on the Band Stop characteristics

Though the DGS parameters shows similar behavior in every substrate; the substrate parameters like dielectric constant ε_r and substrate thickness h influences the location, depth and width of the stop band. To ascertain the influence of dielectric constant ε_r, structures with same DGS parameters were studied for different dielectric materials with thickness $h = 1.6\,mm$. The microstrip line was fabricated to have characteristic impedance $Z_0 = 50\Omega$. It was found that as the dielectric constant increases the pole frequency showed a shift towards the lower side. Moreover lower dielectric constant materials gave wider stop bands when compared with substrates with high dielectric constant. Substrate thickness had a less influence in the stop band characteristics. The observations are as plotted in Figure 4.6.7.

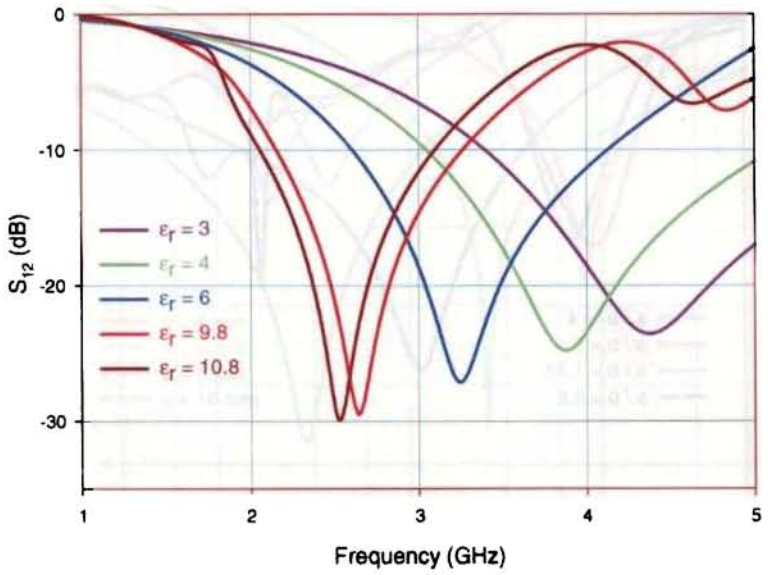

Figure 4.6.7 Stop Band Characteristics for dumbbell shaped DGS in the ground plane, h = 1.6mm, a = b = 8mm, g = 0.2mm, l =W

4.7 Design of a Dumbbell shaped DGS

To predict the resonant frequency of a given dumbbell shaped DGS or to give the dimension for a desired pole frequency one has to give relations connecting the DGS parameters like lattice dimension a, gap width g and the separation between the squares l and substrate parameters like the dielectric constant ε_r and substrate height h with the pole frequency f_o. These parameters are related by a simple expression,

$$f_o = k c \left(\frac{l}{h}\right)\left(\frac{g}{a^2}\right)\left(\frac{1}{\sqrt{\varepsilon_r}}\right) \qquad 4.22$$

c is the velocity of light and k is a constant that is given as

$$
\begin{aligned}
k &= 2.25, \varepsilon_r \leq 3.5 \\
k &= 4.5, 3.6 \leq \varepsilon_r \leq 6 \\
k &= 7, 6.1 \leq \varepsilon_r \leq 10.1 \\
k &= 7.3, \varepsilon_r \geq 10.2
\end{aligned}
\qquad 4.23
$$

In all the cases; the separation between the squares $l = W$ the width of the microstrip line was used. The simulated and predicted pole location using equation (4.22) is depicted in Figure 4.7.1.

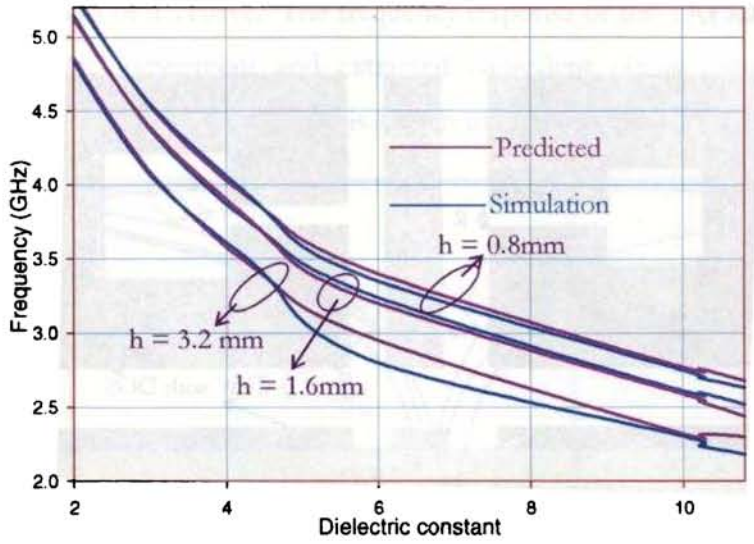

Figure 4.7.1 Pole frequency of the DGS Lattice in the ground plane, h = 1.6mm, a = b = 8mm, g = 0.2mm, l =W

So it could be concluded that DGS is an alternative to PBG for producing a stop band effectively for microstrip lines. How would these structures influence a coplanar wave guide is studied in the following section.

4.8 DGS for Coplanar Waveguide

Filters are an important component in a circuit and are realized in microwave regime using lumped elements. It can be realized in microstrip lines, coplanar waveguides (CPW), strip lines etc. Unlike the microstrip or the strip line the

coplanar structure permits easy parallel and series insertion of circuit elements. Moreover the circuit parameters of CPW are less sensitive to substrate thickness. By etching holes in the ground plane with an open connected to the gap between strip line and ground plane i.e. a DGS cell in the ground plane of a CPW gives effective band gap to certain frequencies.

A unit cell of DGS is implemented by etching square-shaped lattices in the ground plane with an open connected with the gap between strip line and ground plane as in the Figure4.8.1.

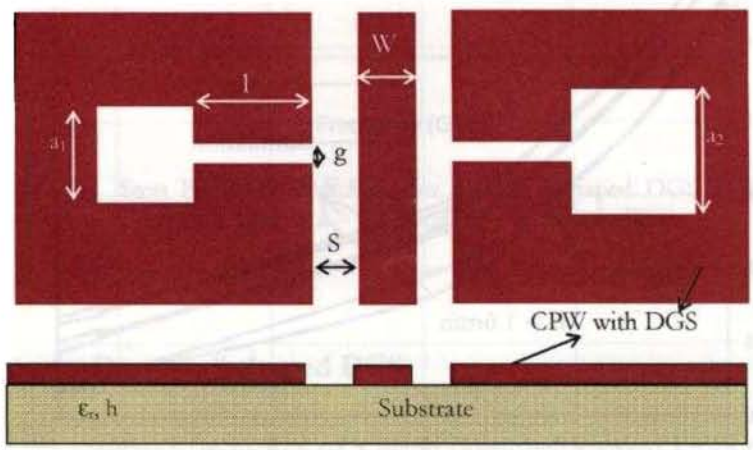

Figure .4.8.1 Geometry of CPW with DGS in the ground plane

The self-resonant characteristic of the DGS unit cell allows desired stop band rejection even with a single unit cell. Equivalent circuit parameters of the proposed CPW DGS unit cell are extracted by simple circuit analysis. The lattice shape etched in the ground plane disturbs the current distribution thus increases the effective capacitance and inductance of the signal strip. So the effective capacitance and inductance of the DGS lattice can be extracted following as

$$R = 2\ Z_0 \left(\frac{1}{|S_{11}|^2} - 1 \right) \qquad 4.23$$

$$C = \frac{\sqrt{|S_{11}|^2 (R + 2Z_0)^2 - 4Z_0^2}}{2Z_0 R \sqrt{1 - |S_{11}|^2} (f_2 - f_1)} \qquad 4.24$$

$$L = \frac{1}{4\pi^2 f_0^2 C} \qquad 4.25$$

In the equations C is the capacitance, L is the inductance Z_o characteristic impedance, f_o is the pole frequency or the stop band center frequency and f_2-f_1 is the *-10 dB* bandwidth of S_{12} curve. The frequency response of this DGS filter obtained from simulation, experiment and extracted equivalent circuit using the above equations are in good agreement and is shown in Figure 4.8.2.

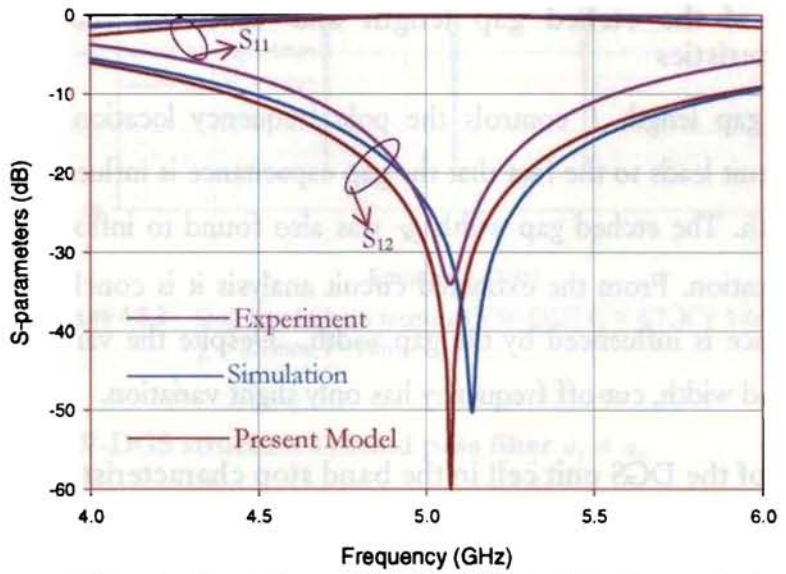

Figure 4.8.2 Stop Band Characteristics for CPW- DGS in the ground plane, ε_r = 4.7, h = 1.6mm, W = 3mm, $a_1 = a_2$ = 5mm, l = 1mm and g = 0.2 mm.

The effect of DGS and substrate parameters in the filtering property of the CPW – DGS is presented in the following sections. The existence of cut-off frequency means that the CPW-DGS increases the effective inductance of the signal strip which corresponds to the etched square area in the lateral ground plane. Meanwhile, the etched gap and width determines the attenuation pole location.

From the extracted equivalent circuit using equations (4.23 to 4.25) we can explain the band stop characteristic. In the lower frequency band, the inductor dominates and determines the cut-off frequency. With the increase in frequency, the series inductance due to the CPW-DGS section increases the reactance of the CPW, and then it starts to reject some frequency regimes. The combination of effective inductance and capacitance provides the attenuation pole, which is the resonant frequency of the LC tank circuit. As the operational frequency increases the capacitor is dominated and the reactance of the capacitance decreases. Thus a band gap occurs between the propagating frequency bands.

4.8.1 Effect of the etched gap length and width on the stop band characteristics

The etched gap length l controls the pole frequency location. Analysis of extracted circuit leads to the fact that the gap capacitance is influenced more by the gap length. The etched gap width g was also found to influence the pole frequency location. From the extracted circuit analysis it is concluded that the gap capacitance is influenced by the gap width. Despite the variations in the gap length and width, cut-off frequency has only slight variation.

4.8.2 Effect of the DGS unit cell in the band stop characteristics

The etched lattice disturbed the current distribution and it lead to disturbance of inductance of the coplanar strip. The proposed CPW-DGS section provides cut-off frequency and pole frequency without periodic perforations as the area of the lattice determines the cut-off frequency. The etched lattice of two types was studied one in which the lattice dimension in both the ground planes were the same: $a_1 = a_2$ and the other when the dimensions were different: $a_1 \neq a_2$.

4.8.2 (a) CPW-DGS structure as band stop filter $a_1 = a_2$

When the etched lattice in the ground planes were kept the same a stop band was observed. The stop band centre frequency varied inversely with the lattice dimension. These observations are plotted in Figure 4.8.3.

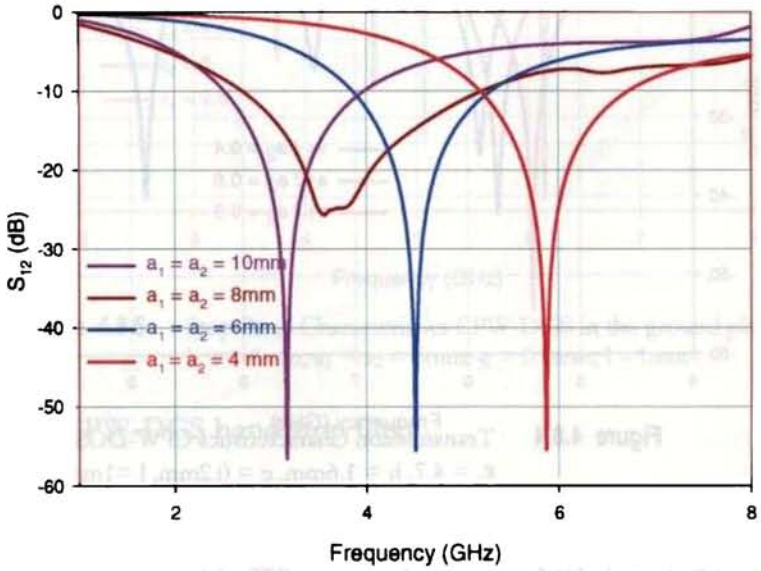

Figure 4.8.3 Stop Band Characteristics CPW-DGS $\varepsilon_r = 4.7$, h = 1.6mm, g = 0.2mm, l =1mm

4.8.3 (b) CPW-DGS structure as band pass filter $a_1 \neq a_2$

The property of self-resonance of a PBG unit cell is used to improve the stop band rejection of a CPW band pass filter. The equivalent circuit is extracted using equations 4.23, 4.24 and 4.25. The frequency response of square lattices of different dimensions in the lateral ground planes is studied. If the ratio $\frac{a_1}{a_2} \leq 0.6, a_2 \rangle a_1$ we have a pass band in the frequency response in between the stop bands. These two pole frequencies may be due to the combination from the

dimension a_1 and a_2. When $a_1 = a_2$ these two frequencies merge to form a single stop band. The frequency response of this filter is as shown in Figure 4.8.4.

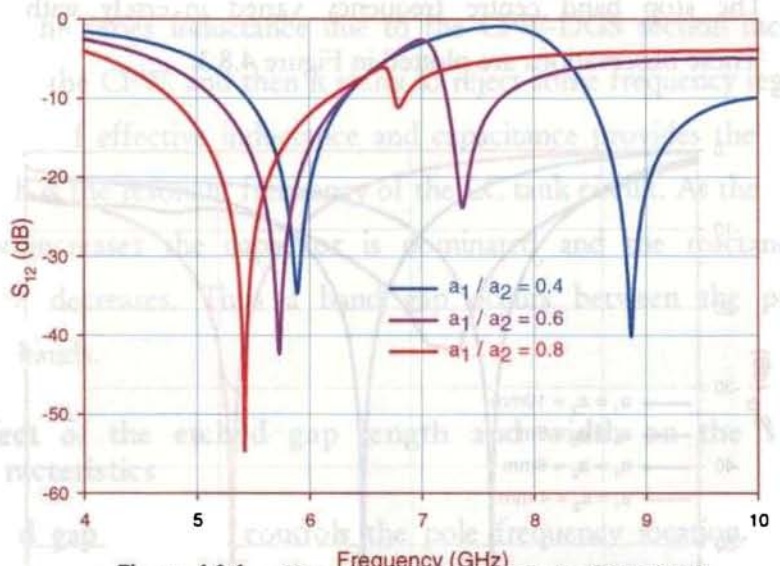

Figure 4.8.4 Transmission Characteristics CPW-DGS
$\varepsilon_r = 4.7$, h = 1.6mm, g = 0.2mm, l =1mm

4.8.4 Effect of Substrate Parameters

The CPW-DGS shows similar behavior in every substrate but the substrate parameters like dielectric constant ε_r and substrate thickness h influences the location, depth and width of the stop band. To ascertain the influence of dielectric constant ε_r, structures with same DGS parameters were studied on different materials. It was found that as the dielectric constant increases the pole frequency showed a shift towards the lower side and the substrate thickness had a less influence in the stop band characteristics. The observations are as plotted in Figure 4.8.5.

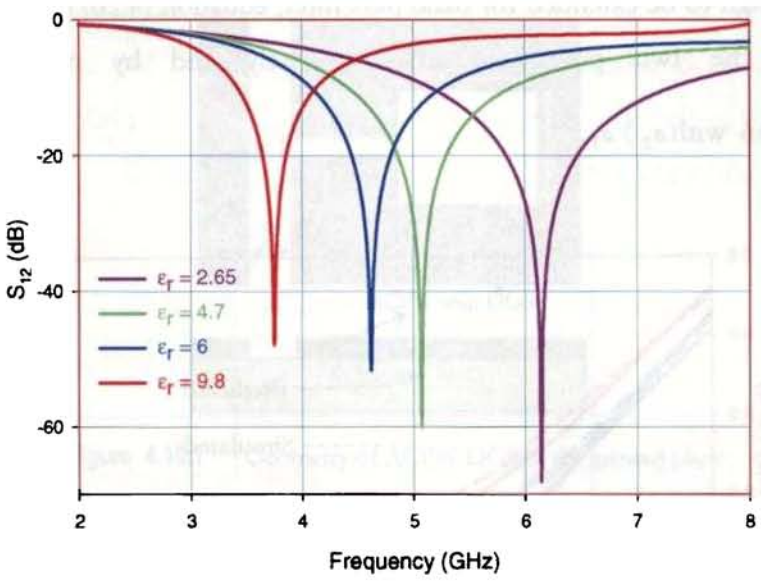

Figure 4.8.5 Stop Band Characteristics CPW-DGS in the ground plane
h = 1.6mm, $a_1 = a_2$ = 5mm, g = 0.2mm, l =1mm

4.9 Design of CPW-DGS band stop filter

From the observations discussed in section 4.8, for a 50 Ω CPW line with slot width 'S', signal strip width 'W' on a substrate with dielectric constant 'ε_r' and substrate thickness 'h' the pole frequency 'f_o' given by the relation

$$f_o = kc\left(\frac{g}{al\sqrt{\varepsilon_r}}\right)\left(\frac{2S+W}{h}\right) \qquad 4.26$$

c is the velocity of light and the constant 'k' is found to be dependent on the dielectric constant and is given as

$$\begin{aligned} k &= 0.4 \ for \ \varepsilon_r \leq 5.8 \\ k &= 0.38 \ for \ 5.9 \geq \varepsilon_r \leq 9.7 \\ k &= 0.32 \ for \ \varepsilon_r \geq 9.8 \end{aligned} \qquad 4.27$$

The cut-off frequency predicted using equation (4.26) and that obtained by simulation are in good agreement and is plotted in Figure 4.9.1.

For the design to be extended for band pass filter, equation (4.26) can be used as it can give the two pole frequencies precisely and by maintaining the ratio $\frac{a_1}{a_2} \leq 0.6$ with $a_2 > a_1$.

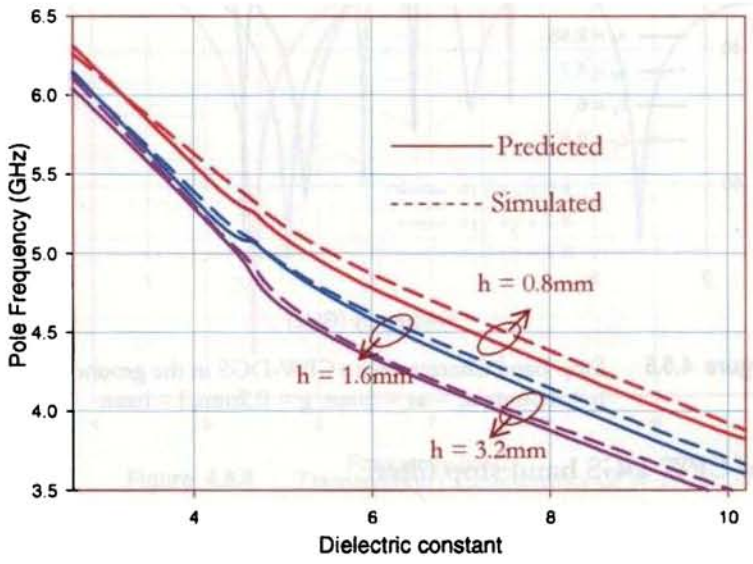

Figure 4.9.1 Variation of cut-off frequency with dielectric constant 2S+W for 50Ω, a = 5mm, l = 1mm and g = 0.2 mm

4.10 DGS for Asymmetric Coplanar Waveguide

The concept of DGS filter is made further compact in an Asymmetric coplanar waveguide (ACPW) which has only one lateral ground plane. By etching holes in the lateral ground plane with an open connected to the gap between strip line and ground plane i.e. a DGS cell in the ground plane of an ACPW gives effective band gap to certain frequencies. A unit cell of DGS is implemented by etching square-shaped lattice in the ground plane with an open connected with the gap between strip line and ground plane as in the Figure 4.10.1.

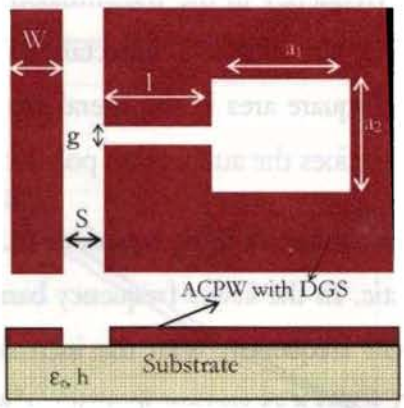

Figure 4.10.1 Geometry of ACPW DGS in the ground plane

As for CPW-DGS the equivalent circuit parameters of the proposed ACPW-DGS unit cell are extracted by simple circuit analysis. So the effective capacitance and inductance of the DGS lattice can be extracted using equations (4.23), (4.24) and (4.25). The frequency response of this DGS filter obtained from simulation, experiment and extracted equivalent circuit are in good agreement and is shown in Figure 4.10.2.

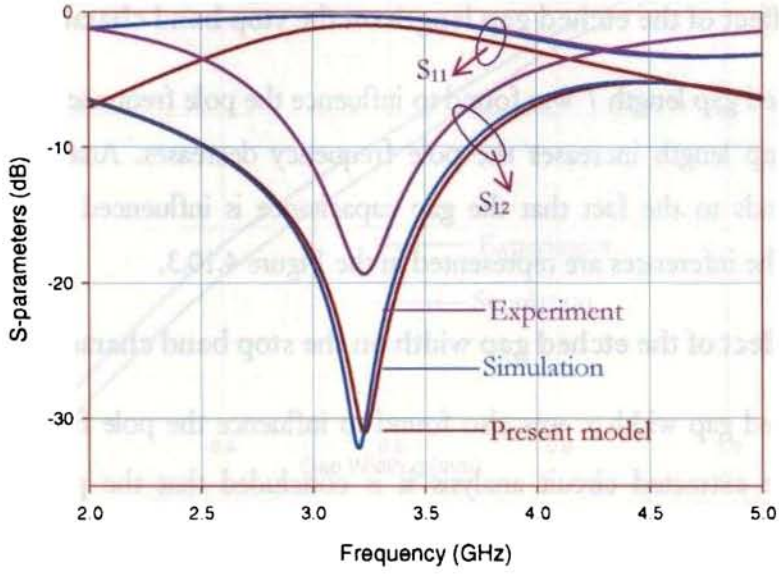

Figure 4.10.2 Stop Band Characteristics for CPW- DGS in the ground plane, $\varepsilon_r = 4.7$, h = 1.6mm, W = 3mm, $a_1 = a_2 = 10$mm, l = 1mm and g = 0.2 mm.

The existence of cut-off frequency in the transmission characteristics means that the ACPW-DGS increases the effective inductance of the signal strip which corresponds to the etched square area in the lateral ground plane. Meanwhile, the etched gap and width determines the attenuation pole location.

From the extracted equivalent circuit using equations (4.23 to 4.25) we can explain the band stop characteristic. In the lower frequency band, the inductor dominates and determines the cut-off frequency. With the increase in frequency, the series inductance due to the ACPW-DGS section increases the reactance of the ACPW, and then it starts to reject some frequency regimes. The combination of effective inductance and capacitance provides the attenuation pole, which is the resonant frequency of the LC tank circuit. As the operational frequency increases the capacitor is dominated and the reactance of the capacitance decreases. Thus a band gap occurs between the propagating frequency bands. The effect of DGS and substrate parameters in the filtering property of the ACPW – DGS is presented in the following sections

4.10.1 Effect of the etched gap length on the stop band characteristics

The etched gap length l was found to influence the pole frequency location. As the etched gap length increases the pole frequency decreases. Analysis of extracted circuit leads to the fact that the gap capacitance is influenced more by the gap length. The inferences are represented in the Figure 4.10.3.

4.10.2 Effect of the etched gap width on the stop band characteristics

The etched gap width g was also found to influence the pole frequency location. From the extracted circuit analysis it is concluded that the gap capacitance is influenced by the gap width. Despite the variations in the gap length and width, cut-off frequency has only slight variation. The inferences are represented in the Figure 4.10.4.

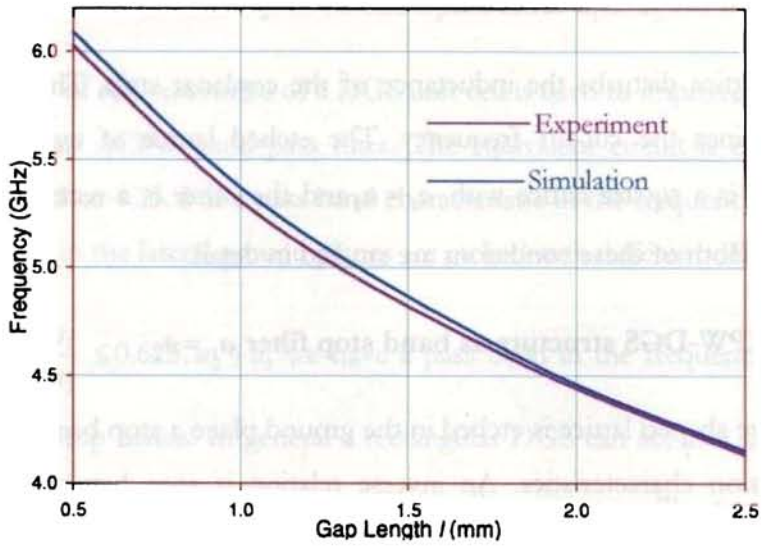

Figure 4.10.3 Variation in Pole frequency of the DGS Lattice in the ground plane, $\varepsilon_r = 4.7$, h = 1.6mm, $a_1 = a_2 = 5$mm, g = 0.4 mm

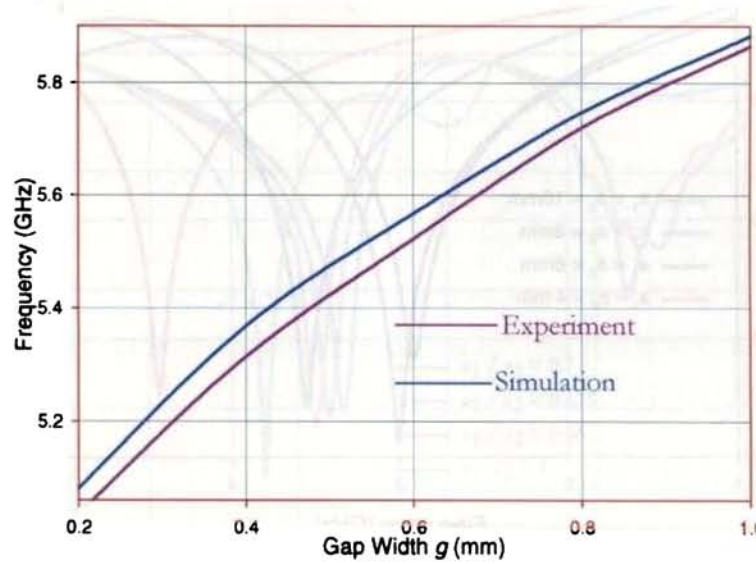

Figure 4.10.4 Variation in Pole frequency of the DGS Lattice in the ground plane, $\varepsilon_r = 4.7$, h = 1.6mm, $a_1 = a_2 = 5$mm, l = 1mm

4.10.3 Effect of the DGS unit cell in the band stop characteristics

The etched lattice disturbs the inductance of the coplanar strip. The area of the lattice determines the cut-off frequency. The etched lattice of two types were studied - one is a square lattice with $a_1 = a_2$ and the other is a rectangular lattice with $a_1 \neq a_2$. Both of these conditions are studied in detail.

4.10.3 (a) ACPW-DGS structure as band stop filter $a_1 = a_2$

When a square shaped lattice is etched in the ground plane a stop band observed in the transmission characteristics. An inverse relation is seen between the lattice dimension and the pole frequency location. These observations are plotted in Figure 4.10.5.

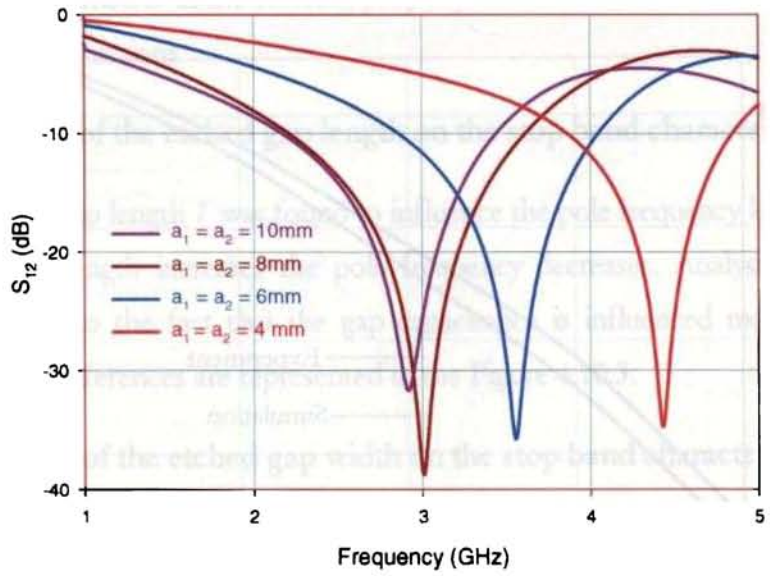

Figure 4.10.5 Stop Band Characteristics ACPW-DGS
ε_r = 4.7, h = 1.6mm, g = 0.4mm, l = 1mm

4.10.3 (b) ACPW-DGS structure as band pass filter $a_1 \neq a_2$

The property of self-resonance of a DGS unit cell is used to improve the stop band rejection of an ACPW band pass filter. The equivalent circuit is extracted using equations 4.23 to 4.25. For a pass band characteristic in the frequency response the square lattice in the lateral ground planes are etched with different dimensions.

If the ratio $\frac{a_1}{a_2} \leq 0.625, a_2 > a_1$ we have a pass band in the frequency response in between the stop bands. In general a rectangular DGS can act as a stop band and pass band filter depending on the selection of $\frac{a_1}{a_2}$ and when $\frac{a_1}{a_2}=1$ we have a pass band filter. The frequency response of this filter is as shown in Figure 4.10.6.

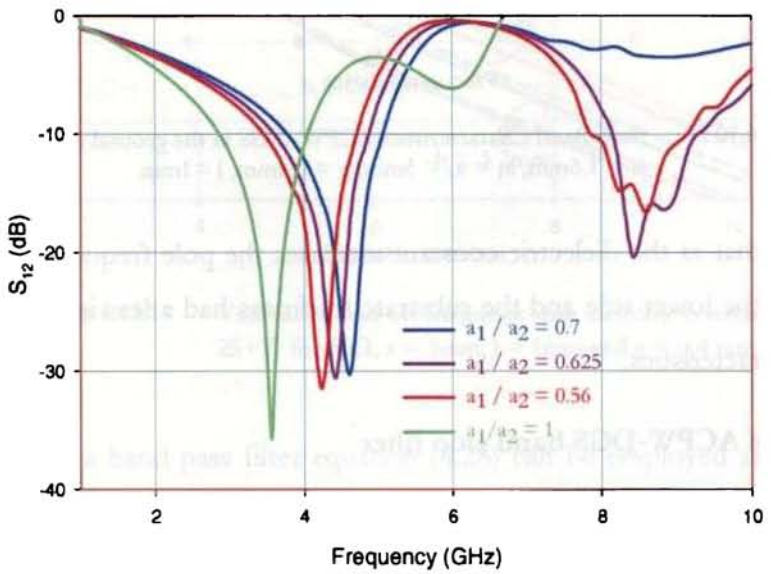

Figure 4.10.6 Transmission Characteristics CPW-DGS
ε_r = 4.7, h = 1.6mm, g = 0.4mm, l =1mm

4.10.4 Effect of Substrate Parameters

A similar behavior is observed in different substrates by the ACPW-DGS but the substrate parameters like dielectric constant ε_r and substrate thickness h influences the location, depth and width of the stop band. The observations are as plotted in Figure 4.10.7.

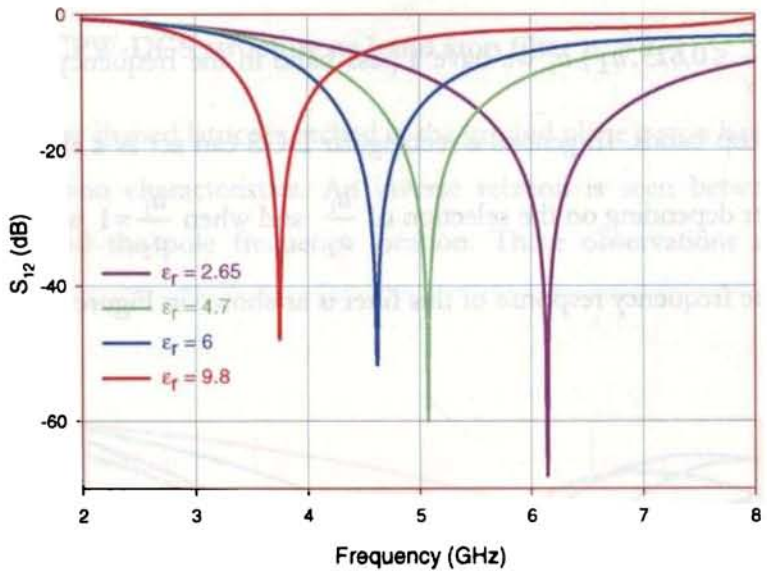

Figure 4.10.7 Stop Band Characteristics ACPW-DGS in the ground plane, h = 1.6mm, $a_1 = a_2$ = 5mm, g = 0.4mm, l =1mm

It was found that as the dielectric constant increases the pole frequency showed a shift towards the lower side and the substrate thickness had a less influence in the stop band characteristics.

4.11 Design of ACPW-DGS band stop filter

From the observations discussed in section 3.13, for a 50 Ω CPW line with slot width 'S', signal strip width 'W' on a substrate with dielectric constant 'ε_r' and substrate thickness 'h' the pole frequency 'f_o' given by the relation

$$f_o = kc\left(\frac{g}{al\sqrt{\varepsilon_r}}\right)\left(\frac{S+W}{h}\right) \qquad 4.28$$

c is the velocity of light and 'k' is a constant that is given as

$$\begin{aligned} k &= 0.4 \ for\ \varepsilon_r \le 5.8 \\ k &= 0.38 \ for\ 5.9 \ge \varepsilon_r \le 9.7 \\ k &= 0.32 \ for\ \varepsilon_r \ge 9.8 \end{aligned} \qquad 4.29$$

The cut-off frequency predicted using equation (4.28) and that obtained by simulation are in good agreement and is plotted in Figure 4.11.1.

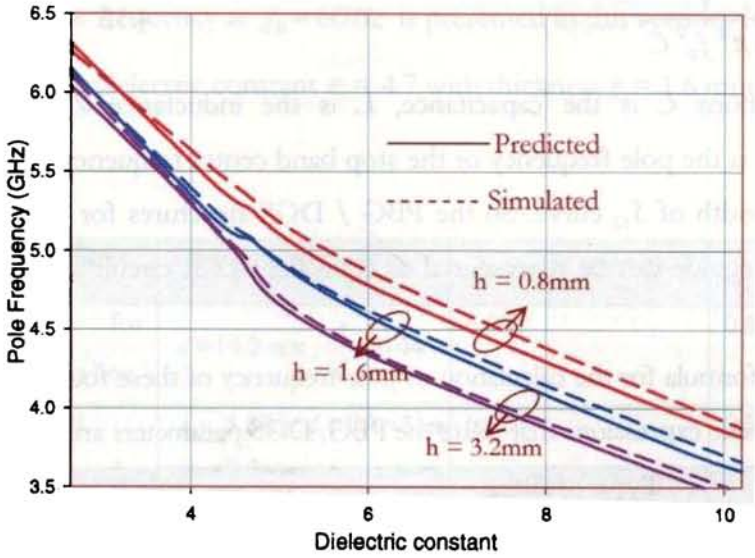

Figure 4.11.1 Variation of cut-off frequency with dielectric constant 2S+W for 50Ω, a = 5mm, l = 1mm and g = 0.4 mm

For designing a band pass filter equation (4.28) can be employed as it could give the two pole frequencies and the pass band frequency can be selected by maintaining the ratio $\frac{a_1}{a_2} \le 0.625$ .When the ratio is unity we have the band stop filter alone.

4.12 Filter Characteristics – in a nutshell

Following the simple circuit analysis in the previous sections equivalent circuit of PBG / DGS structures for microstrip and coplanar waveguide is presented. The equations of the lumped elements being given as:

$$R = 2\,Z_0\left(\frac{1}{|S_{11}|^2} - 1\right) \qquad 4.30$$

$$C = \frac{\sqrt{|S_{11}|^2\,(R + 2Z_0)^2 - 4Z_0^{\,2}}}{2Z_0\,R\sqrt{1 - |S_{11}|^2}\,(f_2 - f_1)} \qquad 4.31$$

$$L = \frac{1}{4\pi^2 f_0^{\,2} C} \qquad 4.32$$

In the equations C is the capacitance, L is the inductance Z_o characteristic impedance, f_o is the pole frequency or the stop band center frequency and f_2-f_1 is the *-10 dB* bandwidth of S_{12} curve. So the PBG / DGS structures for microstrip and coplanar waveguide can be represented as equivalent LCR circuit as in the Figure 4.4.1.

- The formula for the calculation of pole frequency of these four filters is given by simple expressions that relate the PBG/DGS parameters are given below.

Type of filter	Pole frequency
PBG for microstrip line	$f_0 = \frac{c}{\lambda_g}, \lambda_g = 2d$
Dumbbell shaped DGS for microstrip line	$f_o = k\,c\left(\frac{l}{h}\right)\left(\frac{g}{a^2}\right)\left(\frac{1}{\sqrt{\epsilon_r}}\right)$
DGS for coplanar line	$f_o = k\,c\left(\frac{g}{al\sqrt{\epsilon_r}}\right)\left(\frac{2S+W}{h}\right)$
DGS for asymmetric coplanar line	$f_o = k\,c\left(\frac{g}{al\sqrt{\epsilon_r}}\right)\left(\frac{S+W}{h}\right)$

- Return loss: < 0.5 dB (in all the cases).
- Filter selectivity: < 35 dB/GHz ($\xi = \frac{\alpha_{min} - \alpha_{max}}{f_s - f_p}$ dB/GHz ξ is the selectivity, α_{max} is the 3 dB attenuation point α_{min} is the 20 dB attenuation point f_s is the 20 dB stop band frequency and f_p is the 3 dB stop band frequency).

4.13 Design of PBG/DGS filter at 6 GHz

Design of a band stop filter with PBG/DGS parameters for microstrip and CPW line having pole frequency at $f_0 = 6GHz$ is presented in this section. In all the cases a substrate with dielectric constant ε_r = 4.7 with thickness h = 1.6 mm is used.

Type of filter	Design parameters	f_0 GHz observed	% error
PBG for microstrip line	$d = 14.2\ mm$, $\frac{a}{d} = 0.44$	6.05	0.83
Dumbbell DGS for microstrip line	$a = 3.8mm, l = W = 3mm$ $g = 0.2mm$	6.023	0.50
DGS for CPW	$a = 4.3\ mm, l = 1mm,$ $g = 0.2mm, W = 3mm$	5.98	-0.33
DGS for ACPW	$a = 3.4\ mm, l = 1mm,$ $g = 0.2mm, W = 3mm$	6.005	0.083

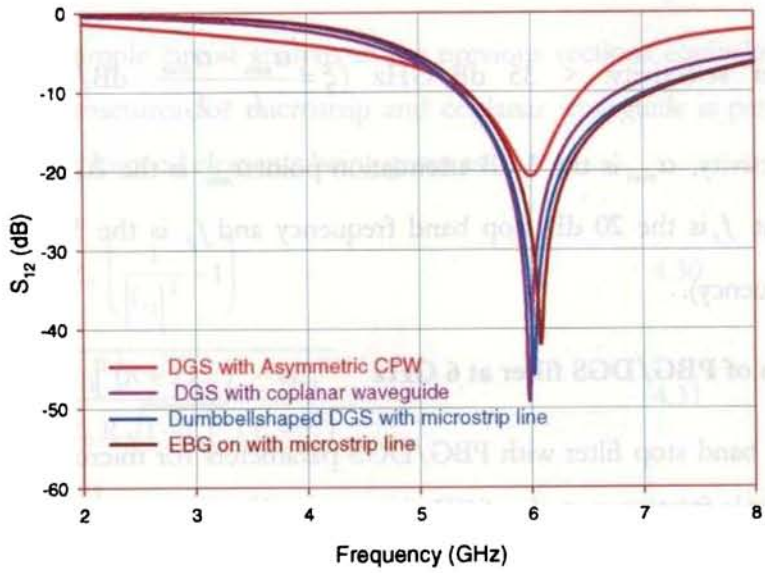

Figure 4.13.1 Stop Band Characteristics h = 1.6mm, ε_r = 4.7

4.14 Conclusion

In this chapter the effect of PBG/DGS structures for band stop filters is presented in detail. For microstrip lines PBG structures offered a wide stop band and the design equations presented can precisely predict the bandwidth and the stop band centre frequency. For miniaturization of the PBG filter DGS is applied to the ground plane of the microstrip line. DGS is extended to the ground plane of a coplanar waveguide and asymmetric coplanar waveguide. These structures are analyzed using FDTD method. In all the cases design equations are presented. The predicted, simulated, FDTD and experimental results are in good agreement.

In the next chapter the application of these ground planes in the reflection and radiation properties of antennas is presented.

5

PLANAR ANTENNAS: REFLECTION AND RADIATION CHARACTERISTICS ON PHOTONIC BANDGAP SUBSTRATES

Contents

Development of broadband microstrip (patch) antennas using substrates containing photonic crystals is illustrated in this chapter. By reducing or eliminating the effect of surface waves with photonic crystals, a broadband response can be obtained from inherently narrowband antennas. In addition, it is also proposed that the behavior of the photonic crystals will lead to improvements in radiation pattern and overall antenna efficiency by the elimination of surface waves. The predicted results are verified through analytical simulations and experimental investigations in the Centre for Research and Electromagnetics and Antennas (CREMA) anechoic chamber.

In this chapter the PBG / DGS structures that were used for filtering action are implemented as substrate for antennas. The idea is to design a patch antenna on a 2D photonic crystal substrate, where the patch becomes the "defect" in the crystal structure. The defect established in the photonic crystal localizes the EM fields. Surface waves along the plane of the patch are forbidden from forming due to the periodicity of the photonic crystal in that plane. This prevention of surface waves enhances operational bandwidth and gain. Since the prevention of surface waves will reduce the edge diffraction, the side lobe level is also reduced.

Further DGS is applied in the ground plane of Coplanar Waveguide (CPW) fed slot antenna. CPW-fed slot antennas have been widely used for wireless applications since they are compatible with monolithic integrated circuits and active solid-state devices. Furthermore, CPW-fed slot antennas exhibit a larger bandwidth with bi-directional radiation patterns. Among the recent researches,

a CPW-fed loop slot antenna with a tuning stub to enhance the bandwidth has been proposed by Chen etal. By adjusting the location of a wide tuning stub, good impedance match can be easily obtained. It is found that more spacing between the ground plane and the widened tuning stub, the larger the bandwidth. However, propagation of higher order modes will increase simultaneously, which may cause low efficiency, cross-polarization - potential problem of the electromagnetic interference and compatibility. To alleviate this, DGS is incorporated in the ground plane of CPW – fed slot antenna. The outcome of the experimental observations of the PBG and DGS integrated planar antenna is given in the following sections.

5.1 Design of Patch Antenna with PBG ground plane – Experimental, Simulated and Theoretical Results

Dielectric substrates with periodic loading can create a Photonic Band Gap whose surface-wave dispersion diagram presents a forbidden frequency band. When this band gap is around the operating frequency of the antenna surface waves cannot propagate along the substrate and an increased amount of radiated power couples to space waves. This mechanism has the effect of increasing the gain, efficiency, reshaping the antenna pattern and can enhance antenna characteristics significantly. We have utilized this property of PBG structures to enhance antenna characteristics. In order to identify the improvements in this novel photonic band gap based patch antenna, the reflection and radiation characteristics of Rectangular Microstrip Antennas (RMSA) are studied. The parameters held constant throughout the study are the shape of the patch (rectangle), and the dimensions and material properties of the photonic crystals. The proposed antenna configuration of RMSA with PBG ground with periodic squares is shown in Figure 5.1.1

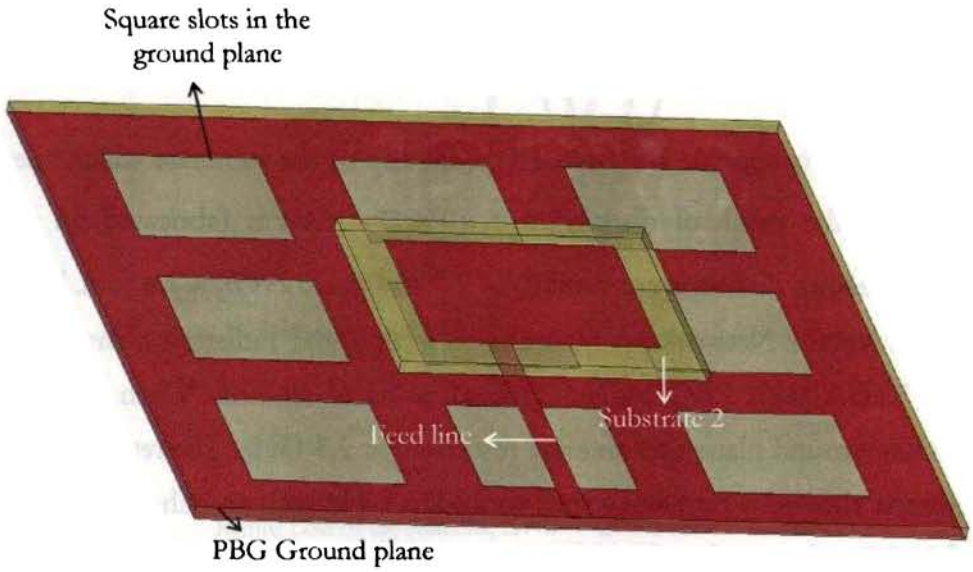

Figure 5.1.1 Proposed antenna Configuration with PBG Ground Plane

As described in Chapter 4, the cut-off frequency of the PBG structure can be computed using equations (4.21, 4.24 and 4.25). Using these equations for a substrate with a dielectric constant ε_r = 4.7 and thickness h = 1.6 mm with a PBG structure placed periodically at a distance $d = 30\ mm$ the pole frequency falls at ~ 2.9 GHz. The resonant frequency 'f_r' of the RMSA given as

$$f_r = \frac{c}{2(L + 2\Delta L)\sqrt{\varepsilon_{reff}}} \qquad 5.1$$

L is the length and the effective dielectric constant ε_{reff} is

$$\varepsilon_{reff} = \frac{\varepsilon_r + 1}{2} + \frac{\varepsilon_r - 1}{2}\left[1 + \frac{12h}{W}\right]^{-1/2} \qquad 5.2$$

In the ground plane of substrate 1 with dielectric constant ε_{r1} = 4.7 and thickness h_1 = 1.6 mm slots are etched periodically at a distance $d = 30\,mm$ and aspect ratio $\frac{a}{d} = 0.44$ as optimized in Chapter 4.

A 50 Ω microstrip line is fabricated on the top of the substrate which energizes a rectangular patch of dimension $L \times W = 27 \times 36\,mm^2$ is fabricated on another substrate with dielectric constant ε_{r2} = 4.7 and thickness h_2 = 1.6 mm. Using HP 8510C Vector Network analyzer the reflection and radiation characteristic of this RMSA with PBG backed ground plane is studied. When placed on a metallic ground plane this antenna resonated at 2.3 GHz. The return loss of the antenna showed a frequency shift to 2.5375 GHz with an enhanced bandwidth of 11.8 % when replaced with PBG ground plane. This confirms the reduction of dielectric constant of the substrate when loaded with PBG structures. Equation (4.14) can predict the resonant frequency of the PBG backed RMSA if ε_r is replaced with ε_{rs} the synthesized dielectric constant. The following things are fixed for the study.

- The PBG material is designed to offer a forbidden frequency band around the wanted operating frequency of the antenna.
- A feeding element is chosen and placed within the crystal to obtain the expected resonant mode in the material.

Variation of return loss as a function of frequency is depicted in Figure 5.1.2. The red colored curve in the return loss characteristics again ascertain the calculated synthesized dielectric constant presented in Chapter 4.

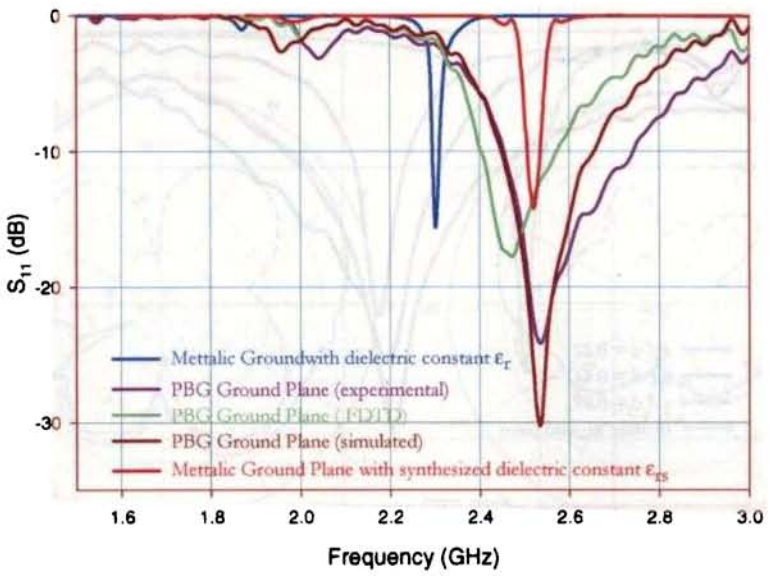

Figure 5.1.2 Return Loss of the Antenna, $L \times W = 27 \times 36\ mm^2$

$\varepsilon_{r1} = 4.7$, $h_1 = 1.6$ mm, $\varepsilon_{r2} = 4.7$, $h_2 = 1.6$ mm $d = 30\ mm$ $\frac{a}{d} = 0.44$

For the optimization of aspect ratio for which RMSA gives better performance different $\frac{a}{d}$ ratios is selected. The reflection characteristics of the patch antenna shows enhanced bandwidth for large $\frac{a}{d}$ ratios. For further optimization of $\frac{a}{d}$ ratio the gain and radiation pattern of the RMSA with PBG ground plane is studied. From these reflection and radiation studies the aspect ratio for better radiation performance of the antenna is optimized to be $\frac{a}{d} = 0.44$. The observations are depicted in Figure 5.1.3, 5.1.4 and 5.1.5. When $\frac{a}{d} = 0.44$, the antenna offered more directive pattern with -30 dB cross-polarization along the bore-sight direction. The gain of the antenna is 10.83 dBi, which is greater than the standard microstrip antenna operating at this frequency. The bandwidth of the antenna is also moderate and greater than that of a conventional RMSA. These observations confirm the suppression of surface waves.

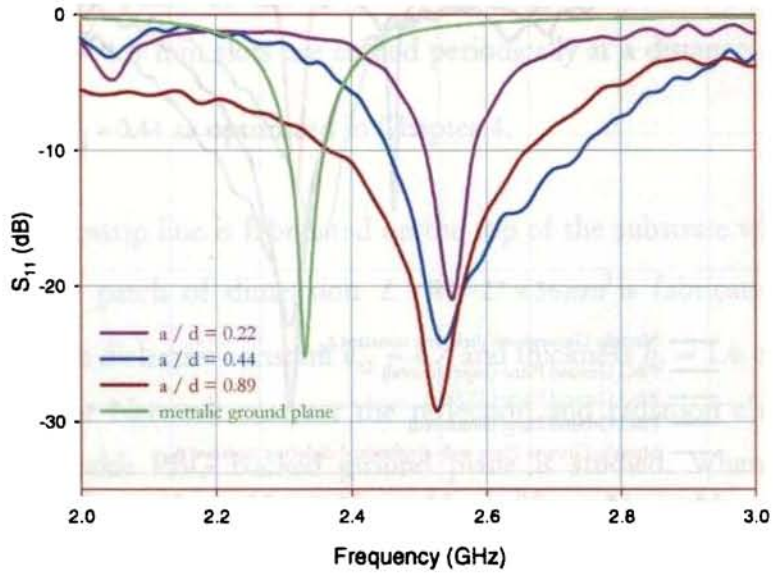

Figure 5.1.3 Return Loss of the Antenna, $L \times W = 27 \times 36\, mm^2$
$\varepsilon_{r1} = 4.7$, $h_1 = 1.6$ mm, $\varepsilon_{r2} = 4.7$, $h_2 = 1.6$ mm $d = 30\, mm$

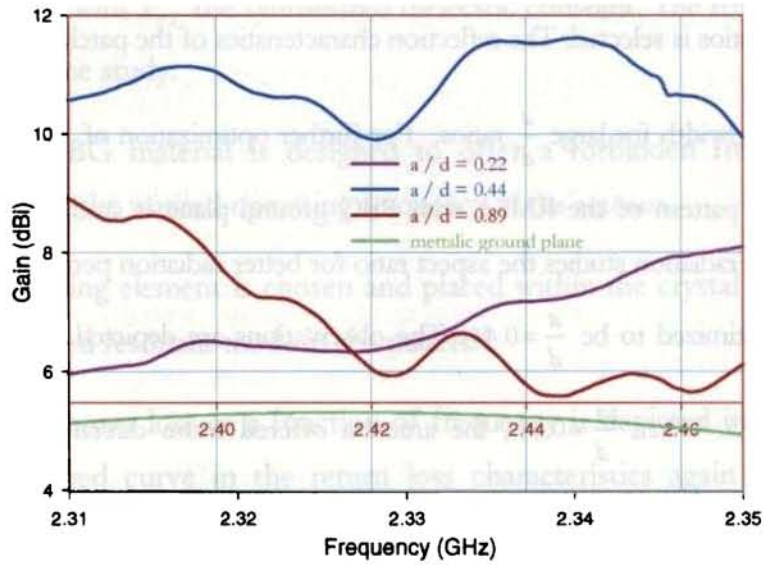

Figure 5.1.4 Gain of the Antenna, $L \times W = 27 \times 36\, mm^2$
$\varepsilon_{r1} = 4.7$, $h_1 = 1.6$ mm, $\varepsilon_{r2} = 4.7$, $h_2 = 1.6$ mm $d = 30\, mm$

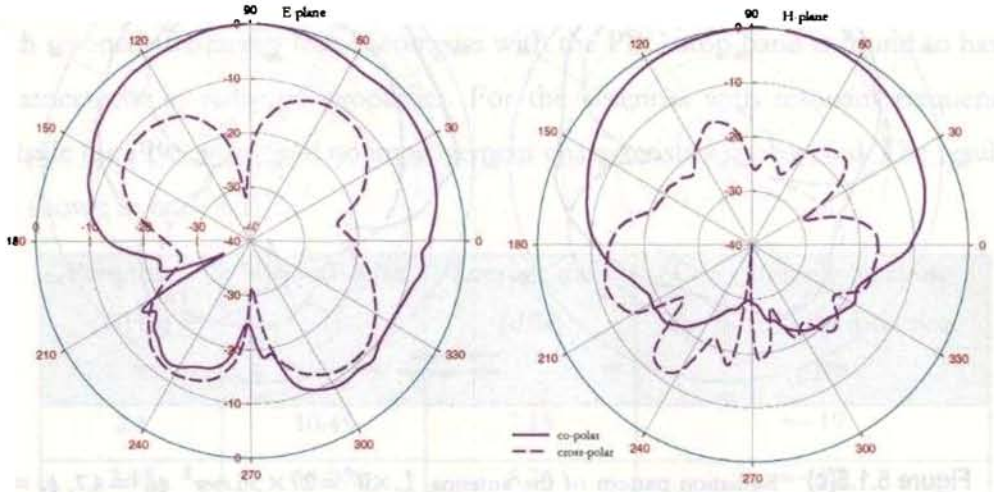

Figure 5.1.5(a) Radiation pattern of the antenna $L \times W = 27 \times 36\, mm^2$ $\varepsilon_{r1} = 4.7$, $h_1 = 1.6$ mm, $\varepsilon_{r2} = 4.7$, $h_2 = 1.6$ mm, $d = 30\ mm$, $\frac{a}{d} = 0.22$

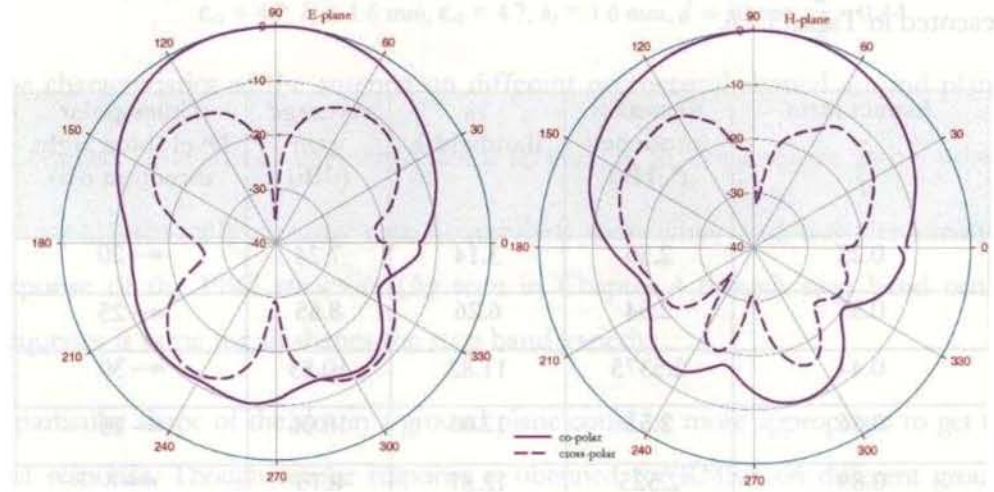

Figure 5.1.5(b) Radiation pattern of the antenna $L \times W = 27 \times 36\, mm^2$ $\varepsilon_{r1} = 4.7$, $h_1 = 1.6$ mm, $\varepsilon_{r2} = 4.7$, $h_2 = 1.6$ mm, $d = 30\ mm$, $\frac{a}{d} = 0.44$

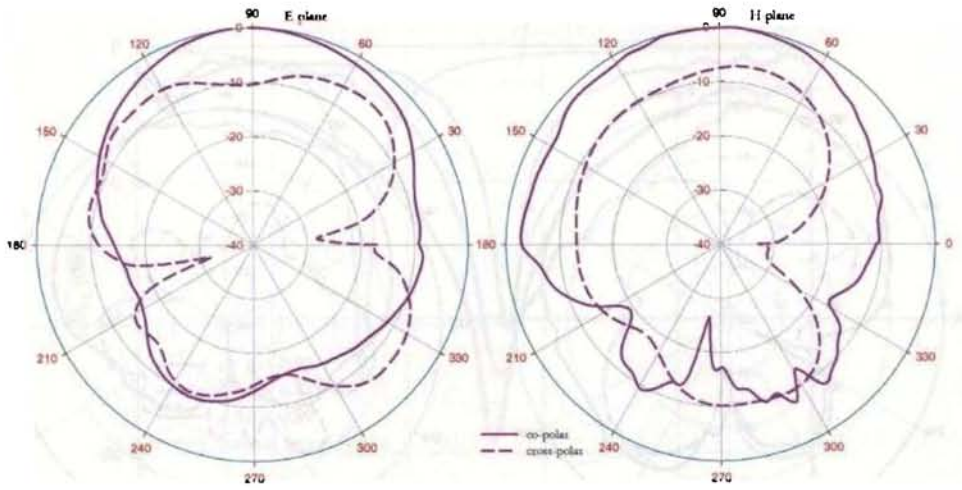

Figure 5.1.5(c) Radiation pattern of the antenna $L \times W = 27 \times 36\, mm^2$ ε_{r1} = 4.7, h_1 = 1.6 mm, ε_{r2} = 4.7, h_2 = 1.6 mm, $d = 30\ mm$, $\frac{a}{d} = 0.89$

The radiation pattern of the PBG backed RMSA showed similar characteristics as of RMSA on metallic ground plane but with more power coupled in the bore-sight direction. The radiation characteristics of the RMSA for different aspect ratio are presented in Table.5.1.6.

Aspect ratio $\frac{a}{d}$	Resonant frequency (GHz)	% Bandwidth	Average gain (dBi)	Cross-polar level (bore sight direction dB)
0.22	2.55	3.14	7.24	≈ -20
0.33	2.54	6.26	8.85	≈ -25
0.44	2.5375	11.82	10.83	≈ -30
0.66	2.53	12.03	10.06	≈ -15
0.89	2.525	12.87	8.75	≈ -8

Table 5.1.6 Radiation properties of the antenna $L \times W = 27 \times 36\, mm^2$ ε_{r1} = 4.7, h_1 = 1.6 mm, ε_{r2} = 4.7, h_2 = 1.6 mm, $d = 30\ mm$

Reflection and radiation properties of RMSA having different dimensions (hence, different resonant frequency) is studied on a PBG ground plane. Only those RMSA with resonant frequency that encompass with the PBG stop band is found to have enhancement in radiation properties. For the antennas with resonant frequency outside the PBG stop band no improvement characteristics is observed. The results are shown in table 5.1.7.

Frequency (GHz)	**% Bandwidth**	**Average gain (dBi)**	**Cross-polar level along the bore sight direction (dB)**
2.1	10.45	7.15	≈ -19
2.15	11.07	8.76	≈ -22
2.5375	11.82	10.83	≈ -30
3.15	9.88	9.97	≈ -28
3.3125	8.61	8.66	≈ -20

Table 5.1.7 Reflection and radiation properties of the different antennas

$\varepsilon_{r1} = 4.7$, $h_1 = 1.6$ mm, $\varepsilon_{r2} = 4.7$, $h_2 = 1.6$ mm, $d = 30\ mm$, $\frac{a}{d} = 0.44$

The characteristics of the antenna on different geometrical shaped ground planes are studied. The area of the etched slot is retained as that of a square with $\frac{a}{d} = 0.44$. An equal area only ensures equal equivalent inductance and not the identical response of the PBG structure (As seen in Chapter 4 though stop band centre frequency is same for all shapes the stop band varied).

A particular shape of the slot in a ground plane could be more appropriate to get the best response. Though similar response is obtained for RMSA on different ground planes, it is observed that PBG ground plane with square lattice is the best. The reflection characteristics of the RMSA for different structures are shown in Figure 5.1.8. The different radiation properties are depicted in Figure 5.1.9 and5.1.10.

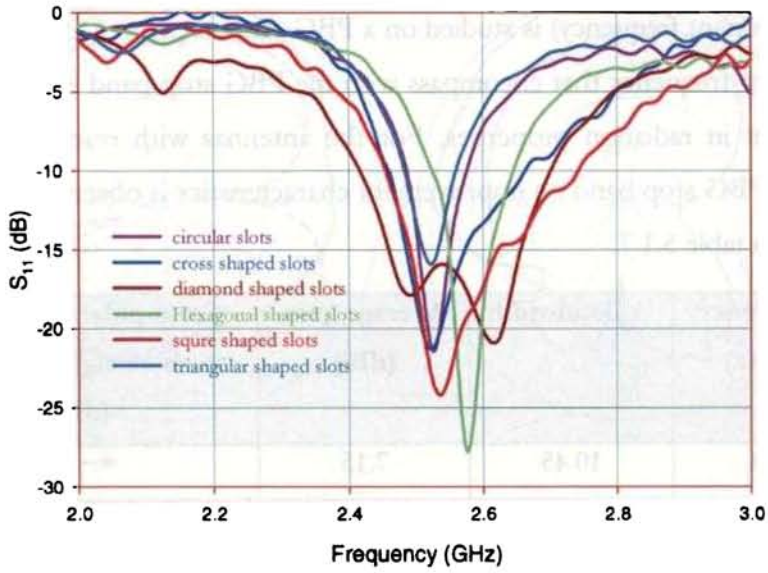

Figure 5.1.8 Return Loss of the Antenna, $L \times W = 27 \times 36\ mm^2$
$\varepsilon_{r1} = 4.7$, $h_1 = 1.6$ mm, $\varepsilon_{r2} = 4.7$, $h_2 = 1.6$ mm $d = 30\ mm$

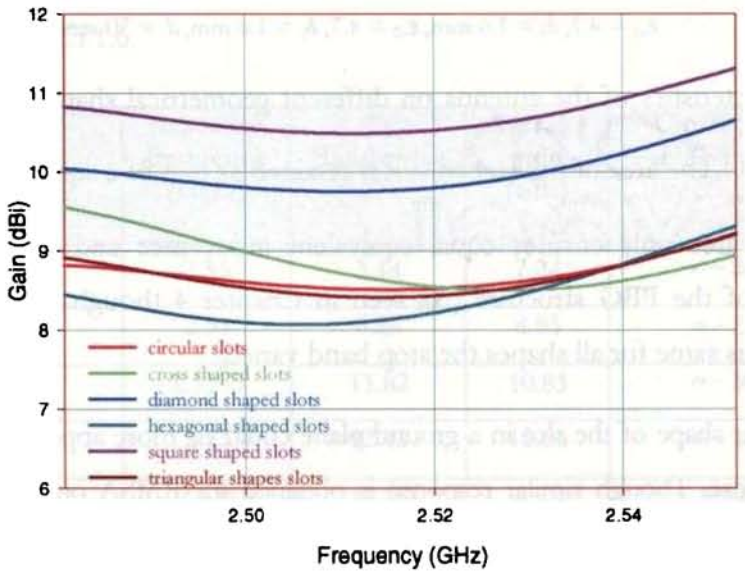

Figure 5.1.9 Gain of the Antenna, $L \times W = 27 \times 36\ mm^2$
$\varepsilon_{r1} = 4.7$, $h_1 = 1.6$ mm, $\varepsilon_{r2} = 4.7$, $h_2 = 1.6$ mm $d = 30\ mm$

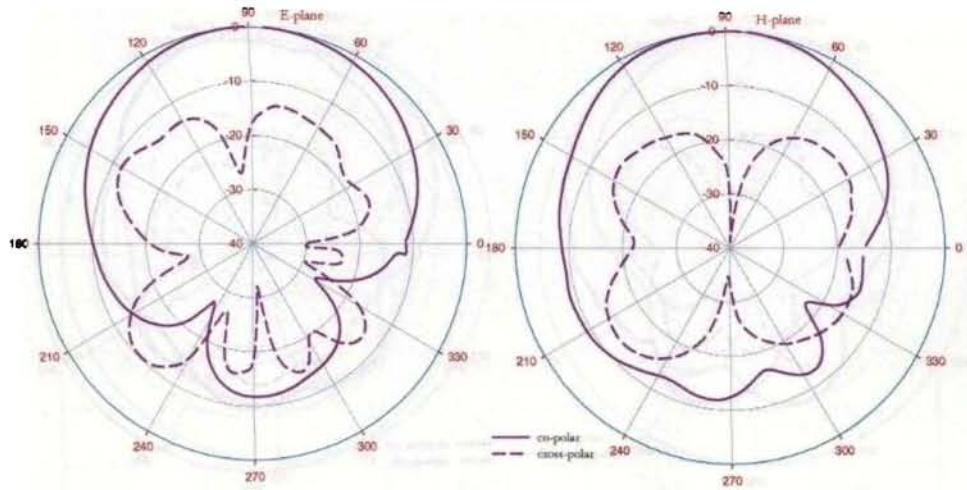

Figure 5.1.10 (a) Radiation pattern of the antenna with PBG ground with circular slots $L \times W = 27 \times 36\, mm^2$ ε_{r1} = 4.7, h_1 = 1.6 mm, ε_{r2} = 4.7, h_2 = 1.6 mm, $d = 30\ mm$

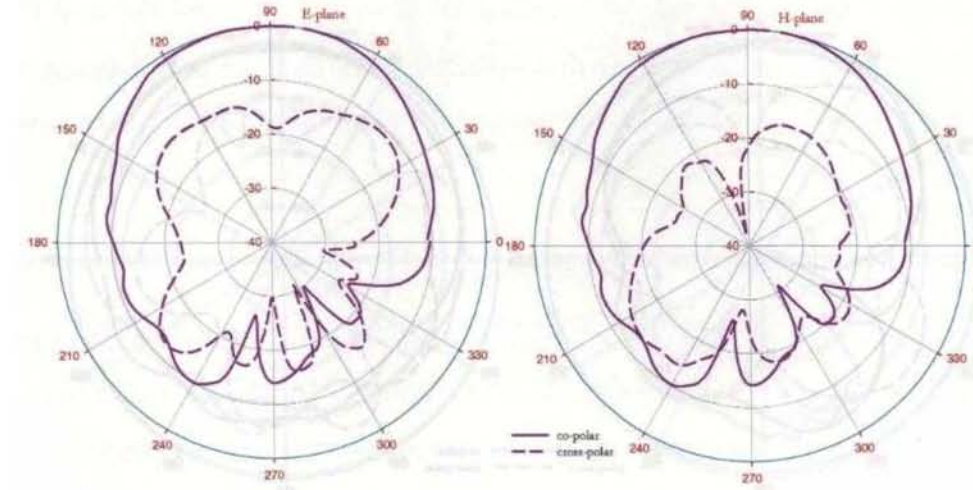

Figure 5.1.10 (b) Radiation pattern of the antenna with PBG ground with cross shaped slots $L \times W = 27 \times 36\, mm^2$ ε_{r1} = 4.7, h_1 = 1.6 mm, ε_{r2} = 4.7, h_2 = 1.6 mm, $d = 30\ mm$

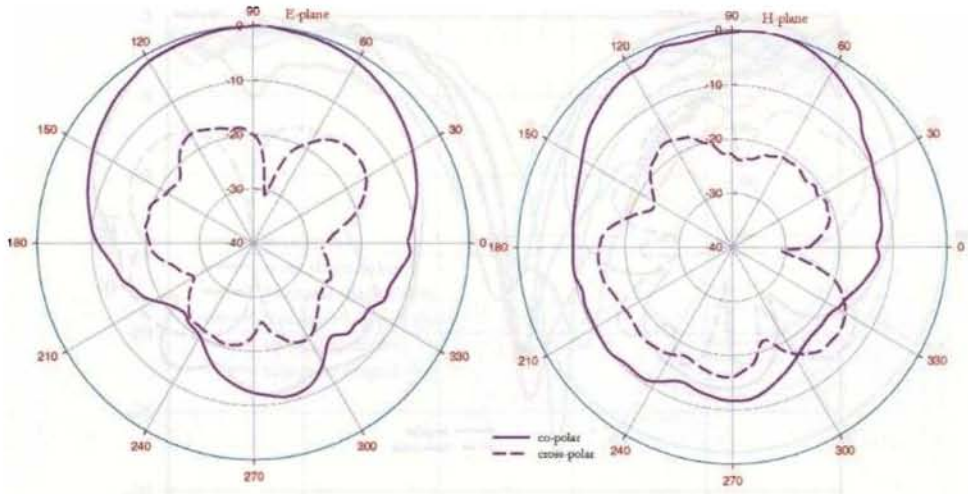

Figure 5.1.10 (c) Radiation pattern of the antenna with PBG ground with diamond shaped slots $L \times W = 27 \times 36\, mm^2$ $\varepsilon_{r1} = 4.7$, $h_1 =$ 1.6 mm, $\varepsilon_{r2} = 4.7$, $h_2 = 1.6$ mm, $d = 30\ mm$

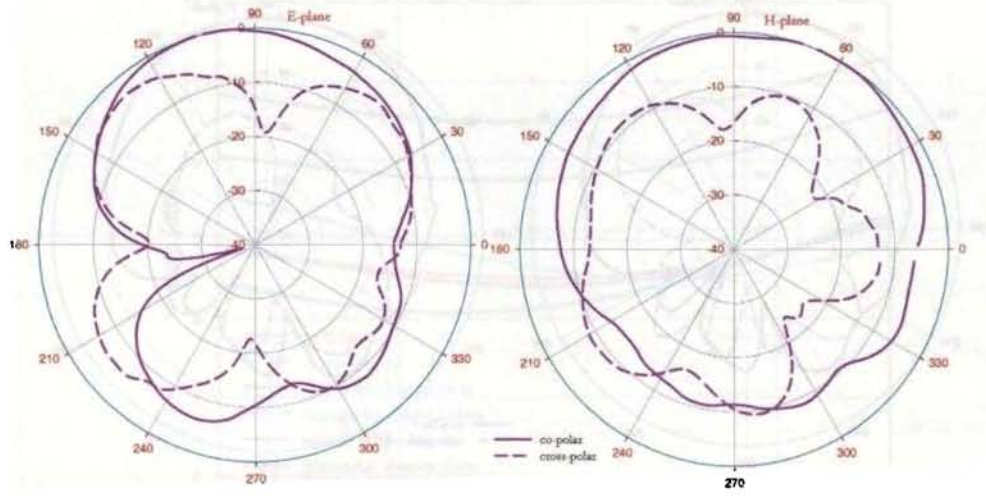

Figure 5.1.10 (d) Radiation pattern of the antenna with PBG ground with hexagonal shaped slots $L \times W = 27 \times 36\, mm^2$ $\varepsilon_{r1} = 4.7$, $h_1 =$ 1.6 mm, $\varepsilon_{r2} = 4.7$, $h_2 = 1.6$ mm, $d = 30\ mm$

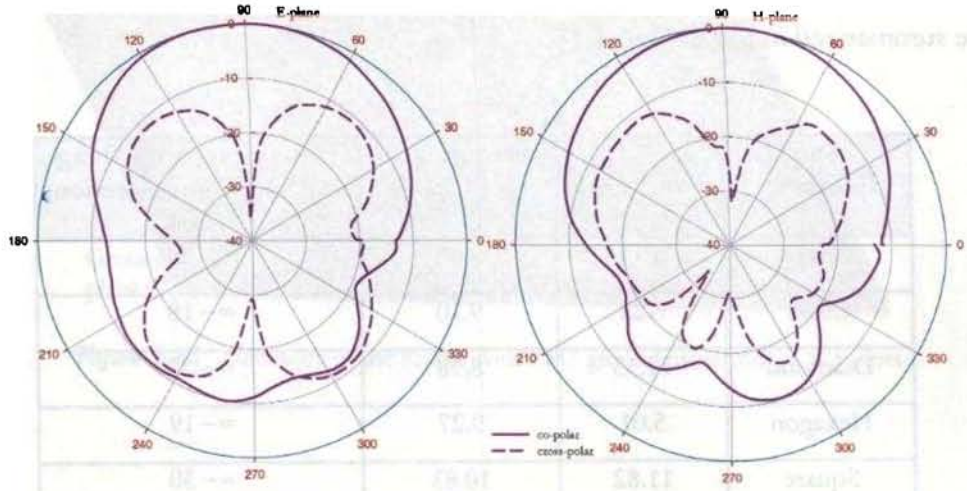

Figure 5.1.10 (e) Radiation pattern of the antenna with PBG ground with square shaped slots $L \times W = 27 \times 36\, mm^2$ $\varepsilon_{r1} = 4.7$, $h_1 = 1.6$ mm, $\varepsilon_{r2} = 4.7$, $h_2 = 1.6$ mm, $d = 30\, mm$

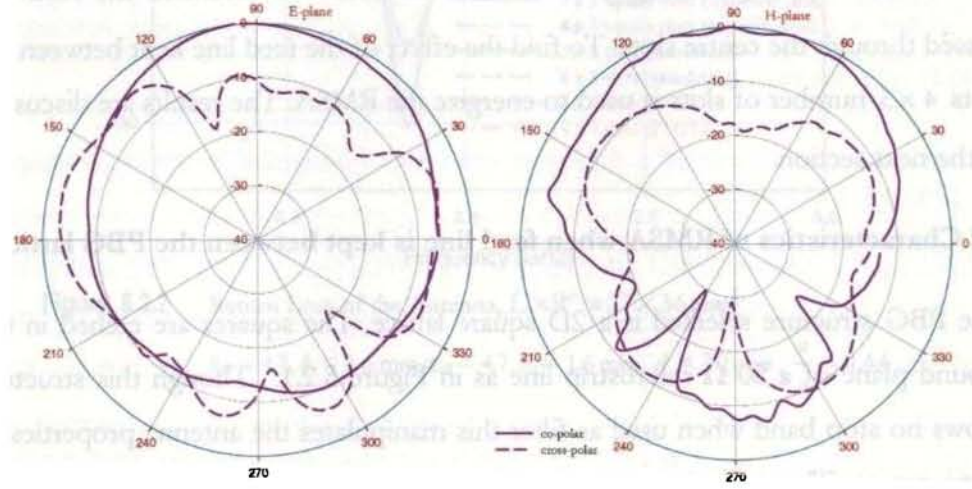

Figure 5.1.10 (f) Radiation pattern of the antenna with PBG ground with triangular shaped slots $L \times W = 27 \times 36\, mm^2$ $\varepsilon_{r1} = 4.7$, $h_1 = 1.6$ mm, $\varepsilon_{r2} = 4.7$, $h_2 = 1.6$ mm, $d = 30\, mm$

The reflection and radiation properties of the RMSA on these PBG ground planes are summarized in the Table 5.1.11.

Slot Geometry	% Bandwidth	Average gain (dBi)	Cross-polar level along the bore sight direction (dB)
Circle	4.11	8.08	≈ -24
Cross	8.21	9.10	≈ -18
Diamond	11.33	8.98	≈ -22
Hexagon	5.01	9.27	≈ -19
Square	11.82	10.83	≈ -30
Triangle	4.11	7.165	≈ -17

Figure 5.1.11 Reflection and radiation characteristics of the antenna with PBG ground $L \times W = 27 \times 36\ mm^2$ ε_{r1} = 4.7, h_1 = 1.6 mm, ε_{r2} = 4.7, h_2 = 1.6 mm, $d = 30\ mm$

In the above cases discussed 3×3 number of slots was used and the feed line passed through the centre slots. To find the effect of the feed line kept between the slots 4×3 number of slots is used to energize the RMSA. The results are discussed in the next section.

5.2 Characteristics of RMSA when feed line is kept between the PBG lattices

The PBG structure selected is a 2D square lattice. The squares are etched in the ground plane of a 50 Ω microstrip line as in Figure 5.2.1. Though this structure shows no stop band when used as filter this manipulates the antenna properties to some extent. The reflection characteristic of this antenna is compared with that having ground plane with 3×3 slots and is shown in Figure 5.2.2.

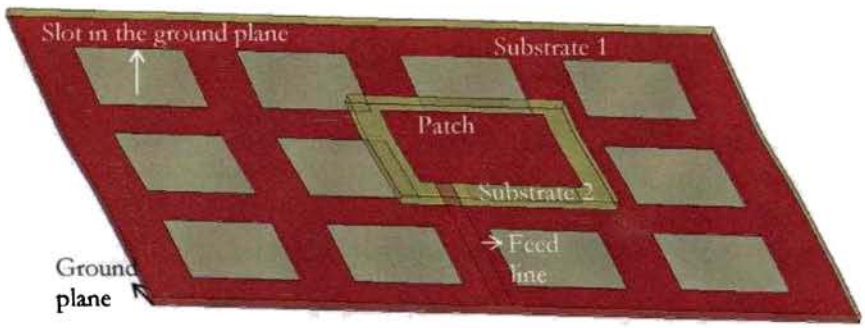

Figure 5.2.1 Geometry of the RMSA with PBG ground plane with 4×3 slots

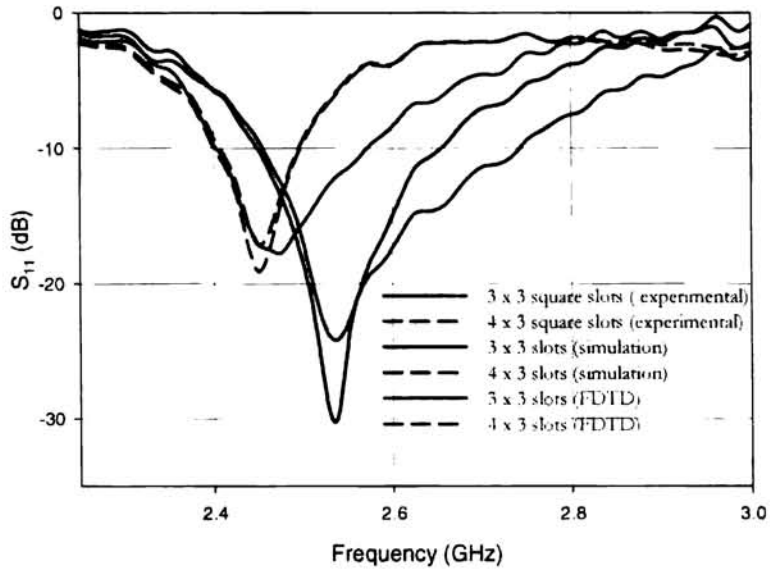

Figure 5.2.2 Return Loss of the Antenna, $L \times W = 27 \times 36\, mm^2$

$\varepsilon_{r1} = 4.7$, $h_1 = 1.6$ mm, $\varepsilon_{r2} = 4.7$, $h_2 = 1.6$ mm, $d = 30\, mm$, $\frac{a}{d} = 0.44$

The bandwidth and the resonant frequency of the RMSA with PBG ground plane having 4×3 slots are found to be lower than that with 3×3 slots. The average gain of the antenna is also found to be ~1.8 dBi less than that with 3×3 slot. So for

better bandwidth the feed line for the antenna should pass through the slots in the ground plane. The radiation pattern of the RMSA is as plotted in Figure 5.2.3.

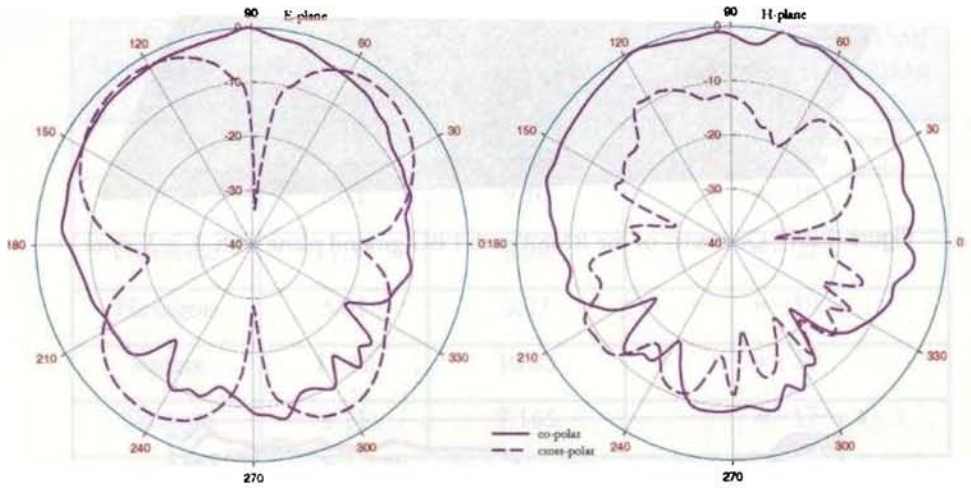

Figure 5.2.3 Radiation pattern of the antenna with 4 ×3 slots in the PBG ground plane, $L \times W = 27 \times 36\, mm^2$ ε_{r1} = 4.7, h_1 = 1.6 mm, ε_{r2} = 4.7, h_2 = 1.6 mm, $d = 30\, mm$ $\frac{a}{d} = 0.44$

Performance of RMSA on the PBG ground plane with two different orthogonal periods is presented in the next section.

5.3 Rectangular Microstrip Antenna on PBG Ground Plane with Unequal Orthogonal Periods

The PBG structure consists of 2x2 slots in the ground plane with orthogonal period d_1 and d_2. These periods are selected such that the stop band center frequency of each period is equal to the operating frequency of the RMSA for TM_{10} and TM_{01} modes. A coaxial probe is used to excite the antenna and performance at different feed locations is studied. The geometry of the proposed antenna configuration is presented in Figure 5.3.1.

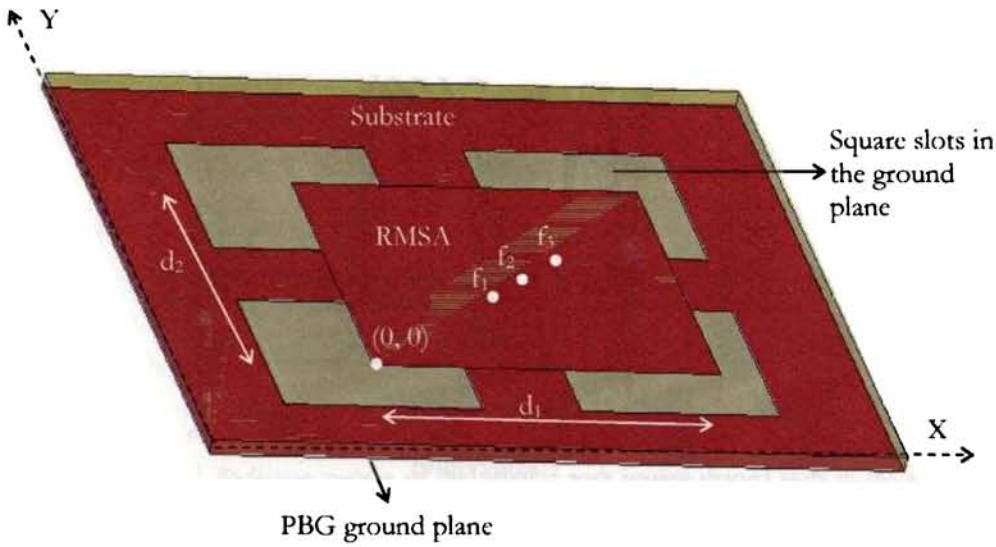

Figure .5.3.1 Antenna configuration with two orthogonal periods in the ground plane $L \times W = 30 \times 40\ mm^2$ ε_r = 4.7, h = 1.6 mm, $d_1 = 40\ mm$ $d_2 = 30\ mm$ a = 0.44 d_2

A RMSA with $L \times W = 30 \times 40\ mm^2$ is fabricated on a dielectric substrate with h = 1.6 mm and ε_r = 4.7. This antenna with metallic ground plane when coaxially fed gave resonance at 1.95 GHz and 2.55 GHz respectively. When PBG ground plane with d_1 = 40 mm and d_2 = 30 mm was incorporated the antenna performance was enhanced. The feed point has considerable influence in the reflection characteristics. Three feed points are selected along the diagonal of the RMSA. Feed points f_1 (1, 1.5) and f_3 (2, 2.5) excites both TM_{10} and TM_{01} mode frequencies of the antenna while f_2 (1.5, 2) merges both the frequencies resulting in a wide band.

Similar studies are conducted with the PBG ground plane with circular slots and in both the cases at the feed points f_1 = (1.5, 1) and f_3 = (2.5, 2) dual frequencies are excited. When the feed point was at f_2 = (2, 1.5) the two orthogonal frequencies merge to give a wide bandwidth. The return loss of the antenna is shown in Figure 5.3.2.

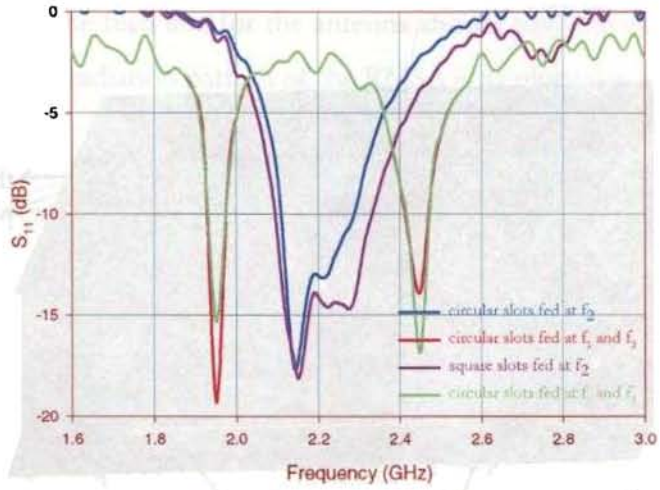

Figure 5.3.2 Return Loss of the Antenna, $L \times W = 30 \times 40\ mm^2$
$\varepsilon_r = 4.7$, $h = 1.6$ mm, $d_1 = 40\ mm$ $d_2 = 30\ mm$ $a = 0.44\ d_2$

The gain of this antenna at the two different feed points is illustrated in Figure 5.3.3. The gain of the antenna is found to be better than conventional RMSA.

The radiation pattern of the antenna at the enhanced band width position is shown in Figure 5.3.4. As far the gain and cross-polar level are concerned the radiation pattern obtained is better than the conventional Rectangular Microstrip Antenna.

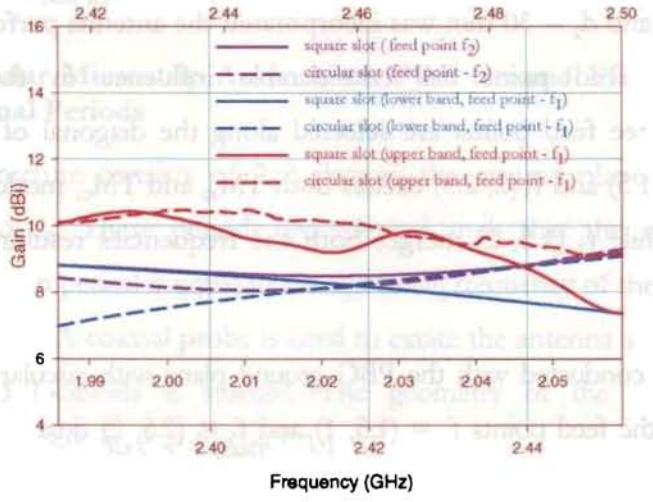

Figure 5.3.3 Gain of the Antenna,, $L \times W = 30 \times 40\ mm^2$
$\varepsilon_r = 4.7$, $h = 1.6$ mm, $d_1 = 40\ mm$ $d_2 = 30\ mm$ $a = 0.44\ d_2$

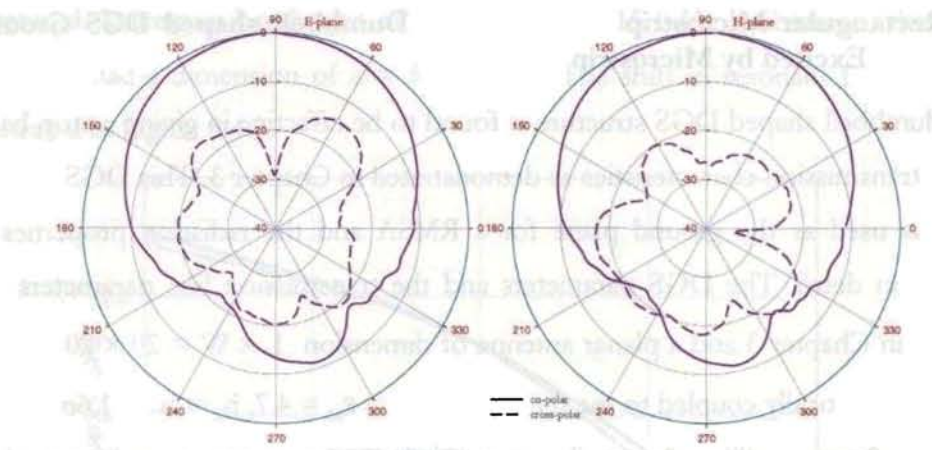

Figure 5.3.4 (a) Radiation pattern of the antenna with square shaped slots in the ground plane fed at the centre. $L \times W = 30 \times 40\ mm^2$ ε_r = 4.7, h = 1.6 mm, $d_1 = 40\ mm$ $d_2 = 30\ mm$ a = 0.44 d_2

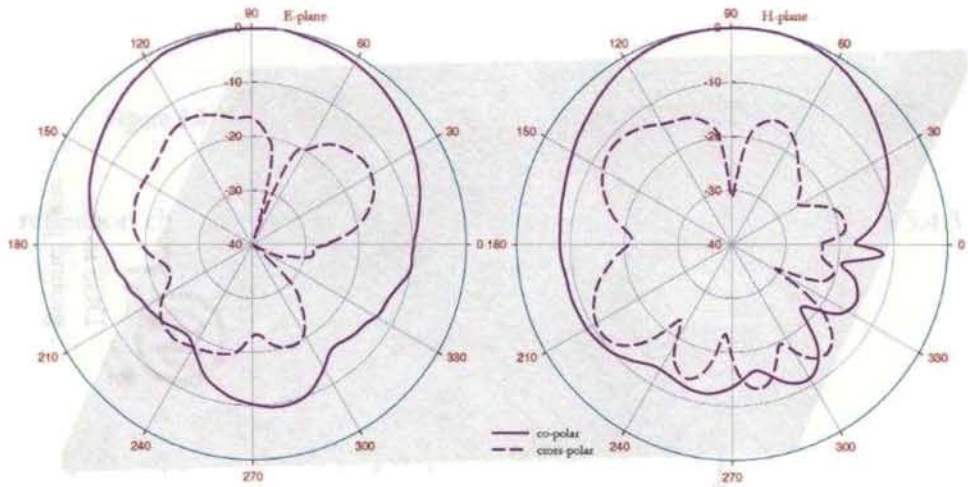

Figure 5.3.4 (b) Radiation pattern of the antenna with circular slots in the ground plane fed at the centre. $L \times W = 30 \times 40\ mm^2$ ε_r = 4.7, h = 1.6 mm, $d_1 = 40\ mm$ $d_2 = 30\ mm$ a = 0.44 d_2

It is concluded that the dual period PBG can enhance the bandwidth of the antenna and desired frequency can be achieved by selecting the feed point. In the following sections DGS is applied to the ground plane of a microstrip line fed RMSA and coplanar waveguide (CPW) fed loop slot antenna.

5.4 Rectangular Microstrip Antenna with Dumbbell shaped DGS Ground Plane Excited by Microstrip Feed

The dumbbell shaped DGS structure is found to be effective in giving a stop band in the transmission characteristics as demonstrated in Chapter 3. This DGS ground plane is used as the ground plane for a RMSA and the radiation properties is studied in detail. The DGS parameters and the transmission line parameters are kept as in Chapter 3 and a planar antenna of dimension $L \times W = 20 \times 20$ mm^2 is electromagnetically coupled to the fee line (i.e. $\varepsilon_{r1} = \varepsilon_{r2} = 4.7$, $h_1 = h_2 = 1.6$mm, a = b, g = 0.2mm, l =W = 3mm). The proposed antenna structure is illustrated in Figure 5.4.1. The numbers of DGS cells (n) were increased to find the response of the antenna but had no effect in the characteristics and so only one cell is incorporated in the ground plane for the studies.

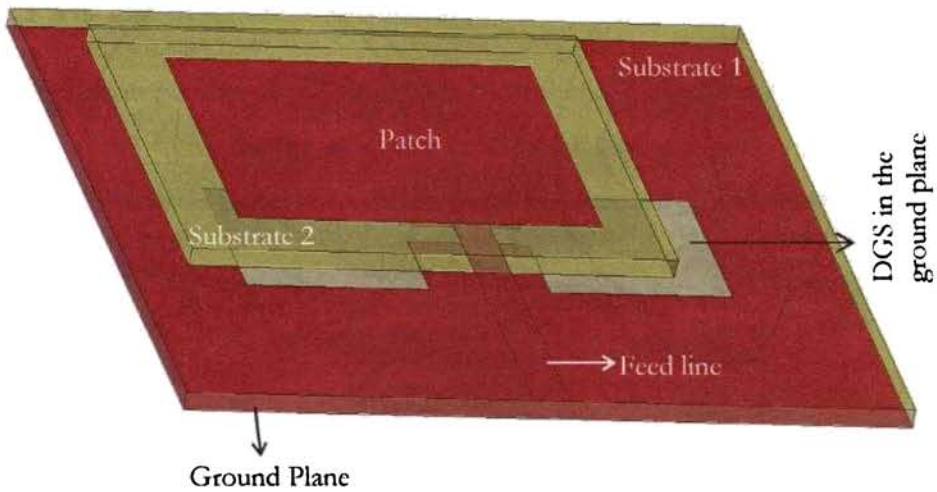

Figure 5.4.1 Geometry of the proposed antenna with DGS in the ground plane. $L \times W = 20 \times 20\ mm^2$, $\varepsilon_{r1} = \varepsilon_{r2} = 4.7$, $h_1 = h_2 = 1.6$mm, a = b, g = 0.2mm, l =W = 3mm

The patch antenna $L \times W = 20 \times 20\ mm^2$ resonated at 3.1 GHz when metallic ground plane is used and the frequency is shifted to a lower side when DGS cell is integrated in the ground plane. As the size of the cell increased the resonant frequency showed more shift towards the lower side but the impedance bandwidth

decreased. Maximum bandwidth of 165 MHz at 2.515 GHz is obtained when the DGS cell had a dimension of $a = b = 8$ mm. The shift in resonant frequency is illustrated in Figure 5.4.2.

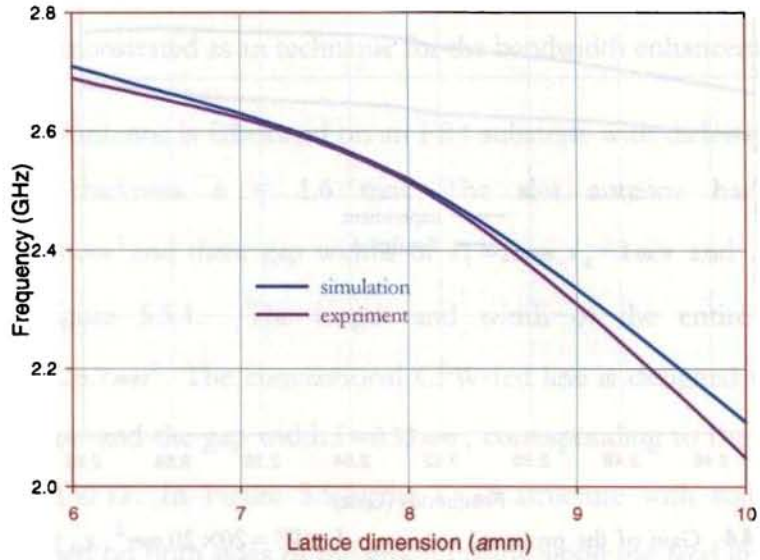

Figure 5.4.2 Variation resonant frequency with lattice dimension '*a*'

The reflection characteristic of the DGS backed antenna is shown in Figure 5.4.3.

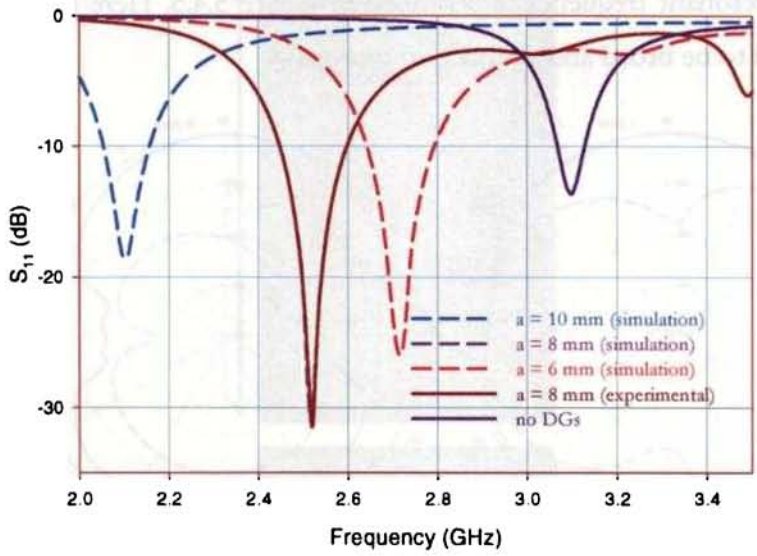

Figure 5.4.3 Return Loss of the Antenna, $L \times W = 20 \times 20 mm^2$, $\varepsilon_{r1} = \varepsilon_{r2} = 4.7$, $h_1 = h_2 = 1.6$mm, a = b, g = 0.2mm, l =W = 3mm

The gain of the proposed antenna is found to be 5.35 dBi at the resonant frequency for maximum bandwidth parameters. The gain plot is as depicted in Figure 5.4.4.

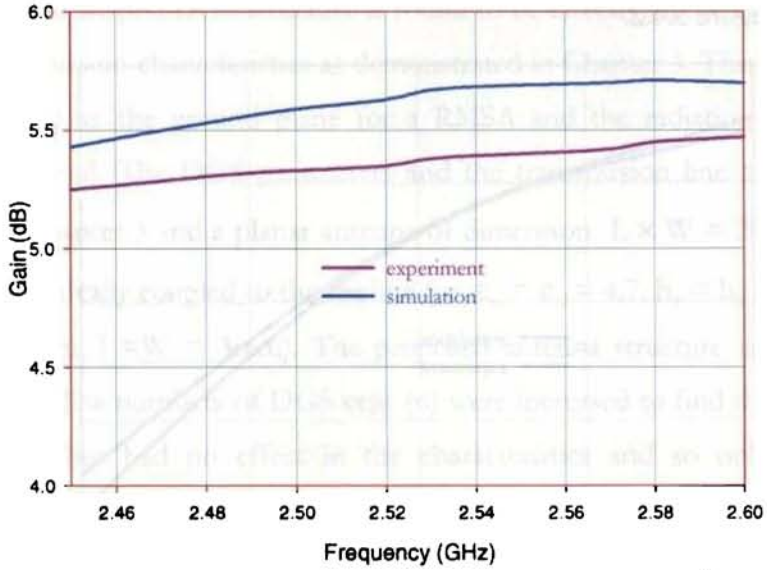

Figure 5.4.4 Gain of the proposed antenna, $L \times W = 20 \times 20\, mm^2$, $\varepsilon_{r1} = \varepsilon_{r2} = 4.7$, $h_1 = h_2 = 1.6$mm, a = b = 8 mm, g = 0.2mm, l =W = 3mm

For the optimized configuration offering maximum bandwidth the radiation pattern at the resonant frequency is described in Figure 5.4.5. Here the radiation pattern is found to be broad and almost bi-directional.

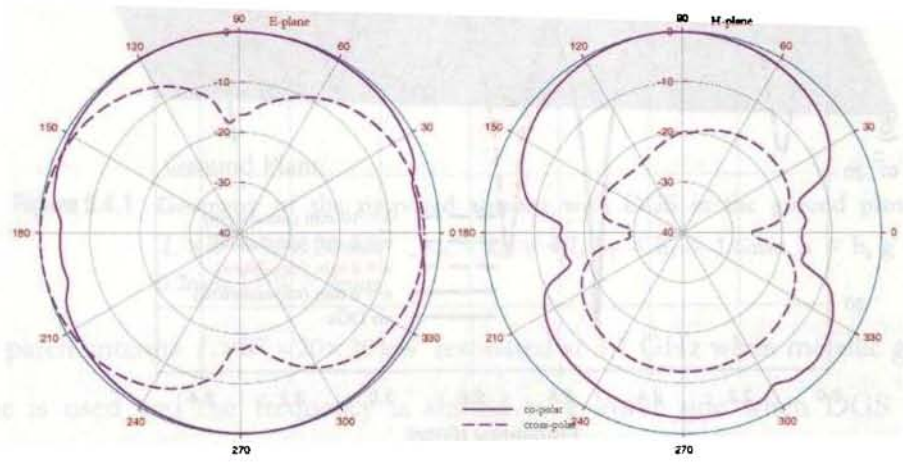

Figure 5.4.5 Radiation pattern of the antenna, $L \times W = 20 \times 20\, mm^2$, $\varepsilon_{r1} = \varepsilon_{r2} = 4.7$, $h_1 = h_2 = 1.6$mm, a = b = 8 mm, g = 0.2mm, l =W = 3mm

5.5 Broadband CPW-fed loop slot antenna

The conventional CPW-fed loop slot antenna incorporated with a DGS structure in the feed network has been proposed and the DGS structure with square-shaped lattices has demonstrated as an technique for the bandwidth enhancement.

The proposed antenna is fabricated on an FR4 substrate with dielectric constant ε_r = 4.7 and thickness h = 1.6 mm. The slot antenna has dimensions $L \times W = 20 \times 20\, mm^2$ and three gap widths of $l_1 = 2\, mm, l_2 = 1\, mm$ and $l_3 = 4.5\, mm$ as shown in Figure 5.5.1. The length and width of the entire structure is $l' \times l'' = 38.5 \times 25.7\, mm^2$. The conventional CPW-fed line is designed with the strip width $W = 3\, mm$ and the gap width $S = 0.33\, mm$, corresponding to the characteristic impedance of 50 Ω. In Figure 5.5.1, the DGS structure with square - shaped lattices is etched on both sides of the ground plane along the feed line. The lattice dimension of the CPW- DGS structure is kept as, $a_1 = a_2$, $g = 0.2\, mm$ and $l = 1\, mm$.

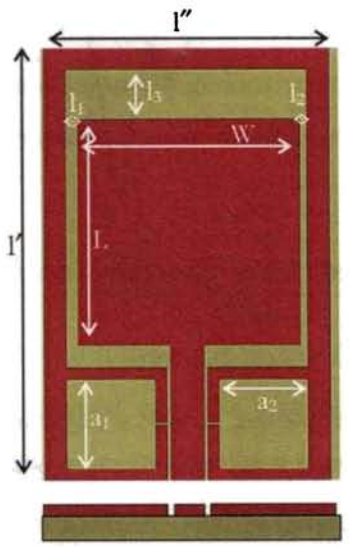

Figure 5.5.1 Geometry of the CPW-fed loop slot antenna $L \times W = 20 \times 20\, mm^2$ ε_r = 4.7, h =1.6 mm, $a_1 = a_2$, $g = 0.2\, mm$, $l = 1\, mm$, $l_1 = 2\, mm, l_2 = 1\, mm, l_3 = 4.5\, mm$, $l' \times l'' = 38.5 \times 25.7\, mm^2$

CPW-fed loop antenna without DGS resonated at 2.825 GHz giving 21% bandwidth. When DGS is incorporated in the ground plane the bandwidth shows variation with a shift in the resonant frequency. Large DGS cell is found to reduce the bandwidth. A slight disturbance in the current path is enough to give a wide bandwidth. The return loss variation as a function of frequency is depicted in Figure 5.5.2. Maximum bandwidth of 57.6% (2.575 – 4.16) at 2.75 GHz is obtained for the CPW – fed slot antenna when the DGS cell is of the dimension $a_1 = a_2 = 2\ mm$. The gain of this antenna with DGS cell of 2 mm is 3.15 dBi while the same antenna without DGS gives a gain of 3.18 dBi. The radiation pattern of the antenna at 2.17 GHz is shown in Figure 5.5.3.

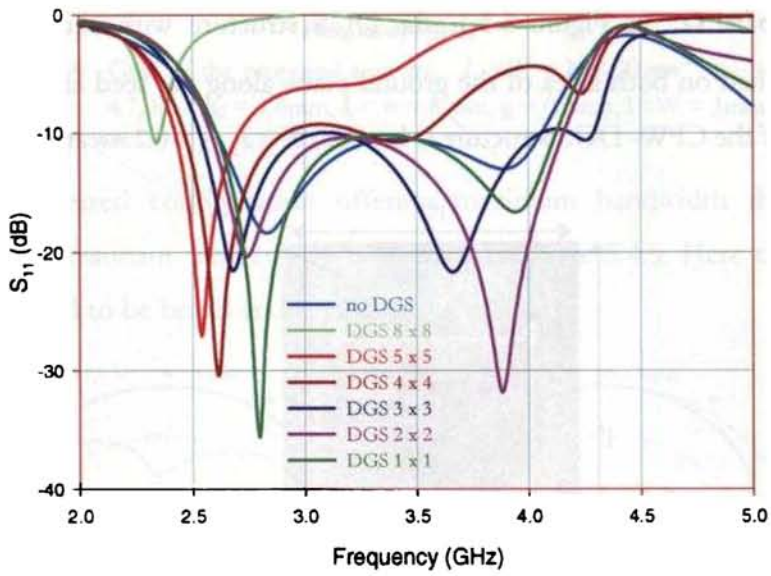

Figure 5.5.2 Return Loss of the Antenna, $L \times W = 20 \times 20\ mm^2$ ε_r = 4.7, h = 1.6 mm, $a_1 = a_2 = 2\ mm$, $g = 0.2\ mm$, $l = 1\ mm$, $l_1 = 2\ mm$, $l_2 = 1\ mm$, $l_3 = 4.5\ mm$

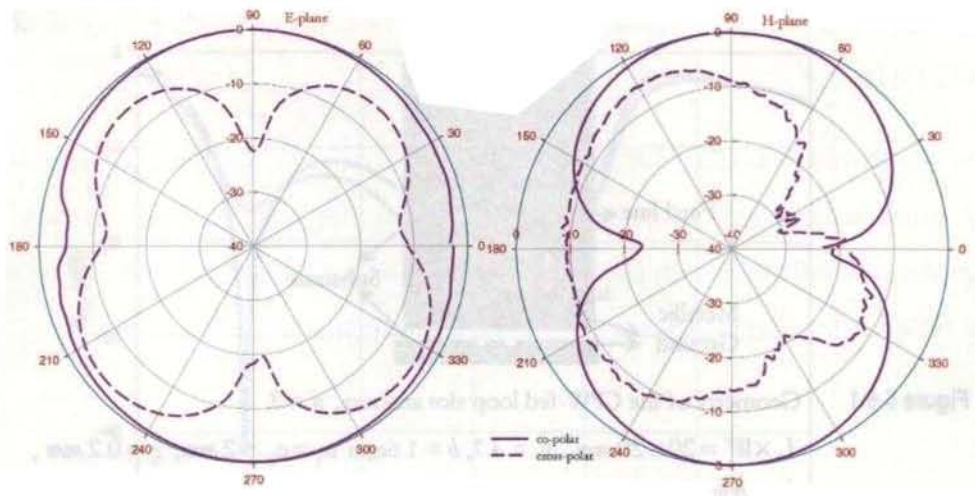

Figure 5.5.3 Radiation pattern of the antenna $L \times W = 20 \times 20\, mm^2$ $\varepsilon_r = 4.7$, $h = 1.6$mm $a_1 = a_2 = 2\, mm$, $g = 0.2\, mm$, $l = 1\, mm$, $l_1 = 2\, mm$, $l_2 = 1\, mm$, $l_3 = 4.5\, mm$

The radiation pattern of the antenna is very broad and almost bi-directional. The antenna is very compact and can be highly suitable for mobile and wireless WLAN.

The CPW-fed loop slot antenna gave a bandwidth of ~ 58 % with only one DGS unit cell in the ground plane. So investigations were done to find out whether more than one DGS cell can enhance the bandwidth or not. This study is discussed in the following section.

5.6 CPW-fed loop slot antenna with more than one DGS cell in the ground plane

The slot antenna dimensions and three gap widths (l_1, l_2, l_3) of this structure and the CPW feed parameters is retained as in the case of the single unit cell for ease of comparison. The DGS parameters also kept the same as $a_1 = a_2 = 2\, mm$. Figure 5.6.1, the DGS structure with square - shaped lattices is etched on both sides of the ground plane along the feed line placed at a distance d with the number of cells etched $n = 2$.

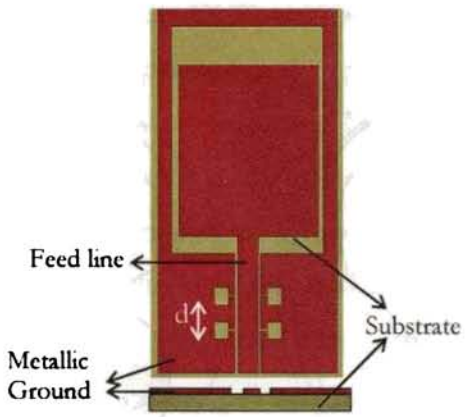

Figure 5.6.1 Geometry of the CPW-fed loop slot antenna, $n = 2$
$L \times W = 20 \times 20\ mm^2$ ε_r = 4.7, h = 1.6mm $a_1 = a_2 = 2\ mm$, $g = 0.2\ mm$,
$l = 1\ mm, l_1 = 2\ mm, l_2 = 1\ mm, l_3 = 4.5\ mm$

CPW-fed loop antenna with 2 DGS cells having $a_1 = a_2 = 2\ mm$ is fabricated on an FR4 substrate. The spacing d between the cells is varied to optimize for maximum impedance bandwidth. As the spacing increased the resonant frequency gets shifted towards the lower side with a decrease in the bandwidth. These results are presented in Figure 5.6.2.

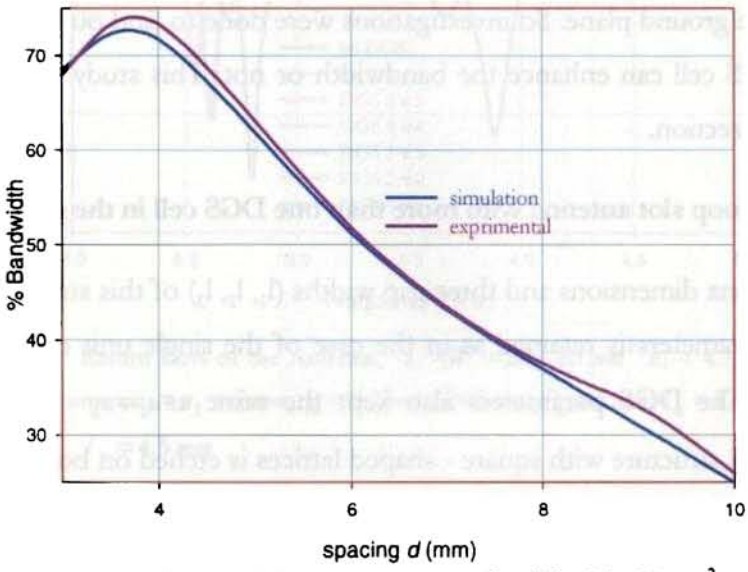

Figure .5.6.2 Variation of % bandwidth with spacing d $L \times W = 20 \times 20\ mm^2$ ε_r = 4.7, h = 1.6 mm, $a_1 = a_2 = 2\ mm$, $g = 0.2\ mm$, $l = 1\ mm, l_1 = 2\ mm, l_2 = 1\ mm, l_3 = 4.5\ mm$

The reflection characteristic for maximum bandwidth spacing is depicted in Figure 5.6.3.

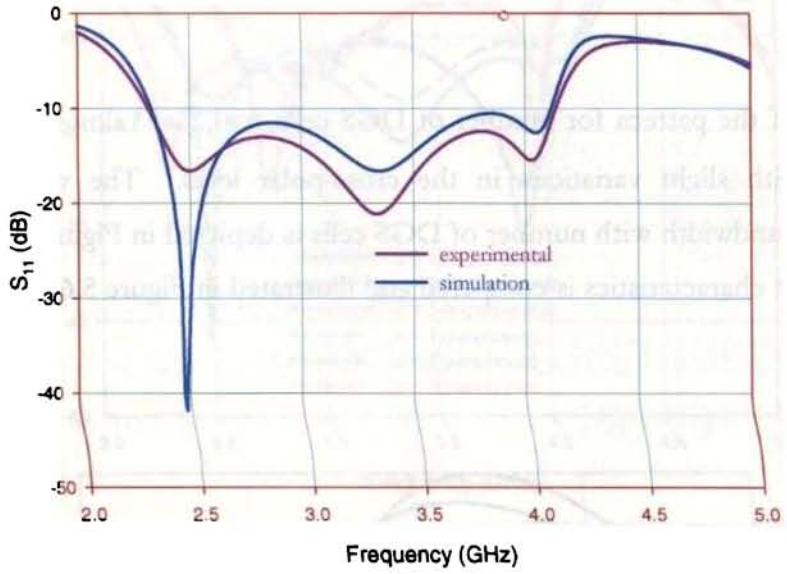

Figure 5.6.3 Return Loss of the Antenna, $n = 2$, $d = 4mm$, $L \times W = 20 \times 20\ mm^2$ $\varepsilon_r = 4.7$, $h = 1.6$ mm, a_1 $2mm$, $g = 0.2mm$, $l = 1\ mm$, $l_1 = 2\ mm$, $l_2 = 1\ mm$, $l_3 = 4.5\ mm$

An optimum bandwidth of 73.4% at 2.48 GHz is obtained when d = 4mm experimentally. The gain of this antenna with DGS cell of 2 mm spaced 4 mm apart is 3.18 dBi. The radiation pattern of the antenna at 2.48 GHz is shown in Figure 5.6.4.

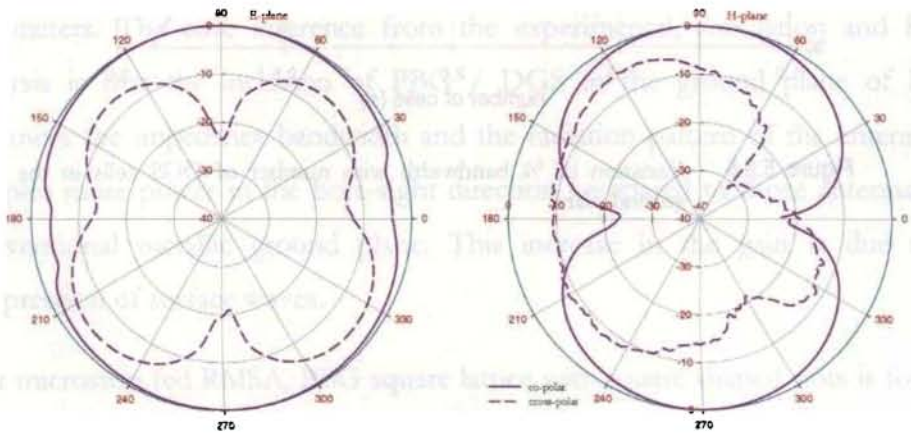

Figure 5.6.4 Radiation pattern of the antenna, $n = 2$, $L \times W = 20 \times 20\ mm^2$ $\varepsilon_r = 4.7$, $h = 1.6$ mm, $d = 4\ mm$, $a_1 = 2\ mm$, $g = 0.2\ mm$, $l = 1\ mm$ $l_1 = 2\ mm$, $l_2 = 1\ mm$ $l_3 = 4.5\ mm$

The impedance bandwidth is found to decrease with 3 DGS cells in the ground plane but the gain gets enhanced to 3.3 dBi with resonant frequency shift to 2.875 GHz.

The shape of the pattern for number of DGS cells $n=1,2$ *and* 3 almost remained the same with slight variations in the cross-polar level. The variation of impedance bandwidth with number of DGS cells is depicted in Figure 5.6.5 and the reflection characteristics is compared and illustrated in Figure 5.6.6.

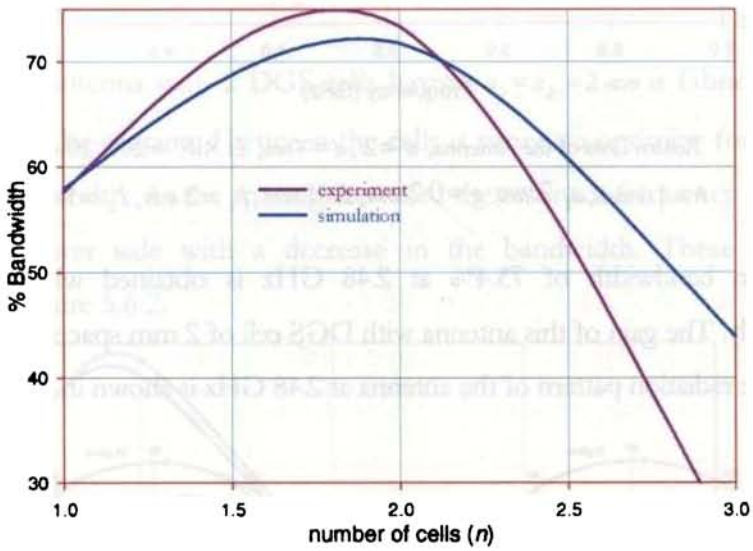

Figure 5.6.5 Variation of % bandwidth with number of DGS cells in the ground plane

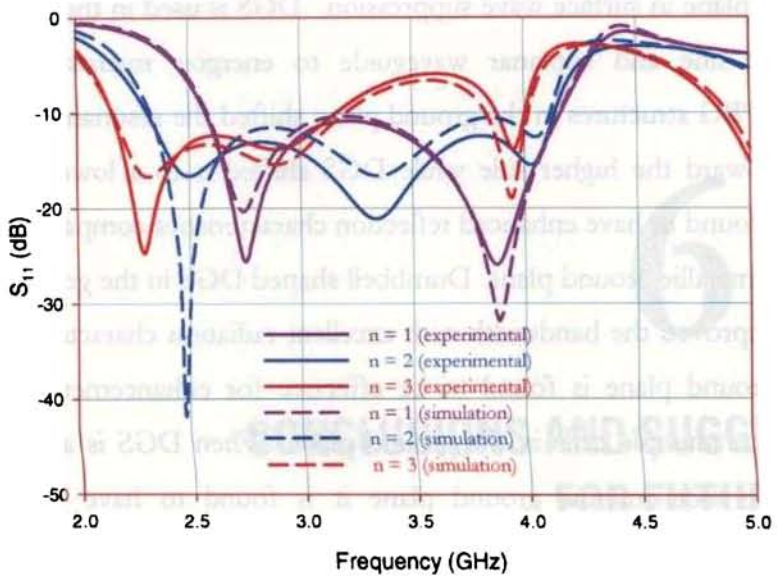

Figure 5.6.6 Return Loss of the Antenna, $n = 2$, $d = 4mm$, $L \times W = 20 \times 20\, mm^2$ ε_r = 4.7, h = 1.6 mm, a_1 2 mm, $g = 0.2\, mm$, $l = 1\, mm$, $l_1 = 2\, mm$, $l_2 = 1\, mm$, $l_3 = 4.5\, mm$

5.7 Antenna Characteristics - Consolidated

The antennas used in the study have rectangular geometry but other shapes will also have the benefit of PBG / DGS property by properly choosing of the parameters. The core inference from the experimental, simulation and FDTD analysis is that the inclusion of PBG / DGS in the ground plane of RMSA enhances the impedance bandwidth and the radiation pattern of the antenna and couples more power in the bore-sight direction compared to those antennas with conventional metallic ground plane. This increase in the gain is due to the suppression of surface waves.

For microstrip fed RMSA, PBG square lattice with square shaped slots is found to be more effective in suppressing surface waves than the other geometrical slots under study. The gain of the antenna is also improved indicating the effectives of

PBG ground plane in surface wave suppression. DGS is used in the ground plane of microstrip line and coplanar waveguide to energize microstrip antennas. Inclusion of PBG structures in the ground plane shifted the resonant frequency of the RMSA toward the higher side while DGS shifted it to a lower side. These antennas are found to have enhanced reflection characteristics compared to that on conventional metallic ground plane. Dumbbell shaped DGS in the ground plane of the RMSA improved the bandwidth with excellent radiation characteristics. Single cell in the ground plane is found to be effective for enhancement of antenna properties than multiple cells in the ground plane. When DGS is applied to the CPW-fed loop slot antenna ground plane it is found to have an improved bandwidth with moderate gain. The 2 DGS cell structure is found to be an ideal choice for wide bandwidth and gain Characteristics of diffrent antennas are presented in the table below.

Antenna		**% bandwidth**	**Gain (dBi)**	**Cross-polar level**
RMSA with PBG ground plane - electromagnetic coupling – microstrip fed (3 x3 slots)		11.8	10.8	-30
RMSA with PBG ground plane (probe fed at centre)		11	8	-30
RMSA with DGS ground plane - electromagnetic coupling – microstrip fed		6.6	5.6	-18
Loop Slot with DGS ground plane of CPW	n = 1	57.6	3.2	- 9
	n = 2	73.4	3.2	- 10
	n = 3	23.9	3.3	- 9

6

CONCLUSIONS AND SUGGESTIONS FOR FUTURE WORK

Contents

Three broad areas are discussed in this thesis

- *Computation of band gap*
- *Design and analysis of compact high performance band stop filters*
- *Analysis of wideband high gain microstrip antennas*

6.1 Computation of band gap

Chapter 2 discusses in depth the fundamental understanding of the electromagnetic waves in a periodic medium and computation of band gap. The Band Gap origin in Photonic crystal is explained with the help of Maxwell's equation and Bloch-Floquet's theorem. The band diagram is computed and presented in chapter 2.

6.2 Design and analysis of compact high performance band stop filters

Filters play important roles in many RF/microwave applications. They are used to separate or combine different frequencies. The electromagnetic spectrum is limited and has to be shared; filters are used to select or confine the RF/microwave signals within assigned spectral limits. Emerging applications such as wireless communications continue to challenge RF/microwave filters with ever more stringent requirements higher performance, smaller size, lighter weight, and lower cost. Depending on the requirements and specifications, RF/microwave filters may be designed as lumped element or distributed element circuits; they may be realized in various transmission line structures, such as waveguide, coaxial line, and microstrip.

We have introduced in this thesis the limitations of classical microstrip line based band stop filters and way to improve the design and response by using the photonic band gap and defected ground plane structures. Four types of planar filters are presented and examined. These filters are

- PBG for microstrip line
- Dumbbell DGS for microstrip line
- DGS for coplanar waveguide
- DGS for asymmetric coplanar waveguide

New investigations are presented on the choice of geometrical shapes for the PBG structure as an element for the band stop filter. Six such geometric shapes are studied. For further compactness the microstrip line is introduced with a dumbbell shaped DGS structure in the ground plane which effectively rejects the frequency range of concern. Idea of DGS is extended to the coplanar waveguide and asymmetric coplanar waveguide. Design and analysis of each of these filters is illustrated in Chapter 4.

6.3 Design of new wideband high gain microstrip antennas

An antenna serves as the "transition" between the RF front-end circuitry and the radiation and propagation of electromagnetic waves in free space. Antennas play a critical role in microwave and other wireless applications systems. Planar oriented antenna, such as microstrip patch has attracted significant attention among antenna engineers due to the tremendous benefits they bring to modern wireless systems in comparison to more conventional designs.

We have introduced in this thesis the PBG backed ground plane for patch antennas to increase its bandwidth. By choosing the suitable substrate, period and shape of the PBG structure a bandwidth of ~ 12 % is obtained from a simple, low profile,

and light weight Microstrip antenna. For many applications such as satellite communications and mobile radio, for which printed antennas are otherwise well suited, low gain may be a serious disadvantage. The electromagnetically coupled RMSA has been investigated to improve the gain and bandwidth with PBG structures in the ground plane. Probe fed PBG backed dual period RMSA further enhanced the bandwidth. These antennas are made compact yet by replacing PBG with DGS elements for microstrip strip fed patch antenna. Insertion of PBG structures in the ground plane of patch antennas shifted the resonant frequency toward the higher side while DGS shifted it to a lower side. DGS is used in the ground plane of CPW and wide bandwidth is achieved. Number of DGS cells for optimum bandwidth is also optimized and presented in Chapter 5. Though rectangular shaped antennas is discussed in detail these inferences hold good for antennas of any geometric shapes.

6.4 Suggestions for future work

Based on observations gathered while completing this thesis certain topics is identified which would benefit further investigation.

- It was found that the geometrical shapes of the PBG - circle, cross, diamond, hexagon, square, triangle etc influence on the sharpness of the transition and stop band rejection. It will be an interesting to investigate the effect of these geometrical shapes as DGS in the ground plane and study the stop band characteristics.
- Since DGS cells have inherently resonant properties, many of them have been used in filtering circuits to improve the stop and pass band characteristics. The DGS have been proposed for improving the spurious response of microstrip band stop filters. Further DGS can be used with couplers, hybrid rings, coupled microstrip line band pass filters etc.

- In all the filters Butterworth response is achieved and further one can design band pass / band stop filters with Chebyshev or pseudo-elliptic responses by applying suitable PBG / DGS elements.
- PBG / DGS can be used to make tunable filters by implementing BST as the host material.
- Complete band gap can be achieved by extending the perforations in three dimensions for PBG structures.
- Gain of CPW – DGS fed antennas can be enhance by incorporating active elements in the circuitry.

APPENDIX

Broad band dielectric resonator antennas excited by modified microstrip line technique is proposed. The effect of geometry modifications of microstrip feed line on the gain, bandwidth and radiation performances of the antenna has also been investigated. For the proposed antennas the radiation performance was comparable and gain was better than that of conventional microstrip patch antennas

A.1 Introduction to Dielectric Resonator Antennas

Ceramic dielectric resonator antennas (DRAs) have the inherent advantages like high radiation efficiency and large impedance bandwidth owing to their lower ohmic loss compared with conventional microstrip patch antennas. The resonant frequency and operating bandwidth of a DRA can be easily controlled by choosing the dielectric constant and dimensions of the dielectric resonator (DR) material used. DRAs can be of any shape and each shape has many resonant modes [1] which have different radiation characteristics.

L and T-shaped microstrip line excitation was used for enhancing the bandwidth of microstrip patch antennas [2,3] and the same technique is implemented for DRAs. In the present study the Dielectric Resonator (DR) used and its material properties is presented in the Table.A.1.1.

Properties	
Material	$Ca_5Nb_2TiO_{12}$
Density	4.05 g/cm^3
dielectric constant	48
$Q_u \times f$	26,000GHz (at 4GHz)
temperature coefficient of the resonant frequency	40 ppm/°C

Table. A.1.1 Material properties of the DR

Different shapes (cylindrical and rectangular) of DR made of $Ca_5Nb_2TiO_{12}$ [4] are prepared via solid-state ceramic technology. The radiation and reflection properties of these DR's are studied on modified microstrip feeds - the L-shaped feed and the T-shaped feed. The characteristics of DRA on these modified feeds are compared with that on microstrip feed. The dimensions of the DR used for the study is shown in the table. A.1.2.

Shape	Dimensions
Cylindrical	Diameter = 24.15 mm Height = 6.81 mm
Rectangular	Length = 22.5 mm Breadth = 11.9 mm Height = 5.55 mm

Table. A.1.2 Dimensions of the DR

A.2 Broad band Cylindrical Dielectric Resonator Antennas

The cylindrical DR with diameter, D = 24.15 mm and height H= 6.81 mm is excited by an L-strip feed fabricated on a substrate of dielectric constant ε_r = 4.28 and thickness h = 1.6 mm. The width of S_1 and S_2 is the same to assure 50Ω impedance of the feed line. Cylindrical DRA loaded on an L-shaped feed is shown in Figure.A.2.1 (a) and the T-shaped feed is shown in Figure.A.2.1 (b).

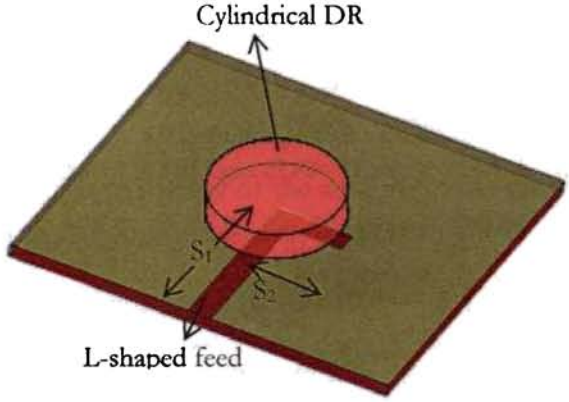

Figure A.2.1 (a) Geometry of the L-shaped fed Cylindrical Dielectric Resonator Antenna

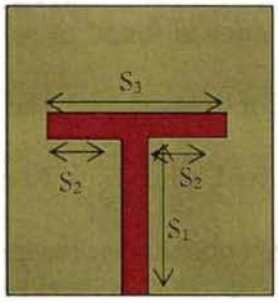

Figure A.2.1 (b) T-shaped feed

The relative position of the DR on the modified microstrip feed is optimized to obtain maximum impedance matching. The feed length S_1 of the feed is kept constant as 50 mm and the feed segment length S_2 is varied from 0 to 40 mm for optimum bandwidth in both the cases. When S_2 = 0, the modified feed acts as a conventional microstrip feed. Variation in the percentage bandwidth with feed segment length (S_2) is shown in Figure A.2.2.

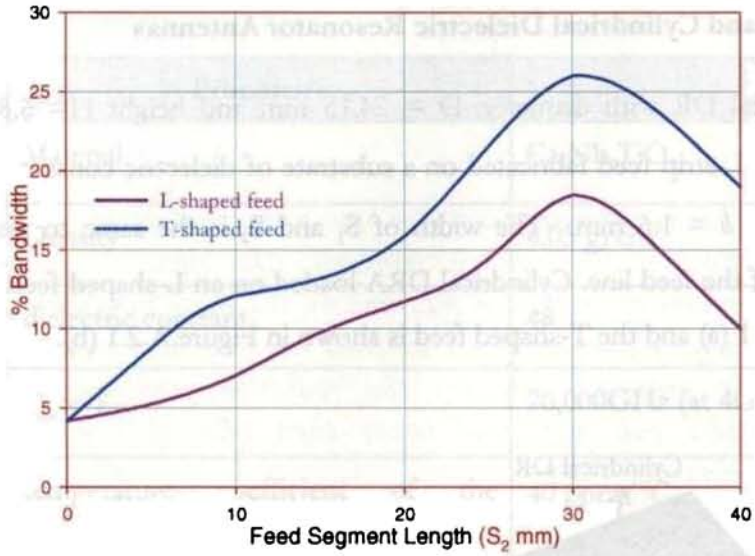

Figure A.2.2. Variation of % Bandwidth with feed segment lengths
h = 1.6mm, ε_r = 4.28, S_1 = 50mm, D = 24.15 mm, H= 6.81 mm, ε_{dr} = 48.

The antenna is found to give a 2:1 VSWR bandwidth of 18.47 % (2.455 - 2.95 GHz) for the L-shaped feed and ~ 26 % (2.4 – 3.075 GHz) is obtained for the T-shaped feed, when S_2 = 30 mm. Variation of S_{11} as a function of frequency at the optimized position for the modified feeds is shown in Figure A.2.3.

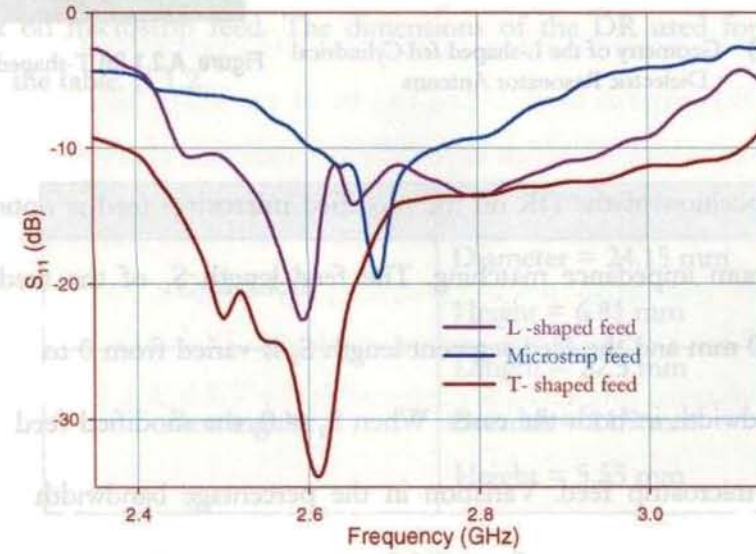

Figure A.2.2. Variation of return loss with frequency
h = 1.6mm, ε_r = 4.28, S_1 = 50mm, S_2 = 30 mm, D = 24.15 mm, H= 6.81 mm, ε_{dr} = 48.

The gain of these antennas is found to be comparable with that of a conventional microstrip antenna. The comparative gain is presented in Table.A.2.3.

Feed used	Gain (dBi) in the bore-sight direction
Microstrip feed	9.1
L – Shaped feed	10.23
T – shaped feed	8.3

Table A.2.3 Gain of the broad band cylindrical dielectric resonator antenna
h = 1.6mm, ε_r = 4.28, S_1 = 50mm, S2 = 30 mm
D = 24.15 mm, H= 6.81 mm, ε_{dr} = 48.

The radiation pattern of the antenna at the resonating frequency for the optimized feed parameters is shown in Figure A.2.4.

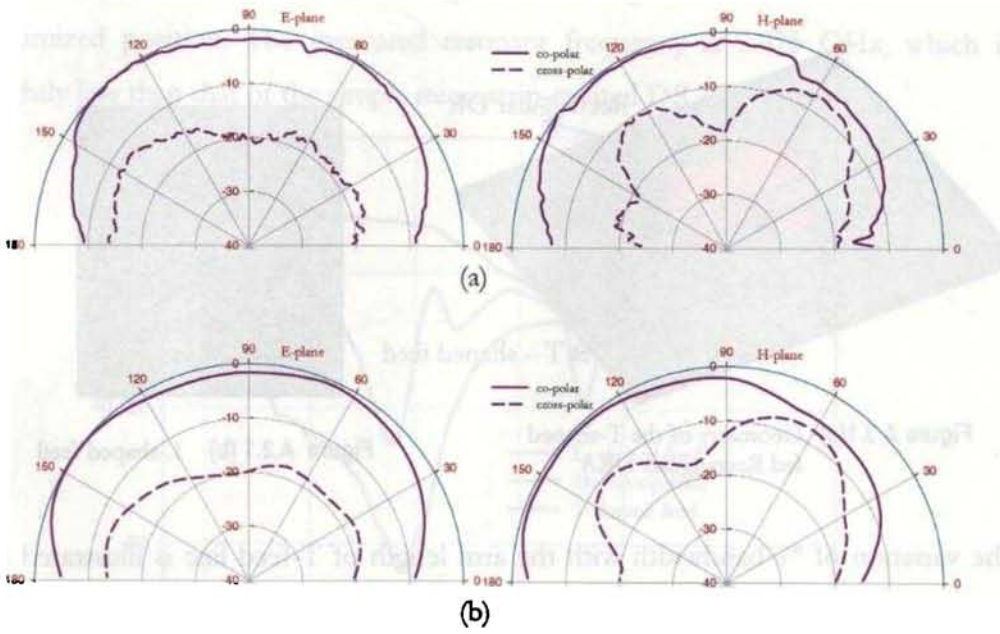

Figure A.2.4 Radiation pattern of the antenna at 2.6 GHz
(a) L-shaped feed (b) T- shaped feed
h = 1.6mm, ε_r = 4.28, S_1 = 50mm, S2 = 30 mm
D = 24.15 mm, H= 6.81 mm, ε_{dr} = 48.

A.3 Broad band Rectangular Dielectric Resonator Antennas

A rectangular DR with Length L = 22.5 m, Breadth B = 11.9 mm and Height H = 5.55 mm is energized by a 50 Ω modified microstrip line printed on a substrate of thickness h = 1.6 mm and dielectric constant ε_r = 4.28.

The feed length S_1 is fixed at 50 mm and the arm length S_2 is varied from 0 to 40 mm. The position of the DR on the feed line is optimized to provide coupling between the microstrip line and the rectangular DR, hence achieving maximum matching at the desired frequency. Excellent matching was observed when the DR was placed at the junction (S_1 = 50 mm) of the branched L and T-feed line with its length exactly over the arm length (S_2) direction, as depicted in Figure A.3.1. For optimum arm length and position on the feed line, the DR was glued to the substrate over the feed line.

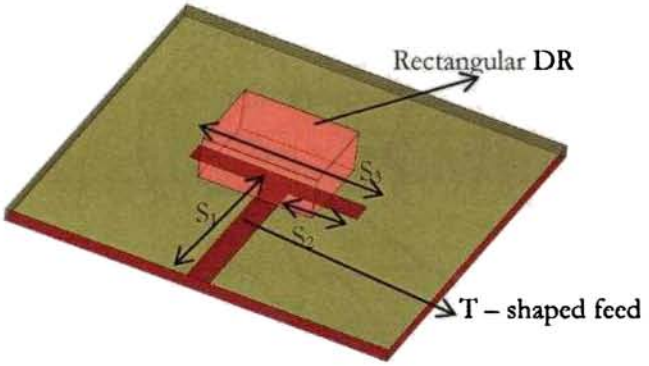

Figure A.3.1(a) Geometry of the T-shaped fed Rectangular DRA

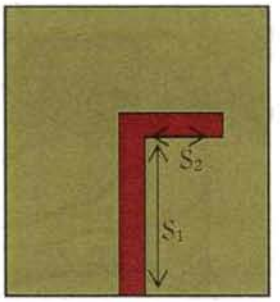

Figure A.3.1 (b) L-shaped feed

The variation of % bandwidth with the arm length of T-feed line is illustrated in Figure A.3.2. The bandwidth increased with the arm length, reached a maximum at S_2 = 35 mm, and then decreased for both the feeds. This was taken as the optimum feed-length dimension and all the antenna characteristics were measured after fixing the DR over the feed line in the optimized position.

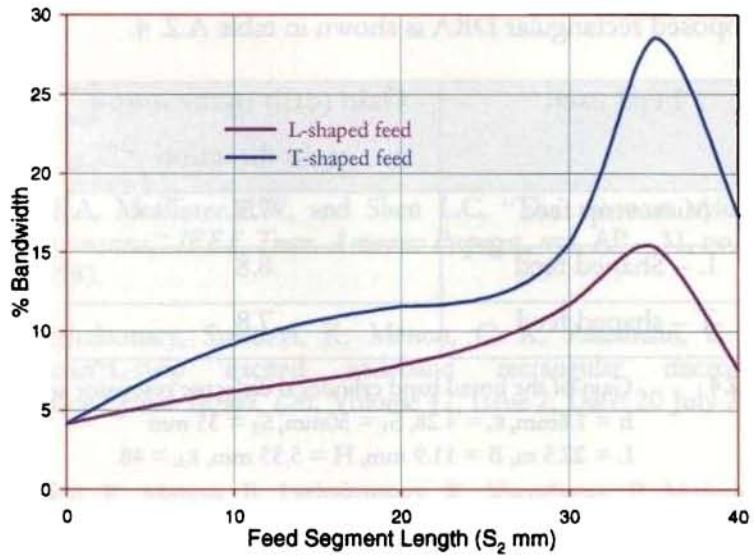

Figure A.3.2. Variation of % Bandwidth with feed segment lengths
h = 1.6mm, ε_r = 4.28, S_1 = 50mm
L = 22.5 m, B = 11.9 mm, H = 5.55 mm, ε_{dr} = 48.

Figure A.3.3 shows the variation of S_{11} of the rectangular DRA, with the DR at the optimized position. The measured resonant frequency is 2.975 GHz, which is slightly less than that of the simple microstrip-excited DRA.

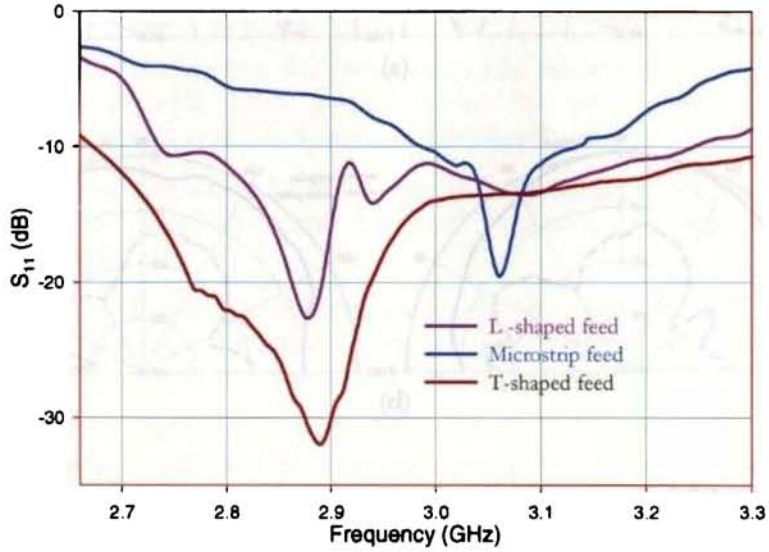

Figure A.3.3. Variation of % Bandwidth with feed segment lengths
h = 1.6mm, ε_r = 4.28, S_1 = 50mm, S_2 = 35 mm
L = 22.5 m, B = 11.9 mm, H = 5.55 mm, ε_{dr} = 48.

The gain of proposed rectangular DRA is shown in table A.2. 4.

Feed used	Gain (dBi) in the bore-sight direction
Microstrip feed	7.5
L – Shaped feed	8.8
T – shaped feed	7.8

Table A.2.4 Gain of the broad band cylindrical dielectric resonator antenna
$h = 1.6mm$, $\varepsilon_r = 4.28$, $S_1 = 50mm$, $S_2 = 35$ mm
$L = 22.5$ m, $B = 11.9$ mm, $H = 5.55$ mm, $\varepsilon_{dr} = 48$.

The radiation pattern of the antenna at the centre frequency of the operating band is shown in Figure A.2.4.

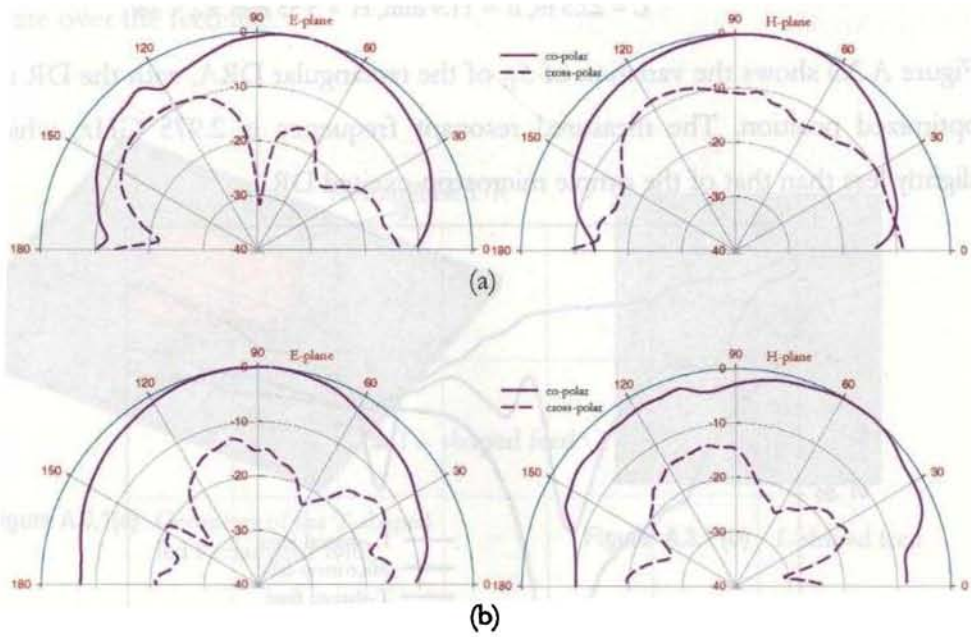

Figure A.2.4 Radiation pattern of the antenna at 2.6 GHz
(a)L-shaped feed (b) T- shaped feed
$h = 1.6mm$, $\varepsilon_r = 4.28$, $S_1 = 50mm$, $S_2 = 35$ mm
$L = 22.5$ m, $B = 11.9$ mm, $H = 5.55$ mm, $\varepsilon_{dr} = 48$.

References

1. Long.S.A, Mcallister.M.W, and Shen L.C, "The resonant cylindrical dielectric cavity antenna," *IEEE Trans. Antennas Propagat.*, vol. AP – 31, no.3, pp.406 – 412, May 1983.

2. B. Lethakumary, Sreedevi. K. Menon, C. K. Aanandan, K. Vasudevan, P. Mohanan"L-strip excited wideband rectangular microstrip antenna" *Microwave Optical Technol. Lett*, Volume 42, Issue 2, Date: 20 July 2004, Pages: 173-175

3. Sreedevi. K. Menon, B. Lethakumary, K. Vasudevan, P. Mohanan "Wide band rectangular microstrip antenna using symmetric T-shaped feed" *Microwave Optical Technol. Lett*, Volume 35, Issue 3, Date: 5 November 2002, Pages: 235-236

4. P.V.Bijumon, Sreedevi K Menon, M.T.Sebastian and P.Mohanan, "Enhanced Bandwidth Microstrip Patch Antennas loaded with High Permittivitty Dielectric Resonators, *Microwave Optical Technol. Lett*, vol. 35, no.4, pp.327-330, November 20 2002.

List of publications of the author

Patents Filed

1. "Microwave dielectric ceramic composition, method of manufacture thereof and devices comprising the same ", M. T. Sebastian, P. V. Bijumon, P. Mohanan and **Sreedevi. K. Menon** . PCT/IN02/00051. US Patent.

2. "Development of novel cylindrical resonator antenna and other devices based on new microwave dielectric ceramic composition in the $Ca_5A_2TiO_{12}$ system [A=Nb, Ta]", M.T. Sebastian, P.V. Bijumon, P. Mohanan and **Sreedevi. K. Menon.** NF/482/2001.

International Journal

1. **Sreedevi. K. Menon,** K. Vasudevan, C. K Aanandan, P. Mohanan " Design and analysis of microstrip lines with EBG-backed ground planes of different geometrical shapes" *Microwave and Optical Technology Letters*, Volume 46, Issue 6, Date: 20 September 2005, Pages: 544-546

2. **Sreedevi. K. Menon,** K. Vasudevan, C. K Aanandan, P. Mohanan "Compact asymmetric coplanar waveguide filter" *IEE Electronics Letters* Vol. 41 No. 11. 26th May 2005

3. **Sreedevi. K. Menon,** K. Vasudevan, C. K Aanandan, P. Mohanan "Coplanar waveguide with DGS ground plane for planar filters" communicated to *Microwave and Optical Technology Letters*

4. **Sreedevi. K. Menon,** K. Vasudevan, C. K Aanandan, P. Mohanan "Coplanar waveguide with DGS ground plane for planar filters and Antennas" communicated to *IEEE Antennas and Propagation.*

5. **Sreedevi. K. Menon,** K. Vasudevan, C. K Aanandan, P. Mohanan "DGS ground plane for planar filters and Antennas" communicated to *Microwave and Optical Technology Letters*

6. **Sreedevi. K. Menon,** B. Lethakumary, K. Vasudevan, P. Mohanan "Wide band rectangular microstrip antenna using symmetric T-shaped feed" *Microwave and Optical Technology Letters* Volume 35, Issue 3, Date: 5 November 2002, Pages: 235-236

7. **Sreedevi. K. Menon,** B. Lethakumary, P. V. Bijumon, M. T. Sebastian, P. Mohanan "L-strip-fed wideband rectangular dielectric resonator antenna" *Microwave and Optical Technology Letters*, Volume 45, Issue 3, Date: 5 May 2005, Pages: 227-228

8. **Sreedevi. K. Menon,** B. Lethakumary, P. V. Bijumon, M. T. Sebastian, P. Mohanan "L-strip-fed wideband rectangular dielectric resonator antenna"

Microwave and Optical Technology Letters, Volume 45, Issue 3, Date: 5 May 2005, Pages: 227-228

9. P. V. Bijumon, **Sreedevi. K. Menon**, M. N. Suma, B. Lethakumari, M. T. Sebastian, P. Mohanan "T-strip-fed high-permittivity rectangular dielectric resonator antenna for broadband applications" *Microwave and Optical Technology Letters*, Volume 47, Issue 3, Date: 5 November 2005, Pages: 226-228

10. M. N. Suma, **Sreedevi. K. Menon**, P. V. Bijumon, M. T. Sebastian, P. Mohanan "Rectangular dielectric resonator antenna on a conductor-backed co-planar waveguide" *Microwave and Optical Technology Letters*, Volume 45, Issue 2, Date: 20 April 2005, Pages: 154-156

11. B. Lethakumary, **Sreedevi. K. Menon**, Priya Francis, C. K. Aanandan, K. Vasudevan, P. Mohanan "Wideband microstrip antenna using hook-shaped feed" *Microwave and Optical Technology Letters*, Volume 44, Issue 2, Date: 20 January 2005, Pages: 169-171

12. B. Lethakumary, **Sreedevi. K. Menon**, C. K. Aanandan, K. Vasudevan, P. Mohanan "FDTD analysis of a symmetric T-strip fed wideband rectangular microstrip antenna" *Microwave and Optical Technology Letters*, Volume 43, Issue 4, Date: 20 November 2004, Pages: 332-334

13. **Sreedevi. K. Menon**, B. Lethakumary, P. Mohanan, P. V. Bijumon, M. T. Sebastian "Wideband cylindrical dielectric resonator antenna excited using an L-strip feed"*Microwave and Optical Technology Letters*, Volume 42, Issue 4, Date: 20 August 2004, Pages: 293-294

14. B. Lethakumary, **Sreedevi. K. Menon**, C. K. Aanandan, K. Vasudevan, P. Mohanan "L-strip excited wideband rectangular microstrip antenna" *Microwave and Optical Technology Letters*, Volume 42, Issue 2, Date: 20 July 2004, Pages: 173-175

15. S. Mridula, **Sreedevi. K. Menon**, P. Mohanan, P. V. Bijumon, M. T. Sebastian "Characteristics of a microstrip-excited high-permittivity rectangular dielectric resonator antenna" *Microwave and Optical Technology Letters* Volume 40, Issue 4, Date: 20 February 2004, Pages: 316-318

16. B. Lethakumary, **Sreedevi. K. Menon**, C. K. Aanandan, P. Mohanan "A wideband rectangular microstrip antenna using an asymmetric T-shaped feed " *Microwave and Optical Technology Letters*, Volume 37, Issue 1, Date: 5 April 2003, Pages: 31-32

17. S. Mridula, **Sreedevi. K. Menon**, B. Lethakumary, Binu Paul, C. K. Aanandan, P. Mohanan "Planar L-strip fed broadband microstrip antenna" *Microwave and Optical Technology Letters*, Volume 34, Issue 2, Date: 20 July 2002, Pages: 115-117

International Conference

18. **Sreedevi K Menon**, B.Lethakumary, C.K.Aanandan, K.Vasudevan and P.Mohanan," Wide band Rectangular Microstrip Antenna using L-shaped feed", Proc, *2002 IEEE Antennas and Propagation Society International Symposium, Texas*, July 2002.

19. **Sreedevi K Menon**, B Lethakumary, C K Aanandan and P Mohanan," Rectangular microstrip antenna with PBG structured ground plane" Proc., *First International Conference on Microwaves, Antennas, Propagation and Remote Sensing (ICMARS 2003)*, International Centre for Radio Science, Jodhpur, Dec. 15-19 2003.

20. **Sreedevi K Menon**, B Lethakumary, C K Aanandan and P Mohanan," Rectangular microstrip antenna with PBG structured ground plane" Proc., of PIERS 2004.

21. **Sreedevi K Menon**, C K Aanandan and P Mohanan," Rectangular microstrip antenna with PBG structured ground plane" *2004 IEEE Antennas and Propagation Society International Symposium*, July 2004.

22. B Lethakumary, **Sreedevi K Menon**,, C K Aanandan K.Vasudevan and P Mohanan " Wide band rectangular microstrip antenna" Proc., *First International Conference on Microwaves, Antennas, Propagation and Remote Sensing (ICMARS 2003)*, International Centre for Radio Science, Jodhpur, Dec. 15-19 2003.

23. S. Mridula, **Sreedevi K Menon**, K.Vasudevan, P.Mohanan, P.V.Bijumon and M.T.Sebastian, "Microstrip Fed Compact Rectangular dielectric Resonator Antenna", Proc., *First International Conference on Microwaves, Antennas, Propagation and Remote Sensing (ICMARS 2003)*, International Centre for Radio Science, Jodhpur, Dec. 15-19 2003.

24. S.Mridula, **Sreedevi K Menon**, Binu Paul, C.K.Aanandan K.Vasudevan, P.Mohanan P.V.Bijumon and M.T.Sebastian, "Experimental investigations on a Microstrip fed Compact Rectangular Dielectric Resonator Antenna", Proc., *International Conference on Computers and Devices for communication (CODEC – 04)*, Institute of Radio Physics and Electronics, University of Calcutta, Jan 1 – 3 2004

25. Binu Paul, S. Mridula, **Sreedevi K Menon**, C.K.Aanandan, P.Mohanan, P.V.Bijumon and M.T.Sebastian, "Time Domain Analysis of a Microstrip Line Excited Compact Rectangular Dielectric Resonator Antenna", Proc., 20th Annual Review of Progress in Applied Computational Electromagnetics, Syracuse, NewYork, April 19 – 23 2004.

26. S.Mridula, Binu Paul, **Sreedevi K Menon**, C. K. Aanandan, K.Vasudevan, P.Mohanan, P.V.Bijumon and M.T.Sebastian, "Wideband Rectangular Dielectric Resonator Antenna For W-LAN Applications" Proc, *2002 IEEE Antennas and Propagation Society International Symposium, Texas*, July 2004.

27. S.Mridula, **Sreedevi.K.Menon,** Binu Paul, C.K.Aanandan K.Vasudevan, P.Mohanan P.V.Bijumon and M.T.Sebastian, "Experimental investigations on a Microstrip fed compact Rectangular Dielectric Resonator Antenna," Proc. International Conference on Computers and Devices for Communication (CODEC-04), Institute of Radio Physics and Electronics, University of Calcutta, January 1-3 2004.

28. Binu Paul, S.Mridula, **Sreedevi.K.Menon,** C.K.Aanandan, P.Mohanan, P.V.Bijumon and M.T.Sebastian, "Time Domain Analysis of a Microstrip Line excited compact Rectangular Dielectric Resonator Antenna," Proc. 20th Annual Review of Progress in Applied Computational Electromagnetics (ACES-04), Syracuse, NewYork, April 19-23 2004.

29. S. Mridula, Binu Paul, **Sreedevi.K.Menon,** C.K.Aanandan, P.Mohanan, P.V.Bijumon and M.T.Sebastian "Wideband Rectangular Dielectric Resonator Antenna for W-LAN applications," Proc. IEEE Antennas and Propagation Society International Symposium, Monterey, June 2004.

National Conference

30. **Sreedevi K Menon,** B Lethakumary, P Mohanan,P V Bijumon,and M T Sebastian "Dielectric Resonator Loaded Microstrip Antenna" *Proc Interactive Integrated Technological Advancement – Recent Trends (IITART), Trivandrum,* 5 – 6 July 2002.

31. **Sreedevi K Menon,** B.Lethakumary, C.K.Aanandan, K Vasudevan and P.Mohanan, "Bandwidth Enhancement of Microstrip Antenna Using Photonic Band Gap Structure", *Proc National Symposium on Antennas and Propagation (APSYM 2002), Cochin,* December 9 – 11 2002.

32. **Sreedevi K Menon,** B.Lethakumary, C.K.Aanandan, K Vasudevan, K. G. Nair and P.Mohanan, "Rectangular Microstrip Antenna with EBG structures with orthogonal periods", *Proc National Symposium on Antennas and Propagation (APSYM 2004), Cochin,* December 2004.

33. B.Lethakumary, **Sreedevi K Menon,** C.K.Aanandan, K Vasudevan and P.Mohanan, "FDTD Analysis of L-strip Fed Microstrip Antenna", *Proc National Symposium on Antennas and Propagation (APSYM 2002), Cochin,* December 9 – 11 2002.

34. P. V. Bijumon, **Sreedevi K Menon,** M. T. Sebastian and P. Mohanan "Enhanced Bandwidth Rectangular Dielectric Resonator Antenna Using Microstrip Feed", *Proc National Symposium on Antennas and Propagation (APSYM 2002), Cochin,* December 9 – 11 2002.

35. Rohith K. Raj, Jayaram P, **Sreedevi K Menon,** K Vasudevan, C.K.Aanandan and P.Mohanan " Fractal PBG Microstrip Antenna", *Proc National Symposium on Antennas and Propagation (APSYM 2002), Cochin,* December 9 – 11 2002.

36. B.Lethakumary, **Sreedevi K Menon**, C.K.Aanandan, K Vasudevan and P.Mohanan, "Circular Microstrip antenna with L-strip Feed", *Proc. National Symposium on Antennas and Propagation (APSYM 2004), Cochin*, December 2004.

37. Suma M N , **Sreedevi K Menon**, C.K.Aanandan, K Vasudevan and P.Mohanan, "Cylindrical Dielectric Resonator Antenna on Conductor Backed Co-Planar Waveguide", *Proc. National Symposium on Antennas and Propagation (APSYM 2004), Cochin*, December 2004

Citation – International Journal

1. **Sreedevi. K. Menon**, B. Lethakumary, P. V. Bijumon, M. T. Sebastian, P. Mohanan "L-strip-fed wideband rectangular dielectric resonator antenna" *Microwave and Optical Technology Letters*, Volume 45, Issue 3, Date: 5 May 2005, Pages: 227-228 *Proc. IEEE Antennas and Propagation Society International Symposium*, Monterey, July 2004 in the paper entitled "Strip fed Rectangular Dielectric Resonator Antennas with/ without a parasitic patch", *IEEE Trans. Antennas Propagat.*, vol.AP-53,no:7, pp. 2200-2207,authored by Bin Li and Kwok Wa Lueng.

2. S. Mridula, Binu Paul, **Sreedevi.K.Menon**, C.K.Aanandan, P.Mohanan, P.V.Bijumon and M.T.Sebastian "Wideband Rectangular Dielectric Resonator Antenna for W-LAN applications," *Proc. IEEE Antennas and Propagation Society International Symposium*, Monterey, July 2004 in the paper entitled "Strip fed Rectangular Dielectric Resonator Antennas with/ without a parasitic patch", *IEEE Trans. Antennas Propagat.*, vol.AP-53,no:7, pp. 2200-2207,authored by Bin Li and Kwok Wa Lueng.

Resume of the author

Sreedevi K Menon
Research Scholar
CREMA, Department of Electronics
Cochin University of Science and Technology
Kochi – 682 022, INDIA
Phone: 91-484-2576418
E-mail: sreedevikmenon@cusat.ac.in

Objective:

To pursue research activities in the field of Photonic Bandgap (PBG) structures, Dielectric Resonators and Electromagnetic Computation.

Education:

M.Sc Physics
Specialization: Electronics
Mahatma Gandhi University (1999)
Score: 67 % - First class

B Sc Physics
Mahatma Gandhi University (1997)
Score: 83% - First class with Distinction

Awards Obtained:

Awarded with Senior Research Fellowship (SRF) by the Council for Scientific and Industrial Research (CSIR) India.

Research Experience:

1. Worked as JRF in the Department of Science and Technology (DST) project, "Preparation characterization and Properties of Ba ($B'_{1/3}$"O_3[B'=Mg ,Zn; B"=Ta, Nb] microwave ceramic resonators" from October 2001 to March 2003.
2. Worked as project associate in the Malaysian consultancy project entitled, "Antenna Design Fabrication and testing for a Pseudo random polarization hopping (PPH) communication system" from July 2003 to July 2004.

Participated and presented research papers at 2 National conferences

Patents	:	2
International	:	1
National	:	1

Publications:

International Journal	17
International Conference	12
National Conference	08

Citation:

In International Journal	:	2 (IEEE Transactions on Antennas and Propagation, Vol. AP – 53, no: 7, pp. 2200 – 2207)

Computer Proficiency:

Assembly level programming, MATLAB
Simulation Softwares: IE3D, Fidelity, Microwave Office, Microstripes, HFFS